BULGARIAN CHEMICAL COMMUNICATIONS

2015 Volume 47 / Special Issue A

Selection of papers presented on the 8th National Conference on Chemistry, June 26-28, 2014, Sofia, Bulgaria

Journal of the Chemical Institutes
of the Bulgarian Academy of Sciences
and of the Union of Chemists in Bulgaria

Bulgarian Chemical Communications, Volume 47, Special issue A (pp. 5-9) 2015

Potential of fast growing poplar, willow and paulownia for bioenergy production

N. Yavorov*, St. Petrin, I. Valchev, S. Nenkova

Department of Pulp, Paper and Printing Arts, University of Chemical Technology and Metallurgy, 8 St. Kliment Ohridski blvd. 1756 Sofia, Bulgaria

Received July 14, 2014; Accepted July 24, 2014

The use of renewable energy sources is one of the possible prospects offering a real alternative to fossil fuels in combination with various eco-oriented advantages. In Bulgaria's forests, there exists an extensive set of fast growing tree species. The most preferred are intensive forest plantations and short-rotation systems from selected clones of poplar, willow, paulownia, acacia, etc. The biomass from plantations of fast growing tree species can be an alternative and attractive base for bioethanol production.

The investigation is performed for determination the potential of fast growing hardwood species from Bulgaria (paulownia (*Paulownia elongata*), poplar (*Populus alba*) and willow (*Salix viminalis rubra*)) as energy crops.

Highest cellulose content is established in *Populus alba*, while the amount of lignin is lowest in *Paulownia elongata*. The obtained lowest calorific value for *Paulownia elongata* is related with the determined content of lignin. The glucose yield after cellulase hydrolysis of steam-exploded *Paulownia elongata* is up to 52%. That result is approximately 24% higher in comparison with corresponding treatment of *Populus alba* and *Salix viminalis rubra*. The obtained result can be explained with the specific structure of *Paulownia elongata*. The chemical composition of wood and especially the cellulose content has no direct effect on the glucose yield.

The plantation harvesting, the calorific value and the glucose yield from fast growing *Populus alba*, *Salix viminalis rubra* and *Paulownia elongata* from Bulgaria make that tree species perspective and suitable for bioenergy production.

Key words: bioenergy, poplar, willow, paulownia, enzyme hydrolysis, steam explosion

INTRODUCTION

Bioenergy is receiving increasing attention because it may reduce greenhouse gas emissions, secure and diversify energy supplies and stimulate rural development. It is well known that transport is almost totally dependent on fossil particularly petroleum based fuels such as gasoline, diesel fuel, liquefied petroleum gas, and compressed natural gas. As the amount of available petroleum decreases, the need for alternative technologies to produce liquid fuels that could potentially help prolong the liquid fuels culture and mitigate the forthcoming effects of the shortage of transportation fuels increases [1, 2].

A potential source for low-cost bioenergy production is to utilize lignocellulosic materials such as crop residues, grasses, sawdust, wood chips, and solid animal waste. Biomass-based fuels, also known as biofuels can be produced via thermochemical and biochemical conversion technologies such as liquefaction [3, 4], pyrolysis [5], gasification [6, 7], hydrolysis [8, 9], fermentation [8], etc. Lignocellulosic biomass has long been recognized as a potential sustainable source of mixed sugars fermentation to biofuels and other biochemical [10, 11]. In the current environment of renewable energy development one option is the production of energy from fast growing forest trees in short rotation intensive culture plantations (SRIC), called bioenergy feedstock. The potential of fast growing forest trees high productivity, coppice ability and ease of vegetative propagation in SRIC plantations has been recognized for over thirty years [12]. One of the most popular fast growing trees are willow [12-14], poplar [12, 13, 15, 16], eucalyptus [15], paulownia [17, 18], etc.

The main object of this study is to establish the suitability of fast growing hardwood species cultivated in Bulgaria (*Paulownia elongata*, *Populus alba* and *Salix viminalis rubra*) as a potential sources of fermentable sugars (glucose) for bioethanol production.

*E-mail: nyavorof@gmail.com

EXPERIMENTAL

Fast growing hardwood tree species of the genus *Paulownia* (species *Paulownia elongata*), *Salix* (species *Salix viminalis rubra*) and *Populus* (species *Populus alba*), were used in these study. They have been harvested for three years in Experimental Station for Fast-growing Forest Tree Species, Svishtov, (north Bulgaria, 43° 37′ N 25° 21′ E).

The tree species were analysed for cellulose [19], lignin (TAPPI standard T222 om-11), ash (TAPPI standard T211 om-12) and calorific value (TAPPI standard T684 om-11).

The steam explosion pretreatment of wood chips was performed in 2 dm^3 stainless steel laboratory installation at the following conditions: a hydromodul ratio 1:10; an initial temperature of 100 ºC; a maximum temperature of 190 and 200 ºC; pressure of 12.8 and 15.85 bar; heating time of 60 min followed by additional 10 min at the maximum temperature. The steam exploded lignocellulosic mass was washed with distilled water and was subjected to enzymatic hydrolysis as a second stage of treatment.

The cellulase complex NS 22086 with activity 1.000 BHU g^{-1} and β-glucosidase NS 22118 with activity 250 CBU g^{-1} of Novozymes AS were used for the enzymatic hydrolysis. The enzyme charge of NS 22086 was 5%, while that of NS 22118 was 0.5%, both referred to the mass. The enzymatic treatment was carried out in polyethylene bags in a water bath previously heated to 50 °C, pH 5.0 – 5.6 and reaction time 72 h.

The glucose, cellobiose, xylose, furfural and HMF content were analysed with a Dionex HPLC system, according to the NREL standard biomass analytical procedure [20].

RESULTS AND DISCUSSION

Properties of the studied materials

The chemical composition and the calorific value of *Salix viminalis rubra*, *Paulownia elongata* and *Populus alba* are presented in Table 1. The results show that higher content of cellulose and lignin is in *Populus alba* and *Salix viminalis rubra*, and the lowest in *Paulownia elongata*. The ash content of the *Salix viminalis rubra*, 1.59%, is very similar to that of *Populus alba* (1.58%).

The calorific value ranging from 17 970 to 19 660 kJ kg^{-1}. The highest calorific value is determined in *Populus alba* and the lowest in *Paulownia elongata*. Relationship between the lignin content and the calorific value of the substrates is found. In the sample with the highest content of lignin was obtained the highest calorific value which may be due to the higher content of carbon and hydrogen in the lignin, which are the main heat producing elements [21, 22].

Table 1. Chemical composition and calorific value of *Salix viminalis rubra*, *Paulownia elongata* and *Populus alba*

Feedstock	Component (%)			Calorific value (kJ kg^{-1})
	Lignin	Cellulose	Ash	
Salix viminalis rubra	24.7	46.43	1.59	18 850
Paulownia elongata	21.87	44.03	1.03	17 970
Populus alba	25.31	49.72	1.58	19 660

Evaluation of pretreatment of various biomass materials used in this study

Pretreatment of the substrates by steam explosion shows that the optimum temperature for full defibrillation of *Paulownia elongata* is 190 °C, while of *Salix viminalis rubra* and *Populus alba* is 200 °C, which is possibly due to the differences in the anatomical structure of tree species. The additional refining of the pulp is necessary at lower temperatures of treatment.

The soluble hemicelluloses are removed with the filtrate during the washing of steam exploded pulp. By the separation of the prehydrolysate from the lignocellulosic mass is effectively reduced the

inhibition products as furfural, hydroxymethyl furfural (HMF), and phenolics. The results of the analysis of the prehydrolysates using HPLC system are summarised in Table 2.

Table 2. Reducing sugars obtained in the prehydrolysates of *Paulownia elongata*, *Salix viminalis rubra* and *Populus alba*.

	Paulownia elongata (190 °C)	*Salix viminalis rubra* (190 °C)	*Salix viminalis rubra* (200 °C)	*Populus alba* (200 °C)
Glucose (%)	1.71	1.62	-	-
Xylose (%)	2.41	1.18	1.43	0.73
HMF (%)	-	0.38	0.10	-
Furfural (%)	0.24	0.18	0.28	0.10

The lowest furfural and xylose yields of 0.10% and 0.73% are obtained from *Populus alba*, while the yield of xylose is greatest from *Paulownia elongata* and that of the furfural from *Salix viminalis rubra* (200 °C).

The studied pulps after steam explosion pretreatment present low glucose conversion of 1.62% and 1.71% for *Salix viminalis rubra* (190 °C) and *Paulownia elongata*, respectively, and absent of conversion for *Populus alba* and *Salix viminalis rubra* (200 °C).

Enzymatic hydrolysis of the pretreated feedstock

The pretreated feedstock are hydrolysed with cellulases (NS 22086) supplemented with β-glucosidase (NS 22118). The yields of glucose and xylose are determined using the HPLC and the results obtained for *Salix viminalis rubra* (190 and 200 °C) are presented in Fig. 1.

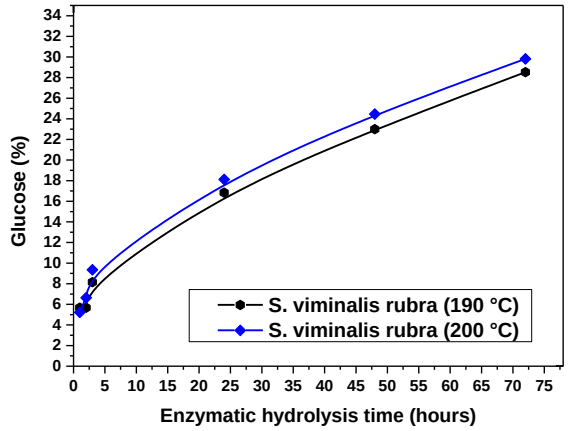

Fig. 1. Glucose yield after hydrolysis of pretreated *Salix viminalis rubra*.

As seen in Fig. 1, the glucose yield reaches nearly 28.7% and 29.8% for *Salix viminalis rubra* (190 °C) and *Salix viminalis rubra* (200 °C), respectively. The results obtained are approximately identical but the short refining must be included at low treatment temperatures. The yields of glucose from *Paulownia elongata* and *Populus alba* are presented in Fig. 2.

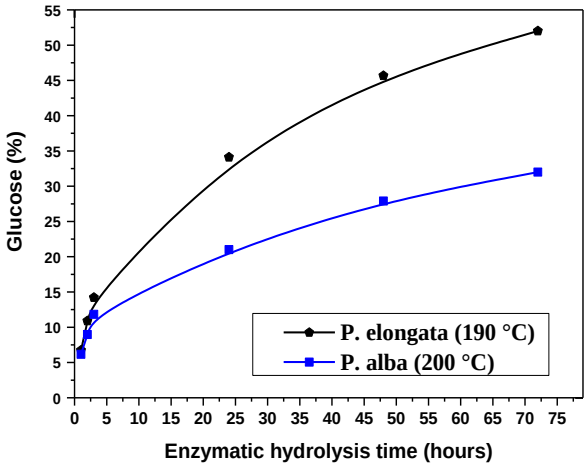

Fig. 2. Glucose yield versus enzymatic hydrolysis time of *Paulownia elongata* and *Populus alba*.

The results show that greater amount of glucose is prepared from *Paulownia elongata* (52%) compared to *Populus alba* (32.1%). This effect is due to the anatomical characteristics and full defibrillation of *Paulownia elongata* during the pretreatment, which contributes to a more efficient enzyme hydrolysis.

The comparing of the obtained results for *Paulownia elongata, Populus alba and Salix viminalis rubra* shows the significant advantage of the paulownia.

The results for *Populus alba* are comparable with those of the enzyme treatment of wheat straw, while the data for *Salix viminalis rubra* are slightly lower [23].

During the cellulase hydrolysis of *Salix viminalis rubra* and *Populus alba* is removed and certain amount of xylose, while for paulownia that effect is

not observed (Fig. 3). That is connected with the steam exploded treatment of wood.

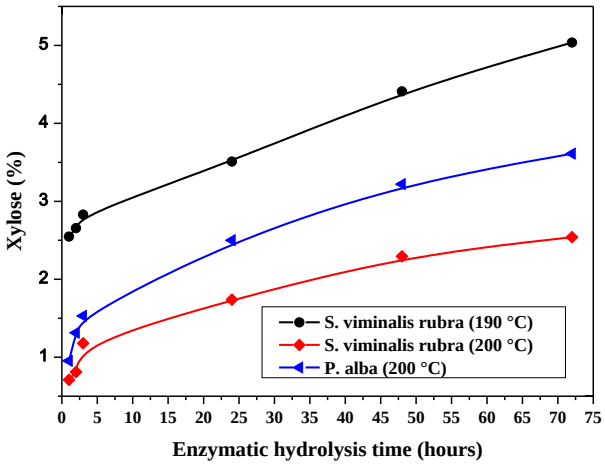

Fig. 3. Xylose yield versus enzymatic hydrolysis time of *Salix viminalis rubra* and *Populus alba*.

CONCLUSIONS

The largest yield of glucose is obtained for *Paulownia elongata* compared with *Populus alba* and *Salix viminalis rubra*.

Poplar and willow, which are a typical tree species on the territory of Bulgaria, shows results comparable with those obtained for wheat straw.

The anatomical structures of tree species, which are selected for testing, explain the different temperatures required for steam exploded treatment.

In conclusion it can be said that the fast-growing tree species, grown in Bulgaria, show a great potential for second-generation bioethanol producing, on the one hand by the high yields obtained sugars, and on the other by the possibility of cultivation in the short rotation plantations.

REFERENCES

1. A. Demirbas, *Appl. Energy*, **86**, Suppl. 1, S108 (2009).
2. M.A. Meyer, J.A. Priess, *Biomass Bioenergy*, **65**, 151 (2014).
3. Z. Liu, F.-S. Zhang, *Energy Convers. Manag.*, **49**, 12, 3498 (2008).
4. M. Balat, M. Balat, E. Kirtay, H. Balat, *Energy Convers. Manage.*, **50**, 12, 3147 (2009).
5. D.R. Vardon, B. K. Sharma, G. V. Blazina, K. Rajagopalan, T. J. Strathmann, *Bioresour. Technol.*, **109**, 178 (2012).
6. M. Balat, M. Balat, E. Kırtay, H. Balat, *Energy Convers. Manage.*, **50**, 12, 3158 (2009).
7. L. Wang, C.L. Weller, D.D. Jones, M.A. Hanna, *Biomass Bioenergy*, **32**, 7, 573 (2008).
8. S. Brethauer, C.E. Wyman, *Bioresour. Technol.*, **101**, 13, 4862 (2010).
9. P. Alvira, E. Tomas-Pejo, M. Ballesteros, M.J. Negro, *Bioresour. Technol.*, **101**, 13, 4851 (2010).
10. Y. Sun, J. Cheng, *Bioresour. Technol.*, **83**, 1,1 (2002).
11. S. Ewanick, R. Bura, in: Bioalcohol production. Biochemical conversion of lignocellulosic biomass, K. Waldron (ed.), Woodhead Publishing Limited, 2010, p. 3.
12. F.A. Aravanopoulos, *Biomass Bioenergy*, **34**, 11, 1531 (2010).
13. C. Hofmann-Schielle, A. Jug, F. Makeschin, K.E. Rehfuess, *Forest. Ecol. Manag.*, **121**, 1–2, 41 (1999).
14. M. Labrecque, T.I. Teodorescu, *Biomass Bioenergy*, **25**, 2, 135 (2003).
15. S. Gonzalez-Garcia, M.T. Moreira, *Biomass Bioenergy*, **39**, 378 (2012).
16. L. Ciadamidaro, E. Madejon, M. Puschenreiter, P. Madejon, *Sci. Total Environ.*, **454**–**455**, 337 (2013).
17. N. Ayrilmis, A. Kaymakci, *Ind. Crop. Prod.*, **43**, 457 (2013).
18. M.E. Lucas-Borja, C. Wic-Baena, J.L. Moreno, T. Dadi, C. Garcia, *Appl. Soil Ecol.*, **51**, 42 (2011).
19. K. Kurschner, A. Hoffer, *Fresen. J. Anal. Chem.*, **92**, 145 (1933).
20. A. Sluiter, B. Hames, R. Ruiz, C. Scarlata, J. Sluiter, D. Templeton, Laboratory Analytical Procedure, National Renewable Energy Laboratory (NREL), 2006.
21. A. Demirbas, *Energy Convers. Manag.*, **42**, 2, 183 (2001).
22. C. Telmo, J. Lousada, *Biomass Bioenergy*, **35**, 5, 1663 (2011).
23. I. Valchev, S. Petrin, in: Proc. 21st EU Biomass Conf. Exhib., Copenhagen, 2013, p. 1547.

ИЗСЛЕДВАНЕ ПОТЕНЦИАЛА НА БЪРЗОРАСТЯЩА ТОПОЛА, ВЪРБА И ПАУЛОВНИЯ ЗА ПОЛУЧАВАНЕ НА БИОЕНЕРГИЯ

Н. Яворов*, Ст. Петрин, И. Вълчев, С. Ненкова

Катедра „Целулоза, хартия и полиграфия“, Химикотехнологичен и металургичен университет, бул. „Св. Климент Охридски“ 8, 1756 София, България

Получена на 14 юли 2014; Приета на 24 юли 2014

(Резюме)

Използването на възобновяеми енергийни източници е една от възможните перспективи, които предлагат реална алтернатива на минерални горива в комбинация с различни еко-ориентирани предимства. В горите на България, съществува богат набор от бързорастящи дървесни видове с потенциал за плантационно отглеждане. Най-предпочитаните са избрани клонове на топола, върба, пауловния, акация и др. Биомасата от насаждения от бързорастящи дървесни видове може да бъде алтернативна и привлекателна основа за производство на биоетанол.

Целта на настоящата работа е изследване и установяване потенциала на бързорастящите, широколистни дървесни видове, отглеждани на територията на България (*Paulownia elongata*, *Populus alba* и *Salix viminalis rubra*) като енергийни култури.

Най-високо съдържание на целулоза е установено при тополата, докато количеството на лигнина е най-ниско при пауловнията, което обяснява получената ниска стойност на калоричност при *Paulownia elongata*. Добивът на глюкоза след целулазна хидролиза на пауловния, предварително третирана с парен взрив е до 52%, който е приблизително 24% по-висок от този при тополата и върбата при равни други условия. Тази разлика най-вероятно се дължи на специфичната структура на пауловнията, т.к. се вижда, че химичният състав на дървесината и особено съдържанието на целулоза няма директно влияние върху добива на глюкоза.

Възможностите за плантационното отглеждане, получените данни за калоричност и високият добив на глюкоза от изследваните бързорастящи дървесни видове, отглеждани в България, прави тези дървесни видове перспективни и подходящи за производство на биоенергия.

Bulgarian Chemical Communications, Volume 47, Special issue A (pp. 10 – 15) 2015

Review and comparative analysis of keratin biocomposites with composites based on collagen

D.I. Zheleva

University of Chemical Technology and Metallurgy – Sofia, Textile and Leather Department, Kl. Ohridsky blvd. 8, Sofia 1756, Bulgaria

Received August 1, 2014; Accepted January 26, 2015

Keratin and collagen are ones of the most abundant proteins which can be used in a variety of biomedical application due to their biocompatibility and biodegradability. Even though, keratin and collagen biomaterials are very high potential for tissue engineering applications. But, the major disadvantages of the natural biomolecules are their poor mechanical properties. Therefore it must be modified or combined with synthetic polymers. More of the synthetic polymers have good mechanical properties and thermal stability and numerous studies of biocomposites based on collagen or keratin and synthetic polymers are performed. The polyurethanes (PUs) are considered the most promising class of synthetic polymers for *in vivo* studies, and fulfill all the criteria for application to medical practice.

Keratin biomaterials have many various advantages over conventional biomolecules, including unique chemical properties due to the high content of sulfur in their structure, high biocompatibility, having aptitude to intracellular recognition and tendency to self-configure. There have been a lot of studies for the composites based on the keratin and one of the following synthetic polymers: poly(ethylene-oxide) (PEO), polyamide (PA6); poly(vinyl alcohol) (PVA), poly(methylmethacrylate) (PMMA), poly(L-lactic acid) (PLLA), etc., with the application in tissue engineering and drug delivery, in the form of gels, sponges, foams, films, fibers, mats and others. In the literature, however, no investigations for the composites based keratin/polyurethane for biomedical applications.

Key words: biocomposites, keratin, collagen, polyurethane, biocompatibility

INTRODUCTION

Collagen is the most abundant used tissue-derived natural polymer, and it is a main component of extracellular matrices of mammalian tissue including skin, bone, cartilage, tendon and ligament. It possesses low immunogenicity, high absorbance and very good biodegradability and it is suitable for preparing of biomaterials with different properties, composition and form by combination with synthetic polymers [1-25].

Keratin is the most abundant non-food protein being the major component of wool, hair, horns, nails and feather. Biomaterials based keratin are proven promising class of natural polymers due to their typical biocompatibility, biodegradation, chemical resistance, biological activity, higher cell adhesion compared to collagen and the possibility of polymerization in the porous structures [26-45].

The disadvantages of the proteins as biomaterials are: their similarity with substances naturally surrounding; poor mechanical properties; proteolytic modification at temperatures below its melting point; difference in the structure of the macromolecular substances which are derived from different animal sources. Each of these polymers is different from one another (specificity of samples) but also by one of the other tissues (tissue specificity) [6,14,18].

In recent years, hybrid polymeric systems of natural and synthetic macromolecules are used as medical biomaterials. The main biopolymers or called animal-based proteins used in preparation of materials for biomedical applications, are collagen, chitin, chitosan, keratin, silk and elastin [12,13,14,28,45].

The term "composite" means having two or more different parts [14]. Most composites are produced to ensure the mechanical properties such as strength, stiffness, toughness and fatigue resistance combined with other necessary qualities: biological functions and biocompatibility. Polyurethanes (PUs) are synthetic materials, which are obtained from isocyanates and hydroxyl containing components, are considered the most promising class of polymers for *in vivo* studies [4,12,13,18]. The reasons are their

*E-mail: darinajeleva@abv.bg

high mechanical strength, elasticity, aging resistance, tissue compatibility. Another advantage is their biodegradability by resorption. The PUs can be varied in a wide range by the proper selection of components, composition and preparation conditions. The PUs have a lot of functional groups: hydroxyl-, isocyanate-, urethane-, ester-, ether, alofanate-, etc. The collagen or other polypeptides, including the keratin, can react with terminal groups of PUs, which may result in bioactive composites. Consequently composites are based on keratin or collagen and polyurethane, combining the advantages of natural and synthetic materials would be promising biomaterials for tissue engineering, drug delivery and others.

The purpose of this study is to review and analyze the established possibilities for obtaining and application the biocomposites based on keratin/ polyurethane in the medicine and other areas as compared to those based on collagen/ polyurethane.

COLLAGEN AND COMPOSITES BASED ON COLLAGEN/ POLYURETHANE

Collagen is the most abundant protein. It is found in all multicellular organisms in the animal world. About 60% of the total content of protein in living organisms falls on collagen. It is available in large quantities, particularly as waste from slaughterhouses and leather industry. During the 80s of XX century, the collagen became a commonly used biomolecule in many medical applications. From a scientific point of view, which appears to collagen is understandable because it belongs to the so-called "grateful" biological objects for investigation. It can easily be isolated in pure form of insoluble fibers; it has a significant chemical and thermal stability as well as highly ordered structure. Due to its valuable biological properties: biocompatibility and biodegradability, which are well studied, there is a growing scientific interest towards it, especially in the field of bone implant surgery [1,3,11-25].

Collagen and elastin are two of the key structural proteins which have been found in the extracellular matrix of many tissues [20,21]. These proteins are important modulators for the physical properties of any engineered scaffolds, affecting cellular attachment, growth and responses to mechanical stimuli.

Natural polymers such as collagen and elastin are usually insoluble both in water and organic solvents [12,14]. The exception is collagen extracted from tissues of young animals, which is soluble in dilute acetic acid. The solubility of collagen in acetic acid provides the possibility to blend it with other water soluble polymers. Mixtures of collagen with synthetic polymers as well as with other natural polymers has been widely studied as biomedical materials, as have been collagen itself [14,26].

Biocomposites based on collagen, water-soluble synthetic polymers, namely polyvinyl pyrrolidone (PVP); polyvinyl alcohol (PVA); polyethylene glycol (PEG); polyethylene oxide (PEO), prepared in the form of thin films, hydrogels and sponges, have been studied in detail in medical practice. For the preparation of biocomposites are used and other synthetic polymers, namely: polyurethanes (PU); polyglycolic-(PGA), polylactic acid (PLA), poly (DL-lactide-co-glycolide) – PLGA [11-25].

Polyurethanes (PUs) are considered the most promising class of polymers for *in vivo* studies such as fulfills all the criteria for applicability to medical practice. PUs are potentially biodegradable materials, have unique chemistry and processability, but there is some limitation on their application due to lack of biologically active groups [4-10].

Jianjun *et al* [17] developed a flexible, biodegradable scaffold structure for cells transplantation in the form of a composite material based on biodegradable poly(esterurethan) urea and collagen type I. Poly(esterurethan)urea was synthesized by poly(caprolactone), 1,4-diisocyanatebutan and putrescine.

Oprea [18] studied the synthesis and properties of the microporous material based on polyurethane and collagen (0-15 wt.%). Polyurethane is prepared by polyadditional reaction on polyetherdiol with an aliphatic 1,6-hexamethylene diisocyanate and castor oil as the three-functional extender of the polymer chains. The obtained two-phase structure is characterized by excellent mechanical properties, pores with required sizes and biocompatibility, which are important parameters for biomedical applications.

The formation of the first primary compact and secondary porous structure can be explained by the surface gelling mechanism, in which the collagen migrates towards the surface of the composite film and the big size pores are formed at this stage. These pores were randomly distributed and interconnected [14,18]. Pore interconnectivity is due to the presence of smaller pores (up to 50 μm) that are positioned adjacent to the collagen fibers. It also has been observed that fewer small numbers of small pores are present in the PU (polyurethane)

phase with a higher content of the collagen. The decomposition temperature in the main stage and mechanical properties decreased with increasing the collagen content. The measurements of the contact angle show that the collagen improves the hydrophilicity of the PU-Collagen composites.

In order to improve the cells adhesion the coatings from collagen onto numerous hydrophilic polymeric scaffolds were applied [19].

The regeneration of damaged or lost tissue requires that certain function reparative cells assemble three-dimensionally around and inside the surrounding scaffold [24]. The nanofibres based on collagen and functionalized thermoplastic polyurethane (TPU/ Collagen) were successfully synthesized by electrospinning technique in order to obtain biomedical material with a porous structure. The results show that electrospun nanofibre composites exhibit features of natural extracellular matrix and can be effectively used as an alternative material for tissue engineering and as functional biomaterials.

The effects of the different parameters on the preparation process of porous structures have been studied in order to obtain optimal polyurethane scaffolds for the cardiovascular engineering.

We synthesized and investigated the composites based on polyurethane (PU) and collagen as a filler in concentrations (5 and 10 wt.%) [25]. The synthesis of the PU was carried out by two-step polyadditional reaction of the polyester polyols and 1,6-hexamethylene diisocyanate (MDI), and 1,4-butanediol as chains extender. Collagen was added *in situ* during the polymerization reaction. *In vitro* tests were conducted of the composites prepared in 1.5 SBF (Simulated Body Fluid) for 7 days under static conditions. FTIR (Fourier Transform Infrared Spectroscopy) and SEM (Scanning Electron Microscopy) methods were used for analysis.

Oprea *et al* [18,20] proved that the appearance of the hydrogen bonds between the collagen and the polyurethane macromolecules which is an indication of crosslinking or hardening of the composite structure. The adsorption bands at 1709 cm^{-1} corresponds to the free and H-bonded C=O groups. The same bands are also observed in our investigations. The intensity of the bands at the composites increases as compared to that of pure PU. The amide and carbonyl regions of spectra provided information for the intermolecular attraction by hydrogen bonding.

The micrographs on *fig.2* show the deposition of hydroxylapatite agglomerates with spherical forms after 7 days stay in SBF. The pores are interconnected in the scaffolds and there is the presence of the micropores in macroporous wall on which they to fulfill the criteria of the scaffold structure.

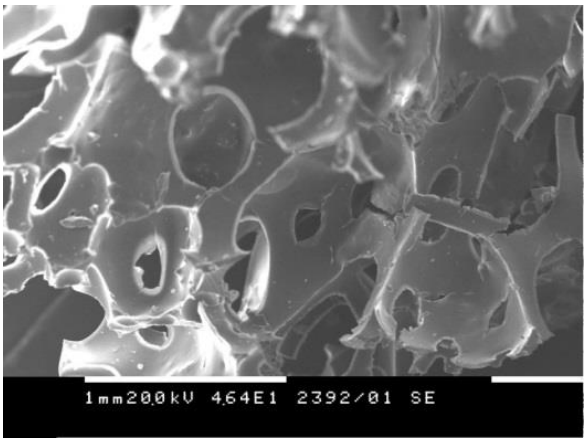

Fig.1. SEM of composites PU/Coll

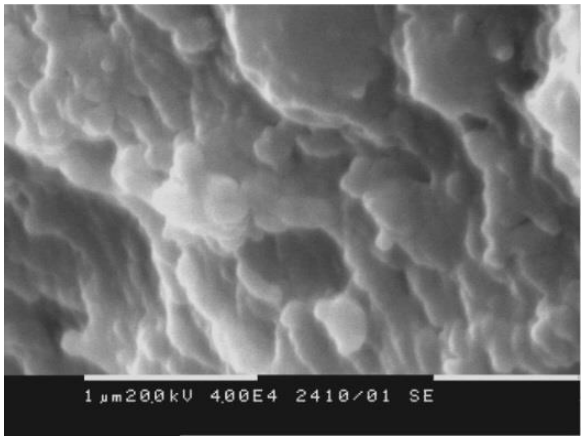

Fig.2. SEM of the PU/Coll after 7 days in SBF

KERATIN AND ITS COMPOSITES

Keratin is one the most abundant animal protein and is a waste from slaughterhouses, the leather and textile industry. It is a major component of hair, horns, nails, feathers, hooves and the stratum corneum of the epidermis. General, which bring together various keratins in one class proteins, is the presence of large amounts of cysteine, and thus the sulfur in its composition. Keratin is characterized by a higher cell adhesion compared to collagen. It has ability to polymerize in the porous structures as collagen and to self-assemble into complex of three dimensional scaffold structures [1,2,12,13,27].

Keratin belongs to the group of fibrous proteins. The extracted keratin can be produced in different forms: sponge scaffolds, mats, films, sheets, gels, micro fibers and bulk materials [26-45].

Wool keratin has been studied for application in cosmetic and tissue engineering for fabrication of sponge scaffolds for cells cultivation due to the close chemical similarity with human skin and hair or has been electrospun with other polymers to produce blend nanofibers with potential applications in different areas, from technical textiles to biomedical commodities [32].

It was limited the use of many biomaterials of natural origin, especially keratin-based products due to their poor mechanical properties. Thus the focus of research shifted to optimize the physico-mechanical properties and the preservation of their excellent biological activity. Several approaches have been considered to control the physical and biological properties, including the addition of natural and synthetic polymers to the keratin compounds and the application of novel preparative techniques to obtain pure keratin films [33,44].

Therefore keratin is suitable basic material for obtaining of hybrid systems with different characteristics, composition and forms, in combination with synthetic polymers. To the keratin is particularly interested in developing new products for the pharmaceutical industry, medicine, cosmetics and biotechnology.

The earliest documented use of keratins for medicinal applications comes from a Chinese herbalist *Li Shi Zhen* in 16th century [26]. A substance made of ground ash from pyrolized human hair that was used to accelerate wound healing and blood clotting called *Xue Yu Tan*, also known as *Crinis Carbonisatus*, was described in his book.

During the years 1905 to 1935, many methods were developed to extract keratins using oxidative-reductive chemistries. These technologies were initially applied to animal horns and hooves, but were also eventually used to extract keratins from wool and human hair.

Advances in the extraction, purification and characterization of keratins, led to exponential growth of keratin materials and their derivatives in the 70s of the last century [26]. The potential uses of keratins in similar applications began to be explored by a number of scientists. In 1982, Japanese scientist published the first study describing the use of keratin coating on vascular grafts as a way to eliminate blood clotting, as well as experiments on the biocompatibility of keratins.

In order to enhance the mechanical properties of the glycerol-containing keratin films by adding the chitosan or keratin experiments were done [35]. The composite films obtained show enhanced anti-thrombo-genetic properties and increased biocompatibility compared with fibroin itself or keratin.

Authors [36] were studied the interaction between keratin and synthetic polymers, namely on the interaction between the poly(ethylene oxide) (PEO) and the keratin film in order to obtain keratin biomaterials with improved properties. These composites can be used as scaffolds supporting the cells growth, dressing materials, membranes for the drug delivery.

It was investigated the intermolecular interactions between keratin and polyamide 6 (PA6) [39] in order to obtain keratin materials with a wide range of applications: from biomedical devices to active water filters and textile fibers.

Various methods for the processing of keratin with synthetic or natural polymers are applied in order to improve its processability in fiber-materials. Materials based on keratin/ PEO have been synthesized by mixing an aqueous solution of keratin and powdered PEO with good mechanical properties [37].

Fibers were obtained from aqueous solutions of the keratin with polyvinyl alcohol (PVA) [38]. The obtained composites showed good mechanical strength, water resistance, and excellent adsorption ability to toxic substances. Therefore with the success can be applied as absorbents for toxic substances, heavy metal ions and toxic gas from the formaldehyde.

Keratin fibers are used as reinforcing filler for the matrix of PMMA (polymethyl methacrylate) [39]. The composites have a high thermal stability and the keratin well distributed in the polymer, which leads to an increase of visco-elastic properties at elevated temperatures.

Keratin fibers are used in composites of polypropylene [43]. Maleic anhydride is grafted to the polypropylene in order to improve the dispersion of the keratin. These keratin materials increase the rate of crystallization of the polypropylene and thus improving its thermal stability.

As a native protein, keratin from wool is used to improve the affinity of the cells to poly (L-lactic acid) (PLLA) [44]. It has been found that the keratin supports interactions between osteoblastic cells and the polymer scaffold.

Wet-spinning techniques have been developed to produce novel keratinous fiber materials with potential use as hygiene articles [42]. Composites are prepared on the basis of keratin derived from feathers and modified bio-cellulose and used

.

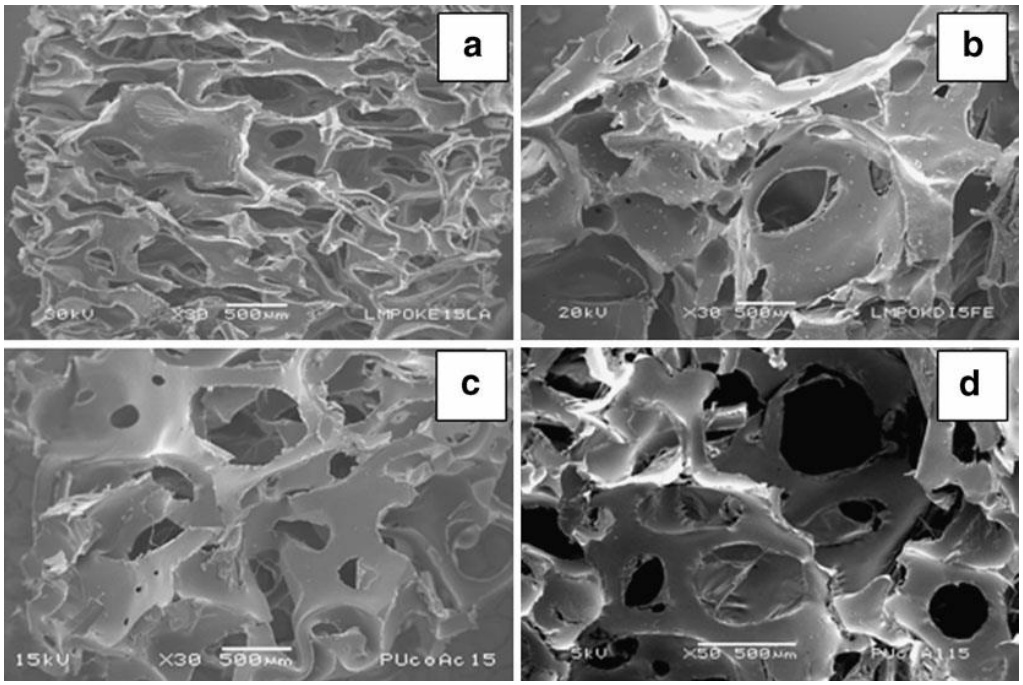

Fig.3. Micrographs of polyurethane-keratin membranes: a) keratin salt, b) dialyzed keratin, c) alkaline biofiber solution, d) acid biofiber solution, all of them at 15 wt.% [40]

to produce fibers, which are characterized by a good sorption properties, higher hygroscopicity and a lower contact angle than the cellulose fibers themselves.

The authors [40] have studied the possibility for use of the porous membrane based on polyurethane/ keratin to remove of hexavalent chromium. Keratin creates active sites for bioabsorption of Cr (VI) and polyurethane plays an important role in supporting the protein

CONCLUSION

Various biomaterials have been developed, some of which serve to support the healing process, acting as implants, others as drug delivery, to increase the adhesion of cells involved in the construction of the extracellular matrix and others. Some of them are based on keratin and synthetic polymers, combining the positive properties of the natural and the synthetic polymer. In the literature there are no reported studies on biomaterials based on keratin/ polyurethane for biomedical applications.

Keratin biomaterials have many various advantages compared to conventional biomolecules, including unique chemical properties due to the high content of sulfur in their structure, remarkable biocompatibility, tendency for self-configuration and internal cell recognition. Since these properties are becoming better studied, monitored and implemented many biomedical applications of keratin biomaterials have made their way in the clinical studies and will undergo revisions and new research in the development of new methods for synthesis of composite biomaterials.

REFERENCES

1. M. Pesheva, L. Papazjan, Fundamentals of Leather and Fur Production, Sofia, 1990, p.3.
2. M. Pesheva, Chemistry and Physics of Raw Leather and Tanning Substances, Sofia, 1982, p.38
3. I. Chakarska, PhD Thesis, UCTM, Sofia, 2008
4. D. Saunders, K. Frish, Chemistry of Polyurethanes, Chem. Ed., Moscow, 1968, p.277
5. K. A. Piez, *J. Dent. Res.*, **45**, 463 (1966)
6. S. Stegman, S. Chu and R. Armstrong, *J. Dermatol. Surg. Oncol.*, **14**, 39 (1988)
7. C. H. Lee, A. Singla and Y. Lee, *Int. J. Pharm.*, **221**, 1 (2001)
8. N. Shanmugasundaram, P. Ravichandran, P. Reddy, N. Ramamurty, S. Pal and K. Rao, *Biomaterials*, **22**(14), 1943 (2001)
9. S. Weiner, H. D. Wagner, *Ann. Rev. Mater. Sci.*, **28**, 271 (1998)
10. K. E. Kadler, D. F. Holmes, J. A. Trotter, J. A. Chapman, *Biochem. J.*, **316**, 1 (1996)
11. E. Khor, *Biomaterials*, **18**, 2, 95 (1997)
12. A. Sionkowska, *Progress in Polymer Science*, **36**, 1254 (2011)
13. Q. Chen, S. Liang, G. Thouas, *Progress in Polymer Science*, **38**(3-4), 584 (2012)

14. B.D. Rather, A.S. Hoffman, F.J. Shoen, J. Lemons, Biomaterials science – An Introduction to Materials in Medicine, USA ISBN: 0-12-582460-2, 1996
15. E. Jabbari, M. Khakpour, *Biomaterials*, **21**, 2073 (2000)
16. M. Huang, J. Wang, J. Luo, *J. Biomedical Sci. and Eng.*, **2**, 36 (2009)
17. G. Jianjun, J. Stanakus, W. Wagner, *Cell Transplant*, **15**, 17 (2006)
18. S. Oprea, *J. Composite Materials*, **44**, 18 (2010)
19. T. Douglas, H. Haugen, *J. Mater.Sci.: Mater. Med.*, **19**, 2713 (2008)
20. M. Popescu, C. Vasile, D. Macocineschi, *Inter. J. of Biol. Macromol.*, **47,** 646 (2010)
21. D. Filip, D. Macocinchi, S.Vlad, *Composites, Part B*, **42,** 1474 (2011)
22. C. Huang, R. Chen, Q. Ke, Y. Ke, K. Zhang, X. Mo, *Colloids and Surfaces B: Biomaterials*, **82**, 307 (2011)
23. D. Sin, X. Miao, G. Liu, F. Wei, G. Chadwick, C. Yan, T. Tris, *Mat. Sci. and Eng.*, **30**, 78 (2010)
24. R. Chen, C. Uang, Q. Ke, C. He, H. Wang, X. Mo, *Coloids and Surfaces B: Biointerfaces*, **79**, 315 (2010)
25. L. Radev, D. Zheleva, I. Michailova, *Centlal Eur. J. Chem.*, **11**(9), 1439 (2013)
26. J. Rouse, M. Van Dyke, *Material J.*, **3**, 999 (2010)
27. J. Cardamone, A. Nunez, R. Garcia., M. Ramos, *Research Letter in Mat. Sci.*, doi: 10.1155/2009/147175 (2009)
28. R. Karthikeyan., S. Balaji, P. Sehgal, *J. Sci.& Industrial Research*, **66**, 710 (2007)
29. K. Yamauchi, A.Yamauchi, T. Kusunoki, *J. Biomed. Mater.Res.*, **31**, 439 (1996)
30. A. Tachibana, S. Kaneko, *Biomaterials*, **26**, 297 (2005)
31. K. Katoh, T. Tanabe, *Biomaterials*, **25**, 4255 (2004)
32. M. Zoccola, A. Aluigi, C. Tonin, *J. Molek. Structure*, **938**, 35 (2009)
33. P. Sierpinski, J.P. Garrett, *Biomaterials*, **29**, 118 (2008)
34. P.J. Apel, A. Atala, J. *Hand Surg. Am.*, **33**, 1541 (2008)
35. T. Tanabe, N. Okitsu, *Biomaterials*, **23**, 817 (2002)
36. C. Tonin, C. Vineis, J. *Therm. Anal. Calorim.*, **89**, 601 (2007)
37. A. Aluigi, C. Vineis, *Eur. Polym. J.*, **44**, 2465 (2008)
38. K. Katoh, M. Shibayama, *J. Appl. Polym. Sci.*, **91**, 756 (2004)
39. K. Wrzesniewska-Tosik, D. Wawro, *Fibres Text. Eur.*, **15**, 157 (2007)
40. V. Saucedo- Rivalcoba, A. Martinez, *Water Air Soil Pollut.*, **218,** 557 (2011)
41. A. Salhi, K. Salah, Conference and Training School Multiphase Polymer and Composite Systems: From Nanoscale to Macro Composites (2011), France
42. A.L.Martinez-Hernandez, C. Velasco-Santos, *J. Composites Part B*, **38**, 405 (2007)
43. F. Bertini, M. Canetti., *J. Polymer Degradation and Stability*, **98**, 980 (2013)
44. L. Jiashen, L. Lin, F. Mak, K. Frank, Q. Ling, *J. Composites: Part B*, **40**, 664 (2009)
45. M. A. Khosa, A. Ullah, *J. Food Processing & Beverages*, **1**, 2332 (2013)

ПРЕГЛЕД И СРАВНИТЕЛЕН АНАЛИЗ НА КЕРАТИНОВИ БИОКОМПОЗИТИ С ТАКИВА НА БАЗА КОЛАГЕН

Д. И. Желева

Химикотехнологичен и металургичен университет – София, Катедра „Текстил и кожи“

Постъпила на 1 август 2014 г.; приета на 26 януари, 2015 г.

(Резюме)

Кератинът и колагенът са едни от най-често срещащите се протеини, които могат да бъдат използвани в различни биомедицински направления благодарение на тяхната биоразградимост и биосъвместимост. Освен това кератиновите и колагеновите биоматериали притежават висок потенциал за приложение особено в областта на тъканното инженерство. Основен недостатък на природните биомолекули са незадоволителните им механични свойства. Това налага модификация или съвместяване със синтетични полимери, характеризиращи се с добри механични свойства и термична стабилност. Проведени са многобройни изследвания на биокомпозити на база колаген или кератин и синтетитичен полимер. Най-обещаващ клас синтетични полимери за *in vivo* изследвания се смятат полиуретаните, които отговарят на всички критерии за биомедицинско приложение.

Кератиновите биоматериали притежават много различни предимства в сравнение с конвенционалните биомолекули, включително и уникални химични свойства, дължащи се на високото съдържание на сяра в структурата им, висока биосъвместимост, склонност към вътрешно клетъчно разпознаване и склонност към самостоятелно конфигуриране. Има много изследвания на композити на база кератин в комбинация с различни синтетични полимери, а именно: полиетиленоксид (PEO), полиамид (PA6); поливинилацет (PVA), полиметилметакрилат (PMMA), поли(L-млечна киселина) (PLLA) и др., с приложение в тъканното инженерство и за доставка на лекарства, под формата на гелове, гъби, пени, филми, влакна, подложки и др. В литературата обаче липсват изследвания специално на композити на база кератин/ полиуретан за биомедицински приложения.

Bulgarian Chemical Communications, Volume 47, Special issue A (pp. 16 - 20) 2015

Artificial ageing of composites based on modified cellulose fibres and polyurethane prepolymer

Ts.N. Ilieva[1*], S.K. Nenkova[1], M. Herzog[2]

[1]*Department of Pulp, Paper and Printing Arts, University of Chemical Technology and Metallurgy, 8 St. Kliment Ohridski blvd. 1756 Sofia, Bulgaria*
[2] *University of Applied Sciences Wildau, 15745 Wildau, Hochschulring 1, Germany*

Received July 17, 2014; Accepted November 4, 2014

Composite materials reinforced with natural short fibres have a number of advantages compared to other composites. These materials have high moulding flexibility, lightweight properties and they are environmentally friendly. Through fibre modification, obtained materials have uses in different areas, such as the automotive industry, conductive composites, building construction, etc.

The ultimate goal of this work is to study the properties of produced composite materials. This research focuses on the production of highly-filled polymer composites from short paper fibres from de-inking process and polymer matrix. The properties of these newly created composites are unknown. This is what forms the principle basis for the need for research.

In this work, a method for the use of waste fibres is provided. The fibres were mixed with liquid polyurethane prepolymer to form the composite. The samples were exposed to artificial ageing for 72, 144, 288 and 384 hours at 90°C and 50% RH. Mechanical properties before and after the ageing were studied.

***Keywords**: Composite materials, Cellulose fibres;, Artificial ageing; Mechanical properties; FT-IR.*

INTRODUCTION

Wood components are natural polymers and their interface has a large quantity of functional polar groups, in particular the cellulose. Waste wood, waste paper and waste plastics are major components in wood-polymer composites and offer great opportunities as recycled ingredients [1,2].

The paper industry generates a source of waste that can be used in further manufacturing. The waste consists of a mixture of fillers, short fibres and ink .

Bonding at the interface can be achieved by modifying the filler-matrix surface with various surface-active additives or coupling agents [3]. The hydrophilic nature of wood particles and cellulose fibres offers additional advantages, in comparison to inorganic fillers, by readily providing the possibility for the incorporation of different chemical groups on the surface [4].

Several classes of adhesives used in wood bonding involve the use of isocyanates. Isocyanates are widely used due to their reactivity with groups that contain reactive hydrogen, such as amine and alcohol groups at room temperature. Isocyanates are most often used to produce polyurethanes by reacting with liquid diols [5].

A great variety of publications offers results in the field of artificial ageing of WPC.

In the present investigation, a new prepolymer based on diphenylmethane diisocyanate (MDI) and long chain polyether polyol was obtained and the effect of cellulose fibres as a filler on the mechanical properties after artificial ageing of composites was studied.

EXPERIMENTAL

Materials

The materials used in this study were waste short cellulose fibres, $CuSO_4.5H_2O$, $Na_2S_2O_3.5H_2O$ (Sigma Aldrich), Desmodur® 44 M Flakes (BAYER), Lupranol®1000 (BASF), catalyst-Stannous Octoate PC CAT T9 (Performance Chemicals Handels GmbH).

Short cellulose fibres are a waste product from the de-inking process in papermaking. The average value of inorganics in this mixture of fibres, fillers and ink is about 22.06 % ± 0.9.

For the purposes of this study, three different ratios of $CuSO_4$ and $Na_2S_2O_3$ were used at hydro modulus 1:6. The goal of fibres modification is obtaining of conductive composites from short fibres [6]. This modification was carried out by the immersion of the fibres in the solution according to Table 1 for 30min at an elevated temperature (80°C). For drying, modified short fibres are kept for 5 hours at a temperature of 105°C.

*To whom correspondence should be sent.
E-mail: ilieva246@gmail.com

Liquid prepolymer was prepared as follows: 0.1 % Stannous octoate is mixed with 1020g Lupranol®1000 (A-component). 350g MDI are melted at 40ºC, and then the A-component is added. The process is carried out for 4 hours at 75ºC. The isocyanate content was determined using back titration - 9.6%.

Preparation of composites

The composites were obtained by melt blending in a chamber of a Brabender mixer, at 120ºC and processed for 30 minutes. After the processing step, each sample was compression moulded at 9.6MPa for 20minutes, at 120ºC.

Investigation methods

FT-IR spectra. Infrared Spectroscopy (FT-IR) was applied with Varian 600-IR equipped with a single reflection ATR accessory, at spectrum range- 400-4000cm^{-1}.

Artificial ageing procedure. All composite samples were placed in a laboratory chamber ESPEC PL-2KPH to accelerate the ageing of the samples. According to TAPPI T544 chamber conditions were 90 ºC and 50% relative humidity. The samples were removed from the chamber at regular intervals after 72, 144, 288 and 384 hours.

Mechanical properties. Tensile and flexural tests were carried out at room temperature on a Zwick 2000 testing machine equipped with activated grips, according to EN ISO 178:1996 and EN ISO 178:2010.

Every sample has dimensions of 4x10x100mm.

RESULTS & DISCUSSION

Compounding characteristics

Fibres modification was carried out with two component system ($Na_2S_2O_3$/ $CuSO_4$) at 120°C for 30 minutes. Ratio between dry mass and liquid in this system was calculated (1:6). Different percentage of modifying agent was used- 20%, 30% and 40%.

Liquid prepolymer DesLu2.8-1 was synthesized and subsequently studied by means of FT-IR. This process was carried out for approximately 4 hours. The samples were collected for 5 minute periods and the changes in OH-group's absorption peak at ~3500 cm^{-1} was used to study kinetic reactions.

Several infrared vibrations, typical of polyurethane systems, could be assigned:

- N-H stretching mode assigned at ~3365 cm^{-1};
- Carbonyl assigned between ~1780 cm^{-1} and ~1600 cm^{-1} (Amide I);

The low intensity of the vibration at ~1643 cm^{-1} (urea carbonyl) compared with that of the overlapped vibration at ~1732 cm^{-1} (urethane carbonyl) indicates that, under the synthesis conditions used, -NH formation is favoured.

- Amide II ~1556 cm^{-1} and amide III ~1244 cm^{-1} vibration modes;
- C- H stretching vibrations are assigned at ~2950 cm^{-1}and ~2880 cm^{-1};
- ~2270 cm^{-1} NCO consumption;
- ~3500 cm^{-1} OH-consumption, ~3365 cm^{-1} – NH formation.

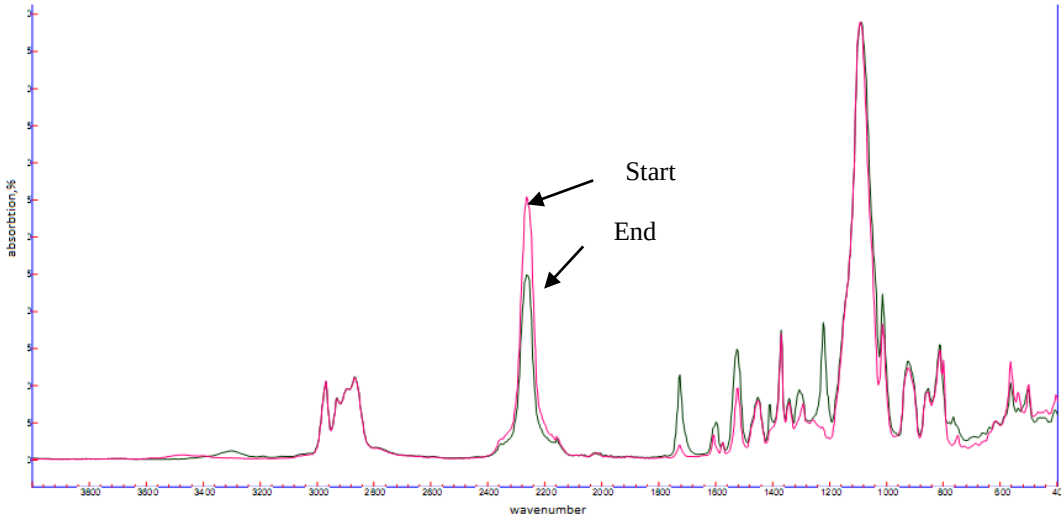

Fig.1: FT-IR spectrum of polyurethane prepolymer DesLu2.8-1 (reaction start and end)

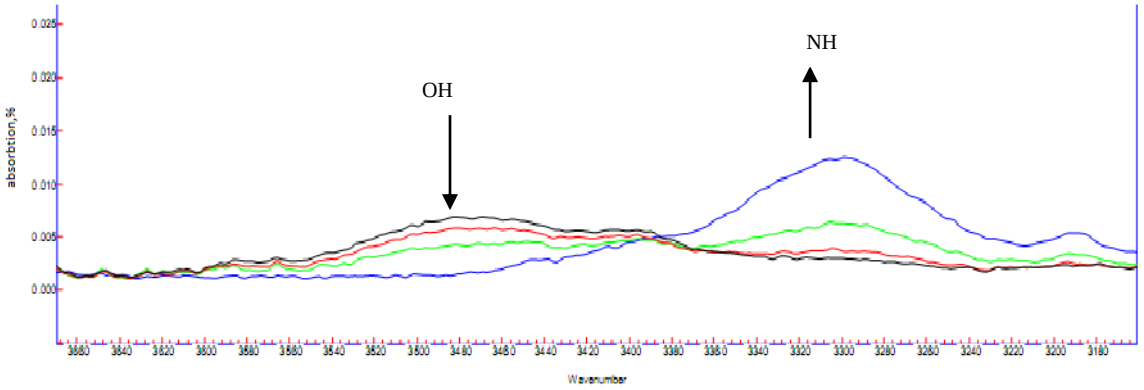

Fig.2: FT-IR characteristic spectrum OH-consumption and –NH formation (DesLu2.8-1, 5min, 10min, 15min, 50min)

Table 2. Composite samples

Composite material	Fibres		Prepolymer, %
	Modification	%	
1-90F10P	Chem1 (60/40)	90	10
1-80F20P	Chem1 (60/40)	80	20
1-70F30P	Chem1 (60/40)	70	30
2-90F10P	Chem2 (70/30)	90	10
2-80F20P	Chem2 (70/30)	80	20
2-70F30P	Chem2 (70/30)	70	30
3-90F10P	Chem3 (80/20)	90	10
3-80F20P	Chem3 (80/20)	80	20
3-70F30P	Chem3 (80/20)	70	30

The peak that occurs at ~3500 cm^{-1} corresponds to the OH-groups of the long chain polyether polyol and the peak at ~3365 cm^{-1} corresponds to the NH-groups of the polyurethane prepolymer. As the reaction takes place the hydroxyl groups of the polyol are reduced in order to form polyurethane groups of the prepolymer. The two characteristic peaks at ~1720 cm^{-1} and ~1530cm^{-1} proved formation of urethane structures. Non- modified fibres were used for reference samples preparation (Table 2).

Table 1. Reference composite samples

Composite	Fibres, %	Prepolymer, %
0-90F10P	90	10
0-80F20P	80	20
0-70F30P	70	30

Composites from modified fibres and liquid prepolymer were obtained. All specimens were artificially aged in a chamber under controlled conditions. For the conditioned samples FT-IR was applied.

A significant difference in FT-IR spectra of modified and non-modified composites was observed. Figure 3 shows that a peak at ~1428 cm^{-1} occurs. This peak is close to the peak of poly (ethyl acrylate) – a component of ink formulation. This component has a boiling point of 99°C and processing the fibres at temperature of 120°C for 30 minutes leads to poly(ethyl acrylate) evaporation.

Mechanical properties

Figure 4 presents the normal behaviour of the fibres after artificial ageing. Non-modified fibres have no significant changes in tensile properties but for the series with modified fibres a collapse in the values was observed. This can be explained with the heat exposure by fibre modification followed by another heat exposure by compression moulding.

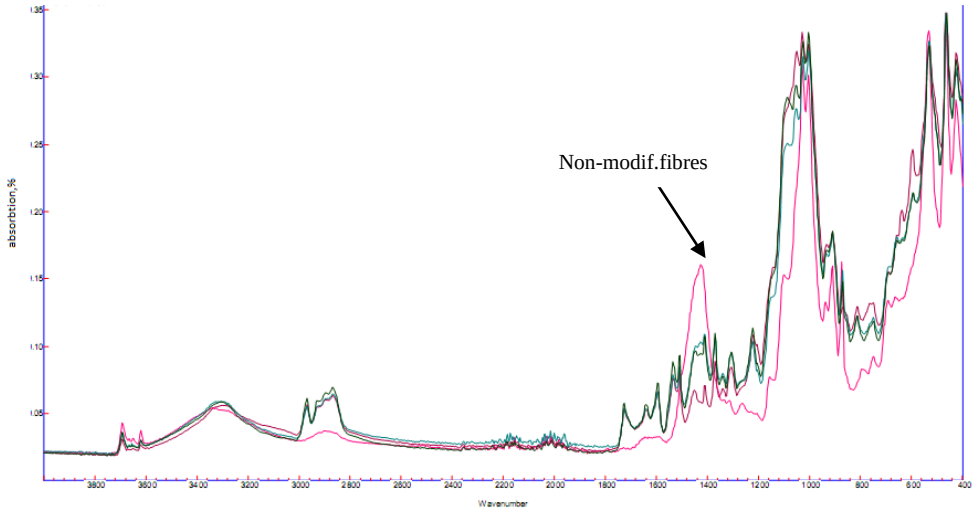

Fig.3. FTIR of composites containing non-modified and modified short fibres.

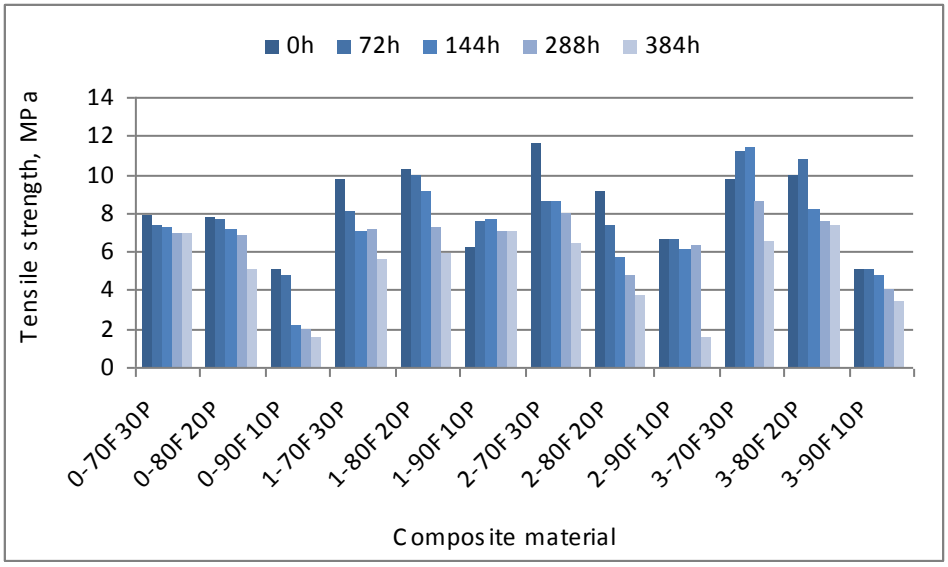

Fig.4. Tensile strength of the composites.

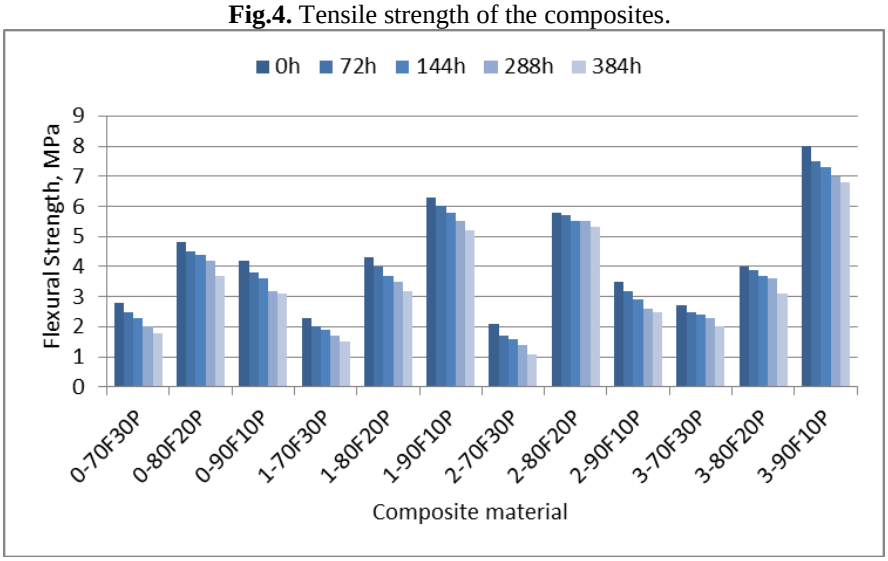

Fig. 5. Flexural strength (ε_B, MPa) of the composites

The modulus of short-fibre-reinforced composites depends in general on the length of fibres and their uniform dispersion in the matrix. A difference is observed by fibre content of 90%, which means higher fibre content and a greater level of ageing.

After the artificial ageing only 3 to 4% collapse in flexural strength values are observed.

It is seen that water affects the strength properties of the composites, but the degree of this influence depends on the compounding process. The absorbed water molecules reduce bonding between the short fibres and establish hydrogen bonds between short fibres and water molecules.

CONCLUSIONS

Polyurethane/Modified cellulose fibres composites were prepared by melt mixing and their behaviour upon controlled weathering was investigated. The influence of artificial ageing on the mechanical properties of short fibres composites was observed. Significant changes at σM after ageing were observed by a sample prepared from 90% fibres and 10% prepolymer. The composites with 20-30 wt% prepolymer recorded a small decrease in mechanical properties after artificial ageing.

REFERENCES

1. A. Najafi, H.K. Eslam, *Bioresources*, **6**,2411 (2011).
2. S.C. Najafi, *J. Waste Management*, **33**, 1898 (2013).
3. H. Dalvag, C. Klason, H.E. Stromvall, *Int. J. Polym. Mater*. **11** (1985).
4. A.Y. Coran, R. Patel, US Patent 4 323 625 (1982)
5. D.A. Lange, J.T. Fields, S.A. Stirn, (2001). Finger joint application potentials for one-part polyurethanes; Wood Adhesives 2000. Forest Products Society, Madison, WI, pp. 81–90.
6. S. Nenkova, R. Garwanska, M. Kulevski, Ts. Ilieva, BG Patent 1329/28.07.2010.

ИЗКУСТВЕНО СТАРЕЕНЕ НА КОМПОЗИТНИ МАТЕРИАЛИ, ПОЛУЧЕНИ ОТ МОДИФИЦИРАНИ ЦЕЛУЛОЗНИ ВЛАКНА И ПОЛИУРЕТАНОВ ПРЕПОЛИМЕР

Ц.Н. Илиева[1*], С.К. Ненкова[1], М. Херцог[2]

[1]Катедра „Целулоза, хартия и полиграфия“, Химикотехнологичен и металургичен университет, 1756 София, България

[2] Университет по приложни науки Вилдау, 15745 Вилдау,Германия

Получена на 17 юли, 2014 г.; Приета на 4 ноември, 2014 г.

(Резюме)

Композитните материали, усилени с къси природни влакна, имат редица предимства в сравнение с останалите познати композити. Тези композити притежават еластичност, ниско тегло и не вредят на околната среда. Чрез модифицирането на влакната, получените материали придобиват специфични свойства, приложими в различни технически области- автомобилна и строителна индустрия, производство на проводими материали и др.

Целта на изследванията е да се изучат свойствата на тези нови композитни материали. Работата е насочена към получаването на високо напълнени полимерни композити от къси целулозни влакна, които са отпадъчен материал при обезмастиляване на хартията и последващото им комбиниране с полимерна матрица. Свойствата на този нов тип композити не са известни, което налага провеждане на обширни изследвания в тази насока.

В процеса на работа са използвани отпадъчни целулозни влакна, които се смесват с течен полиуретанов преполимер за получаване на композитен материал. Композитните образци са подложени на изкуствено стареене в продължение на 72, 144, 288 и 384 часа при 90°C и 50% относителна влажност на въздуха. Изследвани са механичните свойства преди и след стареене на материалите.

Bulgarian Chemical Communications, Volume 47, Special issue A (pp. 21 - 24) 2015

Investigation of the thermal ageing of chemical mechanical pulps obtained from different types of hardwood

R. Boeva[1]*, I. Spiridonov[1], R. Nikolov[1], G. Radeva[2]

[1]*Department of Pulp, Paper and Printing Arts,*
[2]*Department of Physical Chemistry, University of Chemical Technology and Metallurgy,8, Kl. Ohridski Blvd., 1756 Sofia, Bulgaria,*

Received July 30, 2014; Accepted January 30, 2015

The basic raw materials used in papermaking processes are obtained from fibrous materials produced by chemical treatment of various types of wood or annual plants.

In this research were obtained chemical mechanical pulps (CMP) of wood chips from *Paulownia tomentosa* and *Populus deltoides clon-235-15* with improved density (474 kg/m^3).

The obtained chemical mechanical pulp was bleached in two stages by using H_2O_2 and Rongalyt C ($NaHSO_2.CH_2O.2H_2$). The investigation of changes of brightness and yellowness of samples in the process of artificially thermal ageing at 105°C have been performed.

The main goals of the present work are studying of artificial thermal ageing of bleached and unbleached CMP obtained in the laboratory from *Populus* and *Paulownia* woods.

Key words: *wood, thermal ageing, fiber materials.*

INTRODUCTION

During the last years we observe that the production of fibrous materials lags behind from the demand of the market. That trend requires to fabricate higher quality papers, cardboards and packaging obtained by high-grade initial fibrous materials. Therefore, in this research we aim to investigate not only the well knows species *Populus deltoides clon-235-15*, but also the relatively new fast-growing species *Paulownia*, which are suitable for the production of high-yield fibrous materials (HYFM) [1, 2, 3].

Genus *Paulownia* (fam. *Scrophulariaceae*) includes nine species wood [4, 5]. All species of *Paulownia* are fast growing, with excellent timber, but the most promising ones are *P. elongata* (emerald tree) and *P. Fortune* which for a period of 8-10 years reach 20 m in height and 30-40 sm diameter of the stem [6, 7].

EXPERIMENTAL

Production of CMP

The utilized CMP is obtained from the fast-growing poplar timber *Populus* characterized by increased density of and hardwood timber of the specie *P. Tomentosa* [6, 7]. The two types of wood were cleaned from the root parts and later shredded into slices with 20mm thickness. After roots removal the wood was chopped into chips of standard dimensions of 15x20x3 mm.

The fibrous materials utilized in this study are:

- CMP – derived by poplar wood of the specie *Populus deltoides clon - 235-15*, obtained in laboratory conditions;
- CMP – from timber of *P. tomentosa*, obtained in laboratory conditions.

During the process of production of CMP are used: Na_2SO_3, analytical grade, NaOH. During the bleaching are utilized: H_2O_2, analytical grade, Rongalyt C ($NaHSO_2.CH_2O.2H_2O$), produced by the company BASF.

Into the composition of the bleaching solution we included the substances Na_2SiO_3 and $MgSO_4$ which serve as stabilizers of the H_2O_2. Further more NaOH was added to reach the required level of approximately pH 10.5. In order to sequester the ions of the heavy metals - solution of ethylenediaminetetraacetic acid (EDTA) was utilized. The following parameters of the produced CMP have been determined:

- Yield [%], determined by weight method in comparison to the mass of the absolutely dry timber;
- Milling degree, as determined by the device Schopper – Riegler (°SR) as per EN ISO 5267 – 1/AC:2004;

For all used fibrous materials the degree of

To whom correspondence should be sent.
E-mail: r_boeva@abv.bg

Table 1. Conditions of bleaching CMP

Type of Bleaching	Quantity of reagent, (%)	T, (°C)	Duration of process, (min)	Concentration of fibrous materials, (%)	pH of the solution
I stage	2% H_2O_2	80	120	10	10.5
II stage	1.5% Rongalyt C	80	60	6	5

brightness R_{457} (ISO 2470:2002) was determined before and after ageing thanks to the appliance by Spectrophotometer Gretag Magbeth Spectroeye.

Each sample consists of 100g absolutely dry timber of *Populus* and wood of *Paulownia*.

The preliminary weighted chips have been placed in a thermostatic container with the aim to temper it and to maintain the required permanent temperature. Later on they were soaked into required quantity of solution of NaOH and Na_2SO_3. After retention for a specified period, the used solution was removed and the chips have been washed to reach pH 7. The treatment continued by refined in a Sprout-Valdron laboratory mechanical refiner till the moment of production of fibrous materials. Further on it was washed away and sorted out manually between two sieves.

For production of a CMP is performed according to preliminary determined optimization regime: NaOH 7%, Na_2SO_3 5%, temperature 80°C, treatment duration – 120 min and liquor-to-wood ratio 1:5 [4].

The yield of CMP is calculated by the mass method. After soaking for 24 hours in distilled water, the treated chips were washed to reach neutral pH and dried into a drying apparatus at 105°C to achieve absolute dry state.

Bleaching of the different types of fibrous materials

The samples of CMP are destined to two-stage bleaching:

I stage – bleaching with H_2O_2, II stage – bleaching with Rongalyt C.

The conditions of bleaching are given in Table 1.

First stage of bleaching. During the first stage of whitening pH=10.5 and it is maintained thanks to additives like: NaOH 2%, Na_2SiO_3 5%, $MgSO_4$ 0,5%. The aggregation of the ions of heavy metals is performed by 0.5% solution of EDTA [4, 5]. The quantities of all reagents are expressed as percentage regarding the absolute dry fibrous material. After the completion of the first stage, the fiber material is washed properly to obtain pH 7 and in this manner it is able to undergo the next phase.

The fibrous mass is placed in a polyethylene bag where the bleaching solution is poured. The additional reagents are added and the solution is mixed till reaching complete homogenization. Later the bag is placed in thermostatic container which ensures constant temperature during the whole process of bleaching. In order to achieve better degree of degree of whiteness, it is required to ensure mixing of the fiber material, thus facilitating the uniformly distribution of whitening mixture.

Second stage of bleaching. During the second stage of whitening of the two fiber materials, the reagents utilized are Rongalyt C 1.5% and EDTA 0.5% (Table 1). The process of bleaching is similar to the one described in the first stage. After completion of the process, the fibrous mass is washed away again to adjust pH 7.

Ageing of fibrous materials

The samples of both bleached and unbleached fiber materials, are dried and then they undergo artificial ageing in thermal cupboard at 105ºC. In order to characterize the ageing process for bleached and unbleached samples, the degrees of brightness and yellowness for periods of 0, 2, 4, 6, 12, 24, 36, 48 and 72 hours since the commencement of the artificial thermal ageing are determined.

RESULTS & DISCUSSION

The yield of CMP from the specie *Paulownia tomentosa* is 86%, while for the specie *Populus*: the yield is 88%. The milling degrees are: CMP from *P. tomentosa* - 13°SR, and CMP from *Populus* - *12*°SR.

The utilization of HYFM in various brands of paper and cardboard is limited because of the low level of whiteness. This is the reason to perform two-staged process of whitening. Furthermore artificial thermal ageing at 105ºC is conducted. In order to investigate the impact of this ageing over the parameters of the different fiber materials, bleached and unbleached ones, the levels of whitening and yellowness are measured after various periods of time 0, 2, 4, 6, 12, 24, 36, 48 and 72h. Figures 1 and 2 represent the kinetic correlations between the changes in the degree of of brightness and yellowness.

During the process of ageing (Fig. 1) together with the increase of time, the degree of brightness

decreases for both CMP - bleached and unbleached ones. The change in the degree of brightness is most drastically expressed in the beginning of the ageing. The degree of whiteness (Fig. 1) diminishes in various levels for all samples independently of the way of obtaining of fiber materials. The higher degree of brightness of the bleached samples is kept even during the process of artificial thermal ageing.

Even at equal conditions of production and bleaching of fibrous masses, the higher degree of brightness [%] is observed for the timber from *Paulownia*.

During the continuation of the ageing (fig. 2) the degrees of yellowness increase for all samples. Independently of the origin of the sample in bleached and non-bleached, their yellowness increase with time. The yellowness is higher for the sample of unbleached CMP from *Poplar* timber. Almost identical are the recorded levels of yields for the unbleached CMP from *Paulownia* and the two-staged bleached CMP from *Populus*.

Figures 1 and 2 give clearly shows that the CMP from *Paulownia* in their bleached and unbleached form, provides higher degree of brightness, while the level of yellowness is lower in comparison with the bleached and unbleached CMP from *Populus*.

Finally it became clear that at equal conditions of production, bleaching and ageing, the CMP derived from *Paulownia* explicitly proves better results.

CONCLUSIONS

During the study we obtained CMP from the species *Populus* and *P. tomentosa*, under preliminary determined regime the yield obtained was 88% and 86% accordingly, while the degree of milling was 12°SR and 13°SR:

Because of the low level of brightness, the CMP was treated by two-stage bleaching. During stage I the agent utilized was an H_2O_2, while during stage II reduction agent was applied - Rongalyt C. The final degree of brightness achieved for *Paulownia* was 66.4% and for *Populus* - 59.0 %.

- During the processes of bleaching of the two types of fibers materials, it became clear that when treated under the same conditions for preparation and bleaching, the degree of brightness for the specie *Paulownia* is higher.
- The obtained high-yield fibrous materials originating from different timbers are suitable and successfully could be included into compositions of various quality papers and cardboards.

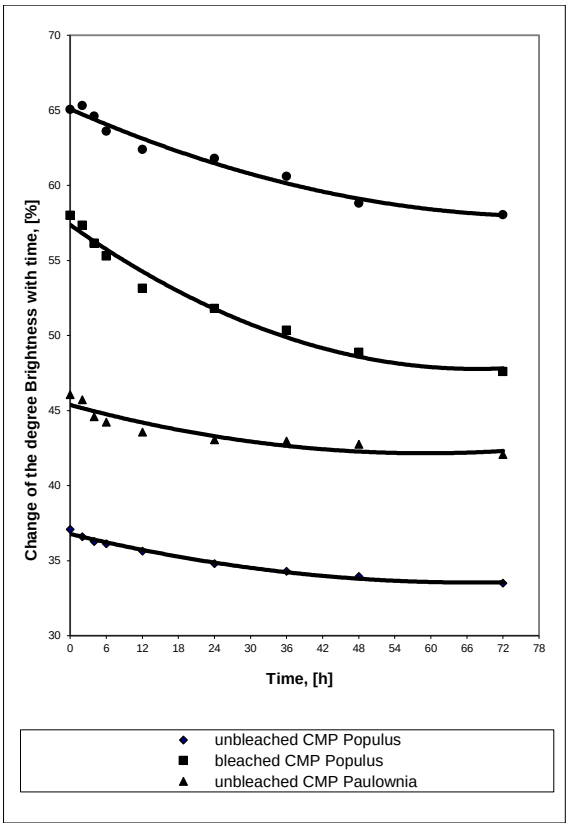

Fig. 1. Change of the degree of Brightness of different bleached and unbleached samples during artificial thermal ageing at 105°C.

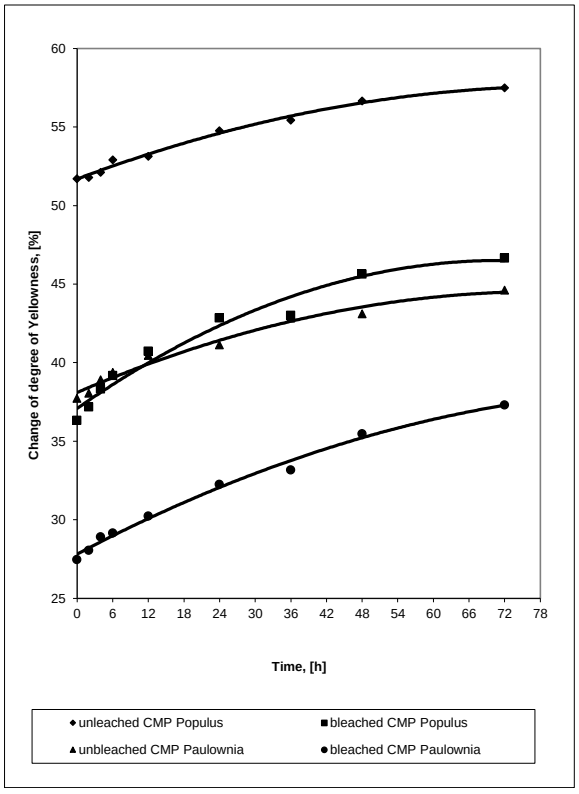

Fig. 2. Change of the degree of Yellowness of different bleached and unbleached samples during artificial thermal ageing at 105°C.

Abbreviations:
CMP - Chemical Mechanical Pulp
EDTA - Ethylenediamine tetraacetic acid
HYFM - High-yield fiber materials

Acknowledgement:. *The authors thank the Scientific Research Centre (contract №11237) at the UCTM Sofia for the financial support of these investigations.*

REFERENCES

1. V.B. Woods, *AFBI Agri-Food and Biosciences Institute*, **7**, 2, 2008.
2. V.H.D. Zuazo, J.A.Jiménez Bocanegra, F.Perea Torres, C.R. Rodríguez Pleguezuelo, J.R. Francia Martínez, *IJRER*, **3**, 789, 2013
3. K.M. Han, R. Dharmawardhana, R.S. Arias, C. Ma, V. Busov, S.H. Strauss, *Plant Biotechnol J*, **9**, 162, 2011.
4. R. Boeva-Spiridonova, E. Petkova, *J. UCTM*, **42**, 41, 2007.
5. R. Boeva, G. Radeva, P. Hinkov, E. Hinkov, *J. UCTM*, **47**, 37, 2012.
6. S. Ates, Y. Ni, M. Akgul, A. Tozluoglu., *African J. Biotechnol.*, **7**, 4153, 2008.
7. A. Ashori, A. Nourbakhsh, *European J. Wood Product*, **67**, 323, 2009.

ИЗСЛЕДВАНЕ НА ТЕРМИЧНОТО СТАРЕЕНЕ НА ХИМИКО МЕХАНИЧНИ МАСИ, ПОЛУЧЕНИ ОТ РАЗЛИЧНИ ВИДОВЕ ШИРОКОЛИСТНА ДЪРВЕСИНА

Р. Боева[1]*, И. Спиридонов[1], Р. Николов[1], Г. Радева[2]

[1]Катедра „ Целулоза, хартия и полиграфия“,
[2] Катедра „Физикохимия“
Химикотехнологичен и металургичен университет, бул. Климент Охридски, 1756 София, България,

Постъпила на 30 юли 2014г.; Коригирана на 30 януари 2015г.

(Резюме)

Основните суровини в хартиеното производство са влакнестите материали, получени при химично преработване на различни видове дървесина или едногодишни растения.

В настоящето изследване са получени химико механични маси от дървесни трески на *Paulownia tomentosa* и бързорастяща тополова дървесина с повишена плътност (474 kg/m^3) от вида *Populus deltoides clon-235-15*. Поради ниската степен на белота двете маси са избелени двустепенно с H_2O_2 и Rongalyt C. Направени са отливки. Проследено е изменението на степента на белота и жълтина в процеса на изкуствено термично стареене при 105^{o}C.

Целта на разработката е изследване на изкуственото термично стареене на избелени и неизбелени химико механични маси, получени в лабораторни условия от тополова дървесина и дървесина на пауловния.

Bulgarian Chemical Communications, Volume 47, Special issue A (pp. 25-29) 2015

Thermoforming–process of biopolymer composites

K.V. Dimitrov[1*], A. Matev[1], M. Herzog[2], S. Nenkova[1]

[1]*University of Chemical Technology and Metallurgy Sofia, Bulgaria*
[2]*Technische Hochschule Wildau, Germany*

Submitted July 17, 2014; Revised January 26, 2015

This work aims to study the behavior of two dimensional composites (2-D composites) during a thermoforming process. Polylactide acid (PLA) films were prepared in a hot press at a temperature of 155˚ C and pressure of 90 kN/m^2. The obtained PLA-films were used as a base for further composite materials synthesis. Various glass fiber types and viscose rayon were used in order to improve the composite behavior. Those materials were further processed to final product packaging, in KIV Kreis GmbH via vacuum thermoforming. The mechanical properties were tested by means of tensile strength, tensile modulus, three point bending and Charpy impact strength. The morphological properties of the composite materials were investigated by digital microscope.

Keywords: *PLA, Viscose rayon, Glass fiber, Thermoforming process*

1. INTRODUCTION

Plastic thermoforming is one of the fastest growing methods of producing plastic packaging. During the thermoforming process, the polymeric sheet is heated to the so-called forming temperature. This temperature depends on the different type of thermoplastic material. The polymer sheet is supple and elastic plastic deformable at the forming temperature [1]. Thermoforming is widely used in manufacturing industries to produce large and labor intensive products. Compared to other manufacturing techniques, thermoforming is an extremely efficient process that is suitable for high-efficiency mass production [2].

PLA is biodegradable and biocompatible polyester, which can be produced from renewable sources [3, 4]. Due to new techniques which allow economical production of high molecular weight PLA, this polymer has attracted great attention recently, being considered as one of the most promising materials for replacing synthetic polymers [5]. PLA has reasonably good optical, physical-, mechanical and barrier properties compared to existing petroleum-based polymers like high density polyethylene (HDPE), polystyrene (PS), polypropylene (PP) and polyethylene terephthalate (PET). The building blocks of PLA can exist in an optically active state. Depending on the enantiomers ratio, the PLA can obtain different mechanical, barrier and surface properties. This allows the production of a wide spectrum of PLA grades matching the performance requirements [6]. The thermoplastic property of those composites enables commercial manufacturing.

Extrusion, injection molding, casting of films and sheets, thermoforming, foaming and fiber spinning are among the methods utilized for PLA processing [7, 8]. The PLA technological waste can be reused to a great extent, which is another significant benefit of this polymer [9].

Despite the above-mentioned advantages the PLA materials show some disadvantages which limit its application, such as high brittleness, poor heat stability, low impact strength. To improve these properties, different modification methods like annealing, adding nucleating agents, fibers or nanoparticles were investigated. Alternatively, some chemical and physical treatments were applied to facilitate the cross linking between PLA molecules. Plasma treatment, UV-light and laser exposures were applied in order to enhance the material adhesion properties. [10, 11].

In this work, glass fiber reinforced, viscose rayon reinforced, and unreinforced PLA sheet were used in experimental thermoforming operation. The results obtained from the experiment and mechanical properties of composite materials were compared with results from unreinforced PLA.

2. EXPERIMENTAL

2.1 Materials

Poly (lactic acid) (PLA; molecular weight, M_w = 20kDa;M_n=10.1 kDa) was obtained from Biomer

To whom correspondence should be sent.
E-mail: kirol_volodiev@abv.bg

Krailling, Germany. Viscose rayon (Cordenka). Cordenka is Super 2 Rayon yarn with high elongation at break and optimized (= reduced) water shrinkage. It is used in mechanical rubber goods, with a focus on radiator hoses. Viscose rayon was obtained from Cordenka GmbH Germany. Glass fiber (stitch) density =300 g/m^2, glass – wool density =440 g/m^2. Both products were obtained from DHD Technology GmbH & Co.KG/ Germany.

2.2 Composites processing

The composites were obtained using press (Servitec Polystat 400S). The fibers were added between two PLA films and pressed. The processing parameters for press are: pressure = 90 kN/m^2, temperature = 155˚ C for 10 minutes. The compositions of the composites prepared are shown in Table 1.

Table 1. Compositions of composites

Materials	Time (min)	Filler (g/m^2)
PLA	5	-
PLA/Cordenka (short fibers)	10	90.5
PLA/Cordenka (stitch)	10	180.5
PLA/Glass fibers (stitch)	10	270.5
PLA/Glass - wool	10	320

The end products were manufactured by KIV Kreis GmbH. The thermoforming process was realized using Visual Thermoforming (HDVS 3036) vacuum skin packager. The processing conditions are shown in Table 2.

Table 2. Thermoforming conditions

Sheet temperature	160 – 170 º C
Heater temperature	350 º C
Heater distance from sheet	10 cm
Mold temperature	35 – 40 º C

Figure 1 shows the thermoform (A), and the thermoforming process (B). Figure 2 shows the thermoformed composites. Figure 2 (A) shows PLA, (B) shows PLA/Viscose rayon (short fibers), (C) shows PLA/Viscose rayon (stitch), (D) shows PLA/Glass fibers (stitch) and (E) shows PLA/Glass – wool.

2.3 Measurements

2.3.1 Mechanical testing. A mechanical testing machine, "Zwick 2000" Zwick GmbH & Co. KG (20 kN), Germany was used to measure the tensile properties according to ISO 14129. The flexural properties of a thermoformed composite were preformed according to the ISO 178. System control and data analysis were preformed using Datum software. All results presented are the average values of five measurements.

An EN ISO 179 charpy impact test was carried out using 10 unnotched samples. In each case a standard deviation < 15% (drop weight) was used to calculate the charpy impact strength.

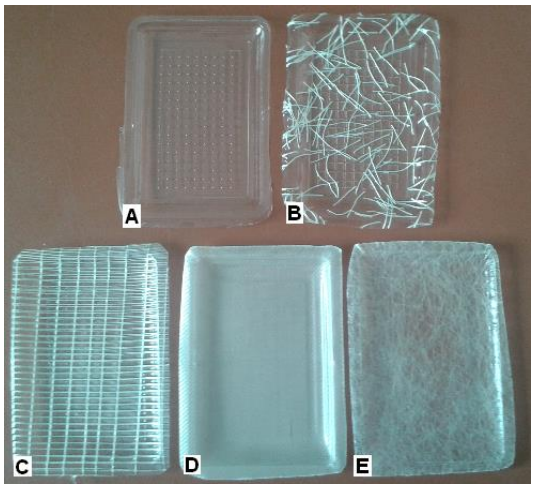

Fig. 1 (A) the thermoform, (B) the thermoforming process.

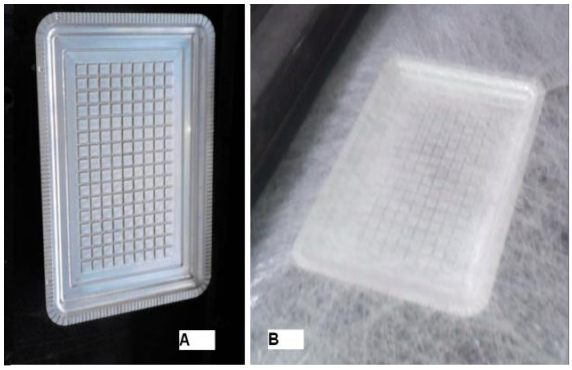

Fig. 2. The thermoformed composites.

2.3.2 Optical microscopy. The morphology of impact cross section of the composites was observed by optical microscopy at room temperature. A microscope (model VHX-600 Series) was used to collect microscopy images for the composite specimen.

4. RESULTS AND DISCUSSIONS

The results of the tensile properties investigation of PLA and PLA - composites are shown in Figs. 3 and 4.The pure PLA has a tensile strength of 58 MPa and a modulus of 3.8 GPa. The addition of glass fiber (stitch and wool) improved the tensile strength 178 MPa, 80 MPa and the modulus of 7 GPa and 5.7 GPA, which indicates that the stress transfers from PLA polymer matrix to the glass fibers. Whereas the addition of Viscose rayon fibers decreased the modulus of 3.9 GPa and the tensile strength of 30 MPa.

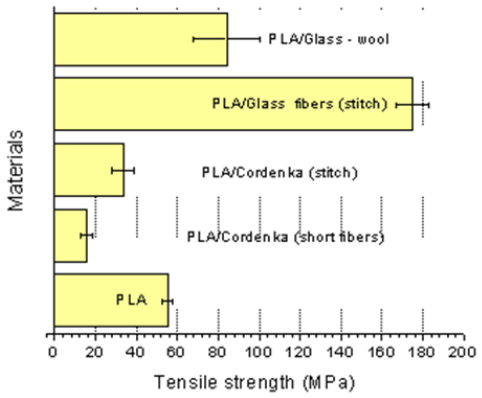

Fig. 3 Tensile strength of composites.

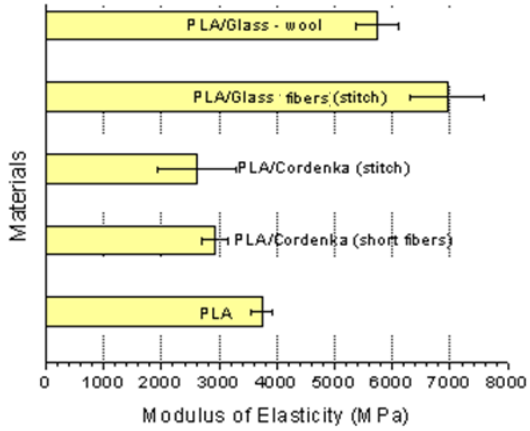

Fig. 4 Tensile modulus of composites.

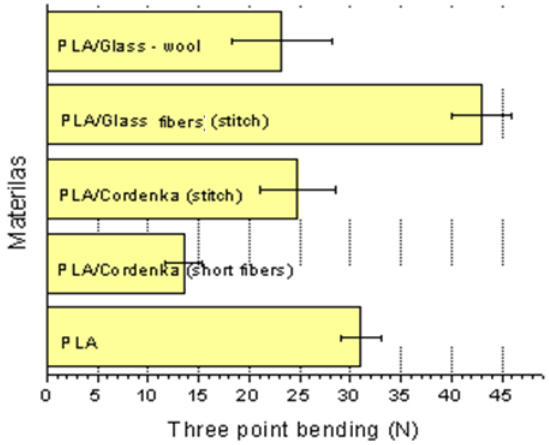

Fig. 5 Three point bending of thermoformed composites.

The three point bending tests of PLA and reinforced PLA composites (Fig. 5) were performed at room temperature. The pure PLA has a flexural tensile of 31 N. Glass fibers (stitch) composite improve the flexural tensile of PLA 42 N. No improvement could be observed in the Viscose rayon composites. Charpy impact samples were prepared by cutting and sanding to dimensions of 80 x 10 x 3.9 mm (length x width x thickness). The results of Charpy impact strength test are summarized in Fig. 6. All composites show improvement in impact strength. Composites with the Viscose rayon (stitch) improved the impact strength of fracture greater than 90 kJ/m^2.

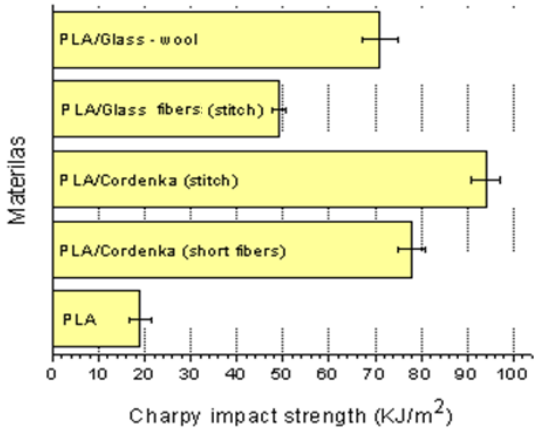

Fig. 6 Charpy impact strength of composites.

The digital microscopy images are shown in Figure 7. The fibers are illuminated white; the matrix is grey and the voids black. Microscopy analysis allows important individual void characteristics to be assessed. For example, the missing adhesion between the polymer matrix and the fibers can be clearly seen in Fig 7B, Fig. 7C and D proof of the bad adhesion based on the greater contrast between fibers and matrix. The best adhesion from all materials is that of the PLA/Glass wool, Fig. 7 (E). One explanation could be the fiber thickness; the thinner the fiber the better the adhesion.

5. CONCLUSIONS

Due to the variety of interesting composites properties, further development of the thermoforming process is highly recommended. One of the biggest advantages of those materials is tailoring their properties according to the application, followed by the economically efficient production process.

In many cases, the physical properties are enhanced dramatically compared to that of the sub-components. The lack of elasticity and the lack of compatibility in adhesion remains a problem as seen in PLA/Viscose rayon composites. The PLA/Glass fibers composites manufactured in this study have a higher tensile strength and a higher specific E-modulus than PLA/Viscose rayon composites. The three point bending test showed that only the glass (stitch) improved the flexure of composite.

PLA/Viscose rayon (stitch) improved the impact strength almost five times. The promising impact properties of the presented PLA/Viscose rayon composites show their potential as an alternative to traditional composites.

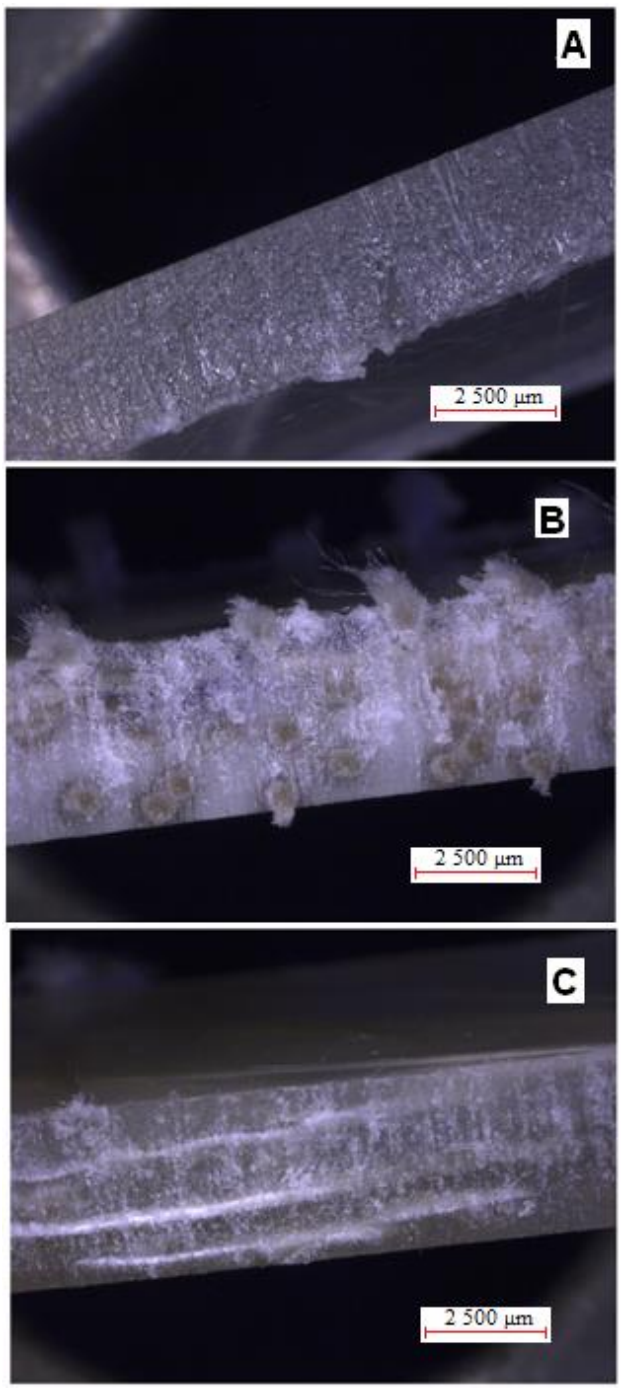

.

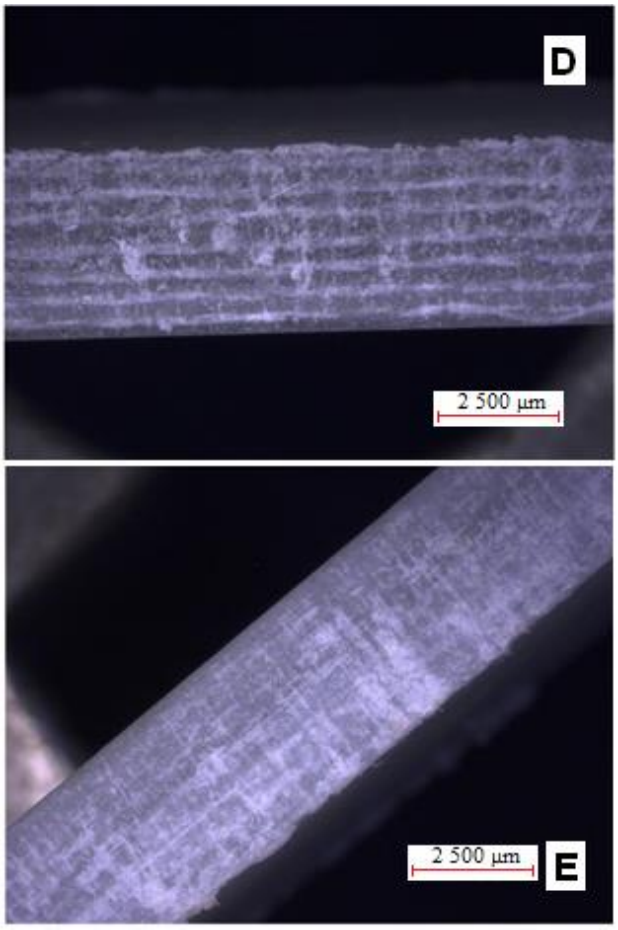

Fig. 7. Composite cross section (A) PLA, (B) PLA/Viscose rayon (short fiber), (C) PLA/Viscose rayon (stitch), (D) PLA/Glass (stitch), (E) PLA/Glass wool.

REFERENCES

1. J. L. Throne, *Polymer-Plastics Techn. & Eng.*, **30**, 685 (1991).
2. S. Erdogan, O. Eksi, *J. of Mech. Eng*., **60**, 195 (2014).
3. A. Sodegard, M. Stolt, *Progress in Polymer Science*, **27**, 1123(2002).
4. L. Yu, K. Dean, L. Li, *Progress in Polymer Science*, **31**, 576 (2006).
5. O. Kenzo, I. Tomokazu, Y. Tadashi, Y. Masayuki, *Europ. Pol. J.*, **48,** 2304 (2009).
6. L. Lim, R. Auras, M. Rubino, *Progress in Polymer Science*, **33**, 820 (2008).
7. L. Lim, R. Auras, M. Rubino, *Progress in Polymer Science*, **33,** 820 (2008).
8. M. Zenkiewicz, J. Richert, *Polymers*, **54**, 299 (2009).
9. M. Zenkiewicz, J. Richert, P. Rytlewski, K. Moraczewski, M. Stepczynska, T. Karasiewicz, *Polymer Testing*, **28,** 412 (2009).
10. P. Rytlewski, M. Zenkiewicz, *App. Surf. Sci.*, **256**, 857 (2009).
11. P. Rytlewski, M. Zenkiewicz, *J. of Adh. Sci. and Techn.*, **24**, 685 (2010).

ТЕРМОФОРМУВАНЕ НА БИО БАЗИРАНИ БАЗИРАНИ КОМПОЗИТИ

К. Димитров[1*], А. Матев[1], М. Херцог[2], С. Ненкова[1]

[1]*Химикотехнологичен и металургичен университет – София*
[2]*Технически университет – Вилдау, Германия*

Постъпила на 17 юли, 2014 г.; приета на 26 януари, 2015 г.

(Резюме)

Тази работа цели изучаване поведението на дву-димензионални композити (2-D композити) чрез термооформящ процес. За получаването на композитите е използвана полимлечна киселина (ПМК), стъклени влакна и вискозни влакна. ПМК беше предварително подготвена във формата на тънки полимерни листове чрез пресоване при температура равна на 155^{o} C и налягане от 90 kN/m^2. Така приготвените листове от ПМК са използвани в по-следващия процес при получаването на композитните материали. Крайните дву димензионални продукти бяха получени във фабирката за производство на термопластични опаковки (KIV Kreis GmbH – Германия), чрез вакум термооформяне. Механчините свойства, якост на опън, модул на еластичност при опън, три точково огъване и якост на удар бяха изследвани. Морфологията на композитите бяха изследвани с дигитален микроскоп.

Bulgarian Chemical Communications, Volume 47, Special issue A (pp. 30 – 33) 2015

Kinetic aspects of enzyme hydrolysis of cellulose fiber material

S. Petrin, N. Yavorov, P. Tzvetkov, I. Valchev, G. Radeva*

University of Chemical Technology and Metallurgy, 8 St. K. Ohridski Blvd., 1756 Sofia, Bulgaria

Received June 30, 2014; Accepted January 29, 2015

The kinetic dependences characterizing enzyme hydrolysis of cellulose fiber material (bleached hardwood pulp) by cellulasic enzyme complexes are studied. It is found that the topochemical mechanism provides a good interpretation of the cellulase action. The kinetics of the process is described by the modified topochemical equation of Prout – Tompkins. It is applied to the processes starting on the easily accessible outer surface of the pulp to continue further through by a gradual penetration to the capillary system of the fiber. The structural features of the system pulp – enzyme control the rate of the process. The activation energy of the hydrolysis is found constant indicating that the energy characteristics of the cellulose are identical on the surface and in the bulk of the fiber matrix. The pre-exponential factor accounts for the accessibility and the varying dimensions of the reaction area, which is formed by the cellulose–enzyme complexes and change during the process. The rate decrease in the course of the process is determined not only by the pre-exponential factor decrease but by the enzyme inhibition as well.

Keywords: *bleached hardwood pulp, enzyme hydrolysis, kinetics.*

INTRODUCTION

The enzyme hydrolysis of cellulose to glucose by cellulases is one of the major steps involved in the conversion of cellulose and lignocellulose material to yield biofuel. The susceptibility of cellulose substrates to cellulase depends on the structural features of the substrate including the cellulose crystallinity, the degree of cellulose polymerization, the surface area, and the lignin content [1]. Cellulose is known to have relatively easily accessible amorphous regions with a few lateral interactions between the cellulose chains as well as crystalline domains that are much harder to hydrolyze. In addition, the hydrolysis product of the cellulase reaction, cellobiose (glucosyl β-1-4 glucose), inhibits severely the cellulase [2]. The optimization of lignocellulosic bioconversion by cellulase enzymes requires good knowledge of the reaction kinetics.

The enzyme processes are generally characterized by relations analogous to those of the heterogeneous catalytic and topochemical reactions. This concept is based on the fact that a specific chemical interaction proceeds between the substrate and the enzyme. It can be limited to the accessible contact surface or can proceed in the bulk of the fiber material. The heterogeneous nature of the macromolecular structure of the cellulose and the lignocellulose matrices hampers the thorough elucidation of the mechanism of the enzyme-substrate interaction [3-6]. Our former investigations on the kinetics of cellulase hydrolysis of wheat straw and maize stalks show that the kinetic model of inhomogeneous surfaces is applicable [7,8]. The explanation refers to the specific structural peculiarities and the highly developed contact surface which result from the hydrothermal pretreatment of these lignocellulose materials. The same kinetic model is also found valid in case of enzyme hydrolysis of steam exploded *Paulownia Tomentosa*. It is worth adding that the cellulase product in the latter case is of lower activity and which is why it attacks only the accessible active centers of the cellulose. Thus the process taking place cannot reach the bulk of the material, which in turn results in low efficacy [9]. According to M. Ioelovich and E. Morag [1] the more active cellulasic enzyme can generate new nano-holes (meso-pores) mainly in the non-crystalline amorphous domains of the cellulose and hence provide access of the enzyme molecules to the inner cellulose structure. The application of a highly active cellulasic complex in the hydrolysis of bleached hardwood pulp preserving its pulp fiber structure, irrespectively of the pretreatment carried out, requires the consideration of the enzyme process from the topochemical point of view.

The aim of the present communication is to present the kinetic relations observed in the course of the enzyme hydrolysis of bleached

*To whom correspondence should be sent.
E-mail: grradeva@uctm.edu

hardwood pulp which in turn provide to elucidate the mechanism of action of the highly active cellulase complex.

EXPERIMENTAL

The investigations were carried out on bleaching hardwood pulp from "Slilocell" AD - Svishtov. The cellulasic hydrolysis was carried out in polyethylene bags in a water bath preheated to the desired temperature. The cellulase complexes NS 22086, with activity 1000 BHU.g^{-1} and β-glucosidase NS 22118, with activity 250 CBU.g^{-1}, were used in a ratio of 10:1 for the enzymatic hydrolysis. The kinetics of the latter was examined at: temperature values of 30°C, 40°C, 50°C; a consistency of 10%; pH range of 5.0–6.0; reaction time of 1h to 48 h and 5% enzyme charge. The glucose content was analyzed by a Dionex HPLC system in accordance with the NREL standard biomass analytical procedure [10].

RESULTS AND DISCUSSION

The amount of glucose obtained, G (%), at different temperatures and reaction times is presented in Table 1.

Table 1. The amount of glucose, G (%) at different temperatures and reaction times

Time, min	G, %		
	T=30^{0}C	T=40^{0}C	T=50^{0}C
60	7.63	9.52	12.94
120	10.20	12.58	16.63
180	12.00	15.90	20.00
1440	26.90	34.00	40.80
2880	33.10	42.28	49.20

The dimensionless quantity α is used as a kinetic variable. It has the meaning of an degree of hydrolysis, i.e. an extent of conversion of cellulose to glucose. It is determined by the relative change of the glucose amount and is calculated in correspondence with Eq. 1:

$$\alpha = \frac{G}{G_{\max}} \quad (1)$$

where G (%) is the current amount of glucose, while G_{max}=87% is the maximal amount.

The degree of conversion α increases with the increase of time and temperature, (Fig. 1).

The applicability of different kinetic equations referring to diffusion, topochemical and other heterogeneous catalytic processes is examined. It is found that the enzyme process is best described by the modified Prout – Tompkins topochemical (P-T) equation:

$$\frac{\alpha}{1-\alpha} = (kt)^{\chi} \quad (2)$$

where k has the meaning of an apparent rate constant, while the power factor χ is an invariable quantity characteristic for the cellulose – enzyme system.

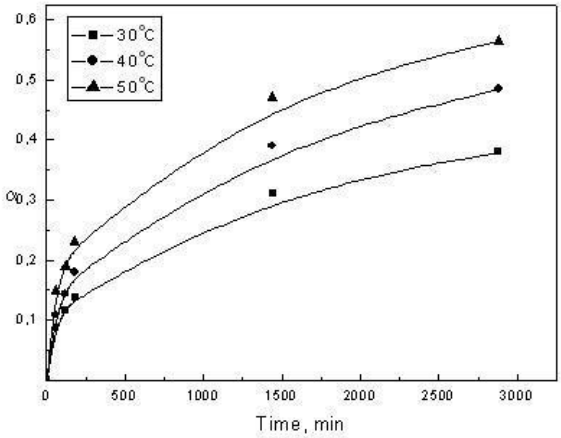

Fig. 1. Kinetic curves of the extent of enzyme hydrolysis at different temperatures.

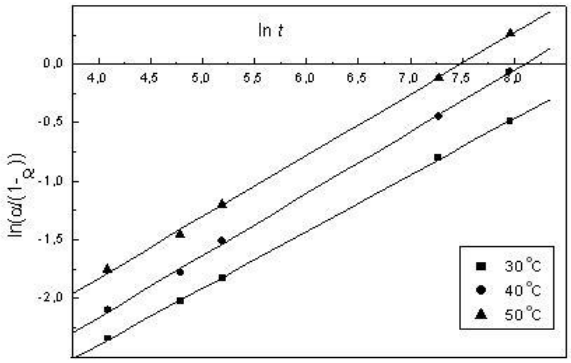

Fig.2. Linearized form of Prout – Tompkins equation for different temperatures.

It is known that Eq. (2) is successfully applied to chain topochemical reactions of chain mechanism [10]. A similar equation can be used in case of diffusion controlled heterogeneous processes. Analogous results have been reported for the xylanase action on kraft pulp [11].

All kinetic curves are linearized in coordinates $\ln\frac{\alpha}{1-\alpha}$ vs. ln t in correspondence with the logarithmic form of Eq. (2):

$$\ln\frac{\alpha}{1-\alpha} = \chi \ln k + \chi \ln t \quad (3)$$

The linear dependences obtained are illustrated by Fig. 2. The apparent rate constant k and power factor χ are calculated. The latter is temperature independent and has an average value of 0.5. The apparent rate constant k depends on the temperature in correspondence with the Arrhenius equation.

On the ground of the linear relation between ln *k* and 1/*T* (Fig. 4), the values of the activation energy *E* and pre-exponential factor ln λ are calculated: *E*=47.5 kJ/mol and ln λ=10.05.

It is of interest to determine the current rate $v = \frac{d\alpha}{dt}$, which varies during the process. The derivative form of the modified Prout-Tompkins equation is applied:

$$v = \chi k \alpha^{\frac{\chi-1}{\chi}} (1-\alpha)^{\frac{\chi+1}{\chi}} \qquad (4)$$

It outlines the dependence of the rate *v* (min^{-1}) on both the amount of the substrate left $(1-\alpha)$ and that of the product formed, α.

The factor $(1-\alpha)^{\frac{\chi+1}{\chi}}$ decreases with α increase. The factor $\alpha^{\frac{\chi-1}{\chi}}$ decreases also with α increase, because the exponent is negative (χ<1). This factor takes account of the glucose inhibiting effect on cellulase, especially near the end of the hydrolysis process when the rate decreases significantly [1]. In case of χ=0.5, Eq. (3) becomes:

$$v = k\frac{(1-\alpha)^3}{2\alpha} \qquad (5)$$

Eq. (5) provides the calculation of the current rates *v* (mim^{-1}) at different α and temperature values. It is shown in Fig. 3.

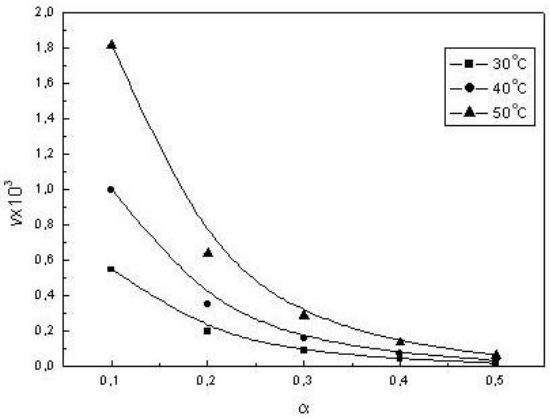

Fig. 3. Dependence of the current rate *v* (mim^{-1}) as a function of α at different temperatures.

It is seen that the process rate is the highest at α values less then 0.2. Then it decreases significantly, probably because of the inhibiting effect of the accumulated glucose at the final stage of the process.

The temperature dependence of the hydrolysis rate is followed in accordance with Arrhenius equation presented in the following form:

$$v = Ae^{-\frac{E}{RT}} \qquad (6)$$

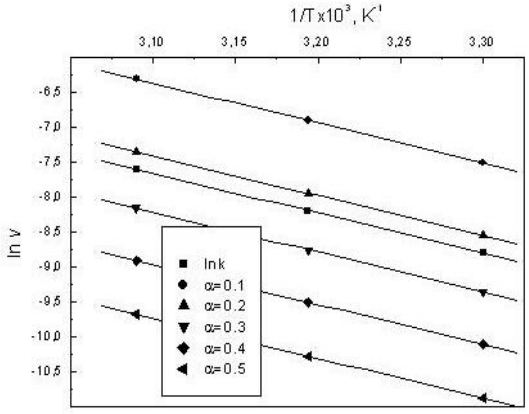

Fig. 4. Temperature dependence of the current rate and the rate constant at α=*const*.

The activation energy *E* and the pre-exponential factor *A* are calculated at different constant values of α (Fig. 4). The activation energy is *E* = 47.5 kJ/mol, i.e. a value which coincides with that found from the temperature dependence of the rate constant. It is evident that the activation energy stays constant during the process, which in turn shows that the cellulose active centers do not change their activity.

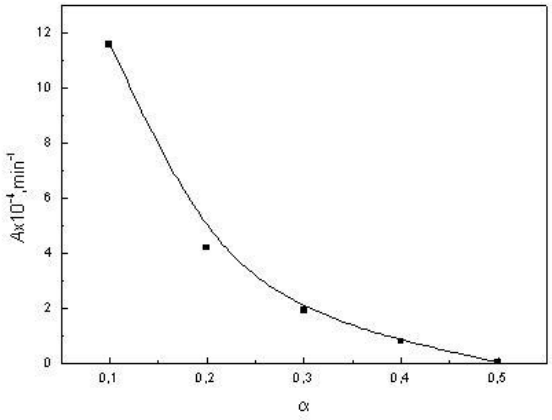

Fig. 5. Dependence of pre-exponential factor *A* (min^{-}1) on the degree of hydrolysis α.

Unlike the activation energy, the pre-exponential factor *A* decreases with the increase of the degree of hydrolysis α (Fig. 5) following the equation:

$$A = \lambda\frac{(1-\alpha)^3}{2\alpha} \qquad (7)$$

The factor *A* can be related to the dimensions and the accessibility of the reaction area, which is formed on the basis of the cellulose-enzyme complexes and changes during the process. It accounts also for the applicability of the

topochemical kinetic model. The rate decrease is due not only to *A* decrease, but also to the inhibition of the enzyme by the product obtained.

The hydrolysis process is starting to take place on the most accessible outer surface of the bleached hardwood pulp to proceed further gradually penetrating the capillary system of the fiber pulp matrix. The structural features of the system pulp – enzyme control the rate of the process. The constant activation energy shows that the energy characteristics of the cellulose are identical on the outer and the inner surface of the capillaries system, i.e. the enzyme interacts chemically with one and the same cellulose active sites. The rate decrease in the course of the process is determined not only by the pre-exponential factor decrease but by the enzyme inhibition as well.

REFERENCES

1. M. Ioelovich, E. Morag, *BioResources*, **6**, 2818 (2011).
2. A., Bommarius, A. Katona, S. Cheben, A. Patel, A. Ragauskas, K. Knudson, Y. Pu, *Metab. Eng*., **10**, 370 (2008).
3. P. Bansal, M. Hall, M.J. Realff, J.H. Lee, A.S Bommarius, *Biotechn. Adv*., **27,** 833 (2009).
4. G. Beldman, A. Voragen, F.M. Rombouts, M. Searle-van Leeuwen, W. Pilnik, *Biotechol. Bioeng*., **30**, 251 (1987).
5. P. Valjamae, V. Sild, G. Pettersson, G. Johansson, *Europ. J. Biochem*., **253**, 469 (1998).
6. K. Ohmine, H. Ooshima, Y. Harano, *Biotechn. Bioeng*., **25**, 2041 (1983)..
7. G. Radeva, I. Valchev, S. Petrin, E. Valcheva, P. Tsekova, *Carbohydrate Polymers*, **87**, 1280 (2012).
8. G. Radeva, I. Valchev, S. Petrin, E. Valcheva, P. Tsekova, *Cellulose Chem. Technol*.,**1-2**, 61 (2012).
9. G. Radeva, I. Valchev, S. Petrin, E. Valcheva, P. Tsekova, *BioResources*, **7**, 412 (2012).
10. A. Sluiter, B. Hames, R Ruiz, C. Scarlata, J. Sluiter, D. Templeton: NREL, **12** (2006): Techn. Rep. NREL/TP-510-42623 (2008).
11. M. Brown, *Themochimica Acta*, 300, 93 (1997).
12. E. Valcheva, S. Veleva, I. Valchev, I. Dimitrov, *React. Kinet. Catal. Lett*., **71**, 231 (2000).

КИНЕТИЧНИ АСПЕКТИ НА ЕНЗИМНАТА ХИДРОЛИЗА НА ЦЕЛУЛОЗЕН ВЛАКНЕСТ МАТЕРИАЛ

С. Петрин, Н. Яворов, П. Цветков, И. Вълчев, Г. Радева*

Химико-технологичен и металургичен университет, бул. Климент Охридски 8,1756 София, България

Постъпила на 30 юни, 2014 г.; Приета на 29 януари, 2015 г.

Изучени са кинетичните зависимости на ензимна хидролиза на целулозен влакнест материал (избелена широколистна целулоза) с целулазен ензимен комплекс. Установено е, че процесът на ензимна хидролиза може да се интерпретира с топохимичен кинетичен модел. За описание на кинетиката на процеса е използвано модифицираното топохимично уравнение на Праут – Томпкинс. То е приложимо за процеси, които започват от най-лесно достъпните външни центрове и постепенно проникват в структурата на целулозното влакно. Определящи за скоростта на процеса са структурните изменения на повърхността. Установено е, че активиращата енергия не се променя в хода на процеса, което показва, че енергетичните характеристики са идентични и на повърхността и във вътрешността на целулозната матрица.

Пред-експоненциалният фактор, който отчита достъпността и особеностите на реакционната зона на системата целулоза – ензим, се променя в хода на процеса. Установено е, че намалението на скоростта се дължи не само на намалението на пред-експоненциалния множител, но и на инхибирането на ензима.

Bulgarian Chemical Communications, Volume 47, Special issue A (pp. 34 - 38) 2015

Ecological utilization of printed waste paper

S.A. Kotlarova, V.G. Lasheva*, D.A. Todorova

University of Chemical Technology and Metallurgy – Sofia, Textile and Leather Department, Sofia 1756, Bulgaria

Received August 12, 2014; Accepted January 26, 2015

The use of printed wastepaper as a source of secondary fiber material for the production of paper and cardboard is related to the process of de-inking through flotation.

The ink removal from waste paper through flotation treatment with enzymes while the pH is neutral leads to modification of the cellulose fibers. The process is fully environmentally friendly.

Restoring the sheet-formation properties of secondary fibers as a result of bio-modification with enzymes helps to increase the number of cycles of waste paper usage and improves some of the characteristics of recycled paper.

The present study is a research on the removal of ink from paper with offset printing through flotation by the usage of the enzymes cellulase and lipase.

Key words: *de-inking, enzymes, printed waste paper*

INTRODUCTION

The use of recycled fiber material for the production of paper and cardboard has a significant role for solving the problems of environmental protection and contributes to energy savings by decreasing the energy consumption.

One of the most important processes used in the recycling of printed waste paper is de-inking, i.e. the removal of ink from the used paper in order to get a whiter recycled fiber pulp. The process includes removing the ink particles from the surface of the fibers and separating them from the fiber suspension through washing or flotation. [1]

A useful method for removing the ink from the waste paper through flotation is the treatment with enzymes while the pH is neutral. When recycling waste paper, enzymes are used to enhance the disintegration of fibers and improve the process of draining, to remove the ink from paper used for Xerox copies and laser printing, as well as to prevent the formation of sticky substances. [2]

Enzymes are complex protein molecules which act as catalysts. The activity of enzymes is essential to the process and is closely related to the chemical and physical environment (temperature, pH), the type and concentration of the substrate. [3]

Offset printing is superficial. The printed and non-printed elements are on the same surface. The printed elements are covered with ink, while the rest are moistened.

Removing the ink with enzymes aims at reaching a balance between the strength of fibers, the strength of interfiber connections and the loss of output, which have to be reduced to a minimum. [4]

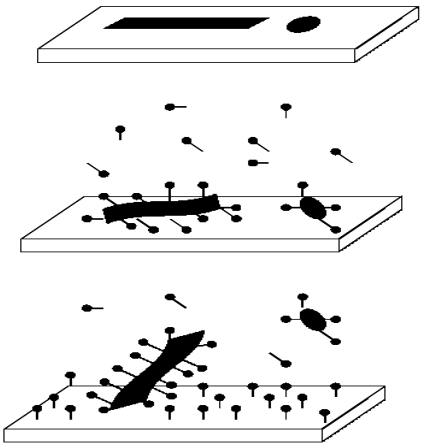

Fig. 1. De-inking in the presence of surfactants

The improved regeneration of the sheet-formation properties of secondary fibers as a result of enzyme treatment is capable of increasing the number of cycles of waste paper usage, as well as improving some characteristics of the paper made from secondary fibres. [2]

The aim of the present study is to investigate the process of removing the ink from waste paper with offset printing through flotation by the use of cellulase and lipase enzymes in combination with surfactants.

The surfactants have the following functions during the process of de-inking through flotation:

- They remove the ink particles from the surface of the fibers and prevent them from settling again on the fibers during the process of de

*To whom correspondence should be sent.
E-mail: *vesla@uctm.edu*

- -inking; They agglomerate the small ink particles into large ones and change the surface of the particles from hydrophilic into hydrophobic;
- They act as foaming agents accumulating froth on the surface of the flotation cell and enhancing the de-inking process [5].

The purpose of this study is to review and analyze the established possibilities for obtaining and application the biocomposites based on keratin/ polyurethane in the medicine and other areas as compared to those based on collagen/ polyurethane.

EXPERIMENTAL

Materials and Reagents

The waste paper with offset printing used in the present research has a grammage of 80 g/m^2. The enzymes flotation is carried out with the following surfactants: BRIJ 35, Sigma Aldrich and the enzymes Cellulase (C) and Lipase(L).

Apparatus

Laboratory hydropulper. An amount of 500 grams of waste paper weighted prior to the experiment is torn into small pieces and is soaked into water for an hour. The soaked pulp undergoes the process of disintegration of the fibers inside the hydropulper.

The laboratory hydropulper has a cylindrical shape and a vertically installed propeller. The apparatus has a volume of 100, l and functions when the concentration of the mass is 2%. The apparatus is working for 2 hours. The produced suspension is drained with a sieve, additionally squeezed to a state of dryness of 20-30% and the secondary fiber pulp is stored in a refrigerator.

Laboratory disintegrator. 20grams of oven dry fiber pulp are taken from the hydropulper and put inside a disintegrator for 10 minutes. Depending on the type of examined pulp samples after the initial time, the necessary reagents are added in a sequence. The fiber suspension is further disintegrated - the process is prolonged by 10 minutes with each one of the reagents. The disintegrator has a working volume of 4 l and a maximum concentration of 2%.

Laboratory froth flotation cell. The suspension of fiber pulp taken out of the disintegrator is then placed into a froth flotation cell (Photo.1). The air is switched on, as well as the stirring paddle. Some flotation froth is formed on the surface which is removed. The process of flotation continues for a certain period of time and the ink-free fiber pulp is stored in a container.

The froth flotation cell consists of a flotation chamber connected to a pipe for air supply and a stirring paddle. The stirring paddle is responsible for turning the fiber pulp into a homogeneous mixture. The even-dispersion of air in the fiber pulp is a condition of utmost importance because it makes it possible for all the ink particles to reach the air bubbles.

Photo 1.

The turbulence inside the froth flotation cell has to be controlled in a way that not a single zone remains stagnant, which would lead to a flotation of fibers and leaving of dirt on the walls of the cell. On the other hand, the turbulence should not be too strong because the fiber pulp can be mixed with the froth on the surface.

Laboratory sheet-moulding apparatus (apparatus Rapid- Keten). The ink-free fiber suspension is divided into a number of moulds which are made up with the help of a laboratory sheet-moulding apparatus Rapid-Keten.

The sheet-moulding apparatus consists of a moulding and a drying sector. The moulding part includes a cylindrical chamber, a sieve and a suction device. The wet pulp settles on the sieve, and then it is drained with the suction device which removes and collects the water. The drying sector consists of two nests for drying.

Laboratory apparatus for establishing the degree of brightness Frank Spectrophotometer Brightness Colour. Brightness is the property of paper to reflect light in a dispersed and homogenous way along the whole range of the visible spectrum.

Brightness is measured as a % of reflected light with a defined wavelength in the blue segment

Table 1. Content of pulp suspension samples.

Name of samples	*Waste paper g/m²*	*Surfactants, %*	*Cellulase, %*	*Lipase, %*
Zero sample	80	-----	-----	-----
Waste paper + Surfatants	80	0,3	-----	-----
Waste paper +Surfatants +0,1 Cellulase	80	0,3	0,1	-----
Waste paper +Surfatants +0,3 Cellulase	80	0,3	0,3	-----
Waste paper +Surfatants +0,1 Lipase	80	0,3	-----	0,1
Waste paper +Surfatants +0,3 Lipase	80	0,3	-----	0,3
Waste paper +Surfatants+0,1Cellulase +0,1Lipase	80	0,3	0,1	0,1

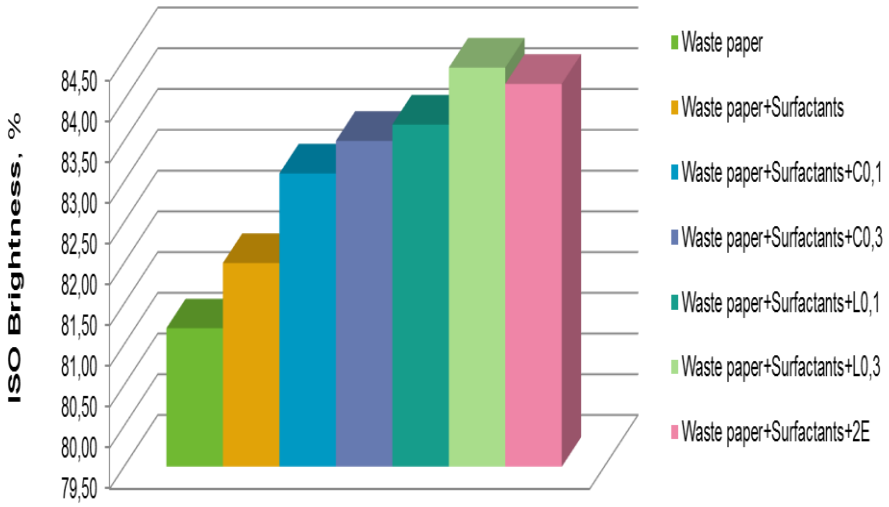

Fig. 2. Brightness of the samples defined according to ISO Brightness.

(457nm) and is termed as Brightness R_{457} (ISO 2470:2002). [6]

RESULTS AND DISCUSSIONS

The waste paper with offset printing undergoes the process of disintegration of fibers, followed by further disintegration with the help of enzymes in combination with surfactants and finally, flotation to separate the cellulose pulp. The following paper samples have been tested, cf. Table 1.

Testing the degree of Brightness of the paper samples. The degree of brightness of the samples is presented in Figure 2.

The results show that the degree of brightness is increased in all samples of de-inked paper. However, it is highest in the samples obtained after flotation with surfactants in combination with lipase enzyme.

De-inking capacity. It is estimated on the basis of a comparison of results after measuring the degree of brightness of the waste paper before de-inking (Zero sample) and the de-inked samples. The following formula is used:

De-inking capacity = {(de-inked sample –zero sample)/zero sample}x 100, [%]

Figure 3 shows the de-inking capacity of enzymes and their possible combinations in percentages. [7]

The greatest de-inking capacity is measured in samples produced after flotation with surfactants in

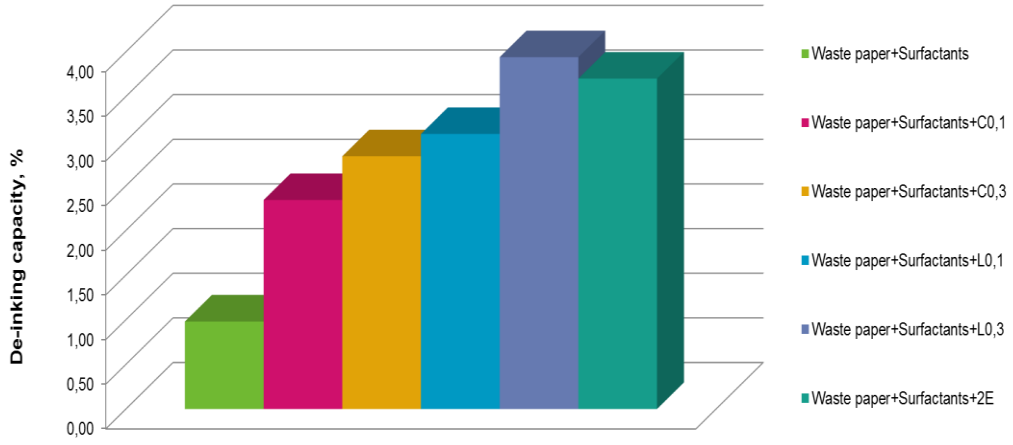

Fig. 3. De-inking capacity

combination with lipase enzyme. The other samples also show an increased de-inking capacity, which leads to the conclusion that both enzymes have a positive effect in the process of de-inking.

Breaking length (L),[m]. This is the length at which a strip of the tested paper with a width of 15mm, suspended at one end, would be torn by the force of its own weight. It is calculated by the formula of Hartig:

$$L=(F.l.100)/d,$$

where:

F – force of tearing in [N], measured by the dynamometer;

l – length of the strip in [m], defined by the distance between the two ends of the dynamometer;

d – weight of the strip in [g], measured after it has been torn from the hooks. [7]

Figure 4 shows the breaking length in [m] of the samples.

A slight increase in the breaking length of the samples is observed, with the exception of those samples obtained after flotation with surfactants in combination with lipase enzyme. The samples obtained after treatment with surfactants in combination with cellulase enzyme have the highest breaking length.

CONCLUSION

Waste paper is a competitive material for the paper industry. During the process of recycling, removing the printed ink from the paper suspension can be a problem. De-inking is a hard task because the different kinds of ink have different ingredients. Therefore, it is necessary to find the most effective and ecological method of removing the ink from the paper.

Restoring the sheet-formation properties of secondary fibers as a result of bio-modification with enzymes helps to increase the number of cycles of waste paper usage and improves some of the properties of recycled paper.

The parameters of enzyme de-inking of printed waste paper have been defined. In the process of flotation the enzymes cellulase and lipase increase the degree of brightness, the de-inking capacity and the physico-mechanical property - breaking length. Adding these enzymes, the de-inking of waste paper is improved.

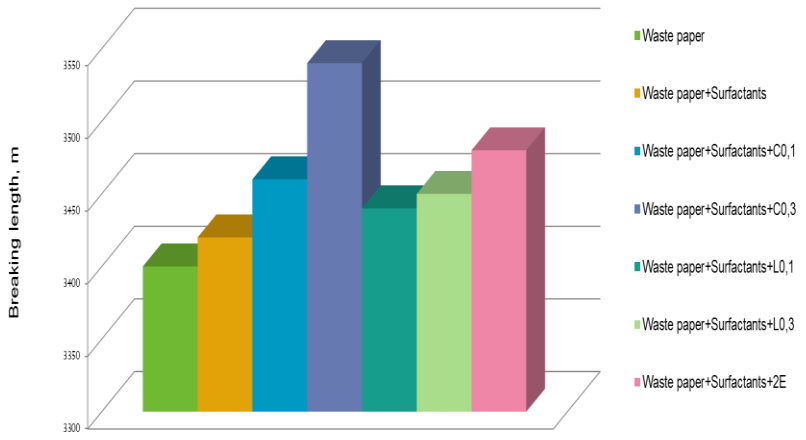

Fig.4. Breaking length of the samples.

REFERENCES

1. P. Pathak, N. Bhardwaj, A. Singh, *Bioresources*, **6**, 447 (2011).
2. E. Bobu, F. Ciolacu, *Wochenblat fur Papierfabrikation*, **1**, 6 (2007).
3. S. Vitforr, Enzymatic pre-treatment of wood chips for energy reductions at mechanical pulp production, Ecotarget, 2008.
4. H. Kippham, Hanbbuch der Printmedien, Heildelberg, 2003.
5. Y. Zhao, Y. Deng, *Roles of Surfactants in Flotation Deinking*, *Progress in Paper Recycling*, **14**, 1 (2004).
6. Lee CK, Darah Ibrahim, Ibrahim Che Omar, Wan Daud Wan Rosli, *Bioresources*, **75**, 3859 (2011).
7. N. Ivanova, S. Bencheva, D. Todorova, Manual for exercises in chemistry, technology and paper properties, Publ. House UCTM, 78-89, 2009 (in Bulgarian).

ЕКОЛОГИЧНО ОПОЛЗОТВОРЯВАНЕ НА ОТПАДЪЧНА ХАРТИЯ С ПЕЧАТ

С. Котларова*, В. Лашева, Д. Тодорова

Химикотехнологичен и металургичен университет – София

Постъпила на 12 август 2014 г.; Коригирана на 11 февруари 2015 г.

(Резюме)

Използването на отпадъчната хартия с печат като източник на вторичен влакнест материал за производство на хартии и картони е свързано с нейното обезмастиляване чрез флотация. Перспективно и екологично е обезмастиляването на отпадъчната хартия по метода на флотация с ензимно третиране при неутрално pH, което води до модификация на целулозните влакна.

В настоящата разработка се изследва влиянието на 2 ензима – целулаза и липаза, както и комбинация от тях, в процеса на флотация.

Регенерацията на гъвкавостта на влакната започва в първия етап на развлакняване на отпадъчната хартия при концентрация 4%. За поведението и характеристиката на получения влакнест материал се съди по кинетиката на отводняване, определенна на апарата Шопер-Риглер.

Ензимната флотация се провежда във флотационна клетка, осигуряваща определени хидродинамични условия на смесване на хартиената суспензия с ензимите и с ПАВ и отделяне на мастилените частици.

За охарактеризиране на физико-механичничните показателите са получени хартиени образци на апарат Rapid-Keten. Определено е съпротивлението на скъсване при опън, съпротивлението на раздиране, съпротивлението на огъване, съпротивлението на спукване. Определена е степента на белота на биомодифицирания обезмастилен рециклиран влакнест материал .

Възстановяването на листообразуващите свойства на вторичните влакна в резултат на биомодификацията с ензими способства за увеличаване броя на циклите за използване на отпадъчната хартия и за подобряване на някои показатели на хартията, получена от рециклирани влакна.

Bulgarian Chemical Communications, Volume 47, Special issue A (pp. 39 - 44) 2015

Copper-based nanostructured lignocellulose materials with antibacterial activity

N. Rangelova, S. Nenkova*, N. Lazarova, N. Georgieva

University of Chemical Technology and Metallurgy, str. bld. 8 Kl. Ohridski, 1756 Sofia, Bulgaria

Received July 17, 2014; Accepted January 29, 2015

In this study we report for successfully preparation of copper-based lignocellulose nanocomposites. The wood fibers (WF) and technical hydrolysis lignin (THL) were used as lignocellulosic materials. To produce copper sulfide lignocellulose nanocomposites a two-component cupri reduction system at saturated steam were used. The copper content in the synthesized samples was determined by Inductive coupled plasma (ICP) analysis, thermal and acid decomposition methods. The linkage of copper ions with lignocelluloses was studied by Infrared (IR) spectroscopy. The IR bands observed at ~3400 cm^{-1} suggest that the main mechanism of interaction between lignocellulose materials and copper ions was realized by oxygen atoms of OH groups in cellulose and in the aromatic nucleus of the lignin macromolecule. SEM-EDS analyses showed the presence of copper particles on the surface of investigated samples. According TEM observations it was found the tendency to formation of clusters from CuNps in different shape. The size of the formed nanoparticles varies between 10-50 nm. The antibacterial activity of modified lignocelluloses was tested against Gram-positive (*Bacillus subtilis* 3562) and Gram-negative (*Escherichia coli* K12 407) bacteria. The results showed that copper-based THL has better antibacterial activity compared to WF material.

Key words: *lignocellulose nanomaterials, modification, copper sulfide, antibacterial activity*

INTRODUCTION

Glucose In recent years, owing to the increased environmental awareness, the usage of lignocellulosic materials as a potential replacement for synthetic fibers such as carbon, aramid and glass fibers in composite materials have gained interest among researchers throughout the world. Lignocelluloses are abundant in nature, renewable raw material and a low cost material. Owing to their low specific gravity, lignocellulose fibers are able to provide a high strength to weight ratio in plastic materials. The usage of lignocellulose materials also provides a healthier working condition than the synthetic fibers [1, 2]. The chemical compositions of lignocellulose materials vary according to the species, growing conditions, method of fiber preparations and many other factors. Lignocelluloses have a large number of reactive groups, a wide range of molecular weight, varying chemical composition, which contribute to their diversity in structure and property [3].

Copper sulfide ($Cu_{2-x}S$) has various phases [4,5]. All of these phases are p-semiconductor due to presence of copper vacancies in their lattice. Copper sulfides are used for solar cells, field emission device, nano switch, photo catalyst, biosensors, p-semiconductor, gas sensors and so on [4,5].

Antimicrobial effects of transition metal nanoparticles have attracted considerable interest from both medical and technological standpoints, because this kind of property plays a crucial role in applications such as protection of medical instruments and devices, water treatment and food processing [6]. Nano-form copper particles (CuNPs) have enhanced antimicrobial activity toward a broad spectrum of microorganisms, including pathogenic bacteria. Apart from their small size, the high surface to volume ratio and derived close interaction with microbial membranes, the source of cytotoxicity were also identified from leached copper–peptide coordination. This complex formation induces a multiple-fold increase in the generation of intracellular reactive oxygen species, reduces cell viability and inhibits overall biomass growth [6].

The purpose of this study is to clarify the modification of lignocelluloses materials (WF and THL) with cupri reduction system at saturated steam. We also examined the structure and antibacterial behavior of obtained copper-based lignocellulose materials.

EXPERIMENTAL

In this study the WF (produced in Lesoplast Inc., Troyan, Bulgaria) and THL (obtained by acid hydrolysis of wood in Pirinhart PLC, Razlog,

To whom correspondence should be sent.
E-mail: nenkova@uctm.edu

Bulgaria) were used as lignocellulosic materials

The copper-based lignocellulose materials were prepared as follows. $CuSO_4.5H_2O$ was used as the metal precursor to produce CuNps. On the other hand $Na_2S_2O_3.5H_2O$ was used as reductor. The modification process was at hydromodule 1:6, and the ratio between the components ($CuSO_4.5H_2O$:$Na_2S_2O_3.5H_2O$) was 1:2 in quantity 45% in term of lignocellulose materials. To produce copper based lignocellulose nanocomposites a method at saturated steam were used [7,18]. All analytical grade reagents were used as without further purification for synthesis of Cu_2S nanoparticles and modification of lignocellulose materials.

The copper content in the samples was determined by ICP (Prodigy High Dispersion ICP Spectrometer – Teledyne Leeman Labs) analysis used thermal and acid decomposition methods. The linkage of copper ions with lignocelluloses was studied by Infrared (IR) spectroscopy (MATSON 7000 Fourier Transforming Infra-Red spectrometer). The shape and size of formed copper nanoparticles was observed by TEM (JEOL 2100). The surface morphology was verified by SE M (JEOL JSM 6390). Energy-dispersive X-ray spectroscopy (EDS) was used as quantitative analysis of elemental composition of samples.

For investigation of antibacterial behavior of lignocelluloses materials bacterial strains used in this study were obtained from the culture collection of Bulgarian National Bank of Industrial Microorganisms and Cell Cultures and included Gram-positive bacteria - *Bacillus subtilis* 3562 and Gram-negative - *Escherichia coli* K12 407.

The cultures growth, bacterial growth-inhibiting effect and the optical density of the culture was described previously [9]. The measurement of antibacterial activity of hybrid materials was calculated according to N. Rangelova *et al.* [9], between the control sample and the test sample.

RESULTS & DISCUSSION

In our previous investigations [7,10] we described the scheme of Cu^{2+} reduction process and Cu_2S formation. The results for copper content are shown on Fig. 1. As can be seen the copper content is higher in the modified THL than the wood fibers. Probably lignin adsorbed in a greater extent the metal ions in comparison with the fibers. As it is known, lignin is very often used as an adsorbent because of its large internal surface area. In this case the metal ions may be adsorbed by both physical sorption or through coordination bonding.

Fig. 2 presents the infrared spectra of lignocellulose and copper-based lignocellulose materials. In these spectra four characteristic absorption regions can be distinguish: from 3700 to 3000 cm^{-1}, 3000 to 1800 cm^{-1}; 1800 to 700 cm^{-1}; and below 700 cm^{-1}. The bands in the first area (3700-3000 cm^{-1}) corresponding to stretching vibration of free (unsubstituted) and hydrogen bonding OH groups in polymer backbone and water [2, 11]. The second area consist intense band at ~ 2940 cm^{-1} and may be attributed to the asymmetric and symmetric stretching vibrations of C-H linkage due to CH, CH_2 or CH_3, and the methyl groups (O-CH_3) in the lignocellulose materials. The area from 1800 to 700 cm^{-1} is unique to each of carbohydrate polymers – "fingerprint region". These include vibrations of the skeletal (C-O-C and C-C) glucosidic bonds, as well as deformation and stretching vibrations of the C-OH linkages in the pyran ring. Here also include the C–H, C–O, C–O–C, C–OH asymmetric, symmetric and deformations stretching vibrations of aromatic skeletal or glycosides linkages and primary alcohol groups [11-13]. The bands at 1600 and 1637 cm^{-1} are

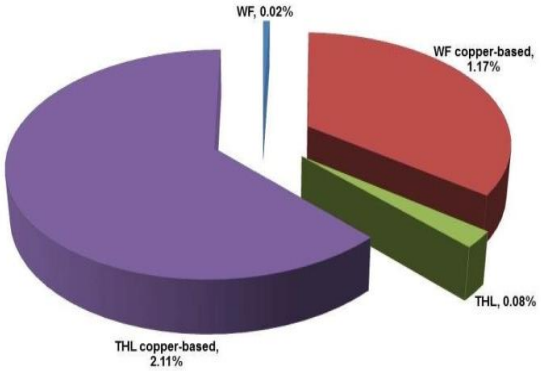

Fig. 1. Copper content in lignocellulose and copper-based lignocellulose materials.

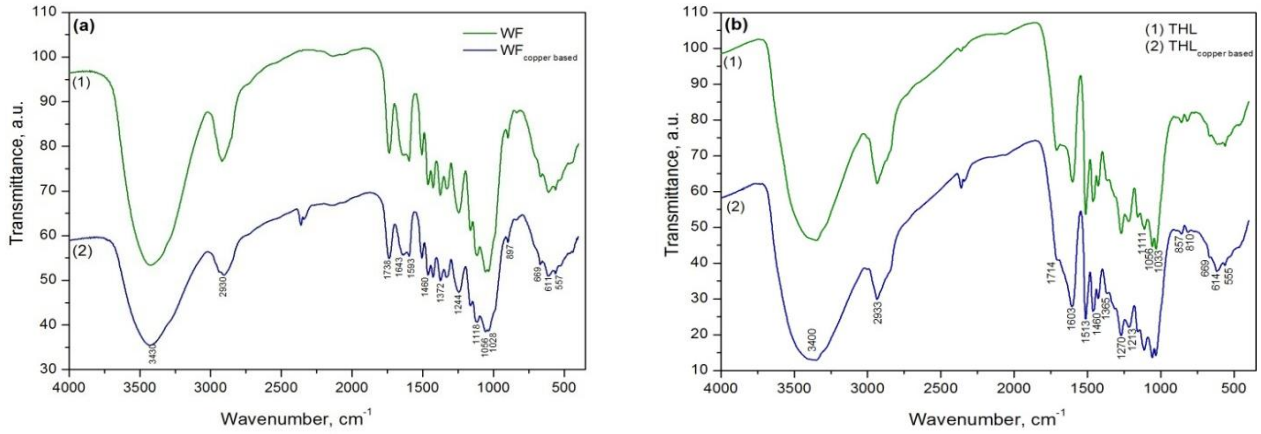

Fig. 2. IR spectra of lignocellulose(a) and copper-based (b) lignocellulose materials.

assigned to the absorbed water and β-glucosidic linkages between the sugar units, respectively. In last area (700-400 cm^{-1}) can be found the characteristic absorption bands of C–OH out-of-plane bending mode in cellulose, skeletal deformation of aromatic rings, substituted groups and side chains in lignin, some heavy atoms stretch in cellulose macromolecules and others [12-14].

The FTIR spectra of lignocellulose and copper-based lignocellulose materials are similar. The main differences in the IR spectra (Fig. 2 a, b) were observed in the range 3500-3200 cm^{-1}. A decrease in the intensity of the O–H absorption band at 3430 cm^{-1} was observed. This fact can be connecting with reduced of content of hydroxyl group in lignocelluloses after reaction. Many authors reported that the bands above 3400 cm^{-1} can be attributed to the vibration of coordination bonding between the copper ions by oxygen atoms from the OH groups of lignocellulose materials [15,16]. On the base of above mentioned results and literature data can be suppose that the probable mechanisms of interaction between copper ions and lignocellulose materials by oxygen atoms of OH groups in cellulose and in the aromatic nucleus of the lignin macromolecule. In details we described previously these results in several papers [7,10].

The SEM images of raw materials and modified lignocelluloses are shown on Fig. 3. On the surface of wood fibers (Fig. 3, a) can be seen the presence of pore with diameter 50 nm. After the modification (Fig. 3, b) on the WF surface are observed bright particles, due to existence of copper nano particles. Moreover as can be seen that the pores disappear on the surface which can be explain with penetration of copper particles in the presented hollows. The micrograph images of THL (Fig. 3, c and d) have shown the heterogeneous, compact structure with rough and disordered surface.

After modification the existence of copper ions on the samples surface is confirm by EDS analysis for both type of copper based lignocelluloses materials. The results of EDS analysis which are

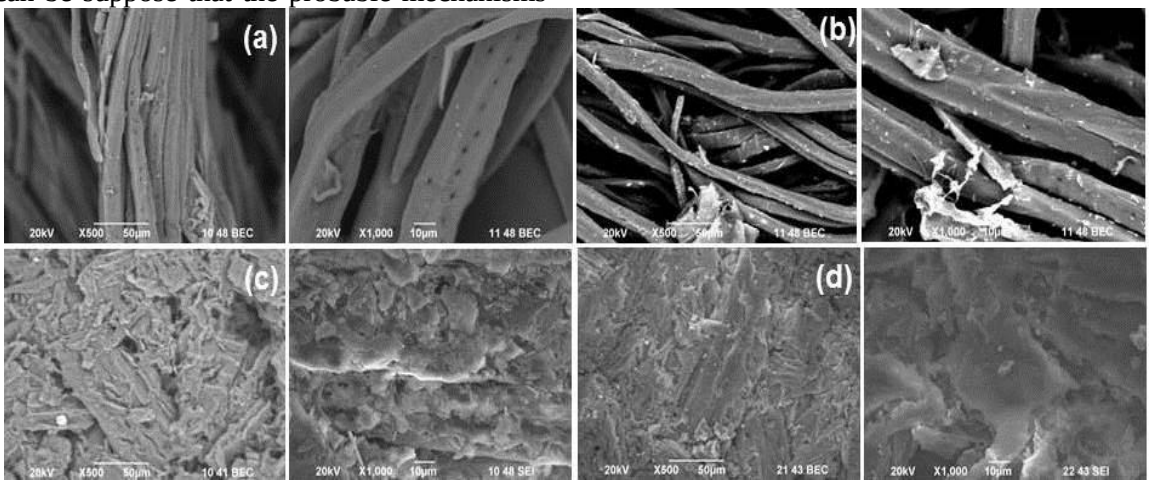

Fig. 3. SEM images of WF (a), WF copper based (b), THL (c) and THL copper based (d).

connected with the present elements in the samples are summarize in Table 1.

TEM observations of WF sample containing copper are shown in Fig. 4. As can be seen the fibers are coated a cluster-forming CuNPs with dimension in the range between 30-50 nm (Fig. 4a) and their shape vary from spherical to elliptical. At higher magnification (Fig. 4b) of the image the present tendencies towards aggregation of copper particles preserve. On the Fig. 4b can be found separated cupper nanoparticles less than 30 nm (from 10 to 30 nm) distributed in the main matrix.

The antibacterial properties of obtained modified lignocelluloses were tested against *B. subtilis* and *E. coli* K12. Bacterial growth of *B. subtilis* was totally suppressed by both materials - WF copper-based materials and THL copper-based materials – 97.42% and 100% respectively (Table 2). This was confirmed by plating a diluted aliquot from each sample onto a LB agar plate and observing bacterial colony after incubation of 24 hours (Fig. 5).

Table 1. EDS elemental analysis of samples

Lignocellulose material	Elemental Composition, wt.%			
	Carbon	Oxygen	Copper	Sulphur
WF	51.14±0.80	48.84±0.80	---	---
$WF_{copper\ based}$	50.09±1.07	46.11±1.07	3.5±0.63	0.3±0.11
THL	59.15±0.76	40.72±0.76	----	----
$THL_{copper\ based}$	58.9±1.47	33.84±1.43	6.12±0.97	1.14±0.18

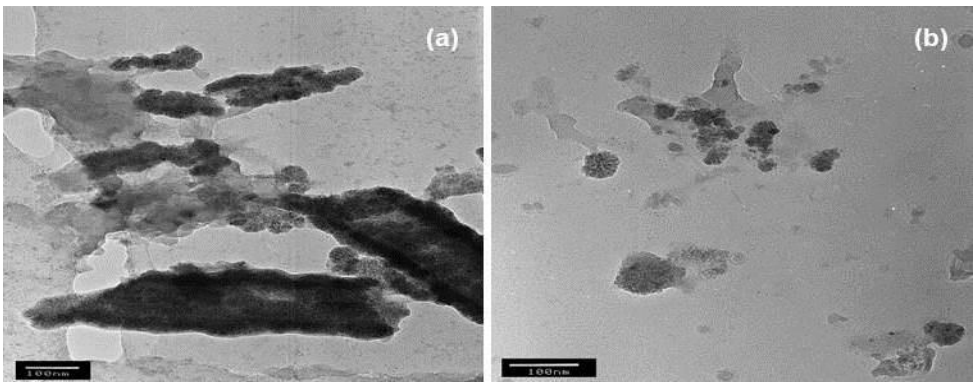

Fig. 4. TEM images of copper-based wood fibers.

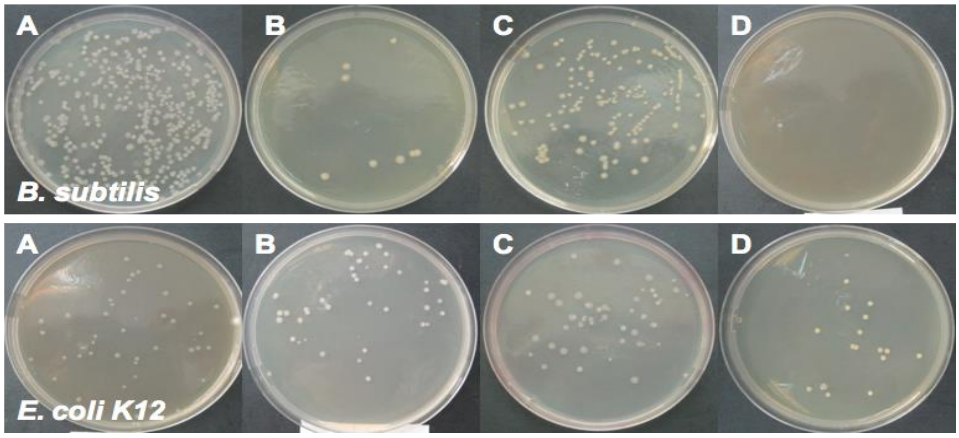

Fig. 5. Test results of *B. subtilis* (upper panel) and *E. coli* K12 (lower panel) for: WF (A), WF copper-based (B), THL (C) and THL copper-based (D).

Table 2. Antibacterial test results of *B. subtilis* and *E. coli* K12 after 24 h cultivation.

Materials	*B. subtilis*		*E. coli K12*	
	CFU/ml	Reduction of bacteria (%)	CFU/ml	Reduction of bacteria (%)
WF	11.6 x10^8	-	9 x10^{10}	-
$WF_{copper-based}$	0.3 x10^8	97.42%	3.9 x10^{10}	56.7%
THL	27 x10^8	-	4.2 x10^{10}	-
$THL_{copper-based}$	n.d.	100 %	1 x10^{10}	76.2 %

These materials caused approximately 56.7% and 76.2 % reduction of *E. coli* K12 growth, indicated that *B. subtilis* is more sensible to CuNPs than *E. coli* K12. Our results demonstrate that THL copper-based materials have more promising effect towards investigated bacteria, compared to WF copper-based materials. The mechanism of biocidal action of copper nanoparticles may be explained with the fact that CuNPs release Cu (II) ions on contact with moisture. These copper ions bind with the COOH and SH groups of protein molecules of bacterial cell wall [17,18].

CONCLUSIONS

Copper-based nanostructured lignocellulose materials (wood fibers and technical hydrolysis lignin) with antibacterial properties were prepared. The quantity of copper is higher in the modified THL than the wood fibers. It was suggested that the most probable mechanism of interaction between lignocelluloses and copper ions is the coordinative binding with the oxygen atoms of OH groups in cellulose and in the aromatic nucleus of the lignin macromolecules. SEM-EDS analyses confirm the presence of copper particles on the samples surface. TEM observation showed cluster-forming CuNPs. The size of the formed nanoparticles varies between 10-50 nm. Antibacterial properties of the copper based lignocelluloses against *B. subtilis* and *E.coli* K12 were demonstrated. The results revealed that the *B. subtilis* strain was more sensitive because it showed larger killing in comparison to *E.coli* K12.

REFERENCES

1. J.S. Van Dyk, B.I. Pletschke, *Biotechnol. Adv.*, **30,** 1458 (2012).
2. T. Hatakeyama, H. Hatakeyama, Thermal properties of green polymers and biocomposites, Kluwer academic publishers, Netherlands, 2004.
3. M. Dragnevska, PhD Thesis, UCTM, Sofia, 2013.
4. Y. Wu, C. Wadia, W. Ma, B. Sadtler, A. P. Alivisatos, *Nano Lett.*, **8**, 2551 (2008).
5. M. Salavati-Niasari, E. Esmaeili, M. Sabet, *J. Clust. Sci.*, **24**, 799 (2013).
6. M. Veerapandian, S. Sadhasivam, J. Choi, K. Yun, *Chem. Eng. J.*, **209**, 558 (2012).
7. S. Nenkova, P. Velev, M. Dragnevska, D. Nikolova, K. Dimitrov, *Bioresources*, **6,** 2356 (2011).
8. M. Dragnevska, P. Velev S. Nenkova, R. Garvanska, *J. Univ. Chem. Technol. Metall.*, **46,** 349 (2011).
9. N. Rangelova, L. Alexandrov, Ts. Angelova, N. Georgieva**,** R. Müller, *Carbohyd. Polym.*, **101**, 1166 (2014).
10. P. N. Velev, S. K. Nenkova, M. N. Kulevski, *Bulg. Chem. Commun.*, **44,** 164 (2012).
11. W. Li, B. Sun, P. Wu, *Carbohyd. Polym.*, **78**, 454 (2009).
12. H. Yang, R. Yan, H. Chen, D. H. Lee, Ch. Zheng, *Fuel*, **86**, 1781 (2007).
13. M. M. Ibrahim, A. Koschella, G. Kadry, T. Heinze, *Carbohyd. Polym.*, **95**, 414 (2013).
14. H. Li, J. Lu, J. Mo, *Bioresources*, **7,** 6 75 (2012).
15. B. Kozlevčar, B. Mušič, N. Lah, I. Leban, P. Šegedin, *Acta Chim. Slov.*, **52**, 40 (2005)
16. J. Zhang, D.P. Kamdem, *Holzforschung*, **54**, 119 (2000).
17. J. Ramyadevi, K. Jeyasubramanian, A. Marikani, G.Rajakumar, G. Rajakumar, A. Rahuman, *Mater. Lett.*, **71**, 114 (2012).
18. M. Grace, N. Chand, S. Bajpai, *J Eng. Fiber Fabr*, **4**, 24 (2009).

МЕДНИ НАНОСТРУКТУРИРАНИ ЛИГНОЦЕЛУЛОЗНИ МАТЕРИАЛИ С АНТИБАКТЕРИАЛНО ДЕЙСТВИЕ

Н. Рангелова, С. Ненкова*, Н. Лазарова, Н. Георгиева

Химикотехнологичен и металургичен университет, бул. Кл. Охридски 8, 1756 София, Бъглария

Постъпила на 17 юли 2014 г.; коригирана на 29 януари 2015 г.

(Резюме)

В представената изследователска работа са показани резултати за получаване на медни лигноцелулозни нанокомпозити. Дървесните влакна (ДВ) и технически хидролизен лигнин (ТХЛ) са използвани като лигноцелулозни материали. За получаването на медно-сулфидни лигноцелулозни нанокомпозити са използвани двукомпонентна медно-редукционна система и лигноцелулозни материали. Модифицирането е проведено по метода на наситена пара. Съдържанието на мед в пробите е определено чрез термичен и киселинен метод на разлагане с последващ ICP анализ (индуктивно свързана плазма), Връзката на медните йони с лигноцелулозния материал бе изследвана чрез инфрачервена (ИЧ) спектроскопия. ИЧ ивиците, наблюдавани при 3400 cm^{-1} показват, че основният механизъм на взаимодействие се осъществява чрез координационно свързване на медните йони с кислородни атоми на ОН групи в целулозата и в ароматно ядро на лигниновата макромолекула. CEM-EDS анализите показват наличието на медни частици върху повърхността на изследваните проби. От TEM изображенията бе установена склонността към образуване на клъстери от CuNps с различна форма. Размерът на образувалите се наночастици варира в интервала между 10-50 nm. Антибактериалната активност на модифицираните лигноцелулози бе тествана срещу Грам-положителни (*Bacillus subtilis* 3562) и Грам-отрицателни (*Escherichia coli* K12 407) бактерии. При сравняване на двата материала резултатите показват, че модифицираният ТХЛ, на медна основа, има по-добра антибактериална активност спрямо дървесно-влакнестия материал.

Bulgarian Chemical Communications, Volume 47, Special issue (pp.45 - 50) 2015

Investigation on the influence of chemical additives over the behavior of paper furnish from recycled newspaper fiber material

D.A. Todorova*, S.P. Bencheva

University of Chemical Technology and Metallurgy, 8 Kl. Ohridski, 1756 Sofia, Bulgaria

Received July 30, 2014; Accepted February 13, 2015

The use of secondary fibers from waste paper itself is a major trend in the production of various types of paper and cardboard, which has a very positive environmental effect; it saves water, electricity, steam and wood raw material. On the other hand the regenerated fibers have reduced sheet-forming-properties and induce problems by the appearance of so-called "stickies". These substances are undesirable components, since reduced and in some cases interfere with the action of the cationic chemical additives (CCA) added for a specific purpose. To solve these issues papermakers use CCA.

What is used primarily in the paper production processes are high-molecular weight hydrophilic synthetic polymers (polyelectrolytes) with different chemical nature. As a result, the dewatering is accelerated, the retention of the components in the paper sheet is improved and this provides a clarified white waters.

The purpose of this study was to investigate the effect of cationic synthetic polyelectrolytes with different chemical nature and charge over the behavior during the dewatering of paper furnish from recycled fiber material from waste paper.

The recycled fiber material is from waste newsprint paper and it mainly consists of chemical-thermo-mechanical pulp. Six types of cationic chemical additives with different chemical nature and charge density are used. The dewatering ability is measured and the turbidity and conductivity of the white waters is determined.

As a result of the studies carried out it is found out that for the improvement of the dewatering and for the clarification of the white waters, the most advisable is the usage of chemical additive based on polyacrylamide.

Key words: *chemicals additives, paper furnish, dewatering, white water, polyelectrolytes*

.

INTRODUCTION

Paper is one of the oldest and widespread industrial products of the world. It is an irrevocable part of everyday life in all its aspects. Fortunately, paper is an ecological product. Its main components are the renewable materials and used paper can be unfenced in natural conditions if it's not being used again for the production of recycled paper or some other method.

Modern paper technology is unimaginable without the use of a great amount of subsidiary materials and chemical additives (CA) as well. Added to the renewable materials they above all things form the necessary features of a paper sheet. With their help a number of technological problems are being solved and also they provide a possibility for saving raw materials when at the same time improving paper quality properties [1-3].

Nowadays the first place among raw materials for paper production takes waste paper which has a very positive environmental effect; it saves water, electricity, steam and wood raw material. On the other hand the regenerated fibers have reduced sheet-forming properties and induce problems by the appearance of so-called "stickies". These substances are undesirable components, since reduced and in some cases interfere with the action of the cationic chemical additives (CCA) added for a specific purpose. To solve these issues papermakers use CCA. One of the problems in using secondary fiber material is its lower drainage ability. This necessitates a specific selection of wet-end chemical additives in the composition of recycled papers [4-6].

What is used primarily in the paper production processes are high-molecular weight hydrophilic synthetic polymers (polyelectrolytes) with different chemical nature. Their role is to cause colloid-chemical changes at the barrier surface of the system "fiber-to-water", and especially the values of the electro-kinetic potential. The obtained larger and smaller agglomerates are better retained onto the web. As a result, the dewatering is accelerated, the retention

To whom correspondence should be sent.
E-mail: todorova.dimitrina@uctm.edu

of the components in the paper sheet is improved and this provides a clarified white waters.

Paper is definitely not a factor interfering with the ecological balance of the world. On the contrary - one of the reasons for that is because a basic requirement towards CA for the paper industry is their ecology – it is being put equally in the triangle "functionality - cost – ecology" [6]. What does this mean? The short answer is – to provide:

- Better utilization of resources – here comes into play the recycling process of waste paper and improved components retention;
- Greater economy of energy – this includes the intensification of refining, dewatering and drying;
- Purer waste waters, which include an improved water circuit with maximum use of white waters.

The behavior of paper furnish during dewatering basically depends on the type of fiber material and the degree of its beating (pulp, chemical pulp, waste paper), fillers, sizing agents and used chemical additives.

A fundamental goal in paper production has always been: to get a greater possible quantity of paper with the highest possible quality at the lowest expense possible all the while acknowledging the ecological requirements.

The purpose of this study was to investigate the effect of cationic synthetic polyelectrolytes with different chemical nature and cationic charge over the behavior during the dewatering of paper furnish from recycled fiber material.

EXPERIMENTAL

The investigations were carried out with secondary fiber material from waste newspaper, containing pulp and chemo-thermo-mechanical pulp (CTPM). The slushing of the paper was made in laboratory vertical pulper and the refining degree was 70 °SR. The objective is to disintegrate fiber slurry so that fibers are separated, wetted and are flexible before entering the chemical additives.

As a Chemical Additives (CA) for the investigation of the drainage ability were used six additives by four types of polymers – Polyacrylamide (PAA), Poly Amine (PA), Poly Ethylene Imine (PEI) and PolyDADMAC + PAA. Its characteristics are shown in Table 1. The consumption of the polymers is 0,025%, 0,05%, 0,075% and 0,1% from o.d.f.

During the process of production of CMP are For straightening out the interactions, the Kinetics of the drainage ability of the suspensions was determined, by Schopper Riegler method. The Dewatering time of paper furnishes were determined for 300ml, 400ml, 500ml, 600ml and 700ml, s.

White waters are also being studied:

- Turbidity – NTU nephelometric acc. ISO 7020 (Turb 350 IR);
- Conductivity - μS acc. ISO 7888 (conductometer EC215).

Measuring the electric conductivity gives an indication of the total concentration of electrolyte in the liquid phase.

RESULTS & DISCUSSION

Influence of the quantity and type of chemical additives, on the drainage ability of the suspensions from recycled fiber material. The accelerated dewatering and increased retention as a result of flocculants effect usually means purer waters in paper mill as well. We are going to present experimental data on the behavior of some CA with dewatering and flocculation effect in the structure of various fiber suspensions. The studies are conducted by products with different chemical nature, molecular weight, conductivity and cationic charge density (Table 1).

The above-mentioned CA are being added in quantity of 0.025% to 0.1% from o.d.f. to water suspensions of secondary fiber material.

The effect of the six examined CA on the drainage ability of suspensions can be presented with the change of dewatering time in seconds (Fig 1-6).

The CA in this case definitely improved the dewatering time, even at 0,025% consumption of

Table1. Characteristics of chemical additives.

	Characteristics of chemical additives			
	Chemical substance	Name	Cationic charge	Conductivity, μS
1.	Polyacryl amide (PAA)	Percol 178	+	61
2.	Polyacryl amide (PAA)	Percol 57	++	117
3.	Polyacryl amide (PAA)	Retaminol PCE-304L	+	73
4.	Poly Amine (PA)	Retaminol K	+++	343
5.	Poly Ethylene Imine (PEI)	Retaminol 2S	+++	410
6.	PolyDATMAC 50% + PAA 50%	Fenosil ES 128	++	174

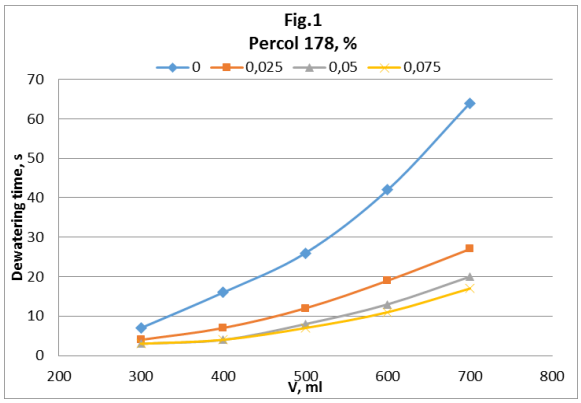

Fig. 1. Dewatering time of secondary fiber suspension at different Percol 178 consumption.

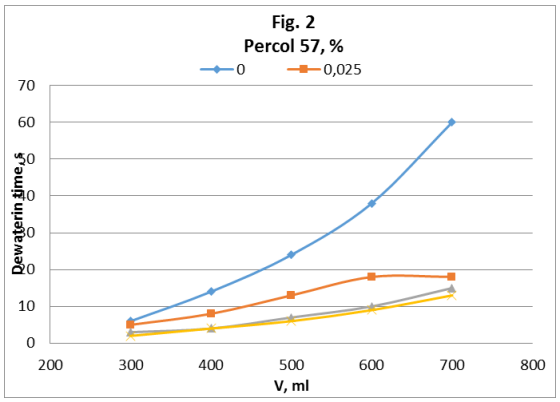

Fig. 2. Dewatering time of secondary fiber suspension at different Percol 57 consumption.

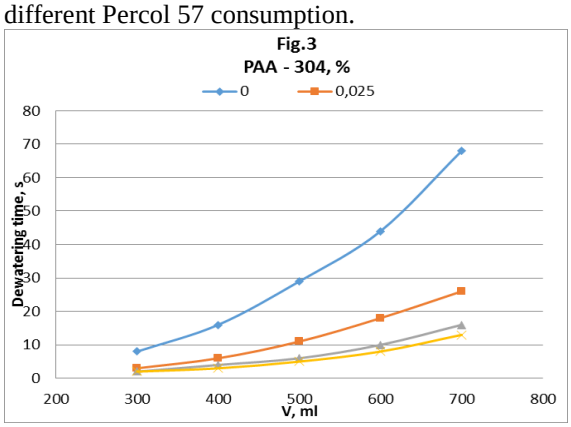

Fig. 3. Dewatering time of secondary fiber suspension at different PAA-304 consumption

the polymers. The figures show that the PAA based CA (Percol 57, Percol 178 and PAA-304) have improved dewatering effect, compared to the other types of polymers (Polyamin K, PEI -2S, PolyDADMAC+PAA). The course of the curves is more uniform with the CA, compared with those without CA.

As it is well known, the cationic PAA are CA with higher molecular weight and lower charge density. They formed agglomerates "water-fibers-cationic-polyacrylamide", through the bridge-

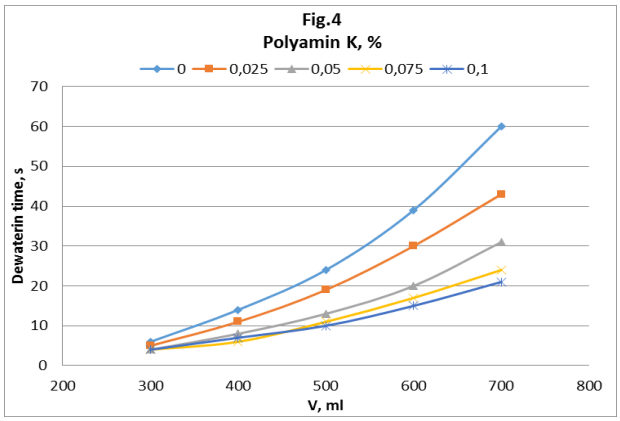

Fig. 4. Dewatering time of secondary fiber suspension at different Polyamin K consumption**.**

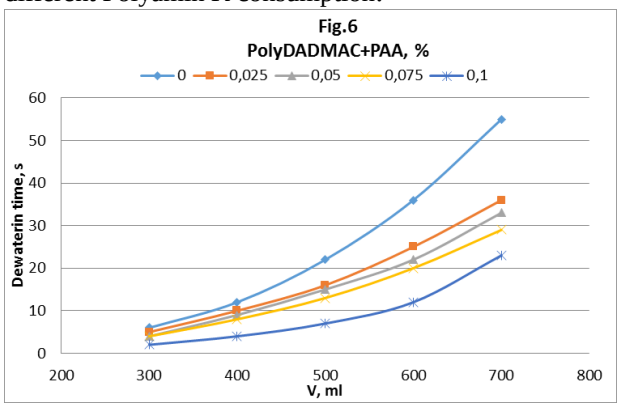

Fig. 6. Dewatering time of secondary fiber suspension at different PolyDADMAC+PAA consumption

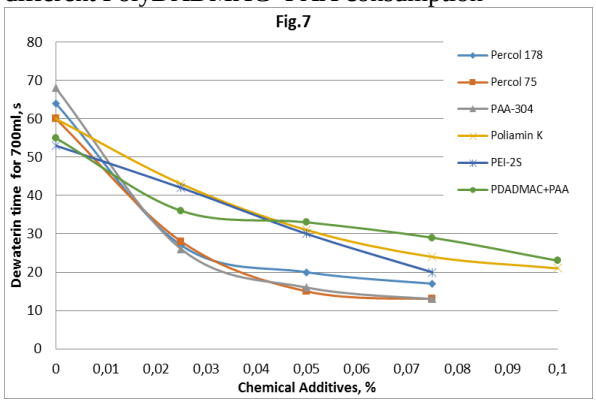

Fig. 7. Dewatering time for 700ml of secondary fiber suspension at different Polyelectrolytes consumption.

forming mechanism. As a result, in the web are formed larger free spaces, without small particles and fines, which results in better water flowing ability. The so- formed flocks are larger with friable structure (macro-flocculation) and the flocculation advanced the dewatering. With increasing the chemical additives, the flocculation capacity is enhanced. With increasing the charge density of the cationic CA, the dewatering is improved.

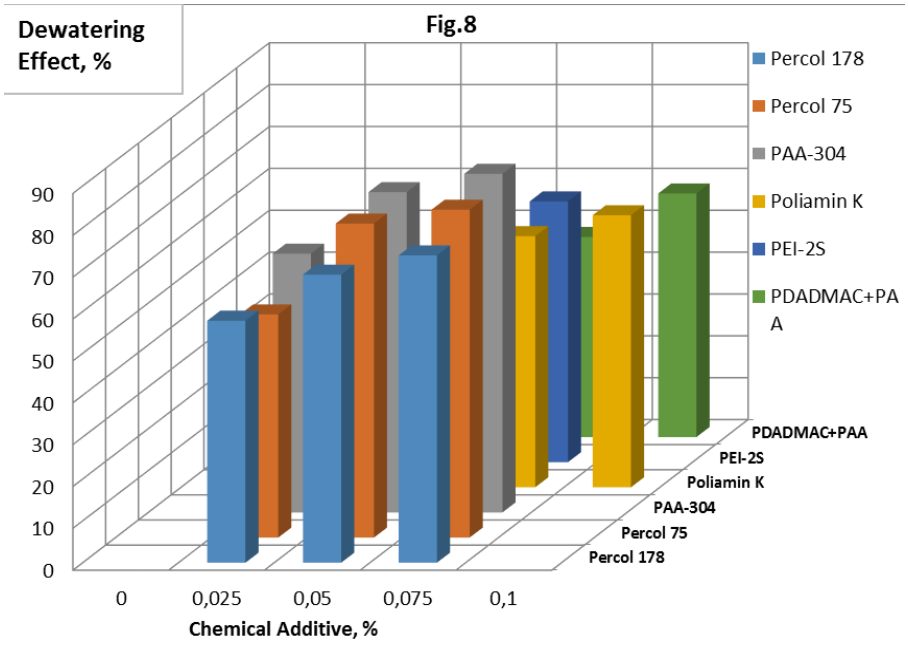

Fig. 8. Dewatering effect of secondary fiber suspension at different Polyelectrolytes and different consumption.

The dewatering effect with the other three CA, based on polyamine, poly ethylene imine and PolyDADMAC, is different and the mechanism of their effect is mainly by the mosaic bonding. They have lower molecular weight and higher charge density. The formed flocks are smaller in relatively compact structure – micro-flocculation.

The effect of the six examined CA on the Dewatering Effect of the secondary fiber suspensions can be presented with the change of dewatering in percentage, calculated with the value of dewatering time at 700 ml filtrate without (T^0_{700}) and in the presence (T_{700}) of certain quantity of chemical additive:

$$Dewatering\ effect = (T^0_{700} - T_{700}) / T^0_{700} .100, \%$$

The obtained experimental results are shown in Fig.8. It can be seen, that PAA-304, at 0,05% consumption, has the highest dewatering effect – 76%. From the other types of CA, the PEI-2S at the same consumption has 43,4% dewatering effect. The CA in this case definitely improved the drainage. According to their dewatering effects at 0,05% consumption, they are being sorted by the nature of the polymers, i.e. the cationic PAA have a better effect: PAA-304 > Percol 57 > Percol 178 > Polyamine K > PEI-2S > PolyDADMAC+PAA. ***Influence of the quantity and type of chemical additives, on the properties of the white waters.*** The investigated secondary fiber material mainly consists of chemo-mechanical pulp, which is a precondition for the appearance of stickies. By the increased mechanical treatment they accumulate more. One of the ways to investigate this process is by measuring the turbidity of the white waters, shown on Fig.9. As it's visible, chemical additives based on cationic PAA, gives the clearest white waters. The other three types are less effective for the clarity of the white waters and with increasing the CA consumption the clarity decreased.

The effect of the six examined CA on the clarification ability of the secondary fiber suspensions can be presented with the change of clarification effect in percentage, calculated with the value of clarity at 700 ml filtrate without (NTU^0_{700}) and in the presence (NTU_{700}) of certain quantity of chemical additive:

$$Clarification\ Effect = (NTU^0_{700} - NTU_{700}) / NTU^0_{700} .100, \%$$

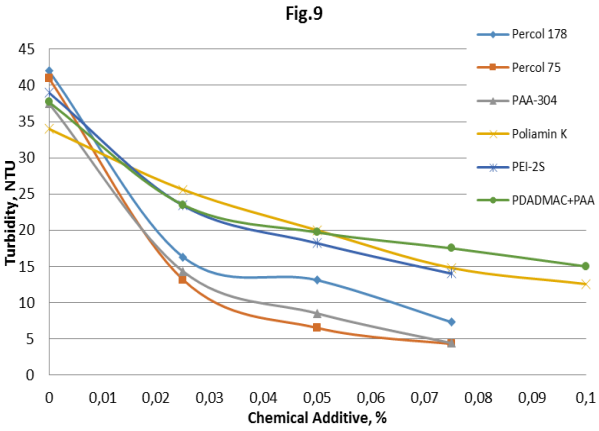

Fig. 9. Turbidity of secondary fiber suspension white waters at different Polyelectrolytes consumption.

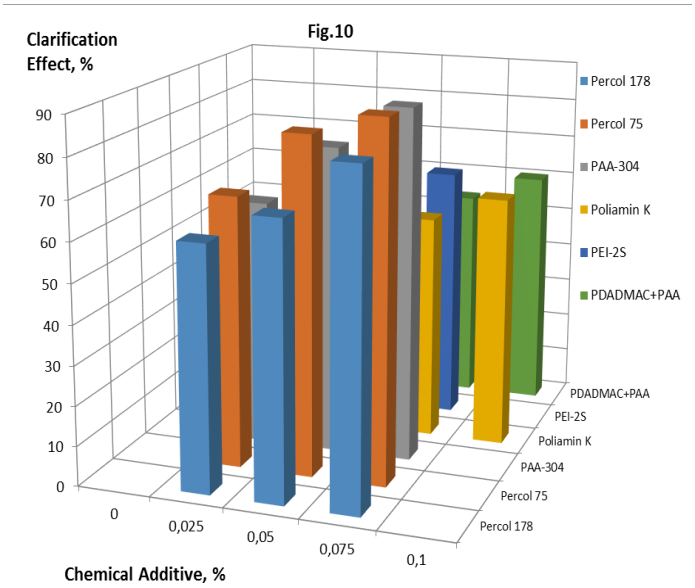

Fig. 10. Clarification effect of secondary fiber suspension at different Polyelectrolytes and different consumption.

Table 2. Conductivity of the white waters.

Conductivity, µS						
Consumption, %	Percol 178	Percol 75	PAA-304	Polyamin K	PEI-2S	PolyDADMAC+PAA
0	152	150	148	146	145	146
0,025	151	149	148	145	145	145
0,05	150	149	148	145	144	144
0,075	150	149	147	145	144	144
0,1				145		143

Fig.10 shows the clarification effect for the sixth investigated polymers at the certain consumption. The highest clarification effect - 84% has the Percol 57 at 0,05% consumption, while with PEI-2S, at the same consumption the clarification effect is 53,4%. The worse effect, at 0,05% consumption, gives the Polyamin K – 41,8%.

The investigations carried out show that for the waste newspaper recycled suspensions the PAA based polymers are particulate, in spite of their low cationic charge. The advisable consumption for the PAA based polymers is from 0,025% to 0,05% from o.d.f., but for the other three types is from 0,05% to 0,075% from o.d.f.

The results for the conductivity of the white waters, shown in Tabl.2 present that with increasing the Percol 178, Percol 57, PAA-304 and PolyDADMAC+PAA consumption, the conductivity parameter decreases. Measuring the electric conductivity gives an indication of the total concentration of electrolyte in the liquid phase. The quantity of the fines in the white waters decreases, because of the enhanced flocculation and retention.

CONCLUSIONS

The obtained experimental results show, that for the acceleration of the dewatering ability of secondary newspaper fiber material, it is appropriate to use chemical additives, based on Polyacrylamide at a consumption of 0,025 ÷ 0,05% from o.d.f.

For enhancing the clarity of the white waters from recycled fiber material it is necessary to use Wet-End chemical additives based on Polyacrylamide.

By its action on accelerating the drainage of the secondary fiber material and the clarification of white water, the studied out chemical additives, used in amount 0.05% from o.d.f. are being sorted by their dewatering and clarification ability, in the following orders:

Dewatering ability:

PAA-304 > Percol 57 > Percol 178 > Poliamin K > PEI-2S > PolyDADMAC+PAA

Clarification ability:

Percol 57 > PAA-304 > Percol 178 > PEI-2S > PolyDADMAC+PAA > Poliamin K.

REFERENCES

1. L. Wagberg, L. Winter, Papermaking chemicals and their function. In: Applications of Wet-End Paper Chemistry, Au C.O., Thorn I. (Eds.), Blackie Academic & Professional, Glasgow, 1-11, (1995).
2. R. Isermann, *Wochenblatt f. Papierfabrikation*, **131**, 629 (2003).
3. M. Soeffge, *Wochenblatt f. Papierfabrikation*, **131**, 28 (2003).
4. J. Gullichsen, H. Paulapuro, "Papermaking Chemistry", TAPPI PRESS, 1999.
5. J. Casey, "Pulp and paper Chemistry and Chemical Technology", Volume III, 1979, USA.
6. S. Kleemann, *IPW / Das Papier*, Nr. 9, 31, (2003).
7. P. Rosenthal, *Wochenblatt f. Papierfabrikation*, **119**, 951 (1991).

ИЗСЛЕДВАНЕ ВЛИЯНИЕТО НА ХИМИЧЕСКИ СПОМАГАТЕЛНИ ВЕЩЕСТВА ВЪРХУ ПОВЕДЕНИЕТО НА СУСПЕНЗИЯ ОТ РЕЦИКЛИРАН ВЛАКНЕСТ МАТЕРИАЛ ОТ ВЕСТНИЦИ

Д.А. Тодорова*, С.П. Бенчева

Химикотехнологичен и металургичен университет, София 1756, бул. Климент Охридски №8

Постъпила на 30 юли, 2014 г.; приета на 13 февруари, 2015 г.

(Резюме)

Използването на вторични влакна от отпадъчна хартия се налага като основна тенденция при производството на различни видове хартии и картони, което има изключителен положителен екологичен ефект, спестява разходи на вода, на електрична енергия, пара и дървесна суровина. От друга страна регенерираните влакна имат понижени листообразуващи свойства и създават проблеми, причинени от появата на т.н."пречещи вещества". Тези вещества са нежелателни компоненти, тъй като редуцират, а в някои случаи смущават действието на катионните химични спомагателни вещества /ХСВ/, добавени с определена цел. За решаването на тези въпроси се използват ХСВ.

Основно се използват високомолекулни хидрофилни синтетични полимери /полиелектролити/ с различна химична природа. В резултат на тяхното действие се ускорява отводняването, подобрява се задържането на компонентите в хартиения лист и се осигуряват по-бистри подситови води.

Целта на настоящото изследване е да се изучи влиянието на катионни синтетични полиелектролити с различна химична природа и заряд върху поведението при отводняване на суспензия от рециклиран влакнест материал от отпадъчна хартия.

Рециклираният влакнест материал, с който се осъществяват експериментите е от отпадъчна вестникарска хартия. При провеждането на изследванията са използвани различни по своята химична природа катионни синтетични полиелектролити, различаващи се по молекулна маса и плътност на заряда.

В резултат на проведените изследвания се установи, че за подобряване на отводняването и за избистряне на подситовите води, най-целесъобразно е използването на ХСВ на основата на полиекриламид.

Bulgarian Chemical Communications, Volume 47, Special issue A (pp. 51 –59) 2015

Effect of dry-heat ageing on label paper quality

V. Radkova, P. Tsekova, T. Ivanova, I. Valchev*

University of Chemical Technology and Metallurgy, 1756 Sofia, Bulgaria

Received July 30, 2014; Accepted January 30, 2015

Ageing of paper can be defined as a sum of all irreversible physical and chemical processes which appear in the material during time. Brightness reversion is of importance for high brightness paper producers. Reversion is a result of chromophores generation via condensation reactions.

The impact of dry-heat ageing on strength and optical properties of label paper was studied. Three types of pigment coated label papers were used. Dependence of Pc number on reaction time for three different temperatures was examined. The studies showed that it increases significantly in the paper with denser surface layer. This was determined by the chromophore structures in pigment surface layer. The kinetics of the ageing process was described most precisely by an exponential kinetic equation for all types of sample papers.

Second examination was carried out to determine the color stability of aged digital prints. The label papers were printed by multicolor printing device and artificially aged using the same technique of accelerated ageing. Differences between aged and non-aged papers were analyzed. Their colorimetric characteristics are represented by means of color difference ΔE^*_{ab}.

***Key words**: dry-heat ageing, label paper, exponential kinetic equation, color difference*

INTRODUCTION

The mechanism of ageing involves numerous interactions between substances in the paper and with its surroundings. These could be defined by deterioration in the mechanical strength, loss of chemical stability and deterioration of the optical characteristics of the paper [1]. The term "permanence" describes the ability of paper to remain chemically and physically stable over long periods of time. The durability depends mainly on the physical and mechanical characteristics of the principal raw materials and on contamination by ions from the environment, the action of light, heat, humidity and microorganisms [2,3]. A study of the natural ageing of paper can take several years to register certain paper properties. To solve these problems of hostile environment which are more aggressive than the normal environment conditions are implemented. The first and the most widespread approach is the exposure to elevated temperatures, usually referred to as thermal accelerated ageing. Accelerated ageing tests are often used to determine the changes of the permanence and durability of paper, as well as to predict the long-term effect of a paper usage [4,5]. Heat is one of the most important environmental influences on the stability of papers [6]. In the accelerated ageing method proposed by TAPPI [7], the material is exposed in a climate chamber at extreme temperature for a certain period of time, during which the changes in the material are measured. The reasons for the loss of strength with ageing are not completely understood, but they are presumed to be directly related to changes that occur at molecular level. Consequently, the concept of chemical kinetics in quantifying the effects of aging is applied. In the chemical kinetics approach, the loss of strength property with time is used to characterize the rate of deterioration of the material [8,9]. "ZOU *et al.* [10,11]" conducted a general kinetic analysis to investigate the aging process of paper. The results from their investigation proved the accurate usage of accelerated aging tests for paper permanence prediction.

In case of label papers the permanence is of great importance. This type of paper is used for different products labeling: bottles, containers etc. Each label carries not only important data but also graphical information for the brand. That is why paper`s color characteristics stability over time is important. Moreover the physical and mechanical properties have to satisfy high demands because the labeled product often experiences a lot of different kinds of environments, which can damage or deteriorate its quality. Depending on the product, the label may be exposed to extreme moisture or dryness, elevated heat or cold, physical tortures and other unforeseen circumstances over time.

The aim of the present study is to determine the impact of dry-heating ageing on the quality of label paper properties. This will allow identification of

To whom correspondence should be sent.
*E-mail: ivoval@uctm.edu

the stability of paper when aged under normal conditions of use and handling over time.

The accomplishment of this goal requires estimation of the impact of dry-heat ageing on the strength and optical properties of the label paper. This was done by analyzing the following parameters:

- mechanical properties of the tested papers;
- ageing by means of ISO Brightness (R457 nm) loss and Pc number (post color number);
- kinetics of the ageing process;
- colour differences between aged and non-aged printed images.

EXPERIMENTAL

Three types of pigment coated label papers were examined. Their properties according to the technical data are presented in Table 1. The specimens were put under accelerated ageing in oven with forced ventilation. Experiments were carried out at 85ºC, 105ºC and 125ºC for 4 hours ageing time.

Table 1. Technical data for the three types of label paper

Paper, [№]	Opacity, [%]	Gloss, [%]	ISO Brightness, [%]
1	90±2	72±3	88±2
2	≥ 84	65±5	92±3
3	94	70	87

In order to characterize the paper some important mechanical and strength properties were examined. The research includes experimental data for tensile strength, tearing resistance and bursting strength. The tests for tensile strength were done according to ISO 1924:2008 [12]. The tearing resistance and bursting strength were determined in conformity with ISO 1974:2012 [13] and ISO 2758:2001 [14] respectively. The selected properties of the three types of paper are compared before and after the second and the fourth hour of ageing.

Since the loss of brightness is an index for the yellowing of paper, ISO Brightness values were studied during the accelerated ageing for the three types of paper. Specimens were measured at regular time intervals within four hours. The measurements were carried out according to ISO 2470-1:2009 [15] with Elrepho "Datacolor 2000" spectrophotometer. Behavior of fiber material subjected to ageing was characterized in term of relative variation of Kubelka-Munk (k/s) function using the experimentally obtained brightness values. In order to show the comparison of the magnitude of yellowing for the three label papers a recalculation of Pc number was accomplished. The kinetics of the ageing process, based on the calculated Pc numbers, was examined and applicability of different kinetic equations valid for heterogeneous processes was verified.

Color stability of printed test charts was investigated in order to determine the usability of the label papers for long periods of time. The charts were printed on the three types of paper with 6 channel ink-jet printing device. Since offset printing is the most popular process device linked profile was created to simulate this type of printing. Chart with 452 patches was generated including patches for determining the color densities of CMYK process colors and halftone values. The device link profiles were applied to the test chart according to the paper types and then were printed. The samples were put under accelerated ageing for 8 hours at 105^0C. Their colorimetric characteristics were measured with X-Rite Spectroscan spectrophotometer at regular time intervals. The color differences between non-aged and aged prints are represented in terms of ΔE_{ab}.

RESULTS AND DISCUSSION

Mechanical properties

Studies of the ageing influence on tensile length and tear index for the three types of label papers were carried out in machine and cross direction. Figure 1 illustrates the obtained results for tensile strength measured at different temperatures. It can be seen that in the course of ageing at different temperatures the tensile length in both directions increases for the three types of examined papers. It was found that after the second hour of accelerated ageing the tensile length changes for Paper No 1 and Paper No 2 are minimal with respect to the initial values. After the fourth hour of ageing the experiments at 85ºC showed marginal changes in the tensile length. Significant changes were observed in the tensile length measured for Paper No 3. As an exception, the experimental data for Paper No 3 showed correlation between tensile length and temperature of ageing.

The measured values for the tensile length in cross direction for Paper No 3 differ significantly from those for the other types. This can be explained with the denser pigment surface layer. When ageing is carried out at higher temperature cross-linking reaction appears. As a result the fiber bonding in cross direction is getting stronger, which increases the tensile length.

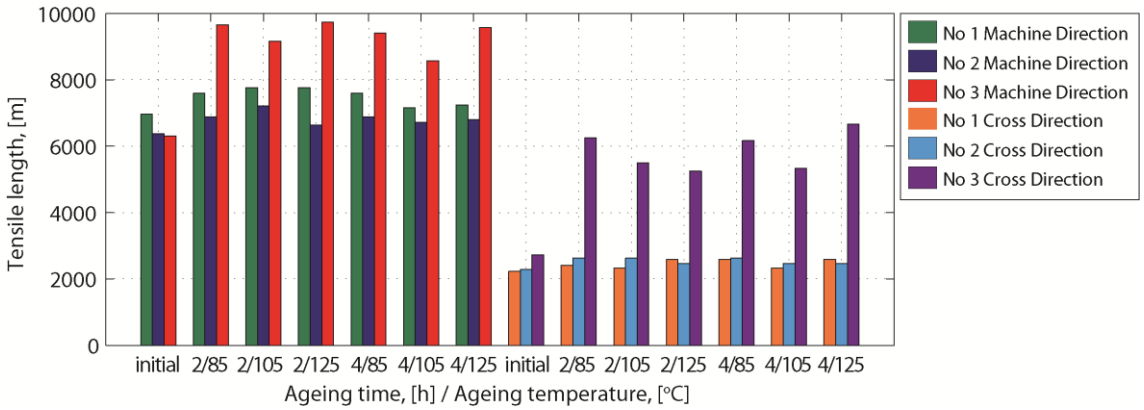

Fig. 1. Effect of ageing time and temperature on tensile length in machine and cross direction for the three types of label paper.

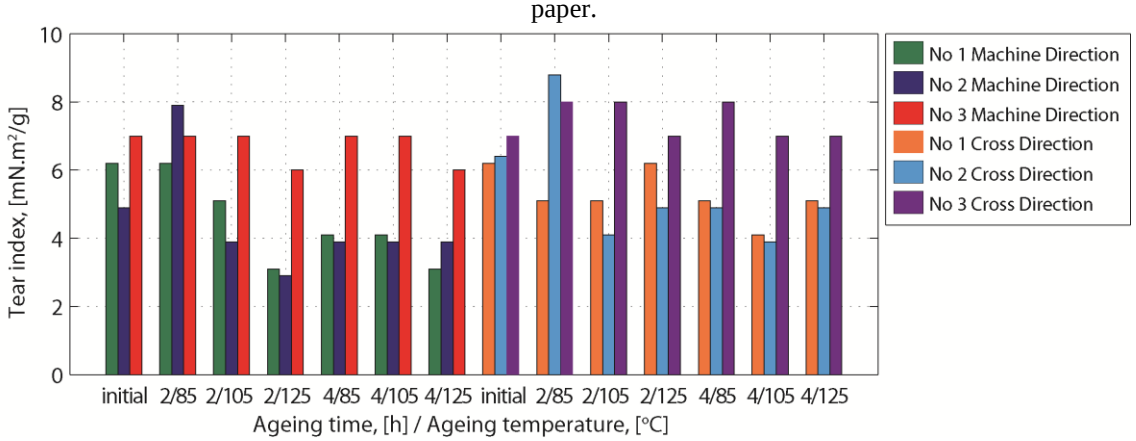

Fig. 2. Effect of ageing time and temperature on tear index in machine and cross directions for the three types of label paper.

The essential chemistry, structure and morphology of the fibers which form the paper as well as their mutual disposition are reflected by the mechanical and strength properties of the paper. The latter also reflect the chemical changes in the paper permanence caused by time. The most commonly used tearing test, measures the internal tearing resistance of paper. Figure 2 shows the obtained results for the tear index measured at different temperatures for the three types of label papers. It is seen that the tear index for Paper No 1 and No 2 decreases with increasing temperature and ageing time. Paper No 3 had slightly different behavior. Its tear index showed correlation to the temperatures used for the experiment rather to the ageing time. The lowest index has been measured at 125ºC.

The tear index measured in cross direction for Paper No 1 decreases most significantly after the fourth hour of accelerated ageing at 105ºC. Measured values of the tear index for Papers No 2 and No 3 after the second hour of ageing at 85ºC increased, while those for Paper No 1 decreased. This experimental data can serve as indicator of the permanence of paper. The results prove that ageing changes the fiber structure, their length and consequently affects the paper permanence.

In support to this conclusion are the results for burst index of the label papers reported in Table 2. This indicator for Paper No 1 and No 2 does not change during the aging process, while increases significantly for Paper No 3. The reason is the polymerization process during ageing which forms a denser surface layer.

Yellowing

Yellowing is reported either as loss of ISO Brightness units or after recalculation as Pc number. The ISO method is used when papers with same ISO Brightness are compared. The main advantage of the approach is the clear understanding of the magnitude of yellowing. The chromophore concentration is not linearly related to the ISO Brightness, but is linked to it via the Kubelka-Munk equation (Eq.1):

$$\frac{k}{s} = \frac{(1-R_\infty)^2}{2.R_\infty} \quad , \qquad (1)$$

Table 2. Effect of ageing time and temperature on the burst index for the three types of label paper

Paper, [№]	Burst index of zero sample, [kPa.m^2/g^{-1}]	Ageing time, [h]	Burst index at 85^{0}C [kPa.m^2/g^{-1}]	Burst index at 105^{0}C [kPa.m^2/g^{-1}]	Burst index at 125^{0}C [kPa.m^2/g^{-1}]
1	2.7	2	2.8	2.9	2.9
		4	2.8	2.8	3.1
2	2.5	2	2.4	2.7	2.4
		4	2.3	2.8	2.4
3	2.2	2	3.5	3.6	3.6
		4	3.7	3.5	3.7

Fig.3. Micrographs of polyurethane-keratin membranes: a) keratin salt, b) dialyzed keratin, c) alkaline biofiber solution, d) acid biofiber solution, all of them at 15 wt.% [40].

where k is the absorption coefficient, s is the scattering coefficient and R_∞ is the ISO Brightness. The values for the k/S factors were calculated using the experimentally obtained brightness units for the three types of label papers aged at different temperatures. In order to achieve better accuracy the Pc number was recalculated according to Eq.2.

$$Pc = 100\left[\left(\frac{k}{s}\right)_{afterageing} - \left(\frac{k}{s}\right)_{beforeageing}\right], \quad (2)$$

where the scattering coefficient s is unaffected by the yellowing.

Physical factors affecting yellowing of paper include humidity, temperature and time. One of the major phenomena of paper ageing is the trend for reduced brightness and increased yellowness. Figures 3, 5 and 7 show the brightness reversion versus time of ageing at various temperatures for each of the examined types of label papers. Obviously the brightness decreases with increasing temperature and time of ageing. The figures have inherent shapes indicating stable correlation between the brightness loss and temperature. The yellowing increases as the retention time increases. The measured values are similar for the first and second type of papers. The third type has slightly different behavior due to differences in the pigment and binder used for coating. The experimental data were sufficiently well described by one-term power series model.

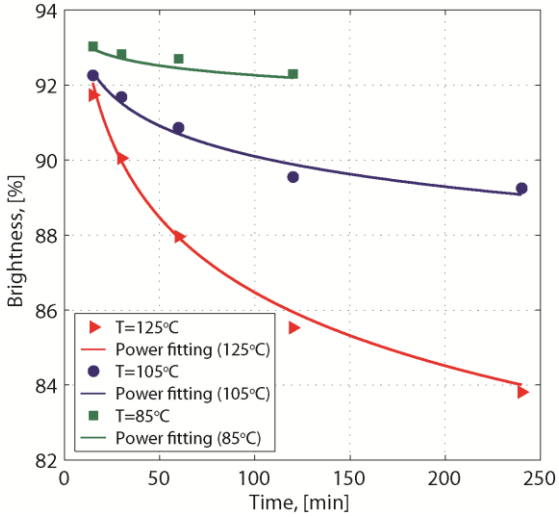

Fig. 3. Brightness dependence on temperatures for paper No 1.

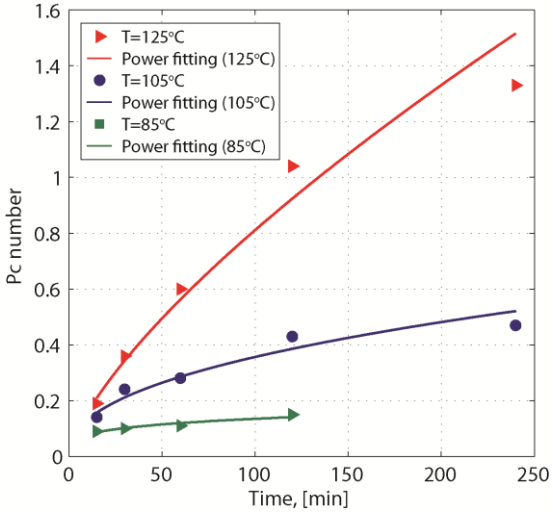

Fig. 4. Pc number dependence on temperatures for paper No 1.

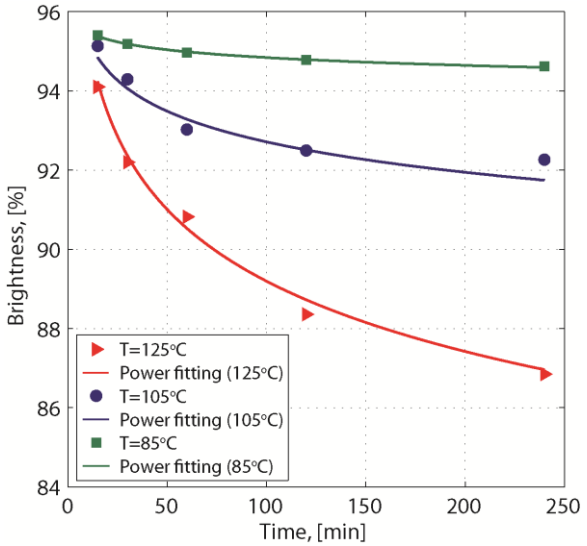

Fig. 5. Brightness dependence on temperatures for paper No 2.

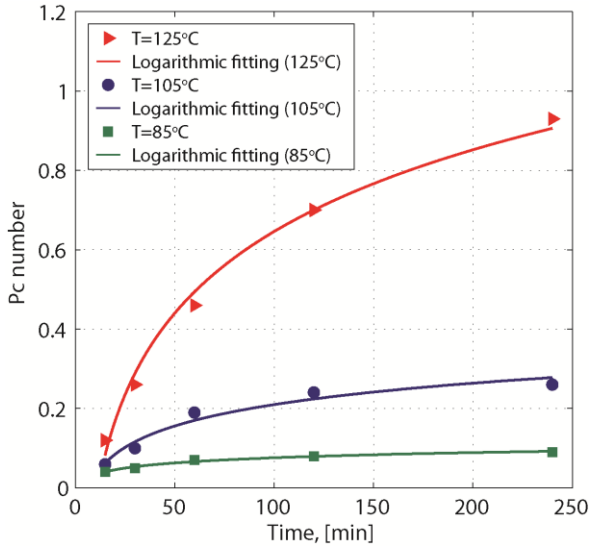

Fig. 6. Pc number dependence on temperatures for paper No 2.

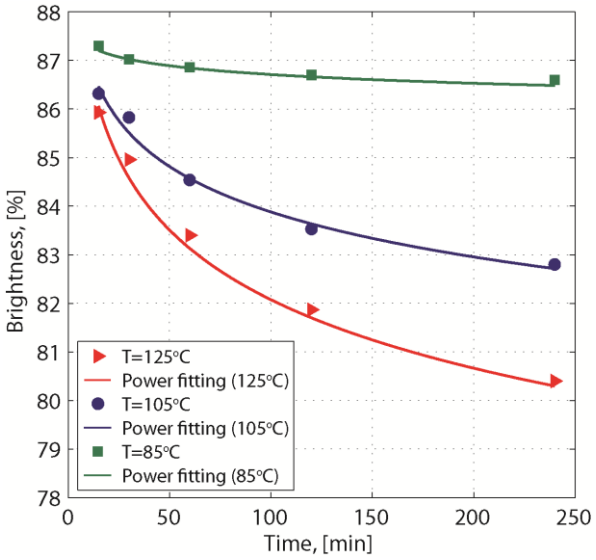

Fig. 7. Brightness dependence on temperatures for paper No 3.

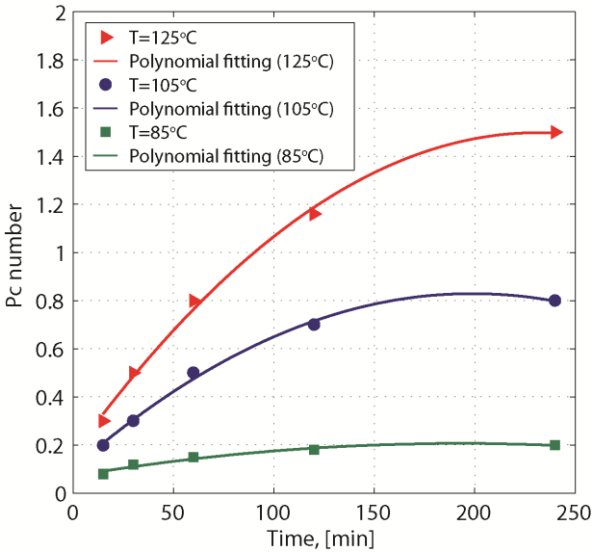

Fig. 8. Pc number dependence on temperatures for paper No 3.

The brightness reversion was also recalculated to Pc number and plotted versus the ageing time. Figures 4, 6 and 8 illustrate the time dependence calculated for the label papers at different temperatures. The figures show good correlation and stability of the ageing process, which proves the general decrease in brightness. The experimental data obtained for Paper No 1 were well described by one-term power series model. Logarithmic equation was used for description of the Pc number data calculated for paper No 2. Second degree polynomial model successfully fitted the calculated data for Paper No 3.

Kinetics of the ageing process

In accordance with Pc number dependences on reaction time kinetic curves were plotted for the three label papers. As already discussed the changes of the Pc number values are with similar characteristics. A representative kinetics of the aging process for Paper No 3 is presented. The experimental data was recalculated in terms of dimensionless quantity α to present the corresponding kinetic curves at different temperature values. The quantity α has a meaning of degree of the ageing and has been used as a kinetic variable. It was calculated in correspondence with equation (Eq. 3):

$$\alpha = \left(\frac{k}{s}\right)_{afterageing} - \left(\frac{k}{s}\right)_{beforeageing}, \qquad (3)$$

where the k/s values changes describe the Pc number values and illustrate the brightness

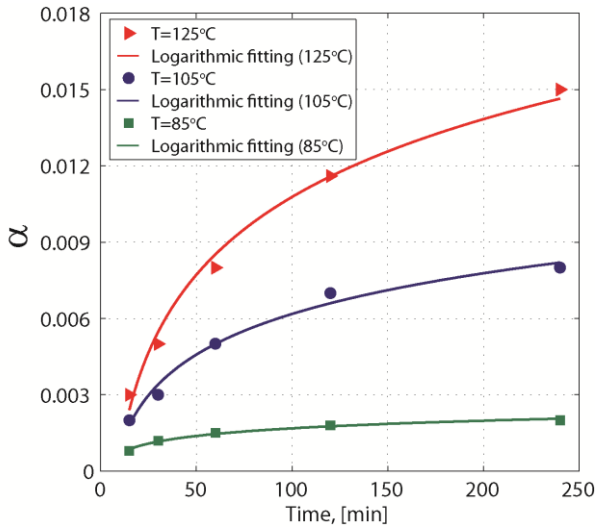

Fig. 9. Described kinetic curves of the ageing at all temperatures for paper No 3.

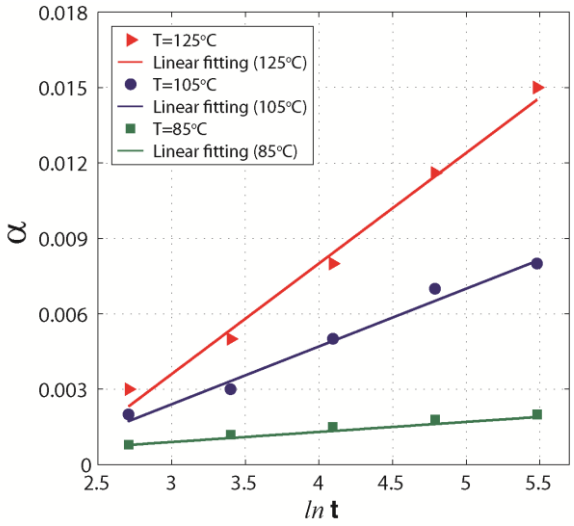

Fig. 10. Linearized kinetic curves of the ageing at all temperatures for paper No 3.

reversion. Figure 9 illustrates α as a function of the ageing time for experimental based recalculations for Paper No 3. As it can be seen the degree of ageing increases with increasing time and temperature.

After verification of applicability of different kinetic equations valid for heterogeneous processes was found that the accelerated ageing process was best described by an exponential kinetic equation. This equation is valid for processes which are taking place on uniformly inhomogeneous surfaces like the label papers surfaces [16]. According to the model of uniformly inhomogeneous surfaces expressed by Eq. 4 the active centers on the surface are distributed linearly referring to their energy and entropy,

$$v = v_0 e^{-a\alpha} \qquad (4)$$

where $v = d\alpha/dt$ is the current rate and v_0 is the initial rate of the ageing process. The kinetic coefficient of inhomogeneity α, which is temperature-dependent term, accounts for the energy and the entropy inhomogeneity of the system [17].

Figure 10 shows α values for three temperatures as a linear function of lnt in correspondence with the approximate integral form of the exponential kinetic equation (Eq.5):

$$\alpha = \left(\frac{1}{a}\right)\ln(v_0 a) + \left(\frac{1}{a}\right) lnt \ . \qquad (5)$$

The kinetic coefficient of inhomogeneity *a*, which is temperature-dependent term, accounts for the energy and entropy inhomogeneity of the system.

Equations 5 and 4 were used respectively for estimation of the initial rate v_0 and current rates v of the ageing process performed at the three temperature values. Their linearized values in accordance with Equation 4 are presented in Figure 11. It is seen that the current rate decreases in the course of the process.

As a proof of this conclusion the results for linearized process rate values calculated at 105°C ageing temperature for the three types of label papers are presented in Figure 12. It is seen that the current rate decreases in the course of the process with increasing of the ageing degree.

The temperature dependence of ageing rate constants was described by the well-known Arrhenius equation (Eq.6):

$$v = Ae^{-E/RT} \ , \qquad (6)$$

where *A* is the pre-exponential factor, *E* is the activation energy (kJmol-l). This dependence was applied for the initial rate and calculations for the initial activation energy and pre-exponential factor were done. In Table 3 are summarized the values calculated for the three types of paper. It can be seen that the differences in the activation energy values are minimal for the examined papers. It was found that the activation energy is a determinant for the decreasing rate of the ageing process. The higher pre-exponential factor value for Paper No 3 could be explained with the different pigment layer of the label paper. The ageing process was localized in the surface layer which is determined by the pigment surface coatings used for the three examined label papers. The initial stage of the process affects more active chromophores. During the ageing process new chromophore groups are generated. This new active centers are with decreasing reactive ability with increasing of the ageing time.

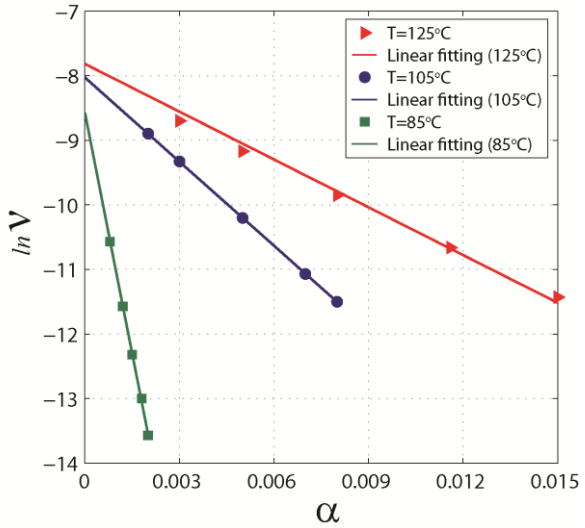

Fig. 11. Linear dependence of process rate vs. ageing degree for paper No 3.

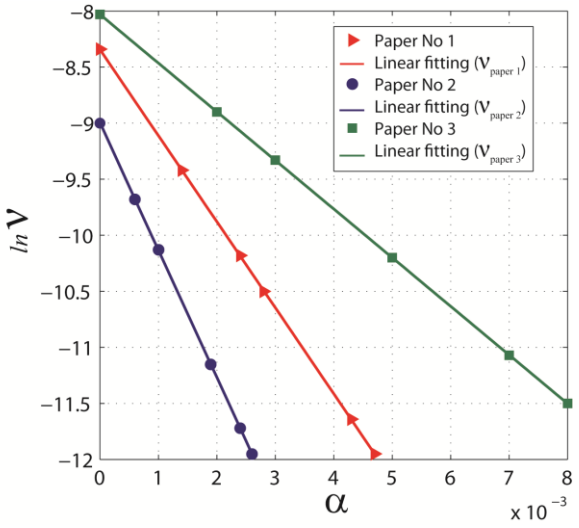

Fig. 12. Linear dependence of process rate vs. ageing degree for all types of paper.

Table 3. Initial activation energy E_0 and pre-exponential factor for all types of paper.

Paper No		2	3
E_0, [kJ/mol]	26.3	26.7	29.7
lnA_0	1.02	0.87	4.06

Colour differences

The permanence of the examined label papers was studied in term of color stability of printed images. Ink-jet system with dye-based inks was used for the printing process. Dye inks are prepared by dissolving of the liquid colored dyes into a fluid carrier. This makes them easy to apply. When they are applied to a paper, the dyes are absorbed very uniformly and reflect light very evenly. During ageing the properties of the paper and ink are simultaneously changing. Hence the durability of the prints depends not only of their chemical composition but also of the physical characteristics of the printed paper.

One of the main quality characteristics of a printed testcharts is the color difference between measured and reference solid process colours. Figure 13 illustrates the obtained colour differences differences were obtained for Paper No 3 due to the denser pigment layer of this paper and its more stable surface structure. The differences are higher at the end of the ageing process.

Figure 14 demonstrates the maximum and averaged colour differences between all ink colours on non-aged samples and aged printouts of the for solid patches of the four process colours on aged papers in relation to the prints on non-aged papers. The color difference was calculated in term of ΔE^*_{ab} in accordance with Equation 7:

$$\Delta E^*_{ab} = \sqrt{(\Delta L^*)^2 + (\Delta a^*)^2 + (\Delta b^*)^2}\ , \quad (7)$$

where $\Delta L^* = L^*_2 - L^*_S$, $\Delta a^* = a^*_2 - a^*_S$, $\Delta b^* = b^*_2 - b^*_S$ are the distances between aged and non-aged colour values in the coordinates respectively of L^*, a^* and b^*. The value of ΔE^*_{ab} is perceptually similar to human's visual perception of color difference. The dimensionless values of ΔE^*_{ab} can be roughly classified into three different levels to reflect the degrees of color difference perceived by human. The color difference is hardly perceptible when ΔE^*_{ab} is smaller than 3; is perceptible but still tolerable when ΔE^*_{ab} is between 3 and 6; and not acceptable when ΔE^*_{ab} is larger than 6 [18]. From the results can be seen that all colour shifts are tolerable. Lowest colour

three types of paper. According to the experimental data Paper No 3 is less influenced by the accelerated ageing but all obtained results are tolerable. The averaged differences are hardly perceptible. This manifests that the prints are stable during time.

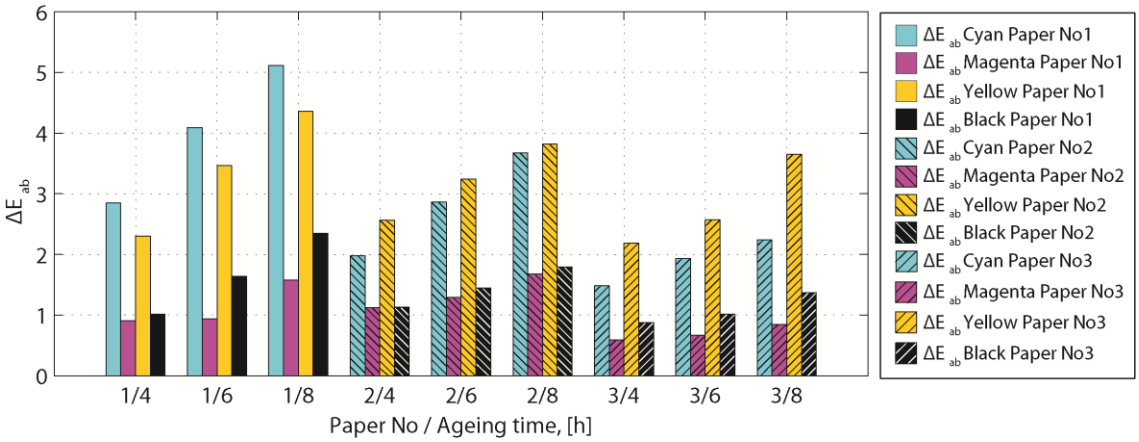

Fig. 13. Ageing influence on color differences for full tone CMYK.

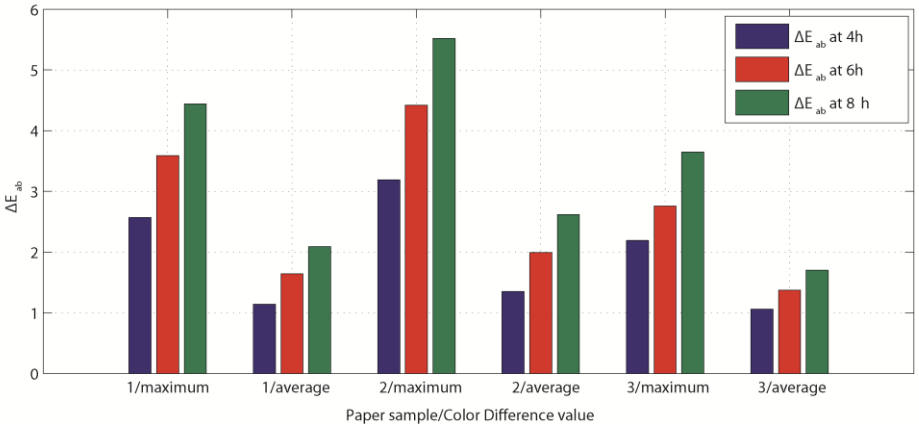

Fig. 14. Ageing influence on color differences of printed testcharts

CONCLUSION

Experimental data showed that paper No 3 has slightly different behavior in respect of brightness reversion compared to other studied label papers. This can be explained with the denser pigment surface layer and different pigment surface coating.

The kinetics of the ageing process was studied. The results indicated that the process takes place at the surface. As the paper surface is uniformly inhomogeneous an exponential kinetic equation valid for this type of processes was successfully applied to describe the experimental kinetic data. The temperature-dependent kinetic coefficient, which takes into account the energy and entropy of the ageing, was determined.

Analysis of the kinetics of the ageing process showed that similar initial activation energies are found for the three types of label papers. The activation energy was found to increase in the course of the ageing process because of the formation of new active centers.

All three types of paper are suitable for labeling applications due to their resistance of mechanical and optical properties to accelerated ageing.

REFERENCES

1. S. Zervos, in: Cellulose: structure and properties, derivatives and industrial uses, A. Lejeune, T. Deprez (eds), 2010. p. 155–203.
2. M. Area, H. Cheradame, Paper aging, methods, *BioResources*, **6**, 5307 (2011).
3. H. El-Saied, A.H. Basta, M.M. Burns, Permanence of paper, *Restaurator*, **21**, 89 (2000).
4. HJ. Porck, Rate of Paper Degradation, *European Commission on Preservation and Access*, Amsterdam, pp. 11-23 (2003).
5. B.T. Hotle, J.M. Considine, M.J. Wald, R.E. Rowlands, K.T. Turner, Effects of Thermal Aging on Mechanical Performance of Paper, *Proc. 11th Int. Congr. and Expos.*, Orlando, Florida, USA, 2008.
6. https://www.imagepermanenceinstitute.org/webfm_send/313.
7. TAPPI UM 200, Brightness loss of bleached pulp (2012).
8. M. Karlovits, D. Gregor-Svetec, Durability of Cellulose and Synthetic Papers Exposed to Various Methods of Accelerated Ageing, *Acta Polytechnica Hungarica*, **9**, 81 (2012).
9. D. F. Caulfield, D. E. Gunderson, Paper testing and strength characteristics, *TAPPI Proc. of the 1988 paper preservation symposium*, pp. 31-40 (1988).

10. X. Zou. T. Uesaka, N. Gurnagul, Prediction of paper permanence by accelerated aging I. Kinetic analysis of the aging process, *J. Cellulose*, **3**, 243 (1996)
11. X. Zou. T. Uesaka, N. Gurnagul, Prediction of paper permanence by accelerated aging II. Comparison of the predictions with natural aging results, *J. Cellulose*, **3**, 269 (1996).
12. ISO 1924-2:2008 Paper and board - Determination of tensile properties.
13. ISO 1974:2012 Paper - Determination of tearing resistance - Elmendorf method.
14. ISO 2758:2001 Paper - Determination of bursting strength.
15. ISO 2470-1:2009 Paper, board and pulps. Measurement of diffuse blue reflectance factor.
16. G. Radeva, I. Valchev, S. Petrin, E. Valcheva, P. Tsekova, Kinetic study of the enzyme conversion of steam exploded paulownia tomentosa to glucose, *BioResources*, **7**, 412 (2011).
17. G. Radeva, I. Valchev, S. Petrin, E. Valcheva, P. Tsekova, Comparative kinetic analysis of enzyme hydrolysis of steam-exploded wheat straw, *J. Cellulose Chem. Technol.*, **46**, 61 (2012).
18. J.Y. Hardeberg, PhD Thesis, École nationale supérieure des télécommunications, Paris, France, 1999.

ВЛИЯНИЕ НА ТЕРМИЧНОТО СТАРЕЕНЕ ВЪРХУ КАЧЕСТВАТА НА ХАРТИЯ ЗА ЕТИКЕТИ

В. Радкова, П. Цекова, Т. Иванова, И. Вълчев*

Химикотехнологичен и металургичен университет, София, 1756, България

Постъпила на 30 юли, 2014 г.; приета на 30 януари, 2015 г.

(Резюме)

Стареенето на хартията може да бъде разгледано като резултат от всички необратими физични и химични процеси, които възникват в материала в течение на времето. Понижаването на белотата е един от тези процеси, които са от значение за производителите на висококачествени бери хартии. Реверсията е в резултат от образуването на хромофорни структури в резултат на реакции на кондензация.

Влиянието на термичното стареене върху механичните и оптични свойства на хартия за етикети е предмет на настоящото изследване. За анализа са използвани три вида пигментно покрита хартия. Изследвана е зависимостта на Pc числото от продължителността на стареене при три различни температури. Резултатите показат значително нарастване при хартията с по-плътен повърхностен слой. Това се определя от хромофорните структури в пигментния повърхностен слой. Кинетиката на процеса на стареене при всички използвани хартии се описва най-точно от експоненциалното кинетично уравнение.

Проведено е допълнително изследване за определяне стабилността на цветовите характеристики на дигитални отпечатъци при термично стареене. Върху хартиите за етикети са направени отпечатъци посредством многоцветно печатащо устройство и подложени на термично стареене, при същите условия. Анализирани са разликите между начални отпечатъци и такива, които са подлагани на стареене. Техните колориметрични характеристики са представени като цветна разлика ΔE^*_{ab}.

Bulgarian Chemical Communications, Volume 47, Special issue A (pp. 60 – 63) 2015

Improvement of the physical-mechanical and optical properties of printing production with biodegradable overprint varnishes

T. Bozhkova, I. Spridonov, Y. Nedelchev*, R. Boeva, A. Ganchev

University of Chemical Technology and Metallurgy – Sofia
Kl. Ohridsky blvd. 8, Sofia 1756, Bulgaria

Received August 1, 2014; Accepted February 23, 2015

Due to limited fossil resources and an increased need for environmentally friendly, sustainable technologies, the importance of using renewable resources in ink and coating industries will increase in years to come. Other than traditional water-based coatings, which are based on petroleum derivatives, biodegradable coatings focus on resins and waxes from nature. Biodegradable coatings are based on natural resources for more than 90% and are biodegradable more than 75%, which makes it possible to dispose coating remains and washing water directly in a clarification plant, after approval from corresponding authorities. To be able to fully replace the conventional water-based coatings, which main components are acrylate and styrene acrylate polymers, the biodegradable coatings should be able to cover the main quality requirements – stable running characteristics on the printing press, scuff and scratch resistance, wet block resistance and satisfying optical properties. The current research highlights the primary quality differences between biodegradable and conventional coatings and their optical, chemical and physical characteristics.

Keywords: *biodegradable coatings, water-based coatings, physical-mechanical characteristics, optical properties*

INTRODUCTION

Nowadays we can classify the overprint varnishes into 4 main groups, depending on their contents, applications and drying methods – oil-based, solvent-based, water-based and UV [4, 5].

They are applied on special coating units that are coupled in-line to the printing press or on off-line coating machines, outside the printing press or even printing house.

The following qualities of the printed product are achieved by coating with a dispersion varnish: abrasion protection, scuff resistance in a wet condition (labels), high gloss, silk finish, or matte effects, hot-seal resistance, gliding quality, deep freeze resistance, fixing of metallic inks. [6]

In recent years an increasing interest is observed in development of eco-friendly materials. Oil-based polymers are slowly being replaced by such from renewable resources. Biodegradability and compostability play very important role for environmental sustainability. Some biodegradable polymers possess excellent mechanical properties, thermal and UV resistance; however production capacity, processing challenges, adhesion, barrier properties and the price are not yet on a sufficient level for the demands of the packaging and printing industries. Biopolymer dispersions find use in various applications, such as adhesives, inks, coatings, etc. From the Biopolymers family only few cover the performance requirements for applying on printing products. Because of their biodegradability, the suitable biopolymers can be used mainly on printing products with limited durability requirements.

The Biopolymers Family can be classified in 4 main groups (Fig.1) [7].

Polymer dispersions are stabilized water-borne emulsion polymers with colloidal particles in water.

Film formation results from the coalescence of the individual particles held apart by stabilizing forces. These forces are overcome by the evaporation of the continuous phase [7].

The goal of this study is to compare 2 types of polymer dispersions, their properties and characteristics, used for the preparation of water-based printing varnish – the reference dispersion, based on synthetic polymer – acrylate dispersion and second one, based on biopolymer.

To whom correspondence should be sent.
*E-mail: yanko.nedelchev@gmail.com

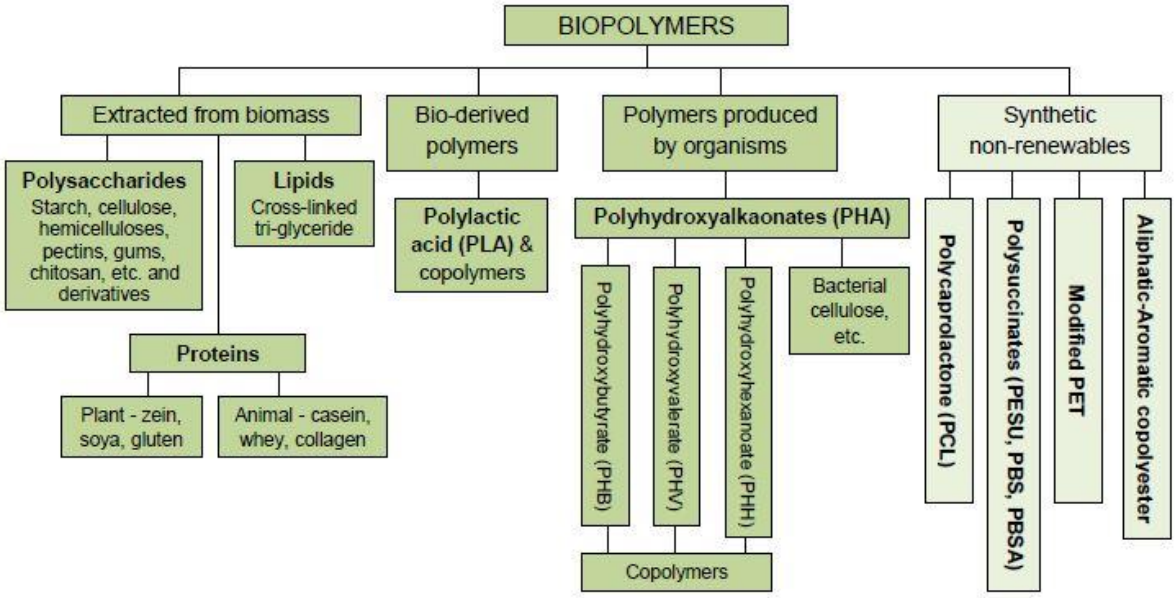

Fig. 1. Classification of biopolymers.

EXPERIMENTAL

Materials. As a reference has been used acrylic water-based multipurpose, gloss varnish with fast drying speed and high wet block resistance – ACTEGA Terra Wet GlossG9/535 (45 sec).[8] The tested varnish was water-based gloss coating, based on renewable resources - ACTEGA Terra Green Gloss G5/200 (45 sec).[9]

Methods. Both varnishes were applied on offset printing press HEIDELBERG CD74 4+L, under same conditions and initial parameters:

- Material – Carboard – LWC 220 g/m^2
- Ceramic Anilox roller – Zecher, 100 L/cm, 60 ^{o,} 35 μ, 13 cm^3/m^2
- IR Lamps power – 15 %, hot air – 100 %
- Temperature in stack – 35^o C
- Equal press speed – 8 000 sheets/hour
- Applied quantity – 3,5 g/m$^{2.}$

RESULTS AND DISCUSSIONS

The researches over both varnish types - acrylic water-based ACTEGA Terra Wet GlossG9/535 (45 sec) and water-based gloss coating from bio-polymer, based on renewable resources - ACTEGA Terra Green Gloss G5/200 (45 sec), in real production conditions, clearly show their characteristics and performances, when applying on printed packaging production. The results are given in Table 1 and Table 2.

Table 1. Properties during coating process.

	G9/535 - acrylic	G5/200 - bio
Runability	Very good	Very good
Drying	Very good	Good
Crackling tolerance	Very good	Very good
Foaming tolerance	Excellent	Acceptable
Two-sided coating	Excellent	Poor

Table 2. Properties in dry condition.

	G9/535 - Acrylic	**G5/200 - Bio**
Gloss (Gloss meter–60^o)	65/73 GU	53/61 GU
Rub resistance	Good	Good
Slip angle (COF)	23^o	21^o
Wet block resistance	Excellent	Good
Cobb $_{(60)}$	5.90 g/m^2	7.33 g/m^2
Whiteness/Yellowness - R 457	80.10/- 4.50	79.50/-2.80
Heat resistance	Up to 120^o C	U to 150^o C

The obtained results in Table 1 and 2 determine that both varnishes have similar key performance parameters during the coating process in the printing machine and don't have significant influence on the normal overall production process. The biodegradable varnish can be used for coating of packaging products without any specific preparations and equipment. Its usage doesn't have any further interference over the printing machine's exploitation. However the results in table 2 are showing obvious performance differences

in water absorption test and in optical characteristics – gloss and whiteness/yellowness, wherefrom can be concluded, that the biodegradable varnish, in this form, cannot meet the criteria for printing packaging from highest quality.

Table 3. Performance during further processing

	G9/535 - Acrylic	G5/200 - Bio
Counter glueing	Excellent	Good
Hot foil stamping	Excellent	Excellent
UV varnishing	Very good	Good
Foil lamination	Good	Satisfying

The printed product, coated with both varnish types is used for the production of food packaging, therefore it needs further processing. Table 3 is showing the performance of the acrylic water-based varnish and the biodegradable varnish during Postpress processing. The research in real production environment shows, that the biodegradable varnish doesn't have significant influence over the production process and its performance is similar to the acrylic varnish. Both varnishes have stable runability parameters and can be used when Postpress finishing is required for the printing production.

When exposed to aging, the printed production, coated with both varnish types shows similar behaviour in their optical characteristics alteration, which can be neglected, when talking about food packaging, because of the limited products expiration dates (cf. Charts 1 and 2).

CONCLUSION

As a result from the tests can be concluded, that the biodegradable varnish covers the main quality criteria, required from a water-based overprint varnish:

– good runability on the printing press
– satisfying properties in dry condition
– sufficiently good performance during further processing,

However the results clearly show that biodegradable varnishes still have to face some

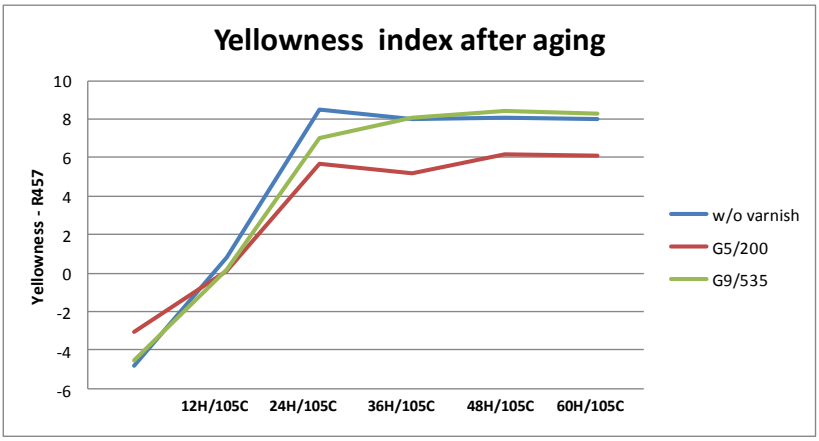

Chart 1. Yellowness after aging.

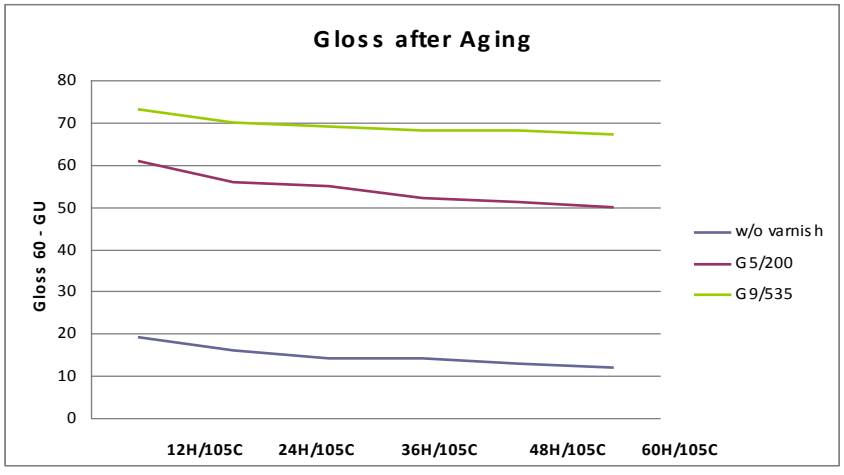

Chart 2. Gloss after aging.

challenges, in order to fully replace the conventional water-based varnishes.

The next step in this direction is the improvement of the optical, adhesion and barrier characteristics of the varnish by modifying the binders or implementing of new additives.

REFERENCES

1. А. В. Несхозієвський, к.т.н., ст. викладач, НТУУ «КПІ», Київ,Україна, ”Управління якістю вибіркового лакуванняна основі зміни параметрів пластин” Технологія і техніка друкарства, 2014, 37-48.
2. T. Bozhkova, *Polygraphy*, **4**, 34 (2008) (in Bulgarian).
3. T. Bozhkova, *Packing and Printing*, **4**, 24 (2008) (in Bulgarian).
4. V. Lasheva, T. Boschkova, *Wochenblatt fur Papierfabrikation*, 14 , 840 (2008).
5. D. Rozalinov, T. Bozhkova, *Celulose and Paper*, **1**, 46, (1994) (in Bulgarian).
6. H. Kipphan, Handbook of Print Media, Technologies and Production Methods, Springer, 2001.ISBN5-8122-0310-5
7. Y. Nedelchev “New types of overprint varnishes in the printing and packaging industry”, COST training school, 24-27September, Hungary, 2013, p 161-176.
8. www.actega.com/terraACTEGA TerraWet Gloss Coating G9/535 Technical Data Sheet
9. www.actega.com/terraACTEGA TerraGreen Gloss Coating G5/200 Technical Data Sheet

ПОДОБРЯВАНЕ НА ФИЗИКО- МЕХАНИЧНИТЕ И ОПТИЧНИ ХАРАКТЕРИСТИКИ НА ПЕЧАТНАТА ПРОДУКЦИЯ С БИОРАЗГРАДИМ НАДПЕЧАТЕН ЛАК

Т. Божкова, И. Спиридонов, Я. Неделчев*, Р. Боева, А. Ганчев

Химикотехнологичен и металургичен университет

Бул. Кл. Охридски 8, София 1756

Постъпила на 1 август, 2014 г.; приета на 23 февруари, 2015 г.

(Резюме)

Поради изчерпване на фосилните ресурси и нарастващата нужда от екологично чисти, устойчиви технологии, необходимостта от използването на възобновяеми източници в производството на мастила и лакове ще нараства през идните години. За разлика от традиционните лакови покрития на водна основа, които са на база петролни деривати, биоразградимите лакове се фокусират върху смоли и восъци от природата. 90% от компонентите на биоразградимите лакове са от природни възобновяеми източници, които са биоразградими на повече от 75%, което прави възможно изхвърлянето на остатъците директно в канализацията, след одобрение от съответните власти. За да бъдат в състояние напълно да заменят конвенционалните лакове на водна основа, чиито основни компоненти са акрилни и стирен-акрилни полимери, биоразградимите лакове трябва да са в състояние да покрият основните изисквания за качество – стабилни характеристики по време на нанасяне в печатната преса, устойчивост на надраскване и изтриване, влагоустойчивост и удовлетворяващи оптични свойства. Настоящето изследване подчертава основните разлики в качеството между биоразградимите и конвенционалните лакове на водна основа, техните оптични, химични и физични характеристики.

Bulgarian Chemical Communications, Volume 47, Special issue A (pp. 64 - 69) 2015

Immobilization of glucose oxidase on porous copolymer

M.N. Kamburov*, T.V. Ivanov, I.G. Lalov

Department of Biotechnology, University of Chemical Technology and Metallurgy, 1756 Sofia, Bulgaria,

Received July 27, 2014; Accepted February 10, 2015

Porous copolymer was prepared by suspension polymerization method of styrene, maleic anhydride and divinylbenzene in a batch type reactor. The characteristics of the copolymer were evaluated using Fourier Transform IR spectroscopy and scanning electron microscopy. The glucose oxidase (GOD) enzyme was selected as a model enzyme to assess its potential applicability for immobilization purpose. Then the glucose oxidase was immobilized on a copolymer under an optimized condition (the incubation time, and pH 6,5, GOD 5 mg/ml). Enzymatic activities of free and immobilized GOD were assessed in terms of the oxidation of D-glucose to D-gluconic acid carried out under stirring by air. The enzyme immobilization yield was 87% with the immobilized GOD activity of 125 U/mg protein. The Michaelis constant for immobilized GOD was disclosed to be 16,3 mmol/l by Lineweaver–Burk plot at 25ºC. The highest enzymatic activity was achieved when the pH of the medium was approximately pH 7.0. Storage stabilities of GOD samples were investigated during 40 days and the retained activity was 70%, higher than the 22% of the free enzyme.

Key words: *maleic anhydride copolymer; glucose oxidase; immobilization*

INTRODUCTION

Glucose-oxidase (GOD, β-D-glucose:oxygen-1-oxidoreductase, EC 1.1.3.4) is a well-characterised enzyme (flavoprotein), that catalyses the oxidation of β-D-glucose to D-gluconolactone which in its turn converts in an aqueous solution into gluconic acid according the following equation:

$$\text{Glucose} + O_2 + H_2O \xrightarrow{\text{GOD}} \text{gluconic acid}$$

$$\text{gluconic acid} + H_2O_2 \xrightarrow{\text{CAT}} CO_2 + H_2O + \tfrac{1}{2} O_2$$

During the catalytic oxidation of glucose, hydrogen peroxide is generated. Under physiological conditions GOD is exposed to very low concentrations of H_2O_2, but in the industrial applications higher H_2O_2 concentrations are usually obtained, which can attack some residues of the proteins and GOD's enzymatic activity is reduced. The gluconic acid accumulates, reducing pH of the solution. Both gluconic acid and hydrogen peroxide can result in product inhibition of GOD. Therefore, it is inevitable to remove hydrogen peroxide, properly with catalase (CAT).

Industrial use of soluble GOD from *A. niger* is the basis of many applications in the food industry, textile bleaching and as a glucose biosensor. The GOD-catalysed reaction removes oxygen and generates hydrogen peroxide, a trait utilised in food preservation [1, 2]. GOD has also been used in baking, dry egg powder production, wine production, gluconic acid production, etc. Maillard non-enzymatic browning is a result of reaction between the amino group of proteins or amino acid and reducing sugars. In the production of dried egg powder, this reaction causes undesirable browning. Thus, soluble GOD-CAT are mixed into egg products in order to remove traces of glucose from them. The GOD-CAT mixture can be added to the beverage to remove oxygen, and thus to prevent damage by oxidation. This is typically a batch process and contains the enzyme as an impurity in the product.

However, because of the relatively high price of GOD it is no competitive. In order to compensate the high price of enzymes, it was proposed to recover them by immobilisation. Through immobilisation, continuous process is possible and the enzyme can also be retained and recycled. Although immobilized enzymes usually show lower catalytic activity than the free ones, they are more stable and can be reused and therefore they are cheaper and more effective in large scale applications [3]. Many studies were performed involving the immobilization of GOD in different matrices to enhance properties such as reusability, recovery, stability, thermostability and shelf life. GOD has been immobilized on numerous carriers, such as sol–gel matrix, porous silica beads, polymer membrane, polymer microsphere. Besides natural polymers, many synthetic organic polymers have been investigated for that purpose. Among them,

To whom correspondence should be sent.
E-mail: m_kamburov@yahoo.com

two common examples are the derivatives of ethylene-maleic anhydride copolymer and those of polystyrene [4,5].

In the present paper, a novel reactive fine powdery copolymer preparation is demonstrated. Its structure and morphology are also investigated. Taking into consideration the economical demands, a simple way of covalently immobilization of GOD is applied. The parameters important for immobilization process were studied. The effect of immobilization on the multiple use of the enzyme was estimated in batch type reactor.

EXPERIMENTAL

Materials

Glucose oxidase isolated from *Aspergillus niger* (Sigma-Aldrich, Product Number GO 49180), its GOD activity was 185 units/mg. Styrene (Lukoil Neftochim Bourgas, Bulgaria, St) was washed successively with a dilute solution of sodium hydroxide and water, dried over anhydrous calcium chloride, and then distilled under reduced nitrogen pressure just before use. Divinylbenzene (DVB), maleic anhydride (MA) and benzoyl peroxide (BPO) used were reagent grade (Sigma-Aldrich). All other chemicals were reagent grade commercial products.

Preparation of copolymer of styrene-maleic anhydride-divinylbenzene (P(St-co-MA-co-DVB)

A glass reaction vessel equipped with a stirrer (l000 rpm), a thermometer, and a reflux condenser was used. 100 ml benzene was put into the reaction vessel and under nitrogen stream a definite weight of the monomers and BPO were added. The copolymerization was carried out at 70°C and stirred for 4 hours. The resultant copolymer was quickly filtered, washed with benzene, and dried up at 70°C under vacuum.

Determination of the maleic anhydride unit content

The total amount of anhydride and free carboxyl groups in copolymer were determined. For this purpose 0,2 g copolymer was hydrolyzed in 25 mL 0,1M NaOH at 90°C for 3 h applying also stirring. After cooling, the mixture was titrated with 0,1 M HC1 using phenolphthalein as indicator. The copolymerized MA quantity was calculated as the MA unit content of the copolymer.

Immobilization procedure

The immobilization of GOD to the active support (P(St-*co*-MA-*co*-DVB) was conducted under defined conditions: 1,0 g of carrier and 100 mg of enzyme were added to 19,0 ml of 0,05 M phosphate buffer (pH 6,5). After incubation at 4°C for 24 hr with occasional stirring, the immobilized enzyme was collected by filtration and washed extensively with several portions of cold buffer to remove the free enzyme.

Determination of protein

Protein determination was performed according to Lowry et al. [6]. The amount of immobilized protein was calculated as the difference between the amount of protein introduced into the coupling reaction mixture and the amount of protein found in the filtrate and washing solutions after immobilization.

Assay of GOD activity

The reaction velocity is determined by an increase in absorbance at 460 nm resulting from the oxidation of o-dianisidine through a peroxidase coupled system [7]. One unit causes the oxidation of one micromole of o-dianisidine per minute at 25°C and pH 6,0 under the conditions specified. The mixture of 2,5 ml dianisidine-buffer mixture, 0,3 ml 18% glucose, 0,1 ml peroxidase and 0,1 ml of appropriately diluted enzyme was added into a cuvette and the increases in A_{460} for 4 - 5 minutes were recorded. ΔA_{460} from the initial linear portion of the curve was measured and GOD activities was calculated:

$$Units/mg = \frac{\Delta A_{460}/\min}{11{,}3.mgGOD/ml}$$

Effect of immobilization on the kinetic constants

The activity assays were carried out applying different glucose concentrations (10,0, 20,0, 30,0, 40,0 and 50,0 mM) in order to determine maximum reaction rates (V_{max}) and Michaelis–Menten constants (K_m) of free and immobilized GOD. V_{max} and K_m for free and immobilized GOD were determined from double reciprocal plots. The stability tests were performed at 4°C with 0.5 ml soluble enzyme or 20 mg immobilized enzyme in 10 ml 0,05M acetate buffer (pH 6.0). After appropriate times of incubation the residual activities were assayed.

RESULTS & DISCUSSION

It is known that the copolymerization of MA with St leads to copolymers with nearly equimolar ratio of monomer units (*alt*-copolymers). The incorporation of a third monomer (DVB) in the polymerization process is a prerequisite for the preparation of a porous solid carrier. Styrene and

divinylbenzene were washed with 2 M sodium hydroxide and water to remove inhibitors. Benzene was distiled before use. P(St-*co*-MA-*co*-DVB) was prepared in a batch type reactor. A mixture of 0,04 M MA, 0,1 M St , 0,005M DVB and 0,04 mM benzoyl peroxide were added to a 300 ml of benzene. The mixture was dispersed and the batch temperature was raised to 70ºC. The reaction mixture was continuously stirred for 3 hour. As the benzene is a poor solvent for the crosslinked copolymer, several minutes after the beginning of copolymerization the reaction system turbid. The resulting reactive fine powdery was filtered, washed with benzene and dried.

The chemical structure of the synthesized polymer was confirmed by Fourier transform infrared spectroscopy (FTIR) by using a spectrophotometer (Varian 660-IR). Absorption bands characteristic of stretching vibrations of aromatic and aliphatic C─H bonds were observed at 3100–3000 and 2926 cm^{-1} (Fig.1). Bands were also detected at 1854.6 cm^{-1} (asymmetric C=O stretching vibrations of the maleic anhydride groups), 1771.7 cm^{-1} (symmetric C=O stretching vibrations of the maleic anhydride groups), 1633.2 cm^{-1} (stretching vibrations of the polystyrene aromatic ring), 1495.1 cm^{-1} (bending vibrations of the aromatic ring), 1454.8 cm^{-1} (C─H bending vibrations of the polymer chain), as well as at 763.1 and 702.4 cm^{-1} (C─H stretching vibrations of the mono-substituted aromatic ring of polystyrene). It can be concluded that the synthesized polymer is a copolymer of styrene, maleic anhydride and divinylbenzene.

The microparticles were analyzed with scanning electron microscopy (JEOL JSM-5510, Japan). As seen from Fig. 2 their surface was a highly porous and rough. The copolymerized MA quantity was calculated as the anhydride and free carboxyl groups in copolymer. The MA unit contents of the copolymers were 32%.

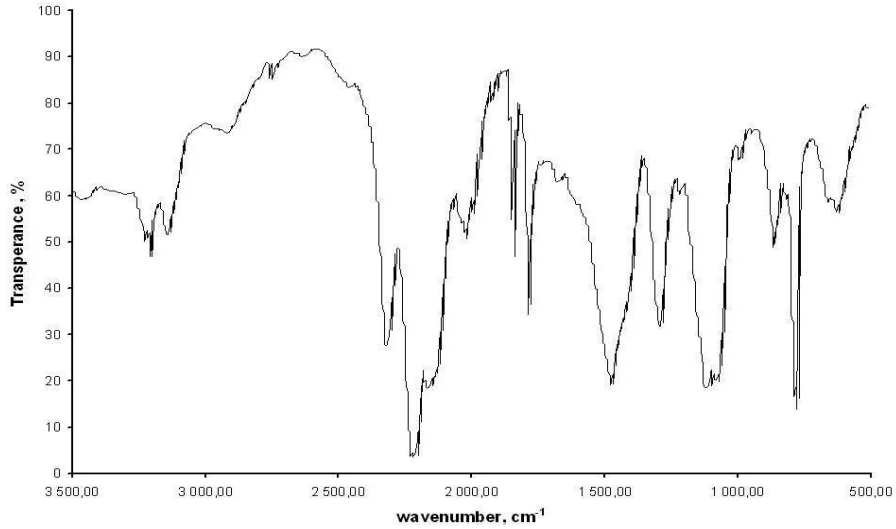

Fig. 1. FTIR spectrum of P(St-co-MA-co-DVB) in KBr pellet.

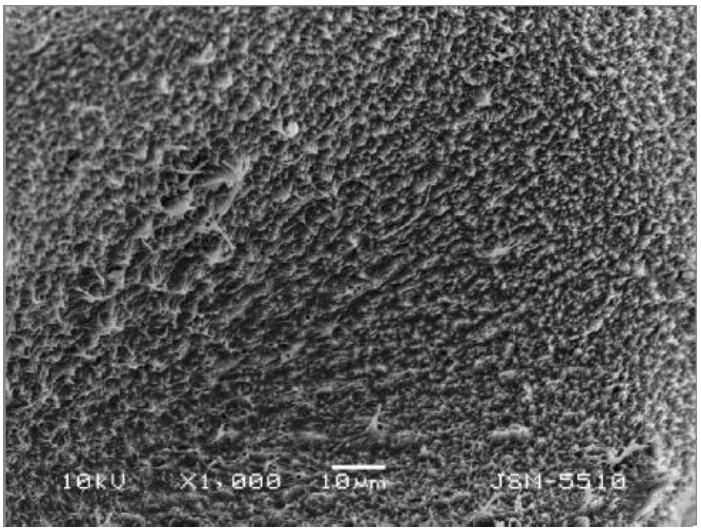

Fig. 2. Scanning electron micrograph of microporous surface of P(St-co-MA-co-DVB).

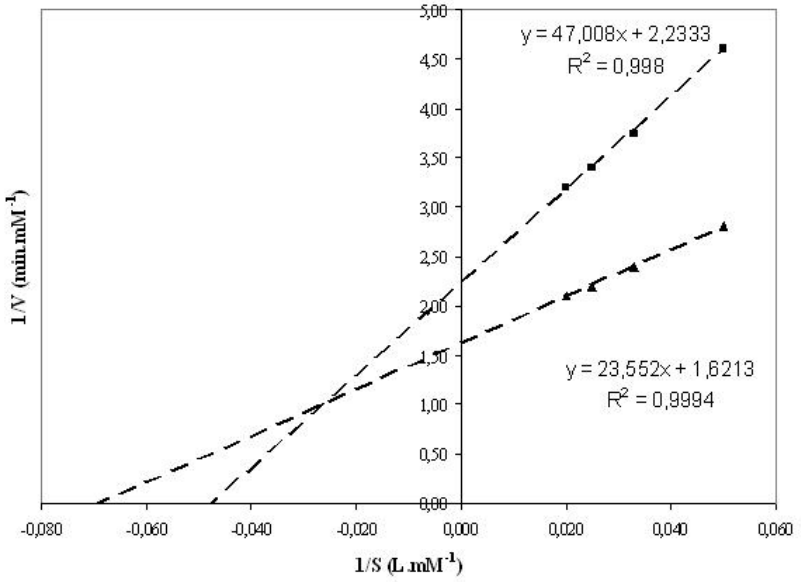

Fig. 3. Lineweaver-Burk plots of free (▲) and immobilized (■) GOD.

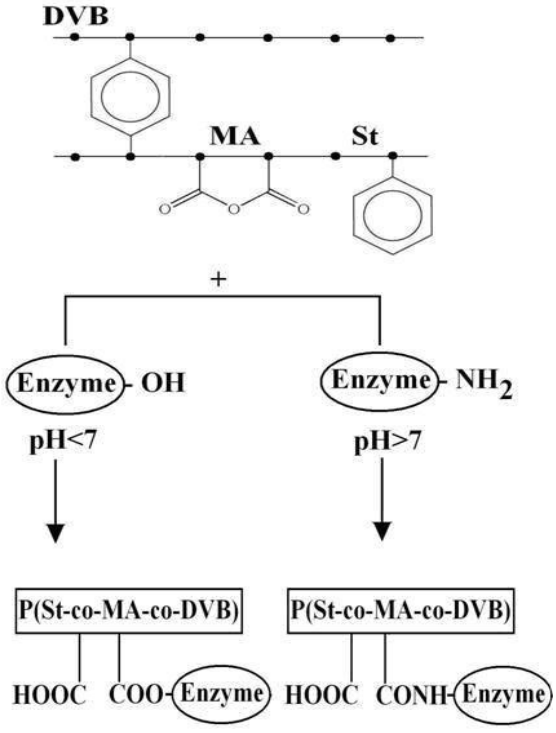

Scheme 1.

It must be pointed out that the P(St-*co*-MA-*co*-DVB) undergo the typical reactions of anhydrides with amines and alcohols. The copolymer may also be affected by the water used in the post-treatment of the samples. The proposed method of immobilization of GOD on P(St-*co*-MA-*co*-DVB) includes the reactions represented on Scheme 1. The presence of reactive anhydride groups allows enzymes to bind covalently to the polymer carrier. There are two possibilities for covalent coupling of enzymes depending on the pH of medium. The copolymer binds proteins via its anhydride groups, which may react with different nucleophiles on the protein as a function of pH:

- Through the formation of an amide bonds between the amino groups of lysyl or arginyl residues.

- Through the formation of ester linkages between the hydroxyl groups of seryl and threonyl residues, or the phenols OH groups of tyrosyl residues.

Parameters, characterizing GOD immobilizationare presented in Table 1. The activity of immobilized GOD and protein binding capacity

Table 1. Characteristics of immobilized GOD.

Parameters	Free GOD	Immobilized GOD
Protein content [mg/g of support]	-	87,1
Specific activity [U/mg protein]	180,2	125,0
Relative activity [%]	-	69,4
Immobilization yield [%]	-	87,0
Storage stability after 40 days [%]	22,0	70,5

reached 125,0 U/mg protein and 87,1 mg/g support. The relative activity was 69,40%, compared with the free GOD.

The effects of immobilization on the properties of the immobilized enzymes were studied. It was found that GOD, immobilized onto P(St-*co*-MA-

co-DVB) exhibited typical Lineweaver-Burk behaviour (Fig.3). The linear nature of the Lineweaver-Burk plots proves that in both cases enzyme reactions followed the Michaelis-Menten kinetics, which permitted the determination of the Michaelis constant (K_m) and the maximum rate of the reaction (V_{max}). As the K_m is a characteristic constant for enzyme activity, it was calculated for both immobilized and free enzymes. It was found that V_{max} of the immobilized GOD (0,45 mM/min) decreased with respect to that of the free enzyme (0,62 mM/min), whereas K_m increased from 16,3 mM for the free enzyme to 19,1 mM for the immobilized one. Since the K_m values were of the same magnitude, this means that the catalytic function of the enzyme was not significantly impaired by the coupling process. Probably the increase in the K_m value after the immobilization of GOD is due to changes in the conformation of the enzyme molecules, which impedes the enzyme–substrate interaction or due to hindered access of the substrate to the active sites of the immobilized enzyme (steric and diffusion effects).

The stability of free and immobilized GOD at 4°C was investigated and results obtained are illustrated in the Fig. 4.

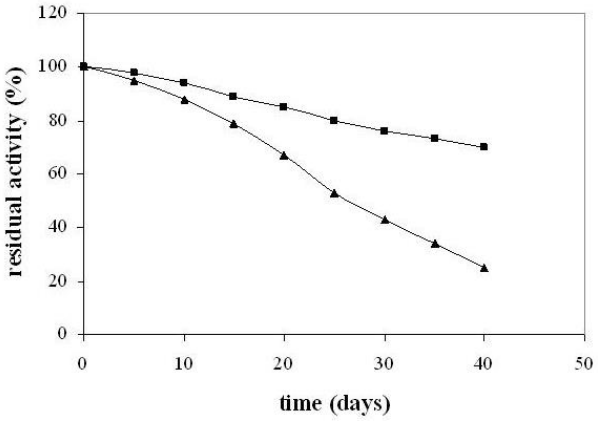

Fig. 4. Storage stability of free (▲) and immobilized (■) GOD at 4 °C. The initial enzyme activity is taken as 100%.

The immobilization procedure stabilized the enzyme structure and the immobilized GOD was much more thermally stable than the free having 70% activity retained compared to 22% for the free GOD after 40 days storage. This phenomenon was also found by Onda *et al*. [8].

The possibility of reuse of the immobilized GOD was studied by measuring its activity after 10 reusing cycles. Covalently bound enzyme shows good operational stability and upon 10 reuses it loses 25% of its activity. This activity reducing is probably due to enzyme deactivation and protein losses from the support upon multiple uses.

CONCLUSIONS

In conclusion, three monomers were used to synthesize porous P(St-*co*-MA-*co*-DVB) with maleic anhydride reactive groups. The immobilized glucose oxidase has better stability upon repeated use than the free enzyme. Probably the covalent immobilization leads to a more stable enzyme conformation in comparison to that of the free enzyme.These properties render the copolymer suitable carrier for immobilization of GOD. The activity values of the immobilized enzyme are suitable for the industrial processing.

REFERENCES

1. W. Gerharrtz, Industrial uses of enzymes. in: Enzymes in industry.Production and applications. New York:VCH Publishers, (1990).
2. C.M. Wong, K. H. Wong, X. D. Chen, *Appl. Microbiol. Biotechnol.*, **78**, 927 (2008).
3. A.Vikartovská, M. Buko, D. Misloviová, V. Pätoprsty, I. Lacík, P. Gemeiner, *Enzyme Microb. Technol.*, **41,** 748 (2007).
4. T. S. Pao, S. Chenga, *Biotechnology and Bioengineering*, **20**, 773 (1978).
5. Y. Mizutani, S. Matsuoka, *J. Appl.Polym. Sci.* **26**, 2113, (1981).
6. O.H. Lowry, N.J. Rosebrough, L. Faer, R.J. Randall, *J. Biol. Chem.*, **193,** 265 (1951).
7. H.U. Bergmeyer, K. Gawehn, M. Grassl, in *Methods of Enzymatic Analysis* Volume I, Second Edition, 457-458, Academic Press, Inc.,NY (1974).
8. M. Onda, K. Ariga, T. Kunitake., *Int. J. Mol. Sci.,***12**, 3052 (2011).

ИМОБИЛИЗИРАНЕ НА ГЛЮКОЗООКСИДАЗА В ПОРЬОЗЕН СЪПОЛИМЕР

М. Н. Камбуров*, Т. В. Иванов, И. Г. Лалов

Катедра „Биотехнология”, Химикотехнологичен и металургичен университет, 1756 София, България

Постъпила на 27 юли 2014 г.; коригирана на 11 февруари 2015 г.

(Резюме)

Синтезиран е носител за имобилизиране на ензими чрез суспензионна съполимеризация на стирен, малеинов анхидрид и дивинилбензен. Съполимерът е охарактеризиран с помощта на FTIR спектроскопия и сканираща електронна микроскопия. Глюкозооксидазата (GOD) е избрана като моделен ензим, за да се изследва възможността за имобилизирането й в полученият съполимер при оптимални условия (време на инкубиране, pH 6,5, GOD 5 mg/ml). Ензимната активност на свободния и имобилизирания GOD са определени чрез окисление на D-глюкозата до D-глюконова киселина при разбъркване и аериране с въздух. Добивът на имобилизиране на ензима е 87%, а активността му е 125 U/mg белтък. Константата на Michaelis за имобилизирания ензим е 16,3 mmol/l, определена с помощтта на графичната зависимост на Lineweaver-Burk. Най-висока ензимна активност е постигната, когато pH на средата е 7.0. Установена е повишена стабилност при съхранение на имобилизирания GOD (остатъчна активност 70%), спрямо свободния ензим (22%).

Bulgarian Chemical Communications, Volume 47, Special issue A (pp. 70- 74) 2015

Denitrification of wastewater with immobilized cells of *Pseudomonas denitrificans*

T.V. Ivanov*, I.G. Lalov, L.K. Yotova,

Department of Biotechnology, University of Chemical Technology and Metallurgy, 8, Kl. Ohridski Blvd., 1756 Sofia, Bulgaria

Received July 24, 2014; Accepted February 18, 2015

Nitrate contamination is one of the major problems in wastewater. The aim of the present investigation is to study the denitrification process with immobilized on different synthetic supports cells of *Pseudomonas denitrificans* (NBIMCC 1625). The bacterium from the agar slants was inoculated into YPD liquid medium. The activated culture was transferred to 100ml of a medium with potassium aspartate or methanol as carbon source. Preliminary study had been carried out with free cells in shake flasks, containing nitrate as KNO_3 and carbon source methanol, C/N ratio was 6. Complete nitrate removal was achieved for 3 hours. In order to determine the kinetic of process the influence of initial nitrate concentration on nitrate removal were examined. By applying linear fit to rate of denitrification vs. initial nitrate concentration Km and Vmax were found to be 63mg NO_3-N/l and 0,671mg NO_3-N/min/g cells respectively. The further investigation of the denitrification process was performed with immobilized on different synthetic supports cells. Denitrification in the continuous-flow column reactor was carried out. After 3 hours the steady state was reached and output concentration of 30mgNO_3-N/l. The result of this study demonstrated that nitrate concentrations up to 45mg NO_3/l can be removed from wastewater. In the continuous column process with immobilized cells at HRT=1h high denitrification rate was achieved.

***Key words**: denitrification, Pseudomonas denitrificans, magnetic support.*

INTRODUCTION

The use of fertilizers and other nitrogen components in various industries, contribute to nitrogen pollution. Ion exchange, adsorption and membrane processes have been developed for nitrogen compounds, like nitrate and nitrite removal. Each of them has advantages and disadvantages, from which biological method is found to be the most commonly used and effective method. The process of biological denitrification has been well studied in last years. There are a large number of bacteria, which can transform nitrogen compounds into harmless nitrogen gas with accompanying carbon removal. The denitrification could be achieved either with pure cultures of *Pseudomonas denitrificans*, *Ps. Stutzery* and other strains or by mixed cultures from wastewater treatment plants [1, 2]. The application of cell immobilization techniques to wastewater treatment process has recently gained much attention, because biological denitrification with free suspended cells is usually slow process [3]. The treatment of wastewater in different types continuous-flow column reactors using immobilized cells is attracting increasing interest and a variety of carriers and immobilization methods have been developed [4]. The advantages of immobilized cells application are in their longer operation stability and in their multiple uses in continuous bioreactors. Several natural materials [5] and synthetic polymers [6, 7] have been applied as support for cell immobilization. Among the various immobilization methods that are available, the immobilization by spontaneous biomass adhesion onto porous support (biofilm formation) has been chosen for its ease of use, low cost and operational stability.

EXPERIMENTAL

Materials and methods

Pure culture of *Pseudomonas denitrificans* was used in this study. A strain of *P. denitrificans* (*NBIMCC* 1625), provided from the Bulgarian National Bank of Industrial Microorganisms and Cell Cultures, was used. In order to prepare the inoculum, the strain was cultured in a medium containing: peptone, 5g/l; meat extract, 3g/l; glucose, 10 g/l, and was incubated for 24 h at 30 °C in a rotary shaker at low agitation speed, 50 rpm. The culture medium for biomass growing and biofilm formation had the following composition (in g/l): potassium aspartate 15; yeast extract 14; KNO_3 8; $MnSO_4$ 0,0025;

To whom correspondence should be sent.
E-mail: todorvelikovivanov@abv.bg

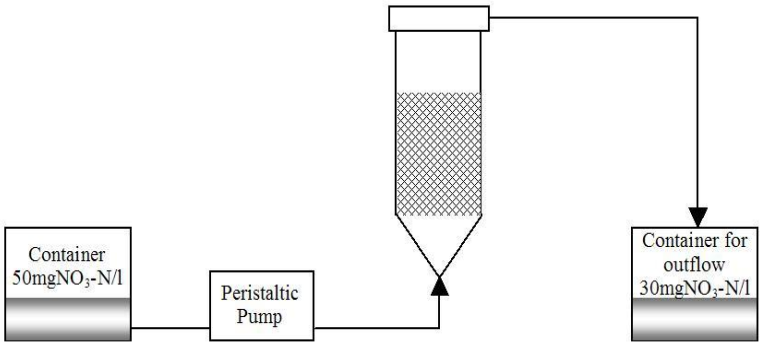

Fig. 1. Fixed bed column bioreactor for denitrification.

$(NH_4)_6Mo_7O_{24}.4H_20$ 0,0025; $FeCl_3.6H_2O$ 0,006; pH 6,75. After cultivation with weak shaking for 24h at 30^0C, cells were harvested by centrifugation (15min, 4000g), washed twice in saline solution and stored at 4^0C. The accessibility to biofilm formation on four different carriers was tested by cultivation for one week. The culture medium was replaced every second day. The first two support materials were a copolymer of acrylonitrile and acrylamide formed as granules with an average diameter of 2mm [8], without and with incorporated Fe_3O_4 nanoparticles. The second two carriers were polyurethane foam (PUF) cut into cubes with approximately 3mm x 3mm x 3mm cubic sizes, also without and included magnetite. Magnetite nanoparticles were incorporated in support matrix by coprecipitation of ferric and ferrous salts with alkaline solution [9], then washed and dried overnight at 50^0C. The study of denitrification activity of free and immobilized biomass was carried out with batch fermentation in shake flasks, containing nitrate as KNO_3 and carbon source methanol, C/N ratio was 6. The continuous-flow reactor for denitrification was set up as an upflow fixed bed, as shown in Fig. 1.The reactor was run in continuous mode at 25°C, and with a flow volume speed of 100 ml/h. It consisted of a container, column reactor with ID=50mm and 100ml total volume, peristaltic pump and container for outflow. The column was packed with 25g support and solution with $50mgNO_3$-N/l was pumped thru the column. Nitrate concentrations were determined through UV-spectrophotometry [7]. Before each spectrophotometric determination of nitrate, the samples were centrifuged for 15 min at 4000 rpm to remove cells from the supernatant. Then 0,1 ml 1N HCl was added to 5 ml of diluted sample. The light absorbance of samples was read against redistilled water at 220 nm on a UV–vis-spectrophotometer (Perkin-Elmer, Germany). In order to avoid the interference of the organic matter, the absorbance of samples was also measured at 275 nm. The corrected UV-light absorbance of nitrate in the sample A was calculated by the equation: $A=A_{220}-2.A_{275}$ and calibration curve was used to determine the concentration of nitrate. The concentration of nitrites in the centrifuged samples was determined spectrophotometrically from the amount of the diazonium salt of sulphanilic acid (formed from the nitrites present) by coupling with α-naphthylamine at pH = 2.0–2.5. The analyses of nitrites were carried out as follows. The assay involved two reagents. The Griess 1 reagent consisted of 0.6 g sulphanilic acid dissolved in 100 ml of distilled water. The Griess 2 reagent contained 0.6 g α-naphthylamine dissolved in distilled water. The solution was mixed with 25ml of glacial acetic acid, and diluted to 100ml with distilled water. Five milliliters of diluted sample was mixed with 1 ml of each of Griess 1 and Griess 2 reagents. The light absorbance of this solution was measured after 40 min using Spekol spectrophotometer at 543 nm against distilled water. When necessary, the samples were diluted prior to the addition of the Griess reagents. The nitrite concentrations were calculated using a calibration curve composed by the same method for concentrations from 0.05 to 1 mg/l. All chemicals were of analytical grade.

RESULTS & DISCUSSION

Batch cultivations with potassium aspartate and methanol as carbon source were performed. The potassium aspartate was replaced with equivalent quantity of methanol in culture medium. The experimental data showed that there are not significant differences between growth kinetics. Results of a typical s-shaped growth curves are presented in Fig.2. The experimental data showed that biomass concentrations after 24h cultivation was 9,6g/l wet biomass, when potassium aspartate

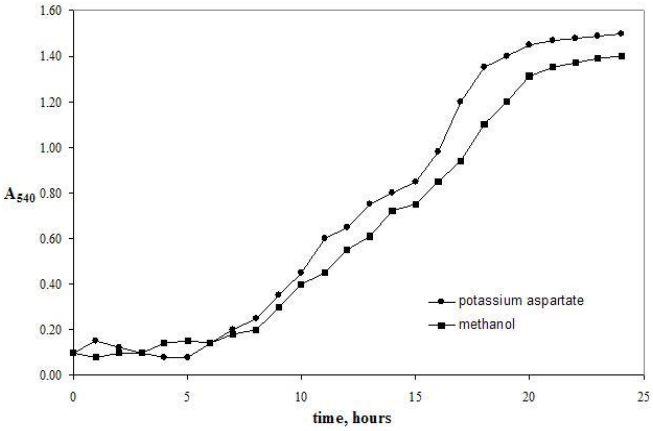

Fig. 2. Kinetics of biomass growth on different carbon sources.

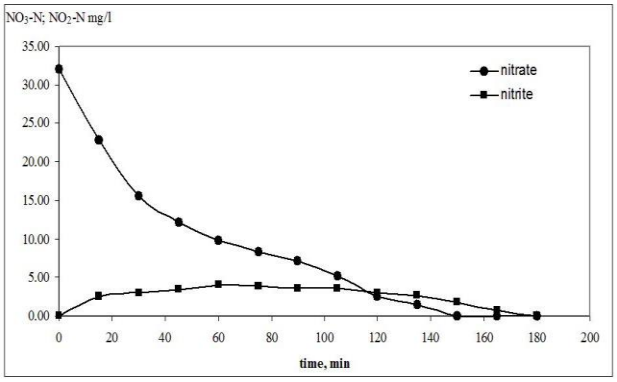

Fig. 4. Nitrate reduction by free cells in culture media containing 32,1mg NO_3-N/l and 2g/l dry biomass

was used vs. 8,8g/l wet biomass when methanol was used like carbon source. It was found that there is no difference between denitrification activities of biomass from two different carbon sources. In orderto determine the optimal conditions of the process nitrate reduction activity of free cells as a function of pH in denitrification media was tested. The denitrification profile obtained for the strain of *Pseudomonas denitrificans* is shown in Fig. 3. The Figure shows that the pH optimum of denitrification activity is between 7.25 and 7.5. At pH higher 9.0 nitrate reduction also was observed. The time profile of denitrification process with free cells is shown in Fig. 4. Complete nitrate removal was achieved after 150 minutes. Slight accumulation of nitrite was observed, during the experiment, but final nitrite concentration was low. In order to determine the kinetic of process the influence of initial nitrate concentration on nitrate removal was examined. The effect of different initial nitrate concentrations is shown in Fig. 5. The data from batch experiments were used to calculate the rate of nitrate reduction as a function of initials concentrations.

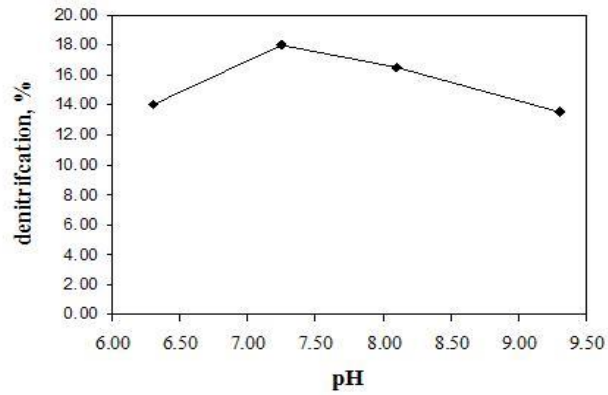

Fig. 3. pH optimum of the nitrate reduction by free cells.

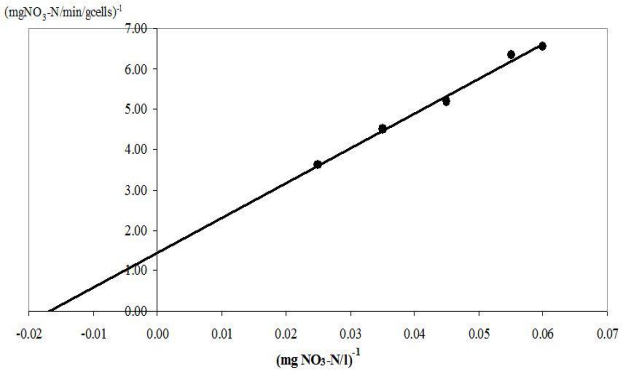

Fig. 5. Lineweaver-Burk plots (1/v versus 1/[S]) derived from initial rate of nitrate reduction at different nitrate concentration.

The rate of nitrate reduction was observed to depend on its concentration as predicted by the Michaelis–Menten equation. By applying linear fit to rate of denitrification vs. initial nitrate concentration Michaelis-Menten constants Km and Vmax were found to be 63mg NO_3-N/l and 0,671mg NO_3-N/min/g cells respectively. A comparison of the experimental results for the processes using immobilized on different supports cells in batch culture is shown in Fig. 6.

It is clearly seen from fig. 6 that nitrate removal increases when the polyurethane foam beads are used. The best results were obtained with magnetite containing polyurethane foam support. There are many investigations on bacterial biofilm application, but initiation of biofilm formation is poorly understood, and in particular, the contribution of chemical bond formation between bacterial cells and metal oxides (titanium dioxide and iron (II, III) oxide) has received much attention [10]. The Fe_3O_4 probably has a complex effect on the bacterial community, but did not show a straightforward toxic effect. It was found that nanoparticles of Fe_3O_4 changed the hydrolytic activity and bacterial community composition.

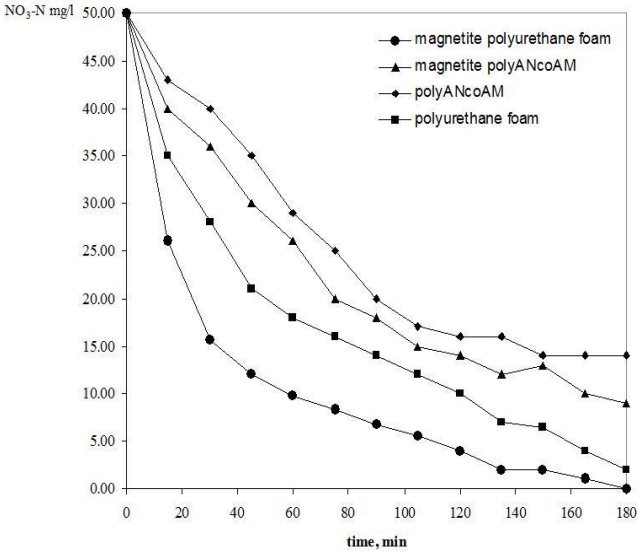

Fig. 6. Nitrate reduction by immobilized cells in culture media containing 50,0mg NO_3-N/l and 100g/l beads.

Generally, magnetite tends to cover cell surfaces, but no damage to the cell's integrity was reported in different studies dealing with this problem [11]. Overall, magnetite nanoparticles did not affect bacteria in culture media and model waste waters enough to indicate significant risk.

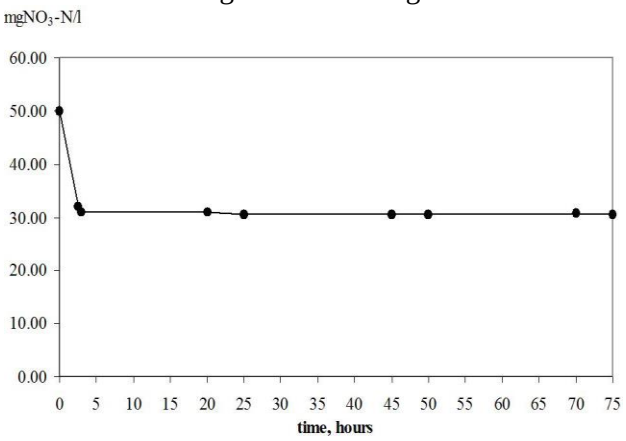

Fig. 7. Denitrification in continuous-flow column reactor.

The results from denitrification in continuous-flow column reactor are shown in Fig. 7. The results of column experiments show that after 3 hours the steady state was reached and output concentration of 30mgNO_3-N/l.

The result of this study demonstrated that nitrate concentrations up to 45mg NO_3/l can be removed from wastewater. In the continuous column process with immobilized cells of *Pseudomonas denitrificans* at HRT = 1 h high denitrification rate was achieved. Through the description of the Fig. 7, it can be concluded that flow rate of 0.1l/h should be chosen as the optimum hydraulic loading, and two columns should be used to reach desired nitrate reduction.

CONCLUSIONS

The microbial cells of gram-negative bacteria *Ps. denitrificans* were immobilized by adhesion onto four different kinds of polymer supports. Denitrification processes with free and immobilized cells have been investigated. Our findings, based on the experimental results, suggested that the use of immobilized cells in column bioreactor for water denitrification ensured a stable process over a long period of time without biomass wash out. An increase in the efficiency of the denitrification was observed in the presence of a magnetite (Fe_3O_4 nanoparticles) embedded in a matrix. The effect of the iron oxide nanoparticles on biofilm formation and denitrification should be studied better. The technique of using magnetic biomass carriers was shown better results. An accumulated biomass of microorganisms was achieved inside the reactor during a continuous process when applying this technique. Magnetite containing PUF was the most appropriate carrier of the particles evaluated and could be applied in Magnetic carrier technology. Our results confirm that stabilized magnetite nanoparticles interact with bacterial surfaces without causing damage sufficient to inhibit cell growth. Magnetite is also relatively cheap and available, why magnetic separation and reintroduction can be achieved to a relatively low cost in large-scale production.

REFERENCES

1. Y. Wen, Y. Ren, C. Wei, *African J. Biotechnol.*, **9**, 869, (2010)
2. A. Rezaee, H. Godini, S. Dehestani, S. Kaviani, *Iran. J. Environ. Health. Sci. Eng*., **7**, 13, (2010).
3. R. Nair, P. Dhamole, S. Lele, S. D'Souza, *Chemosphere*, **67**, 1612, (2007).
4. B.A. Bolto, *Waste Management*, **10**, 11, (1990).
5. S. Andersson, M. Nilsson, G. Dalhammar and G. K. Rajarao, *VATTEN*, **64**, 201, (2008).
6. S. Naik, Y. P. Setty, *Int. J. Biol. Ecol. Environ. Sci*., **1**, 42 (2012).
7. T. Parvanova-Mancheva, V. Beschkov, *Biochem. Eng. J.*, **44,** 208, (2009).
8. T. Ivanov, V. Ivanova, M. Kamburov, *Int. Rev. Chem. Eng.*, **1**, 308, (2009).
9. I. Šafařík, L. Ptáčková, M. Koneracká, M. Šafaříková, M. Timko, P. Kopčanský, *Biotechnol.Lett.*, **24**, 355, (2002).
10. D. Marinkova, D. Danalev, S. Serfaty, L. Yotova, E. Caplain, P.Griesmar, *Phosphorus, Sulfur, and Silicon and the Related Elements*, **187,** 926, (2012).
11. S. Frenk, T. Ben-Moshe, I. Dror, Br. Berkowitz, D. Minz, *PLOS ONE*, **8**,12, (2013)

ДЕНИТРИФИКАЦИЯ НА ОТПАДНИ ВОДИ С ИМОБИЛИЗИРАНА БИОМАСА ОТ *Pseudomonas denitrificans*

Т.В. Иванов*, И.Г. Лалов, Л.К. Йотова

Катедра Биотехнология, Химикотехнологичен и металургичен университет, бул. Кл.Охридски №8, 1756 София, България

Постъпила на 2014 г.; коригирана на 18 февруари, 2015 г.

(Резюме)

Един от основните замърсители в отпадните води са нитратите. Целта на настоящата работа е да се изследва и оптимизира процес на денитрификация с имобилизирана върху различни носители биомаса *от Pseudomonas denitrificans* (NBIMCC 1625). От твърдата хранителна среда микроорганизмите бяха развити на течна среда съдържаща калиев аспартат или метанол като въглероден източник. При използване на метанол в процеса на денитрификация и съотношение на C/N = 6 със свободна биомаса беше достигнато пълно отстраняване на нитратите за 3h. Определени са и основните кинетични параметри Km = 63 mg NO_3-N/l и Vmax=0,671 mg NO_3-N/min/g клетки. Процеса на денитрификация беше изследван и с имобилизирана на различни синтетични носители биомаса. При използване на колонен реактор запълнен с имобилизирана биомаса в непрекъснат процес е достигната концентрация от 30 mg NO_3-N/l на изход от колоната и е установено че времепрестой от 1 час е достатъчен за достигане на висока степен на денитрификация.

Bulgarian Chemical Communications, Volume 47, Special issue A (pp. 75 -79) 2015

Synthesis and bioactivity of new platinum and ruthenium complexes of 4-bromo-spiro-(fluorene-9,4'-imidazolidine)-2',5'-dithione

P.E. Marinova[1*], M.N. Marinov[2], M.H. Kazakova[3], Y.N. Feodorova[3], V.S. Sarafian [3], N.M. Stoyanov[4]

[1]*University of Plovdiv, Faculty of Chemistry, Department of General and Inorganic Chemistry with Methodology of Chemistry Education, 4000 Plovdiv, Bulgaria*
[2]*Agricultural University – Plovdiv, Faculty of Plant Protection and Agroecology, Department of General Chemistry, 4000 Plovdiv, Bulgaria*
[3]*Medical University – Plovdiv, Department of Medical Biology, 4000 Plovdiv, Bulgaria*
[4]*University of Ruse – Razgrad Branch, Department of Chemistry and Chemical Technology, 7200 Razgrad, Bulgaria*

Received July 24, 2014; Accepted February 19, 2015

The present study is focused on platinum and ruthenium complexes of 4-bromo-spiro-(fluorene-9,4'-imidazolidine)-2',5'-dithione (L), synthesized from $(NH_4)_2[PtCl_4]$ and $RuCl_3.H_2O$, and their potential cytotoxicity properties. The structure of the complexes obtained is researched by elemental analysis and means of spectroscopic UV-Vis, IR, FT-ATR methods. We have examined for the first time biological potential of new complexes on a retinoblastoma human cell line (WERI-Rb-1). The cytotoxic effect is evaluated by WST-assay (Roche Applied Science).

Key words: *4-bromo-spiro-(fluorene-9,4'-imidazolidine)-2',5'-dithione, metal complexes, cytotoxic effect*

INTRODUCTION

Hydantoin derivatives possess a wide array of important biochemical and pharmacological properties. Several of these (phenytoin, methetoin, mephenythoin, fosphenytoin, norantoin) are well-known anticonvulsive drugs [1], whereas others have been suggested to act as antiarrhythmics and antimicrobial agents, skeletal muscle relaxants and nonsteroidal antiandrogens [2]. Recently, antitumor effect of hydantoin derivatives has been described by several authors [3, 4].

Although hydantoin compounds are studied extensively, there is not much research on their anticancer effects. In a previous work of ours, we have reported a method for obtaining 4'-bromo-(9'-fluorene)-spiro-5-(2,4-dithiohydantoin) (4-bromo-spiro-(fluorene-9,4'-imidazolidine)-2',5'-dithione) [5] and 3-amino-9'-fluorenespiro-5-hydantoin [6]. In the studies cited above, we have investigated cytotoxic activities of the two compounds on the retinoblastoma cell line WERI-Rb-1 and antibacterial effects towards Gram-positive, Gram-negative bacteria, as well as yeasts *C. albicans*. Recently, we studied the complexation properties of (9'-fluorene)-spiro-5-hydantoins and its 2-thio derivative [7]. The two platinum complexes show significant effects on cancer cell growth compared to their ligands.

In the current work we described the synthesis and reaction conditions to obtain of new Pt(II) and Ru(III) complexes of 4-bromo-spiro-(fluorene-9,4'-imidazolidine)-2',5'-dithione (L) with general formula given in Figure 1**,** as well as characterization of the obtained complexes and *in vitro* antiproliferative activity on human tumor cell line.

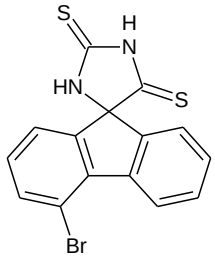

Fig. 1. General formula of (L).

EXPERIMENTAL

Metal salts ($(NH_4)_2[PtCl_4]$ and $RuCl_3.H_2O$ - Sigma-Aldrich or Merck) and solvents used for the synthesis of the complexes were with a p. a. qualification. UV/Vis spectra of L and its metal complexes were measured on a Lambda 9 Perkin-Elmer UV/Vis/NIR Spectrophotometer from 200 nm to 1000 nm. The IR spectra of L and its complexes were registered in KBr pellet on a Bruker FT-IR VERTEX 70 Spectrometer from 4000 cm^{-1} to 400 cm^{-1} at resolution 2 cm^{-1} with 25

To whom correspondence should be sent.
E-mail: marinova@uni-plovdiv.bg

scans. Attenuated Total Reflection (ATR) spectra were registered on the same instrument by ATR accessory MIRacle™ with a one-reflection ZnSe element (Pike); the stirred crystals of L and its complexes were pressed by an anvil to the reflection element; the spectra were from 4500 cm^{-1} to 600 cm^{-1} at resolution 2 cm^{-1} with 16 scans.

1. Synthesis of Pt(II) and Ru(III) complexes of L

0.0004 mol (0.1445 g) of L in 10 cm^3 THF; 0.0002 mol (0.0746 g) $(NH_4)_2[PtCl_4]$ or 0.0002 mol (0.0450 g) $RuCl_3.H_2O$ in 10 cm^3 H_2O; 0.1 M solution of NaOH. 1 cm^3 of 0.1 M NaOH was added slowly to an L solution while stirring at pH = 9. The solution of the metal salts was added dropwise from a burette during stirring with electromagnetic stirrer. The precipitation of the formed complexes started after 72 h for Pt(II)L or 48 h for Ru(III)L, respectively. The complexes were formed as a brown or a black amorphous precipitates. The precipitates was filtered and washed with 10-20 cm^3 H_2O. These were dried over $CaCl_2$ for 2 weeks. It was found out that the complexes were soluble in THF and DMSO.

Elemental analysis for $PtL_2.2H_2O$; $C_{30}H_{20}N_4S_4Br_2PtO_2$; Mw = 951.65 g/mol; calc./(exp.) C% - 37.8 / (37.2); H% - 2.1 / (2.0); N% - 5.9 / (6.2); $Ru_2L_2L_{-4H}Cl_2.2H_2O$; $C_{90}H_{54}N_{12}S_{12}Br_6Ru_2O_2Cl_2$; Mw = 2472.72 g/mol; calc./(exp.) C% - 43.7 / (43.1); H% - 2.2 / (2.1); N% - 6.8 / (7.0)

IR (ν_{max}, cm^{-1}) L: 3374, 3150, 3066, 2919, 1605, 1575, 1515, 1465, 1448, 1407, 1232, 1216, 1194, 1102, 1064, 773, 754

IR (ν_{max}, cm^{-1}) Pt(II)L: 3500, 3392, 3250, 3065, 2922, 1607, 1513, 1465, 1448, 1405, 1233, 1215, 1191, 1103, 1064, 773, 757

IR (ν_{max}, cm^{-1}) Ru(III)L: 3400, 3100, 3065, 2973, 2872, 1606, 1508, 1465, 1448, 1406, 1234, 1215, 1194, 1106, 1064, 774, 757.

The ATR spectral data obtained of the free ligand L and its new complexes are on situation in University of Plovdiv, Department of the corresponding author.

2. WST-1 cell proliferation assay

The cytotoxic effect of Pt(II)L and Ru(III)L complexes were assessed on a retinoblastoma cell line (WERI-Rb1, ATCC-HTB-169) using WST-1 assay (Cat. No11 644 807 001, Roche). Cells were seeded in 96-well flat-bottom plates at a density of $6{,}5x10^4$ cells/well. After a cultivation period of 24h, the compounds were added at a concentration of 50 μM and incubated for 24 and 48h respectively. WST-1 was added to the cells at these time points and incubated for 4h. WST-1 is a colorimetric assay for the nonradioactive quantification of cell proliferation, viability and cytotoxicity. Absorbance was measured on ELISA SUNRISE Reader. The wavelength for measuring the absorbance of the formazan product is 450 nm and the reference filter was set at 620 nm in accordance with the WST-1 manual. Cells grown in culture media alone and in appropriate concentrations of DMSO were used as controls. The percentage of viable cells was calculated as a ratio of the OD value of the sample to the OD value of the control. Descriptive statistics was done in Excel to determine mean and SD values.

RESULTS AND DISSCUSION

Complexation with Pt(II) and Ru(III) were conducted under alkaline conditions using metal salts namely $(NH_4)_2[PtCl_4]$ and $RuCl_3.H_2O$ at molar ratio $M:L:OH^- = 2:4:1$. Neutral complexes were synthesized and isolated as brown and black precipitates, respectively. All complexes were investigated by means of elemental analysis, UV-Vis FT-ATR and IR spectroscopy. The elemental analysis data show metal-to-ligand ratio 1:2 and presence of two water molecules for Pt(II)L complex. All UV/Vis spectra were registered in THF. Maxima in the UV/Vis spectra of the free ligand L were observed at λ_{max} = 234 nm, 241 nm, 268 nm, 279 nm, 294 nm. Maxima in the UV/Vis spectra of Pt(II)L and Ru(III)L complexes were observed at 238 nm, 243 nm, 271 nm, 290 nm, 380 nm and 239 nm, 269 nm, 294 nm, 380 nm, respectively. In the UV/Vis spectra of the two metal complexes, one new maximum appeared at 380 nm.

The presence of two thioamide groups renders four donor atoms for coordination to the metal center: two S-atoms from C=S groups and two N-atoms from NH groups. The fact that both thioamide groups are part of a common heterocycle, where p-conjugation occurs, makes almost impossible the unambiguous assignment of the observed IR frequencies to individual vibrational modes. Selected vibrational frequencies observed in the IR spectra of the complexes and the free ligand L are given in Experimental part. The bands at 3374 cm^{-1} and 3150 cm^{-1} of the free ligand L may refer to the stretching vibrations of two N-H groups of the hydantoin ring. In the IR spectrum of the PtL complex, the same bands have been observed at 3392 and 3250 cm^{-1}. The two bands shift to higher frequency by 18 and 100 cm^{-1} as compared to the corresponding free ligand bands. In the IR spectrum of the RuL complex one of the N-H band has disappeared and the second band

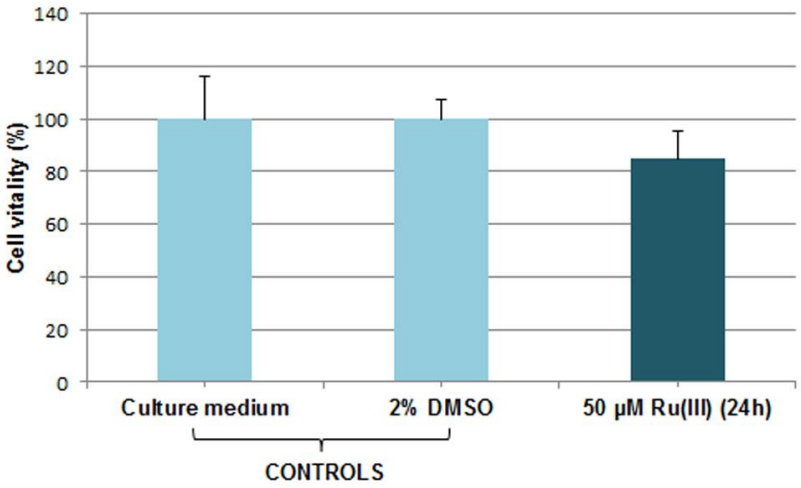

Fig. 2. Effect of the Ru(III)L complex on the proliferation of WERI-Rb 1 cells measured by WST-1 assay at 24h of treatment. The results represent mean values of three measurements. Error bars are SD values.

shifts to a lower frequency by 50 cm^{-1} as compared to the corresponding free ligand. The bands of free ligand L at 1605 cm^{-1} and 1575 cm^{-1} can be attributed to the stretching vibration of the two C=S groups of the hydantoin ring. In the IR spectrum of PtL and RuL complexes the band at 1607 cm^{-1} and 1606 cm^{-1} can be attributed to the stretching vibration of C=S group, respectively. In the IR spectrum of PtL and RuL complexes the second band of C=S group has disappeared. This fact shows that one of the two thiocarbonyl groups of the ligand hydantoin ring participates in the coordination with a metal ion. In the IR spectrum of the PtL and RuL complexes one new band has been observed at 3500 cm^{-1} and 3400 cm^{-1}, respectively. This band may refer to the stretching vibrations of OH^- group. In the IR spectra of the free ligand and its PtL and RuL complexes the band at 3066 cm^{-1} and 3065 cm^{-1}, 3065 cm^{-1} have been for stretching vibrations of CH in fluorene moiety, respectively.

Our results show that the Ru(III)L complex has a moderate cytotoxic effect on the human retinoblastoma cell line WERI-Rb1 (Figure 2). We have found that prolonged incubation periods do not influence cell viability. In contrast, the complex Pt(II)L does not perturb cell proliferation at all. This could be explained by the fact that this compound has a low solubility and the highest achievable concentration at which we were able to test it was only 50 µM. We have previously shown that the ligand 4'-bromo-(9'-fluorene)-spiro-5-(2,4-dithiohydantoin) significantly reduces the number of cells in a time-dependent manner [5].

CONCLUSIONS

The synthesis of two new Pt(II) and Ru(III) complexes with 4-bromo-spiro-(fluorene-9,4'-imidazolidine)-2',5'-dithione have been described. The structure of the obtained complexes was verified by elemental analysis, UV-Vis, FT-ATR and IR spectroscopy. Our results imply that two newly synthesized compounds could not act as potential anticancer agents since they do not significantly inhibit the growth of retinoblastoma cells at the tested concentration.

Acknowledgements. *Financial support by the National Science Fund of Bulgaria, (Contract DFNI BO1/0014) is gratefully acknowledged.*

We are grateful also to Assoc. Prof. P. Penchev from University of Plovdiv for spectra measurements.

REFERENCES

1. D.A. Williams, T.L. Lemke, Foye's principles of medicinal chemistry, Philadelphia: Lippincott Williams & Wilkins, 6th edition by T. L. Lemke, D. A. Williams, 2002.
2. A. Kleemann, J. Engel, B. Kutscher, D. Reichert, Pharmaceutical Substances: Synthesis, Patents, Applications of the most relevant APIs, Vol. 2, Thieme: Stuttgart, New York, 5th Edition, completely revised, 2001.
3. C. Kavitha, M. Nambiar, C. Ananda Kumar, B. Choudhary, K. Muniyappa, K. Rangappa, S. Raghavan, *Biochem. Pharmacol*., **1**, 77, 348 (2009).
4. M. Azizmohammadi, M. Khoobi, A. Ramazani, S. Emami, A. Zarrin, O. Firuzi, R. Miri, A. Shafiee, *Eur. J. Med. Chem*., **59**, 15 (2013).
5. P. Marinova, M. Marinov, Y. Feodorova, M. Kazakova, D. Georgiev, E. Trendafilova, P. Penchev, V. Sarafian, N. Stoyanov, *University of Ruse "A. Kanchev" Proceedings,* **52**, *Chemical technologies*, 33 (2013).
6. P. Marinova, M. Marinov, M. Kazakova, Y. Feodorova, D. Georgiev, V. Lekova, P. Penchev, N. Stoyanov, *Compt. Rend. Acad. Bulg. Sci*., **67**, 513 (2014).
7. P. Marinova, M. Marinov, M. Kazakova, Y. Feodorova, P. Penchev, V. Sarafian, N. Stoyanov, *Biotechnol. Biotec. Eq.*, **28**, 316, (2014).

СИНТЕЗ И БИОЛОГИЧНА АКТИВНОСТ НА НОВИ Pt(II) И Ru(III) КОМПЛЕКСИ НА 4-БРОМО-СПИРО-(ФЛУОРЕН-9,4'-ИМИДАЗОЛИДИН)-2',5'-ДИТИОН

П.Е. Маринова[1*], М.Н. Маринов[2], М.Х. Казакова[3], Я.Н. Феодорова[3],
В.С. Сарафян[3], Н.М. Стоянов[4]

[1]ПУ „П. Хилендарски", Химически факултет, Катедра „ОНХ с МОХ", Пловдив 4000*
[2] Аграрен университет-Пловдив, Факултет по растителна защита и агроекология, Катедра „Обща химия", Пловдив 4000
[3]Медицински университет-Пловдив, Катедра „Медицинска биология", Пловдив 4000
[4]Русенски университет-Филиал Разград, Катедра „Химия и химични технологии", Разград 7200

Постъпила на 24 юли, 2014 г.; приета на 19 февруари, 2015 г.

(Резюме)

Целта на настоящата разработка е получаването на нови Pt(II) и Ru(III) комплекси на 4-бромо-спиро-(флуорен-9,4'-имидазолидин)-2',5'-дитион и изследване на техните потенциални цитотоксични свойства. Структурата на получените метални комплекси е изследвана с елементен анализ и UV-Vis, ИЧ, FT-ATR спектроскопия. За пръв път е проучен потенциалният цитотоксичен ефект на новополучените комплекси върху човешка ретинобластомна клетъчна линия (WERI-Rb-1, ATCC-HTB-169). За оценка на клетъчната пролиферация и жизненост е използван комерсиалния Cell Proliferation Reagent - WST-1 тест (Cat. No11 644 807 001, Roche Applied Science).

Bulgarian Chemical Communications, Volume 47, Special issue A (pp. 79 - 86) 2015

Cross-linked star (co)polymers containing core of C-tetraalkylcalix[4]resorcinarene

P.P. Petrova[1*], S.M. Miloshev[1], Ch.P. Novakov[2]

[1]*University of Chemical Technology and Metallurgy, Polymer Engineering Department, l756 Sofia, Bulgaria*
[2]*Institute of Polymers, Bulgarian Academy of Sciences, 1113 Sofia, Bulgaria*

Submitted July 25, 2014; Revised December 20, 2014

An adapted method for synthesis of ATRP macroinitiator based on C-tetra-pentylcalix[4]resorcinarene was demonstrated. Studies on optimization the process of preparation of star-shaped acrylic polymers by ATRP controlled radical polymerization were performed.

The possibility to obtain butyl acrylate/ (hydroxyethyl) methacrylate (HEMA) copolymer in one pot synthesis initiated by octa-functionalized C-tetra-pentylcalix[4]resorcinarene macroinitiator has been shown. It was found that the polymerization process carried out at [macroinitiator]/[monomer] ratio below 1/1000 for polymeriztion time over 30 min yields to a formation of star-branched (co)polymers containing tetraalkylcalix[4]resorcinarenes core.

Key words: C-tetrapentylcalix[4]resorcinarene, ATRP polymerization, star polymers, star-branched polymers

INTRODUCTION

Star-branched polymers with nonlinear structure exhibit specific properties and therefore the subject of intensive research during last decade [1-6]. The synthesis of materials of controlled composition and architecture may be accomplished by the methods of controlled/living radical polymerization. For example, atom transfer radical polymerization (ATRP) enables the synthesis of well-defined macromolecular architectures such as block copolymers, graft copolymers and other branched structures [7,8]. Among branched macromolecules star polymers and dendrimers are those that show interesting rheological properties, due to their specific spatial architecture and existence of a large number of functional groups [9-12]. Regular star polymers consist of a core located in the center of the molecule and a different number of radiating linear chains (arms, branches) of a symmetrical structure with identical chemical composition connected to the core [2]. They are synthesized using two different approaches: "arm first" and "core first". There are two ways for the synthesis of star polymers by the use of a 'arm first" methodology [13-17]. In the first method the formation of the cross-linked core consists of the following: "living" linear polymer chain copolymerized with divinyl monomer in the presence of mono-functional macro initiator. Another method is based on direct copolymerization of macro monomer with divinyl monomer in the presence of low molecular weight initiator [18,19]. By using the "core first" approach the controlled polymerization is carried out by the initiator with a defined number of initiating groups [20-25] or by not entirely well-defined multifunctional macromolecule [26-29].

To hold a low degree of component heterogeneity star-branched polymers are required to have cores of an accurate and known structure and function. These requirements are satisfied by calix[4] resorcinarenes and their derivatives. As cyclic oligomeric precursors they are superb output fragments for construction of such architectures.

Their high functionality allows for greater variety of synthesis and modification of the polymer structures containing calixarenes fragments [30].

The *aim* of the present study was to synthesize a series of star (co)polymers of well defined predetermined structure based on suitably functionalized calix[4]resorcinarenes using ATRP polymerization technique.

EXPERIMENTAL

Materials

Triethylamine (TEA), α-bromoisobutyryl bromid (98%, Acros), 2,2'-bipyridine, cuprous chloride (CuCl), propylene glycol, dichloromethane were used as received (Acros). Tetrahydrofurane (THF) (99.5 %, Fisher) and DMSO (Fisher, 99 %) were purified by distillation over calcium hydride before use. Butyl acrylate (99%,Acros) and 2-(hydroxy-ethyl) methacrylate (HEMA) (97%, Acros) were purified to remove the stabilizers according to the following procedure: about 1% by volume deionized water was added to the liquid

To whom correspondence should be sent.
E-mail: p.petrova1@abv.bg

monomer, the mixture was cooled and after removing the frozen water with dissolved therein stabilizer the purified monomer was dried over magnesium sulfate. C-tetra-pentylcalix[4]resorcinarene was synthesized according to the procedure described in [31] and was used without further purification.

Syntheses

Synthesis of octa-functionalized C-tetra-pentylcalix[4]resorcinarene-ATRP macroinitiator. C-tetrapentylcalix[4]resorcinarene 1 mmol (0,769 g), triethylamine 24 mmol (2,43g), dry THF 12 ml and DMSO 8 ml were placed into a two-necked flask fitted with a reflux condenser and magnetic stirrer. The mixture was cooled to 0^0C and under constant agitation slowly drop wise α-bromo-isobutyryl bromide 24 mmol (5,52 g), previously dissolved in 12 ml dry THF was added. The reaction mixture was intensively agitated and purged with N_2 for 48h at room temperature. Then the reaction mixture was concentrated on a rotary evaporator. The resulting highly viscous mixture was dissolved in 100ml of dichloromethane washed with deionized water and again concentrated on a rotary evaporator. The product was precipitated in cold methanol and the resulting precipitate was filtered and dried.

Synthesis of star polymer: polymerization of butyl acrylate initiated by octa-functionalized C-tetrapentylcalix[4]resorcinarene ATRP macro-initiator. Octa–functionalized C-tetrapentylcalix[4] resorcinarene 0,1mmol (0,196 g), 2,2'-bipyridine 1,6 mmol (0,2498 g), CuCl 0,8 mmol (0,0792 g), butyl acrylate 160 mmol (22.93 ml) and propylene glycol 30,72 mmol were placed in a two-necked flask fitted with a reflux condenser and magnetic stirrer. The reaction mixture was intensively agitated and purged with N_2 for 30 min then the temperature was raised to 135^0C. The reaction was continued for 2 hours. Then the reaction mixture was cooled, 30 ml of THF was added and the resulting mixture was filtered through a column filled with neutral Al. The final product was precipitated in 40ml mixture of MeOH/H_2O (v/v=80/20).

One pot synthesis of star–branched copolymers: ATRP polymerization of butyl acrylate and (hydroxyethyl) methacrylate (HEMA) initiated by octa-functionalized C-tetrapentylcalix[4] resorcin-arene macroinitiator. Octa–functionalized C-tetrapentylcalix[4]resorcinarene 0,1mmol (0,196 g), 2,2'-bipyridine 1,6 mmol (0,2498g), CuCl 0,8 mmol (0,0792g), butyl acrylate 40 mmol (5,73 ml) and propylene glycol 7,68 mmol were placed in a two-necked flask fitted with a reflux condenser and magnetic stirrer. The reaction mixture was intensively agitated and purged with N_2 for 30 min then the temperature was raised to 135^0C. The reaction was continued for 20 minutes. Then HEMA 40 mmol (4,85 ml) was added and was stirred at the same temperature for a further 20 minutes. After the completion of the second step of the polymerization process the reaction mixture was cooled, 25 ml of THF was added and the resulting mixture was filtered through a column filled with neutral Al. The finally obtained copolymer was precipitated in 40ml mixture of MeOH/H_2O (v/v=80/20).

Instrumentation. ^{1}H NMR spectra were recorded on a *Bruker Avance DRX 250* (250 mHz) instrument. The samples were dissolved in deuterated solvent (dimethyl sulfoxide-d_6). Tetramethylsilane was used as an internal NMR standard.

Infrared spectra of the samples were recorded on a Varian Scimitor 1000 FTIR spectrophotometer equipped with a MIRacle Attenuated Total Reflectance Attachment.

The molecular weight characteristics were determined on a chromatography line consisting of a 510 HPLC pump, a U6K universal injector, a tunable absorbance detector M 484, a differential refractive index detector M 410 (all Millipore Co., Waters Chromatography Division) and a set of three *Phenogel* columns (Phenomenex) with nominal pore sizes of 50Å, 100Å and 10000 Å. THF was used as an eluent at 40°C and a flow rate of 1.0 ml.min^{-1}. Molecular weight characteristics were calculated using a calibration curve constructed with monodisperse poly(styrene) standards on a station for collection and processing of data through Clarity software. 1,3-dihydroxybenzene was used as an internal standard.

RESULTS AND DISCUSSIONS

Synthesis of octa-functionalized C-tetra-pentylcalix[4]resorcinarene-ATRP macroinitiator. The synthesis of octa-functionalized C-tetra-pentylcalix[4]resorcinarene was performed accor-ding to the methodology proposed in [32] and adapted in analogy to [33] as shown in Scheme 1.

The methodology is optimized to achieve maximum reproducibility of well defined products and to avoid the step of product purifying by column chromatography or repeated re-crystallization as described in the literature [15,24,30,32]. The methodology is optimized to achieve maximum reproducibility of well defined

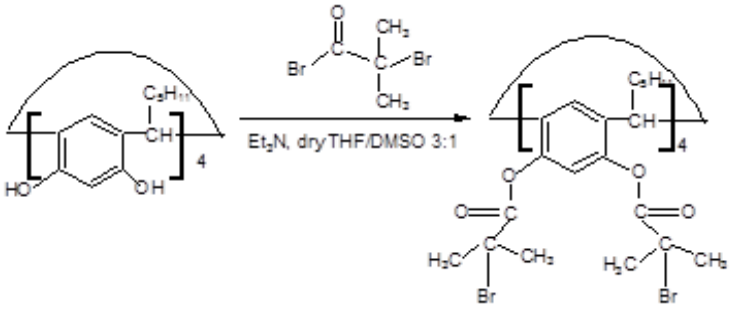

Scheme 1. Synthesis of octa-functionalized C-tetrapentylcalix[4]resorcinarene

products and to avoid the step of product purifying by column chromatography or repeated recrystallization as described in the literature [15,24,30,32].

GPC, ^{1}H NMR and IR spectroscopy were used to characterize the products obtained.

In the IR spectra of both C-tetra-pentylcalix[4]resorcinarene (Fig. 1a) and of the functionalized product (Fig. 1b), an oscillation band evidence that the product was functionalized. at about 3200cm^{-1} characteristic for the OH groups was not observed. A strip oscillation at about 1753 cm^{-1} was appeared which is characteristic for the C=O bond of the carbonyl group. A doublet at about 1100 cm^{-1}, characteristic for the methyl group (-CH_3) of the substituent was also detected. The appearance of an intense band at about 1255 cm^{-1}, which is characteristic for the (Ar) C-O-C bond is further

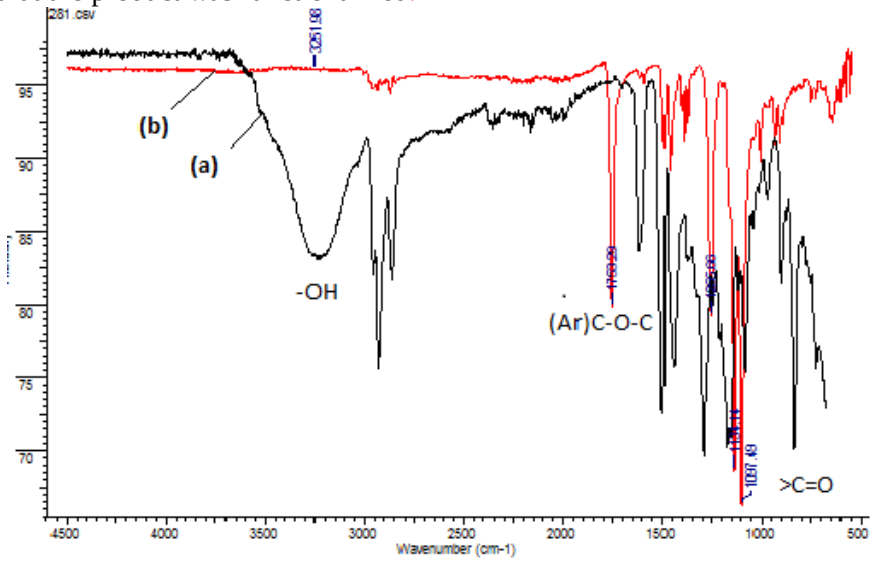

Fig. 1. IR spectra of C-tetrapentylcalix[4]resorcinarene (a) and octa-functionalized derivative (b)

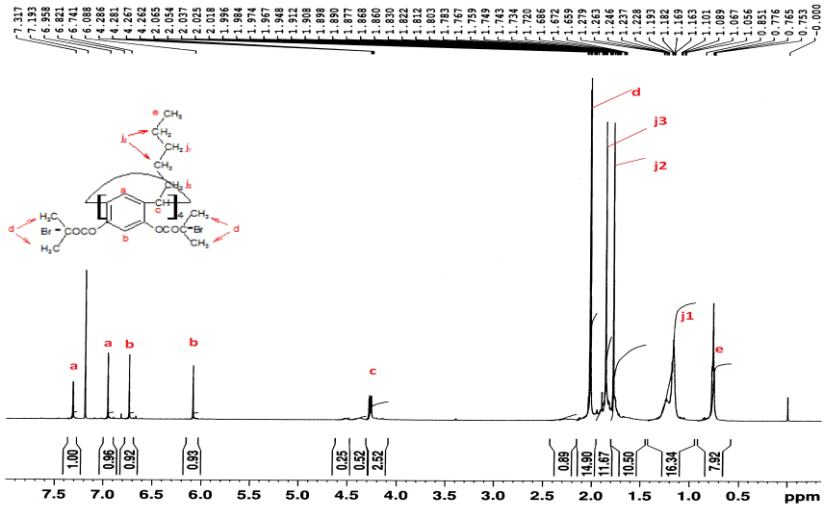

Fig. 2. ^{1}H NMR spectrum of octa-functionalized C-tetrapentylcalix[4]resorcinarene.

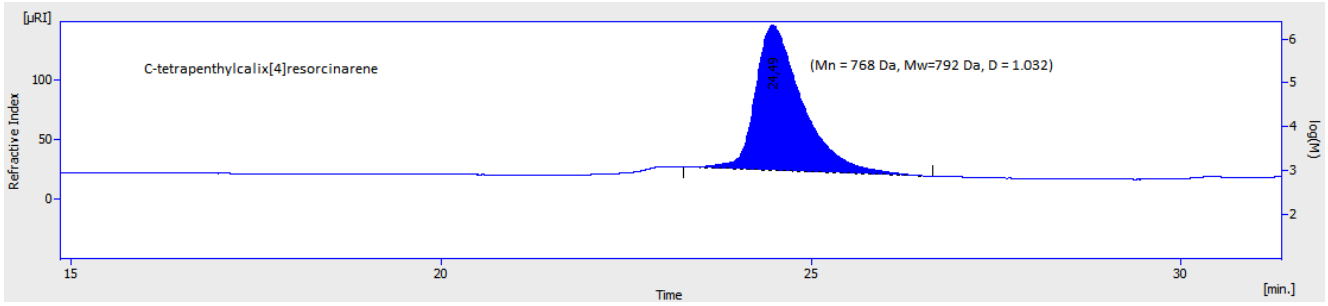

Fig. 3a.

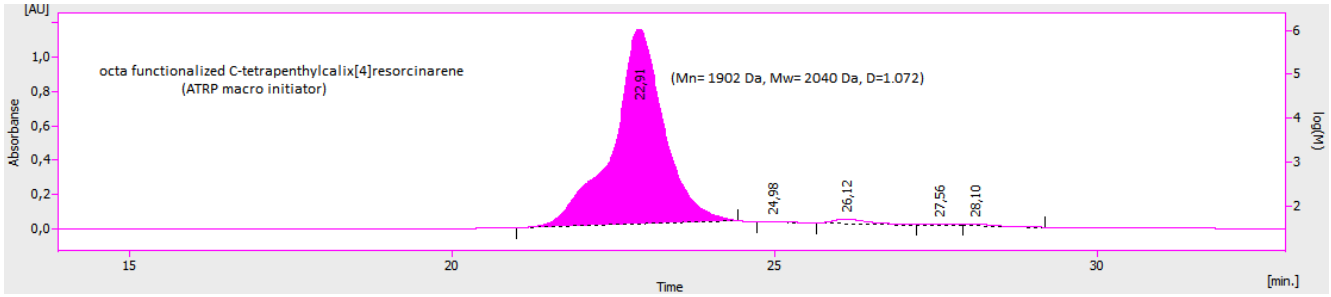

Fig. 3b.

Fig. 3. GPC traces of C-tetrapentylcalix[4]resorcinarene (a) and octa-functionalized ATRP macroinitiator (b).

The structure of ATRP macroinitiator obtained was proved from ^{1}H NMR spectrum (Fig. 2) where signals characteristic for the protons of the expected structure are observed.

The molecular weight characteristics of the C-tetrapentylcalix[4]resorcinarene and its octa-functionalized derivative are shown in Fig. 3. The calculated from GPC traces molecular mass of the functionalized calixarene based macroinitiator of about 2000 Da (Fig. 3) corresponds to the theoretically calculated one (1960 Da).

Synthesis of star polymer: polymerization of butyl acrylate initiated by octa-functionalized C-tetra-pentylcalix[4]resorcinarene ATRP macroinitiator. The synthesis of star polymer with a core comprising octa-functionalized tetrapentylcalix[4]-resorcinarene was carried out according to the adapted methodology described in [33] as shown in Scheme 2.

The dependence of formation of star polymer of the time in ATRP polymerization of acrylate monomer initiated by octa-functionalized C-tetra-pentylcalix[4]resorcinarene was investigated. It was found that under the adopted reaction conditions almost complete conversion of the monomer was observed within about two hours. The studies were conducted at various macroinitiator/monomer ratios (1:1600; 1:1200, 1:800, 1:400). The type of reactions taking place within this time interval is determined by the data taken from the GPC eluograms.

It was found that at [In]/[M] ratio of 1/1600 (close to the value cited in [7]) polymer with a gradual increase over time molecular weight and low polydispersity was obtained.

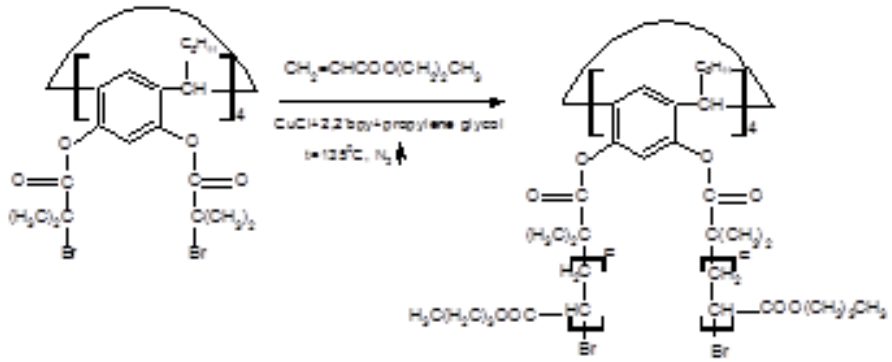

Scheme 2. Synthesis of star polymer via ATRP of butyl acrylate initiated by octa-functionalized C-tetra-pentylcalix[4]resorcinarene macromonomer.

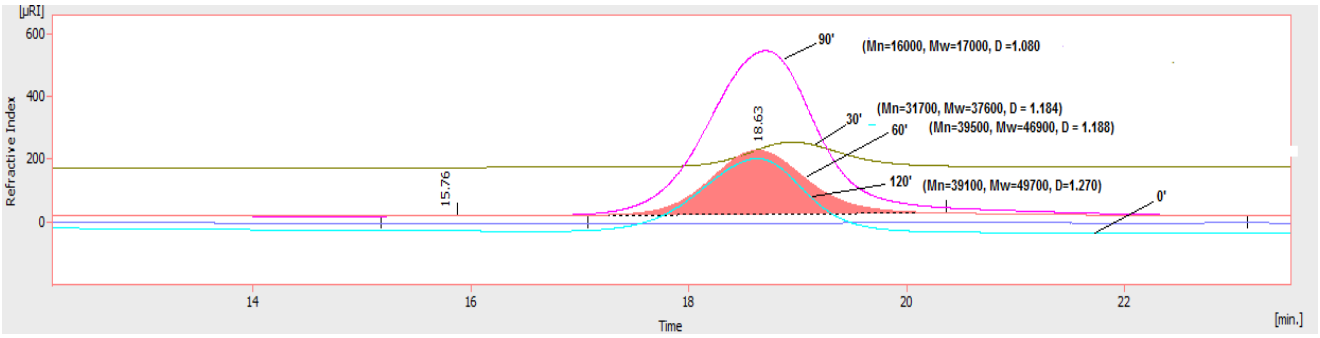

Fig. 4. GPC traces of star polymer prepared by ATRP of butyl acrylate initiated by octa-functionalized C-tetra-pentylcalix[4]resorcinarene macromonomer at [macroinitiator]/ [monomer] ratio = 1/1600.

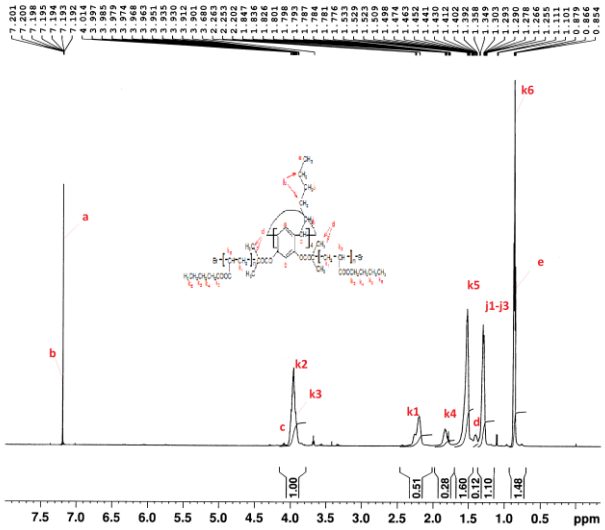

Fig. 5. ^{1}H NMR of star polymer prepared by ATRP of butyl acrylate initiated by octa-functionalized C-tetra-pentylcalix[4]resorcinarene macromonomer at [macroinitiator]/ [monomer] ratio =1/1600.

The values for molecular mass of polymers synthesized at different times are marked in chromatograms shown in Figure 4. It can be seen that the star polymer with a relatively narrow molecular mass distribution and molecular mass of about 40,000 ÷ 50,000 Da was prepared at reaction time of about 60 min.

The prepared star – structure was proved by ^{1}H NMR spectroscopy. The signals characteristic for the protons of the expected structure are observed as shown in spectrum presented in Fig. 5.

There is a tendency to increase the degree of monomer conversion and to obtain a higher yield of star polymer with lower polydispersity by reducing the amount of monomer, i.e., [In]/[M] ratio. The amount of star polymer obtained against reaction time is plotted on Fig. 6.

In addition, the maximum amount of star polymer was prepared in a relatively shorter reaction time reducing the monomer content as seen from Fig. 6. When the polymerization is carried out at [In]/[M] ratio above 1/1000 the complete conversion of the monomer in selected research time interval was not occur. The optimum yield of star polymer for ATRP at [In]/[M] ratio of 1/1200 at at polymerization time of 38 min was found to be of about 64% while for polymerization at [In]/[M] ratio of 1/1600 at polymerization time of 60 min the amount of star polymer reached value of only 50%.

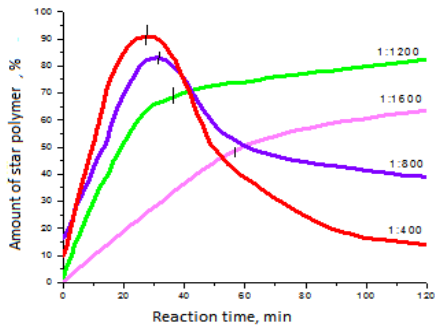

Fig. 6. Plot of the amount of star polymer against reaction time for ATRP of butyl acrylate initiated by octa-functionalized C-tetrapentylcalix[4]resorcinarene at various [In]/[M] ratios: 1/1600 (a); 1/1200 (b); 1/800 (c); 1/400 (d)

At [In]/[M] ratio up to 1:1000 the dependency of the yield of the star polymer versus the reaction time reaching a pronounced maximum at a reaction time of about 30 minutes. The almost complete monomer conversion was observed - 87.30% at [In]/[M] ratio of 1:400 and reaction time of 28 min, and 81.46% at [In]/[M] 1:800 ratio and reaction time of 32 min, respectively. The GPC traces of the reaction mixtures taken at larger reaction times showed the presence of a copolymer fraction of increased molecular weight and index of polydispersity. The amount of these polymer fractions versus reaction time was plotted in Fig. 7.

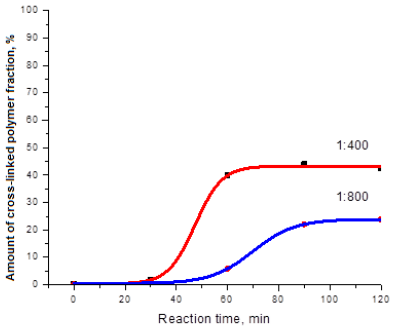

Fig.7. Plot of the amount of cross-linked polymer fraction against reaction time for ATRP of butyl acrylate initiated by octa-functionalized C-tetrapentylcalix[4]resorcinarene at [In]/[M] ratio of 1/800 (a) and 1/400 (b).

Possibly after initial almost complete monomer consumption a process of intermolecular interactions of preformed star polymer was occurred, namely coupling reactions between star macromolecules was initiated. These side effects lead to the observed decrease in the amount of star product of the desired molecular weight and polydispersity when polymerization was carried out at larger reaction times (see curves *b* and *c* shown in Fig. 6).

One pot synthesis of starcopolymer: ATRP polymerization of butyl acrylate and (hydroxyethyl) methacrylate (HEMA) initiated by octa-functionalized C-tetrapentylcalix[4]resorcinarene macroinitiator..

Determined optimal reaction conditions for obtaining defined product at higher yield, namely the [In]/[M] ratio and polymerization time, was used in reaction of preparation of star *co*polymers by the addition of second monomer to the reaction mixture.

"One pot" synthesis was used to prepare star – branched copolymer by sequential addition of two different acrylic monomers, namely butyl acrylate and (hydroxyethyl) methacrylate **(**HEMA). The reaction course of ATRP polymerization was monitored by GPC. GPC traces of polymer obtained polymerizing butyl acrylate and the copolymer formed after the addition of second HEMA monomer are presented in Fig. 8. The two monomers were added in equimolar ratio. Each polymerization step was carried out for 20 minutes. After the first-stage of reaction – polymerization of butyl acrylate the number average molecular weight (M_n) of star homopolymer obtained was of about 15 000 Da and PDI = 1,14. At the end of the polymerization of HEMA, the second polymerization stage, the M_n was reached a value of about 21 000 Da while the polydispersity remains unchanged. Probably the reaction capability of the second monomer is less, since it established conversion rate is significantly lower (45%) for applied reaction time of 20 minutes. However, a possibility of obtaining a star-shaped (cross-linked) (co)polymers of branches of various lengths and composition by ATRP polymerization initiated with calyx resorcinarene macroinitiator is demonstrated.

CONCLUSIONS

An optimized method for synthesis of ATRP calix[4]resorcinarene macroinitiator was demonstrated and the structure of octa-functionalized C-tetrapentylcalix[4]resorcinarene prepared was proved.

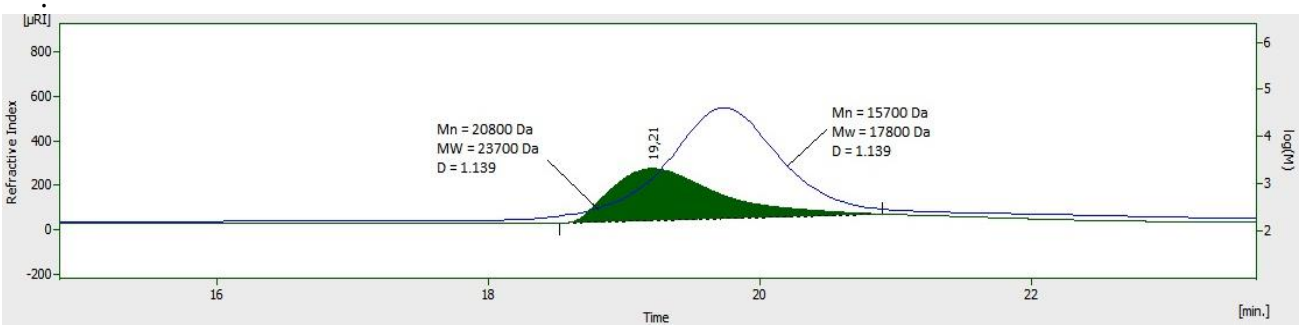

Fig. 8. GPC traces of star-branched copolymer formed via ATRP of butyl acrylate and HEMA initiated by octa-functionalized C-tetrapentylcalix[4]resorcinarene macroinitiator at macroinitiator/monomer ratios [In]/[M1]/[M2] = 1/400/400; reaction time – 60 min.

The possibility for preparation of various star–branched homo- and (co)polymers of well defined architecture via ATRP polymerization initiated by functionalized calixarene macroninitiator was established.

Butyl acrylate / (hydroxyethyl) methacrylate (HEMA) copolymer has been prepared in one pot copolymerization initiated by octa-functionalized C-tetrapentylcalix[4]resorcinarene macroinitiator.

The structure of star–branched homo- and copolymers prepared was studied by various conventional instrumental methods.

Acknowledgment. *The authors are thankful for the financial support from the Research and Development Fund of University of Chemical Technology and Metallurgy- contract 11248. Ch. Novakov acknowledge the financial support from the European Commission project "POLINNOVA".*

REFERENCES

1. Zheng A., Xue Y., Wie D., Guan Y., Xiao H., *Mater. Sci. Eng*. **C 33**, 519 (2013).
2. W. Burchard, *Adv Polym Sci*, **143**, 113 (1999).
3. S. Grest., L. Fetters, J.L. Huang, D. Richter, *Adv Chem Phys*, **XCIV**, 67 (1996).
4. J. Roovers, L.L. Zhou, P.M. Toporowski, M. van der Zwan, H. Iatrou, N. Hadjichristidis, *Macromolecules*, **26**, 4324 (1993).
5. A. Hult, M. Johansson, E. Malmstrom, *Adv Polym Sci*, **143**, 1 (1999).
6. O.A. Matthews, A N. Shipway, J F. Stoddart, *Prog Polym Sci*, **23**, 1 (1998).
7. S. Strandman, H. Tenhu, *Polymer*, **48**, 3938 (2007).
8. K. Matyjaszewski, Xia J. *Chem Rev*.,**101**, 2921 (2001).
9. L.J. Fetters, A.D. Kiss, D.S. Pearson, G.F. Quack, F.J. Vitus, *Macromolecules* ,**26**, 647 (1993).
10. C.J. Hawker, P.J. Farrington, M.E. Mackay, K.L. Wooley, J.M.J. Fre´chet, *J Am Chem Soc* **117**,4409 (1995).
11. A.W. Bosman, R. Vestberg, A. Heumann, J.M.J. Fre´chet, C.J. Hawker, *J Am Chem Soc*, **125**, 715 (2003).
12. H. Yang, S.T. Lopina, *J Biomater Sci Polym Ed*.,**14,** 1043 (2003).
13. D. Rein, J.P. Lamps, P. Rempp, P. Lutz, D. Papanagopoulos, C. Tsitsilianis, *Acta Polymerica*, **44**, 225 (1993).
14. Xia J., X. Zhang, K. Matyjaszewski, *Macromolecules*, **32**, 4482 (1999).
15. Zhang X., J.Xia, K. Matyjaszewski, *Macromolecules*, **33**, 2340 (2000).
16. K-Y. Baek, M. Kamigaito, M. Sawamoto, *Macromolecules*, **34**, 7629 (2001).
17. Gao H., K. Matyjaszewski, *Macromolecules*, **39**, 3154 (2006).
18. Gao H., S. Ohno, K. Matyjaszewski, *J. Am. Chem. Soc*., **128**, 15111 (2006).
19. Gao H., K. Matyjaszewski, *Macromolecules*, **40**, 399 (2007).
20. Li M., N.M. Jahed, K. Min, K. Matyjaszewski, *Macromolecules*, **37**, 2434 (2004).
21. Wang J.S., D. Greszta, K. Matyjaszewski, *Polym. Mater. Sci. Eng*., **73**, 416 (1995).
22. K. Matyjaszewski, J.S. Wang, in: PCT Int. Appl. (Carnegie Mellon University, USA), WO 9630421, 1996, p. 129 .
23. K. Matyjaszewski, P.J. Miller, J. Pyun, G. Kickelbick, S. Diamanti, *Macromolecules*, **32**, 6526 (1999).
24. S. Angot, K.S. Murthy, D. Taton, Y. Gnanou, *Macromolecules*, **31**, 7218 (1998).
25. J. Ueda, M. Kamigaito, M. Sawamoto, *Macromolecules*, **31**, 6762 (1998).
26. S.G. Gaynor, S. Edelman, K. Matyjaszewski, *Macromolecules*, **29**, 1079 (1996).
27. K. Matyjaszewski, S.G. Gaynor, A. Kulfan, M. Podwika, *Macromolecules*, **30**, 5192 (1997).
28. K. Matyjaszewski, S.G. Gaynor, A.H.E. Mueller, *Macromolecules*, **30**, 7034 (1997).
29. K. Matyjaszewski, S.G. Gaynor, *Macromolecules*, **30**, 7042 (1997).
30. T. Krause, PhD Thesis ,Tech.Univ. Dresden, 2006.
31. D. Plachkova-Petrova, S. Miloshev, C. Novakov: *Bulg. Chem. Comm.* **44,** 208 (2012)
32. St. Angot, D. Taton, Y. Gnanou, *Macromolecules*, **33,** 5418, (2000)
33. S. Strandman, M.Luostarinen, S.Mienela, K.Rissanen, H.Tenhu, *J. Polym.Sci.Part A; Polym.Chem*.,**42** ,4189 (2004)

НАПРЕЧНО СВЪРЗАНИ ЗВЕЗДОВИДНИ СЪПОЛИМЕРИ, СЪДЪРЖАЩИ ЯДРО ОТ С-ТЕТРА-АЛКИЛКАЛИКС[4]РЕЗОРЗИНАРЕНИ

П.П. Петрова[1*], Ст. М. Милошев[1], Христо П. Новаков[2]

[1]Химикохтехнологичен и металургичен университет, Катедра „Полимерно инженерство“, l756 София, България

[2] Институт по полимери, Българска академия на науките, 1113 София, България

Постъпила на 25 юли, 2014 г.; коригирана на 20 декември, 2014 г.

(Резюме)

По адаптирана методика е синтезиран ATRP макроинициатор на основата на С-тетрапентилкаликс[4]резорцинарен. Проведени са изследвания за оптимизиране на метода за получаване на звездовидни акрилатни полимери чрез ATRP контролирана радикалова полимеризация. Показано е, че при определени условия е възможно получаването на бутилакрилат-хидроксиеталакрилатен съполимер чрез едноетапен метод. Установено е, че при съотношения макроинциатор/мономер под 1:1000 и реакционно време над 30 минути се получават и омрежени звездовидни полимери, съдържащи С-тетраалкилкаликс[4]резорцианаренови ядра.

Bulgarian Chemical Communications, Volume 47, Special issue A (pp. 87 - 92) 2015

Preparation of poly(ethylcyanoacrylate) nanofibers by vapor phase polymerization using alcohol initiators

N. Marinov, M. Simeonova*

Department of Polymer Engineering, University of Chemical Technology and Metallurgy Sofia, Bulgaria

Submitted July 30, 2014; Revised February 9, 2015

Anionic initiators, containing either hydroxyl or thiohydroxyl group as initiating moieties, were used for preparation of poly(ethylcynoacrylate) (PECA) nanofibers by vapor phase polymerization. The hydroxyl (alcohol) and thoalcohol groups as nucleophilic entities are capable to attack the double bond of monomer resulting in polymerization in vapor phase and formation of nanofibers at high relative humidity atmosphere. Different techniques such as scanning electron microscopy, thermogravimetric analysis, differential scanning calorimetry, gel permeation chromatography and Fourier transformed infrared spectroscopy were used for characterization of the morphology, thermal behavior, molecular weight and structure of polymer nanostructures (nanofibers).

The results obtained show differences in the properties of PECA nanofibers formed via vapor phase polymerization more probably due to the different nucleophilicity of both initiating species.

Key words: *Nanofibers, poly(ethylcyanoacrylate), vapor phase polymerization, alcohol initiators*

1. INTRODUCTION

Alkyl-2-cyanoacrylates (ACA) are known as one of the most reactive monomers that easily undergo anionic polymerization by nucleophilic attack of strongly activated double bond even by traces of nucleophiles or weak bases such as water or alcohols [1]. The high susceptibility to anionic polymerization of the ACA originates from the monomer property of the 1,1 di-substituted strong electron withdrawing groups, nitrile (CN) and ester (COOR). The attacking nucleophile causes strong electromeric effects, which make the nitrile and ester groups highly negative. This leads to the polarization of the double bond and activates the monomer to the nucleophilic attack. Polymerization of cyanoacrylate vapors is used in forensic science for development of latent fingerprints [2,3] and for replication of ice crystals [4]. In the recent years, Mankidy et al. [5,6] were prepared nanofibers of poly(ethyl-2-cyanoacrylate) (PECA) by a vapor phase polymerization directly on surface modified glass substrates. The vapor phase polymerization of ethyl-2-cyanoacrylate (ECA) accomplished under high relative humidity conditions resulted in different polymer morphologies depending on the type of initiator used [7]. As the best of our knowledge mercaptoethanol is not investigated as initiator of ECA vapor phase polymerization.

•To whom correspondence should be sent.
•E-mail: msimeonova@uctm.edu

2. EXPERIMENTAL

2.1 Materials

Ethyl-2-cyanoacrylate monomer was purchased from Specialty Polymers Ltd, Bulgaria. Ethanol (96%), sulfuric acid (97%) and hydrogen peroxide (30%) were from Valerus Ltd, Bulgaria. 1N–(3-methoxy silyl propyl)diethylenetriamine was obtained from Sigma Aldrich (USA) and mercaptoethanol (96%) was from Merck (USA). Tetrahydrofuran (THF) was from Merck (Germany). All chemicals were of laboratory grade purity and used as obtained.

Microscope slides (coverglasses) with size of 18x18 mm were from Knittel Glass (Germany).

2.2. Methods

2.2.1. Preparation of poly(ethylcyanoacrylate) (PECA) nanofibers by vapor phase polymerization. The closed glass chamber was used at room temperature with a humidity of 89.6-90.3% for preparation of PECA nanofibers. Glass substrates used for nanofibers deposition were cleaned by immersing for 30 min in a freshly prepared Piranha etching solution, then rinsed carefully with deionized water followed by ethanol and dried. Silanation of the cleaned substrate surfaces was performed by 2% aqueous solution of 1N–(3-methoxy silyl propyl)diethylenetriamine in deionized water. For this purpose the cleaned substrates were immersed in this silane solution for

45 min and after that were removed and immediately rinsed with ethanol. The substrates were then placed in a drying-oven maintained at 110°C for 2 hours. Both anionic initiators at a volume of 0.3-0.5 ml were scattered onto processed glass substrates and dried. The substrate was then placed in the chamber with humidifying solution (8 % aqueous solution of sulfuric acid) and humidified for about 10 hours at 89-90% RH. Subsequently (after wetting of substrates), 50 μl of liquid ECA monomer was placed in a plate inside the chamber and vapor phase polymerization was carried out for 12 hours. The circulation in the gas phase inside the chamber was provided by a fan. Humidity was monitored by a Thermo-/Hygrometer model 306 (Germany).

The nanofibers samples were carefully scraped away from the glass substrates, washed by distilled water and dried before characterization by Infra Red Spectroscopy, Gel Permeation Chromatography and Thermal analyses.

2.2.2. Scanning electron microscopy (SEM). The morphology of PECA nanofibers was examined using a scanning electron microscope SEM 515 Philips (Holland) operated at 25 kV of acceleration voltage. Before the observation the samples were coated with thin gold film by BH-30 coater (Philips).

2.2.3. Fourier Transformed Infrared Spectroscopy Fourier Transformed Infrared (FT-IR) spectra of the PECA nanofibers were recorded on an IR Affinity-1 "SHIMADZU" FTIR spectrometer with MIRacle Attenuated Total Reflectance Attachment. A total of 50 scans were used and data were recorded with a spectral resolution of 4 cm^{-1} over the range 4000–400 cm^{-1} spectral region.

2.2.4. Gel Permeation Chromatography. Molecular weight and molecular weight distribution of the PECA nanofibers were determined by Gel Permeation Chromatography (GPC). GPC was performed on a Waters chromatographic system equipped with a double detection - Differential Refractometer M410 and an UV M484 (254 nm) detector. The analyses were performed on Phenogel 50Å, Phenogel 100Å and Phenogel 10000Å columns (Phenomenex) calibrated with polystyrene standards. THF was used as a mobile phase with a flow rate of 1.0 ml/min at 40°C. Data collection and processing were done by the Clarity software.

2.2.5. Thermal analyses. Thermogravimetric **(**TGA) – Differential Scanning Calorimetry (DSC) analyses were performed using DSC-TGA Perkin-Elmer Sapphire machine in flowing N_2 with an average heating rate of 10°C/min between 25 and 300°C.

Thermal degradation and the weight loss of the nanofibers samples were obtained by TGA. The TGA experiments were carried out under a nitrogen flow from 25°C to 300°C at a scan rate of 10°C/min. The glass transition temperatures (Tg) of the PECA nanofibers were measured with DSC. For each measurement, a sample of approximately 5 mg was used, placed in aluminum pan and sealed. The samples were firstly heated from 25°C to 170°C and cooled down (2.5°C/min) to 25°C. Then the analyzed samples were heated to 300°C at a scan rate of 10°C/min. Glass transition temperatures were determined from the first derivative of second scan and the midpoint of the transitions was taken as Tg.

4. RESULTS AND DISCUSSIONS

Poly (ethyl 2-cyanoacrylate) nanofibers were synthesized via vapor phase polymerization initiated either by ethanol or mercaptoethanol. ECA monomer introduced in the vapor phase polymerizes on a glass substrate coated with the alcohol initiators of polymerization. The formation of PECA nanofibers was observed using scanning electron microscopy. SEM analyses of the surface morphology of the obtained polymer nanostructures substantiate the availability of nanofibers deposited on the glass substrates (Figs. 1-2).

The examination of the micrographs shows that the glass substrates with deposited PECA nanofibers initiated with mercaptoethanol are more densely populated (Fig.2-A,B) as compared to these, on which nanofibers initiated with ethanol are deposited (Fig. 1). However there were observed areas, in which the nanofibers deposited are not homogenous in diameter as shown in Fig. 2-A,B. The reason for this higher nanofibers yield could be the different rate of polymerization. The diameters of nanofibers initiated with ethanol were between 125-250 nm (mean diameter of 175.75 nm), while these of nanofibers initiated with mercaptoethanol were between 100-200 nm (mean diameter of 141.75 nm).

IR spectra show no differences between the two vapor phase synthesized polymer nanofibers regarding their chemical structure (Fig. 3). The characteristic bands for PECA are well seen in both spectra: CH_3 at 2988 and 2880 cm^{-1}, CH_2 at 2943 cm^{-1}, CN at 2250 cm^{-1}, C=O at 1745/6 cm^{-1}, C-O-C at 1247 and 1013 cm^{-1}. The C-CN band was observed at 1156 cm^{-1}.

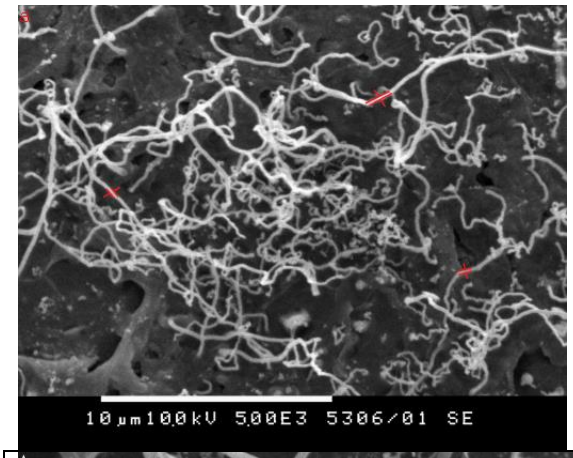

Fig. 1. SEM micrograph of PECA nanofibers prepared by vapor phase polymerization initiated with ethanol

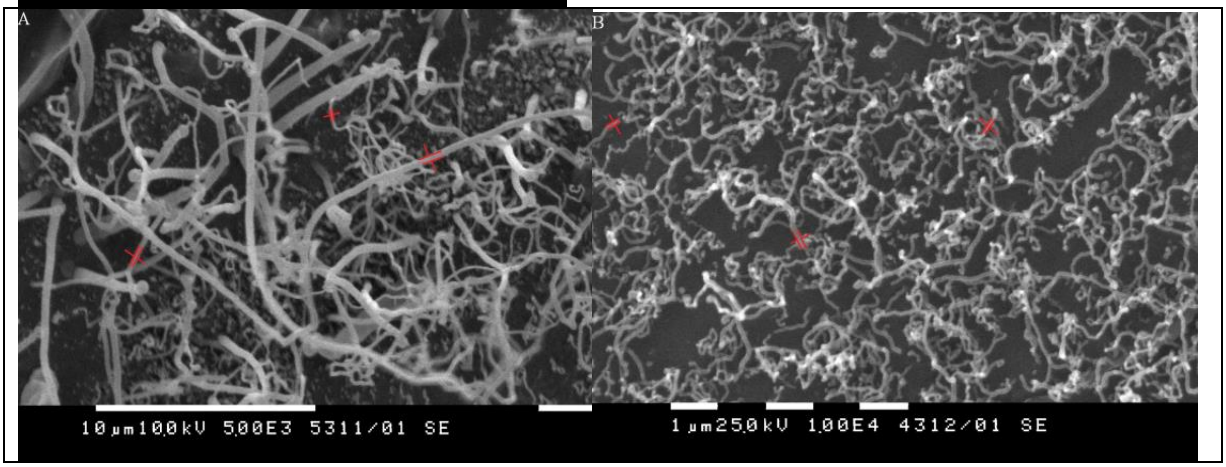

Fig. 2A,B. SEM micrographs of PECA nanofibers prepared by vapor phase polymerization initiated with mercaptoethanol

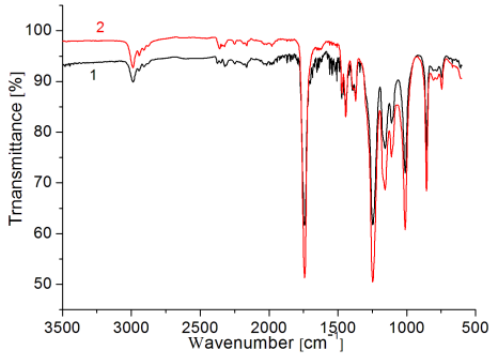

Fig. 3. FT-IR spectra of PECA nanofibers prepared by vapor phase polymerization initiated by ethanol (1) and mercaptoethanol (2)

Molecular weight estimations of PECA nanofibers analyzed were made out using universal polystyrene calibration curve as the standard. Figure 4 depicts the traces obtained from the Refractive Index (RI) detector on the GPC as a function of elution time for both PECA nanofibers samples.

Although the peak molecular weights (Mp) are almost the same (Mp=15163 and 15581 for ethanol and mercaptoethanol initiated sample, respectively) there are significant differences in the number

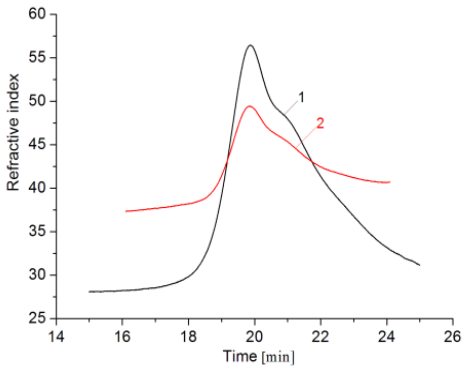

Fig. 4. GPC traces of PECA nanofibers made via vapor phase polymerization using ethanol (1) and mercaptoethanol (2) as initiators.

average (Mn) and weight average (Mw) molecular weight values, as well as in the molecular weight distribution (polydispersity, PD) of the two nanofibers samples (Table 1). PECA nanofibers made using mercaptoethanol as initiator have higher Mn and Mw than these made using ethanol as initiator. Furthermore, the initiated by mercaptoethanol nanofibers show more than twice

narrow PD (1.5) in comparison to initiated by concentration of both initiators as well as the time of polymerization (about 12 hours) were the same, the differences are probably due to the differences in the rates of initiation, propagation or chain transfer (termination) during the polymerization. The lower molecular weight for PECA nanofibers prepared with ethanol as initiator could be due to a slower rate for initiation in contrast to the PECA nanofibers obtain in the presence of mercaptoethanol as initiator. This finding is in good accordance with the nucleophilicity of $^{-}$OH and $^{-}$SH species. HO^{-} is smaller, more solvated, and less nucleophilic than HS^{-} [8]. The IR data analysis indicated that transfer or termination reactions are identical in the two PECA nanofibers since no differences were observed in the IR spectra (Fig. 3). If so the lower molecular weight for PECA nanofibers obtained with initiator ethanol could be a result of a slower rate of initiation.

Table 1. Molecular weight characteristics of PECA nanofibers prepared by vapor phase polymerization initiated with ethanol and mercaptoethanol.

Initiator	Mp g/mol	Mn g/mol	Mw g/mol	PD (Mw/Mn)
Ethanol	15163	2857	10898	3.81
Mercaptoethanol	15581	8462	12749	1.50

Mn, Mw and Mw/Mn values relative to PS standards.

The thermal stability of the synthesized PECA nanofibers was studied by TGA. The TGA curves of PECA nanofibers prepared by two alcohol initiators differing by the nucleophilicity of their initiating species, $^{-}$OH and $^{-}$SH respectively, are shown in Fig. 5. Both curves appeared in the same temperature interval showing similar shapes. The initial (2%) and the maximum mass loss temperatures for PECA nanofibers studied are set in Table 2. The PECA nanofibers samples obtained by vapor phase polymerization initiated by ethanol and mercaptoethanol are relatively stable until 143 and ethanol ones (3.8). As the quantity and 146°C, respectively. Nanofibers obtained with ethanol as initiator start degrading at slightly lower temperature than these prepared with mercaptoethanol. Their maximum degradation rate is registered significantly earlier (at 247°C) than that of mercaptoethanol initiated nanofibers (at 297°C). The two nanofibers samples completely degraded at around 300°C. The results obtained are in accordance with the suggestion of a previous study that the stability of the PACA depends on the nature of initiator and polymerization method [9].

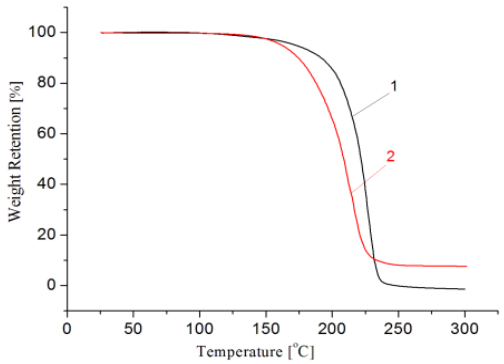

Fig. 5. TGA curves at a heating rate of 10°C/min of PECA nanofibers prepared by vapor phase polymerization with initiators ethanol (1) and mercaptoethanol (2).

The glass transition temperature of PECA nanofibers samples synthesized by vapor phase polymerization process initiated with ethanol and mercaptoethanol were determined by DSC analysis. The PECA nanofibers synthesized using initiator ethanol showed rather unclear glass transitions during the 1st DSC scan (Fig 6).

During the first DSC scan, two endothermic processes/peaks can be identified in the nanofibers sample obtained with initiation by mercaptoethanol. The first one, weak and relatively wide peak was registered around 64°C. The second relatively narrow and sharp endothermic peak superimposed over the Tg transition is registered at 138°C.

Table 2. Temperatures of initial (2%) and maximal weight loss and transition temperatures of PECA nanofibers, prepared by vapor phase polymerization depending on the initiator used.

Weight loss temperatures and transition temperatures* of PECA nanofibers					
Ethanol			Mercaptoethanol		
2% loss, °C	Max. loss, °C	Tg, °C	2% loss, °C	Max. loss, °C	Tg, °C
143.05	247.19	104	146.28	297.66	128.5

*Tg values were determined after the second DSC scan.

Denchev and co-authors [10] described the same behavior of PECA films synthesized in bulk assuming that neither of these transitions could be due to degradation with weight loss. They attributed the endothermic peak close to Tg rather to structural relaxation due the intensified chain mobility often found in other polymer systems [11].

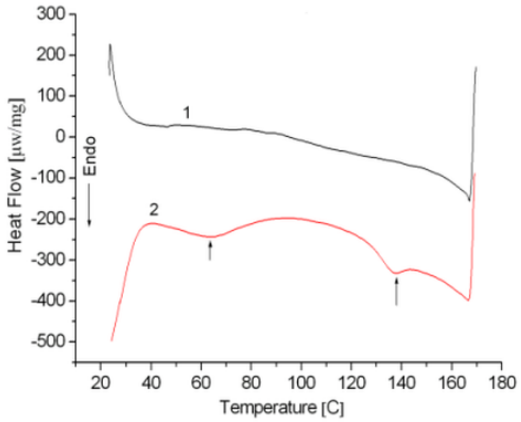

Fig. 6. DSC thermogramms of PECA nanofibers prepared by ethanol (1) and mercaptoethanol (2) used as initiators of vapor phase polymerization, 1st DSC scan.

To more exact determination of the Tg, the first derivative of the second DSC scan was calculated, showing a step instead of a peak. Glass transition temperatures were determined from the first derivative of second scan and the midpoint of the transitions was taken as Tg (figures are not shown). The individual data for both nanofibers are listed in Table 2. The glass transition temperatures in the PECA nanofibers increase with increasing the nucleophilicity of the initiating species of the alcohol used and the molecular weight of the respective nanofibers. Thus PECA nanofibers, depending on the initiator of vapor phase polymerization used and the molecular weight display a Tg between 104 and 128.5°C. As a linear polymer chain PECA has two chain ends, on decreasing molecular weight, the concentration of chain ends increases and the mobility averaged over all repeat units is enhanced, resulting in decrease Tg.[12].

5. CONCLUSIONS

Poly(ethylcynoacrylate) nanofibers were successfully synthesized by vapor phase polymerization initiated by anionic (alcohol) initiators differing by the nucleophilicity of their initiating species, $^{-}$OH and $^{-}$SH, as documented by SEM. Mercaptoethanol was used for the first time for initiation of vapor phase polymerization of ECA aiming to synthesize polymer nanofibers.

Characterization of the morphology, termal behavior, molecular weight and structure of polymer nanofibers by different techniques clearly showed strong dependence of the properties of PECA nanofibers on the nucleophilicity of the initiator used for the vapor phase polymerization process.

Investigations dealing with preparation of PACA nanofibers by vapor phase polymerization initiated by different initiators are in progress.

REFERENCES

1. H.W. Coover, D. W. Dreifus, J. T. O'Connor, *Handbook of Adhesives*, V. N. Reinhold (ed.), New York, 3rd edn, 1990.
2. H. Lee, R.E. Gaensslen, Advances in fingerprint technology, H. Lee, R. E. Gaensslen (eds.), Boca Raton, FL: CRC Press, 2001.
3. D.L. Exline, C. Wallace, C. Roux, C. Lennnard, M.P. Nelson, P. J. Treado, *Forensic Sci.*, **48**, 1047 (2003).
4. R. Smith - Johannsen, *Science*, **171**, 1246 (1971).
5. P.J. Mankidy, R. Rajagopalan, H.C. Foley, *Chem. Commun*., **10**, 1139 (2006).
6. P.J. Mankidy, R. Rajagopalan, C.G. Pantano, H.C. Foley, *Chem. Mater*. **21**, 831 (2009).
7. P.J. Mankidy, R. Rajagopalan, H. C. Foley, *Polymer*, **49**, 2235 (2008).
8. F.A. Carey, *Organic Chemistry*, 4th edition, K. A. Peterson (edr.), McGraw-Hill, 2000, chapter 8, p. 313.
9. K.G. Chrobadjiev, PC. Novakov, *Eur. Polym. J*., **27**, 1009 (1991).
10. Z. Denchev, M. Tomanova, A. Lederee, *J. Polym. Sci., Part A: Polymer Chemistry*, **46**, 5142 (2008).
11. J. Zhao, J. Wang, C. Li, Q. Fan, *Macromolecules*, **35**, 3097 (2002).
12. K.L. Ngai, In: Physical Properties of Polymers, 3 edition, J. Mark (ed.), Cambridge University Press, 2004, Part I., Chapter 2, p. 72.

ПОЛУЧАВАНЕ НА ПОЛИЕТИЛЦИАНАКРИЛАТНИ НАНОВЛАКНА ЧРЕЗ ПОЛИМЕРИЗАЦИЯ В ПАРОВА ФАЗА С АЛКОХОЛНИ ИНИЦИАТОРИ

Н. Маринов, М. Симеонова*

Катедра Полимерно инженерство, Химикотехнологичен и металургичен университет, София, България

Постъпила на 30 юли 2014 г.; Коригирана на 9 февруари 2015 г.

(Резюме)

Анионни инициатори, съдържащи хидроксилна или тиохидроксилна група като инициращи групи, са използвани за получаване на полиетилцианакрилатни (ПЕЦА) нановлакна чрез полимеризация в парова фаза. Хидроксилната (алкохолна) и тиоалкохолна групи като нуклеофилни единици са способни да атакуват двойната връзка на мономера, в резултат на което протича полимеризация в парова фаза и формиране на нановлакна в атмосфера с висока относителна влажност. Различни техники като сканираща електронна микроскопия, термогравиметричен анализ, диференциална сканираща калориметрия, гелово-проникваща хроматография и инфрачервена спектроскопия с Фурие трансфомация са използвани за охарактеризиране на морфологията, термичното поведение, молекулната маса и структурата на полимерните наноструктури (нановлакна).

Получените резултати показват различия в свойствата на ПЕЦА нановлакна, формирани чрез полимеризация в парова фаза, най-вероятно поради различната нуклеофилност на двете инициращи групи.

Bulgarian Chemical Communications, Volume 47, Special issue A (pp. 93 - 99) 2015

Surface modified poly (butyl cyanoacrylate) nanoparticles loaded with indomethacin: preparation and physicochemical characterization

V. Staneva[1], G. Ivanova[2], M. Simeonova[1*]

[1]*University of Chemical Technology and Metallurgy, Department of Polymer Engineering, 1756 Sofia, Bulgaria;*
[2]*REQUIMTE, Departamento de Quıımica, Faculdade de Ciěncias, Universidade do Porto, 4169-007 Porto, Portugal*

Received July 25, 2014; Accepted February 9, 2015

Poly(butylcyanoacrylate) nanoparticles (PBCN) as biodegradable and biocompatible devices have gained interest as a colloidal drug delivery system. Their main technological advantage is the possibility of preparation by anionic polymerization in aqueous medium without addition of any initiator that could have undesirable side effects. Unfortunately, in such conditions arises a problem with the encapsulation of poorly water-soluble drugs.

Aiming to overcome this problem the modifying ability of hydroxypropyl-beta-cyclodextrin (HPBCD) in the preparation of PBCN loaded with indomethacin was investigated. Surface modified HPBCD-PBCN were prepared by anionic polymerization of the monomer in the presence of HPBCD. The loading of indomethacin was performed simultaneously with the formation of nanoparticles.

The physicochemical characterization of indomethacin loaded HPBCD-PBCN was made by Dynamic Light Scattering, laser Doppler electrophoresis, Infra Red and NMR spectroscopy. All of these verify the presence of the drug into the polymer matrix of nanoparticles.

Key words: *Poly(butylcyanoacrylate) nanoparticles, hydroxypropyl-β-cyclodextrin, indomethacin, drug delivery, NMR.*

INTRODUCTION

Indomethacin (Ind) (Fig 1), a non-steroidal anti-inflammatory drug is widely used in the treatment of arthritic diseases to reduce inflammation, pain and fever [1]. However it is well known to cause side effects including gastrointestinal disturbances. This can be avoided by delivering the drug to the targeted site of the body [2,3]. Indomethacin is poorly water-soluble drug and shows low bioavailability, but encapsulation of the drug within biodegradable polymer nanoparticles can increase its bioavailability.

Different types of polymer nanoparticles [4-7] were used as carriers for Ind aiming to improve its bioavailability and undesirable side effects. Complexes of soluble cyclodextrins and their derivatives with Ind were also prepared for improving drug bioavailability [8,9]. Different types of cyclodextrins are used in the preparation of poly(alkylcyanoacrylate) (PACA) nanoparticles, loaded with various poorly water-soluble drugs. The loading capacity of nanoparticles for poorly water soluble drugs is significantly increased as shown on a series of steroids and on saquinavir [10]. Hydroxypropyl-beta-cyclodextrin/Flurbiprofen (HPBCD/FP) inclusion complex was used for preparation of HPBCD/FP/PACA nanoparticles for improving the oral bioavailability of FP [11].

The aim of the present study was the preparation of hydroxypropyl-beta-cyclodextrin modified poly(butylcyanoacrylate) nanoparticles (PBCN) loaded with Ind and their physicochemical characterization.

EXPERIMENTAL

2.1. Materials

n-Butyl-2-cyanoacrylate (n-BCA) monomer was purchased from Specialty Polymers Ltd, Bulgaria. Hydroxypropyl-β-cyclodextrin, 97% was from ACRŌS ORGANICS (Belgium) and citric acid as monohydrate was from Auldrich. Indomethacin (Reagecon, Ireland) was a gift from Sopharma Ltd. Other chemicals were of laboratory grade purity and used as obtained.

2.2. Methods

2.2.1. Preparation of unloaded HPBCD modified poly(butylcyanoacrylate) nanoparticles (HPBCD-PBCN). HPBCD modified poly(butylcyanoacrylate) nanoparticles were prepared by an *in situ* anionic dispersion polymerization. Basically, the monomer, n-BCA

To whom correspondence should be sent.
E-mail: msimeonova@uctm.edu

(20 mg/ml) was instilled into aqueous polymerization medium, containing citric acid (2 mg/ml) and HPBCD (5 mg/ml) serving as

at room temperature with continuous magnetic stirring for 6 hours. The formed polymer suspension of nanoparticles was then adjusted to pH 7 by 1N sodium hydroxide.

2.2.2. Preparation of Indomethacin-loaded nanoparticles (HPBCD-PBCN-Ind). Nanoparticles-loading of Ind was accomplished during the interfacial polymerization simultaneously with formation of nanoparticles. Powdered Ind was dissolved (0.4 mg/ml) in 2 ml of acetone and the monomer was added to this organic phase. Then this organic phase was carefully added to the aqueous solution of HPBCD (5 mg/ml) and the polymerization was carried out under the same experimental conditions as the unloaded nanoparticles.

2.2.3. Photon Correlation Spectroscopy. The mean (hydrodynamic) diameters of unloaded and Ind-loaded nanoparticles were determined by photon correlation spectroscopy (PCS). The dynamic light scattering measurements were performed on a Zetasizer Nano ZS (Malvern Instruments, Malvern UK) using a detection angle of 173º at a temperature of 25ºC. Zeta-potential (ξ-potential) was measured by laser Doppler electrophoresis on the same apparatus using a detection angle of 17º of the scattered light at above temperature (25ºC). The analyzed samples were appropriately diluted with deionized water.

2.2.4. Fourier Transform Infrared Spectroscopy characterization. Fourier Transform Infrared (FTIR) spectroscopy was used as a preliminary tool to verify the presence of Ind into polymer matrix of HPBCD-PBCN. FTIR spectra of the nanoparticles both unloaded and Ind-loaded as well as of Ind were recorded in KBr pellets on a Varian Resolutions Pro spectrometer with resolution of 2 cm^{-1} over the range 4000–400 cm^{-1}.

Samples of the analyzed polymer suspensions were filtered over a 0.1 μm pore sized Cellulose nitrate membrane (Whatman, England) and the isolated wet nanoparticles were dried and used for characterization by FTIR and NMR spectroscopy.

2.2.5. NMR Spectroscopy. All NMR experiments were recorded on a Bruker Avance III 400 spectrometer, operating at 400.15 MHz for protons, equipped with pulse gradient units, capable of producing magnetic field pulsed gradients in the z-direction of 56 G/cm. The NMR spectra were acquired in DMSO-d_6 as a solvent at a temperature of 30°C. NMR spectra of Ind, HPBCD, HPCBD-PBCN, HPBCD-PBCN-Ind and physical mixture of acidifying agent and steric colloidal stabilizer, respectively. Polymerization was carried out

HPBCD-PBCN and Ind were measured. The solvent resonance peak at 2.49 ppm was used as a chemical shift reference in ^{1}H NMR spectra. ^{1}H NMR experiments were acquired with relaxation delay 1.5 s, 128 or more transients of a spectral width of 4000 Hz were collected into 64 K time domain points.

Two-dimensional ^{1}H/^{1}H correlation spectra (COSY) and gradient-selected ^{1}H/^{13}C heteronuclear single quantum coherence (HSQC) spectra were recorded using the standard Bruker software. 2D-COSY spectra were acquired with a multiple quantum filter, gradient pulses for selection, a gradient ratio of 16:12:40 and a relaxation delay of 1.5 s. A total of 2048 data points in F2 and 256 data points in F1 over a spectral width of 5000 Hz were collected. ^{1}H/^{13}C HSQC experiments (Bruker pulse program hsqcedetgpsisp2.2) [12-15] recorded in phase sensitive mode using echo/antiecho-TPPI gradient selection, with decoupling during acquisition time and multiplicity editing during selection were carried out with a spectral width of 6000 Hz for ^{1}H and 20000 Hz for ^{13}C, relaxation delay 1.5 s, Fourier transform (FT) size 2 K × 1K.

The two dimensional Nuclear Overhauser effect (NOE) spectroscopy (NOESY, ROESY) experiments were acquired in phase sensitive mode with gradient pulses in the mixing time, using the standard pulse sequences with optimized mixing time in the range between 200 and 800 ms. Generally, 64 scans and 512 F1 slices were obtained and the spectral width in both dimensions was 8000 Hz.

The Diffusion-ordered NMR (DOSY) experiments were acquired employing Bruker 2D pulse sequence (dstebpgp3s) with double stimulated echo for convection compensation and LED (Longitudinal Eddy Delay) using bipolar gradient pulses for diffusion [16,17] The experimental conditions (amount of the solute and the solvent, temperature, air flow, no sample rotation) for all DOSY experiments were kept constant. Before all NMR experiments, the temperature was equilibrated and maintained at 30°C, as measured using the spectrometer thermocouple system. All measurements were carried out in DMSO-d_6 and the diffusion coefficient of the residual water in DMSO-d_6 (1.2×10^{-9} m^2s^{-1}, calculated standard deviation of 1.4×10^{-3}) was used as an internal reference for the diffusion measurements. The spectra were recorded in 5 mm NMR tubes with an air flow of 535 l/h. Typically, in each experiment a

number of 16 spectra of 16K data points were collected, with values for the duration of the magnetic field pulse gradients (δ) of 3 for Ind and 3.6 ms for the rest of the samples, diffusion times (Δ) of 100 or 200 ms and an eddy current delay set to 5 ms. The pulse gradient (g) was incremented from 2 to 98% of the maximum gradient strength in a linear ramp. The spectra were first processed in the F2 dimension by standard Fourier transform and after baseline correction; the diffusion dimension was processed with the Bruker Topspin software package (version 3.2). The diffusion coefficients are calculated by exponential fitting of the data belonging to individual columns of the 2D matrix. The diffusion coefficients (D) were obtained by measuring the signal intensity at more than one place in the spectra and all scaled to the D value obtained for residual water in DMSO-d_6. At least two different measurements were done for the determination of each diffusion coefficient.

The amount of Ind included into the HPBCD-PBCN-Ind was determined by quantitative NMR analysis, using the relative quantitative method [18].

2.2.6. Drug Loading Determination. The amount of Ind included into the HPBCD-PBCN-Ind was determined by quantitative NMR analysis, using the relative quantitative method [18].

RESULTS & DISCUSSION

HPBCD-PBCN were prepared by an *in situ* anionic polymerization skilled as a dispersion polymerization process since a polymeric stabilizer (HPBCD) was used instead of an emulsifier. The loading of Ind into HPBCD-PBCN was performed during the interfacial anionic polymerization because of the insolubility of Ind in water. Alkylcyanoacrylate monomers are highly predisposed to anionic polymerization proceedings by initial addition of an anion to the strongly activated carbon-carbon double bond. Because of the presence of two powerful electron-withdrawing groups (ester, -COOBu and cyano,-CN), n-BCA monomer holds a remarkable reactivity toward nucleophiles (OH, NH_2, etc.), resulting in an extremely high polymerization rate. Due to its insolubility in the continuous aqueous phase the formed polymer precipitates into a new particulate phase stabilized by the polymeric stabilizer used. The aggregation of these precipitated growing polymer chains after their length exceeds a critical value resulted in formation of nanoparticles [19].

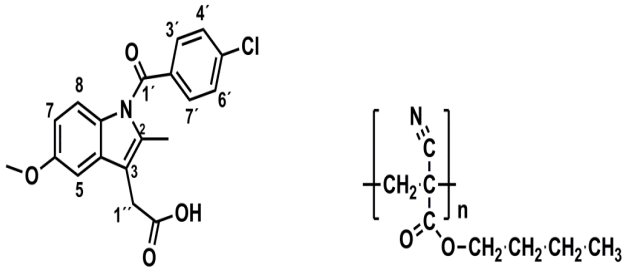

Fig.1. Chemical structure of Indomethacin (Ind) and poly(butylcyanoacrylate).

The obtained HPBCD-PBCN, unloaded and indomethacin loaded were characterized by size, size distribution, and ζ-potential, all considered as main colloid characteristics. Both nanoparticles show a narrow size distribution (polydispersity index, PDI<0.1). The mean hydrodynamic diameter of unloaded HPBCD-PBCN was 209 nm (PDI = 0.086), while those of indomethacin loaded ones was 197 nm (PDI = 0.044), (Fig. 2). A possible reason for the smaller mean diameter of Ind loaded nanoparticles could be an intermolecular interaction between the drug molecules and polymer chains leading to change in the particle compactness. Such behavior of the size of PBCN loaded with other drug molecules was described earlier [20]. The surfaces of both nanoparticles are negatively charged. The ζ-potentials of HPBCD-PBCN and HPBCD-PBCN-Ind in water were -42.3± 6.32 mV and -34.5±6.80 mV, respectively. The reduced surface negativity of Ind-loaded nanoparticles suggests that some of the drug molecules are located (adsorbed) on the nanoparticles surface.

FTIR studies were performed attempting to confirm drug inclusion into the nanoparticles. The comparative FTIR spectra of Ind, unloaded HPBCD-PBCN and drug loaded HPBCD-PBCN-Ind are present in Fig. 3.

In the FTIR spectrum of Ind (Fig. 3a), the characteristic C=O doublet at 1691.41 and 1715.14 cm^{-1}, and C-Cl band at 749.58 cm^{-1} are clearly observed (see molecular structure of Ind in Fig. 1). The FTIR spectrum of HPBCD-PBCN (Fig. 3b) shows the CH_3 at 2963.29 and 2875.96 cm^{-1}, and CH_2 at 2937.23 cm^{-1}. The characteristic CN stretching mode of the poly(butylcyanoacrylate) (see Fig. 1 for molecular structure) was observed at 2250.28 cm^{-1}. The prominent band at 1751.44 cm^{-1} corresponds to the C=O stretching mode of the polymer ester group, while the feature at 1257.75 cm^{-1} corresponds to the asymmetric C-O-C stretch. The C-CN band was observed at 1161.68 cm^{-1}. The wide OH band appears at 3463.23 cm^{-1}.

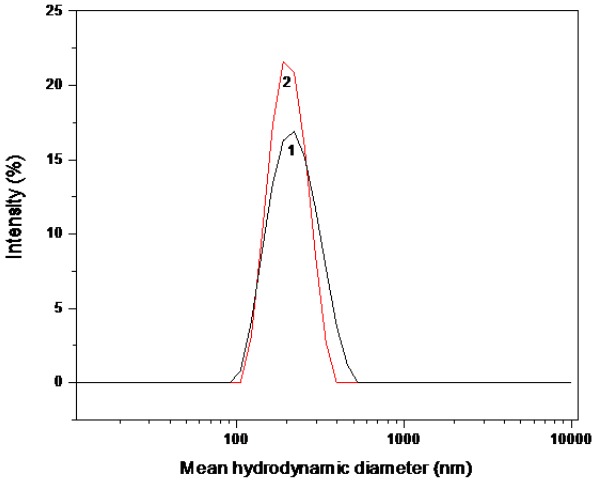

Fig. 2. Size distribution by intensity of HPBCD-PBCN (1) and HPBCD-PBCN-Ind (2)

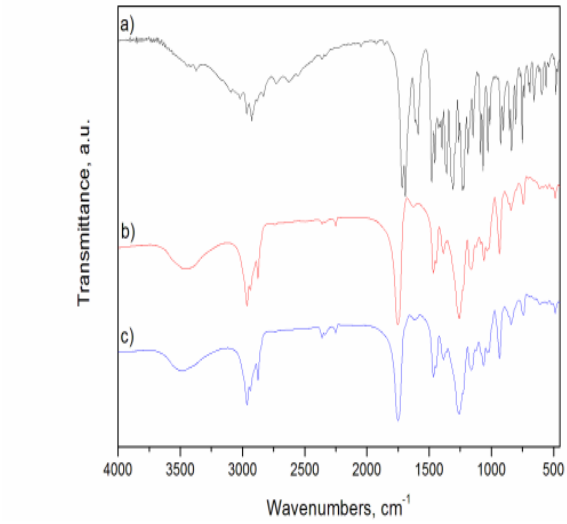

Fig. 3. FTIR spectra of Indomethacin (a), unloaded HPBCD-PBCN (b) and HPBCD-PBCN-Ind (c).

In the FTIR spectrum of HPBCD-PBCN-Ind (Fig. 3c) all characteristic bands of HPBCD-PBCN assigned to the CN stretching at 2250.20 cm^{-1}, C=O at 1750.22 cm^{-1} C-O-C at 1258.39 cm^{-1} and C-CN at 1159.97 cm^{-1} were observed. The characteristic OH band shifted significantly from 3463.23 to the 3482.41 cm^{-1} that evidenced some interactions of Ind molecules with the polymer matrix of nanoparticles.

The ability for inclusion of Ind into the polymer matrix of poly(butylcyanoacrylate) nanoparticles, prepared by an anionic polymerization of n-BCA in the presence of HPBCD was studied by proton NMR spectroscopy. The role of HPBCD in the polymerization process, the possible mechanisms of drug inclusion into the polymer matrix of HPBCD-PBCN and structural characterization of unloaded (HPBCD-PBCN) and Ind loaded (HPBCD-PBCN-Ind) nanoparticles were estimated by studying structurally important NMR parameters, such as chemical shifts, line shape and translational diffusion. For comparison, NMR spectroscopic investigations of Ind, HPBCD-PBCN and their physical mixture (HPBCD-PBCN+Ind) were carried out. The assignment of the resonance signals in ^1H NMR spectra of the samples studied was confirmed by an analysis of their $^1H/^1H$ COSY and $^1H/^{13}C$ HSQC spectra. Typical 400 MHz ^1H NMR spectra of HPBCD-PBCN, HPBCD-PBCN-Ind, Ind with assignment of the resonance signals are presented in Figure 4. The ^1H NMR spectrum of the physical mixture (HPBCD-PBCN+Ind) is included for comparison.

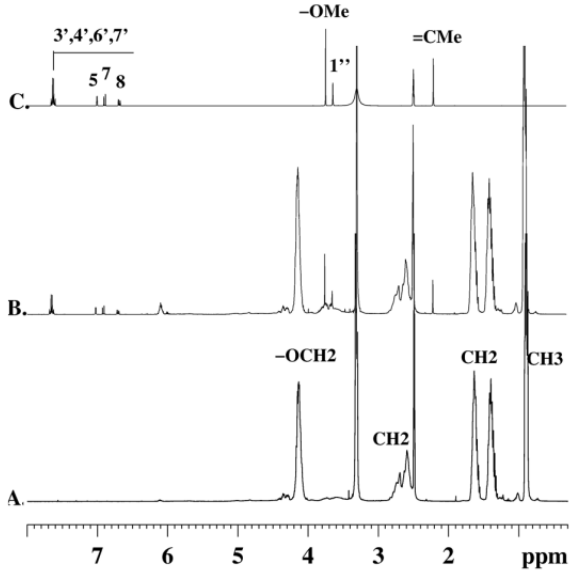

Fig. 4. 400 MHz ^1H NMR spectra of: HPBCD-PBCN (A), HPBCD-PBCN+Ind (B), HPBCD-PBCN-Ind (C) and Ind (D). The assignment of the resonance signals is included.

The ^1H NMR spectra of HPBCD-PBCN and HPBCD-PBCN-Ind are dominated by the intense resonance signals of protons belonging to poly(butylcyanoacrylate) (PBCA), i.e. resonances at 0.89 (CH_3), 1.40 (CH_2), 1.64 (CH_2), 4.14 (OCH_2) and 2.60 ppm (CH_2, main polymer chain). Weak and broad resonance signals characteristic for HPBCD at 5.1-4.8 ppm (anomeric protons), 3.9-3.4 ppm (-OCH and –OCH_2) and 1.04 ppm (CH_3) were additionally registered (Fig. 4). The line broadening of HPBCD resonance signals in ^1H NMR spectra of HPBCD-PBCN and HPBCD-PBCN-Ind reveals an interaction of HPBCD molecules with polymer chains of PBCA.

The available HPBCD hydroxyl groups could behave like an initiator in the anionic polymerization of n-BCA in aqueous medium resulting in covalently bonded to the polymer

Table 1. ^{1}H NMR chemical shifts (δ, ppm) of Ind in the presence and absence of HPBCD-PBCN

	H5	H7	H8	CCH_3	OCH_3	H3'-H7'	H1"
Ind	7.022	6.703	6.914	2.202	3.747	7.648	3.643
HPBCD-PBCN_Ind	7.024	6.705	6.915	2.207	3.751	7.651	3.647
HPBCD-PBCN+Ind	7.023	6.704	6.915	2.206	3.750	7.650	3.646

Table 2. Diffusion coefficients ($D \times 10^{10}$ (m^2s^{-1})) of Ind, HPBCD and HPBCD-PBCN in the samples studied.

Sample	Size, nm	Ind	HPBCD	HPBCD-PBCN
Ind		2.98		
HPBCD			1.38	
HPBCD-PBCN	209		1.01	1.22
HPBCD-PBCN-Ind	197	2.81	1.04	1.29
HPBCD-PBCN+Ind	209	2.92	1.02	1.21

chains HPBCD molecules. In the ^{1}H NMR spectrum of HPBCD-PBCN-Ind, resonances arising from Ind included in the polymer nanoparticles were clearly observed (Fig. 4). Relative to the sample of pure Ind, down field shifts of the resonance signals of Ind in ^{1}H NMR spectra of HPBCD-PBCN-Ind, more significant for the protons in the close proximity to the carboxyl group were registered (Table 1). These chemical shifts alterations were attributed to intermolecular interactions between Ind and HPBCD and/or polymer chains of PBCA. The NOE studies based on the analysis of the two-dimensional NOESY and ROESY spectra have shown no evidence of Ind inclusion into the cavity of HPBCD. Therefore, a presence of electrostatic or dipole-dipole interactions between the oxygen bearing functional groups of Ind, HPBCD and polymer molecules was assumed as a main contribution for the chemical shifts changes observed.

The drug content into the polymer matrix of HPBCD-PBCN was defined by quantitative NMR analysis, using the relative quantitative method according to Malz and Jancke [18]. The drug loaded HPBCD-PBCN in the scope of this investigation were considered as a two componentsystem composed by drug and polymer. The amount of Ind incorporated into HPBCD-PBCN was determined from the relative integral intensity of characteristic signals in ^{1}H NMR spectra of HPBCD-PBCN-Ind, considering the number of the contributing nuclei and molecular weights of Ind and monomer unit (n-BCA) in PBCN. The integral intensities of more than one resonance signal belonging to the individual compounds were measured. The Ind content (weight %) in HPBCD-PBCN-Ind was calculated using the following equation:

$$\text{Ind}\ (\%) = \frac{I_{Ind} \times E_{Ind}}{(I_{Ind} \times E_{Ind}) + (I_{BCA} \times E_{BCA})} \times 100 \quad (1)$$

where, **I** is the integral value for selected protons of Ind and monomer units (n-BCA), respectively; **E** is the molecular weight of the corresponding compound divided by the number of the absorbing protons. The Ind content (%) in the drug loaded HPBCD-PBCN (HPBCD-PBCN-Ind), was found to be 3.4 %.

Diffusion NMR spectroscopy (^{1}H DOSY) was further applied to confirm the Ind incorporation and location into HPBCD-PBCN. The diffusion coefficients (D) of Ind, HPBCD and poly(butylcyanoacrylate) in HPBCD-PBCN-Ind and the physical mixure HPBCD-PBCN+Ind were measured and compared with the corresponding values obtained for the free Ind, HPBCD and HPBCD-PBCN. The diffusion coefficients were obtained by measuring the signal intensity at more than one place in the spectra and all scaled to the D value obtained for residual water in DMSO-d_6. The results are presented in Table 2.

The diffusion coefficients measured for poly(butylcyanoacrylate) in the unloaded HPBCD-PBCN and the physical mixture of HPBCD-PBCN

with Ind were found to be similar but slightly lower than the corresponding value in the drug loaded HPBCD-PBCN (HPBCD-PBCN-Ind). The results are relevant to the smaller nanoparticales size determined for the drug loaded formulation (HPBCD-PBCN-Ind). The observed decrease of HPBCD diffusion in HPBCD-PBCN, HPBCD-PBCN-Ind and HPBCD-PBCN+Ind samples was attributed to the participation of molecules in the polymerization process of n-BCA most probably as an initiator and direct bonding of HPBCD molecules to the polymer chains of PBCA. The reduction of Ind diffusion in the polymer matrix of HPBCD-PBCN was found to be more significant when the drug was present in the polymerization medium through the process of polymer nanoparticles formation (HPBCD-PBCN-Ind). These results reveal the existence of association processes or/and intermolecular interactions between drug molecules and polymer matrix of HPBCD-PBCN. The diffusion behavior of Ind could be interpreted as a fast exchange between two sites, i.e. bound to the polymer and free (physically entrapped) in the polymer matrix of HPBCD-PBCN drug molecules [21,22]. In this case, the observed diffusion coefficients (D) are weighted-average values between the free and bound drug species and if we consider fast exchange between these two states, the mole fractions of the free or physically entrapped and bound drug molecules could be calculated using the following equation:

$$D = f_{free}D_{free} + f_{bound}D_{bound} \quad (2)$$

where **f** and **D** denote the molecular fractions and diffusion coefficients of the free and bound drug molecule and $f_{free} + f_{bound} = 1$. The fractions of the bound Ind in HPBCD-PBCN-Ind and HPBCD-PBCN+Ind were estimated using the diffusion coefficient of the free Ind (D_{free}) measured separately and assuming the diffusion coefficient of the bound drug molecules (D_{bound}) to be equal to that of the HPBCD-PBCN in the sample. The fraction of the bound Ind was found to be 10 and 3% from the total found (presenting) drug in the systems for HPBCD-PBCN-Ind and the physical mixture HPBCD-PBCN+Ind, respectively. The results suggest an inclusion of Ind in the polymer matrix of HPBCD-PBCN-Ind and existence of strong drug-polymer interactions. The low fraction of bound Ind in HPBCD-PBCN+Ind indicates weak drug-polymer interactions and drug molecules predominantly adsorbed on the surface of these NP was assumed.

4. CONCLUSIONS

The results of NMR analyses suggest an inclusion of Ind in the polymer matrix of HPBCD-PBCN-Ind and existence of strong drug-polymer interactions but no inclusion in the hydrophobic cavity of HPBCD. But the Ind content (%) in the drug loaded nanoparticles was found to be low (3.4 %). The presence of Ind molecules decreases the surface negativity (ζ-potential) of the formed drug-loaded nanoparticles supporting the contribution of Ind in the composition of nanoparticles. The FTIR study also evidenced some interactions of Ind molecules with the polymer matrix of nanoparticles.

Acknowledgments: *Financial support of the Research and Development Fund of the University of Chemical Technology and Metallurgy, Sofia, contract no.11246 is kindly acknowledged. The Nanosizer Nano ZS was purchased with the financial support of the Bulgarian Science Fund, contract no. DO 02-168/2008. The NMR spectrometers are part of the National NMR Network and were purchased in the frame work of the National Program for Scientific Re-equipment, contract REDE/1517/RMN/2005, with funds from POCI 2010 (FEDER) and Fundação para a Ciência e a Tecnologia (FCT).*

REFERENCES

1. N. Chieng, J. Aaltonen, D. Saville, T. Rades, *Eur. J. Pharm. Biopharm.*, **71**, 47 (2009).
2. A. K. Jain, *Eur. J. Pharm. Biopharm.*, **68**, 701 (2008).
3. T. S. Anirudhan, D. Dilu, S. Sandeep, *J. Magn. Magn. Mater*., **343**, 149 (2013).
4. K. Bury, F. D. Prez, D. Neugebauer, *Macromol. Biosci.*, **13**, 1520 (2013).
5. K. Tomoda, H. Terashima, K. Suzuki, T. Inagi, H. Terada, K. Makino, *Colloid. Surf. B Biointerfaces*, **88**, 706 (2011).
6. L. Upadhyaya, J. Singh, V. Agarwal, R. P. Tewari, *Carbohyd. Polym.*, **91**, 452 (2013).
7. A. T. S. Miyazaki, K. Wataru, *J. Pharm. Pharmaceut. Sci.*, **6,** 238 (2003).
8. S. Jambhekar, R. Casella, T. Maher, *Int. J. Pharm.*, **270**, 149 (2004).
9. P. J. Salústio, G. Feio, J. L. Figueirinhas, J. F. Pinto, H. M. C. Marques, *Eur. J. Pharm. Biopharm.*, **71**, 377 (2009).
10. D. Duchêne, G. Ponchel, *J. Incl. Phenom. Macro.*, **44**, 15 (2002).
11. X. Zhao, W. Li, Q. Luo, X. Zhang, *Eur. J. Drug Metab. Pharmacokinet.*, **39**, 61 (2014).
12. G. Bodenhausen, D. J. Ruben, *Chem. Phys. Lett.*, **69**, 185 (1980).
13. A. G. Palmer III, J. Cavanagh, P. E. Wright, M. Rance, *J. Magn. Reson.*, **93**, 151 (1991).

14. L. E. Kay, P. Keifer, T. Saarinen, *J. Am. Chem. Soc.*, **114**, 10663 (1992).

16. A. Jerschow, N. Mueller, *J. Magn. Reson. A,* **123**, 222 (1996).
17. A. Jerschow, N. Mueller, *J. Magn. Reson. A,* **125**, 372 (1997).
18. F. Malz, H. Jancke, *J. Pharm. Biomed. Anal.*, **38**, 813 (2005).
19. R. S. R. Murthy, L. H. Reddy, in: Nanotechnology for cancer therapy, M. A. Mansoor (ed), Taylor & Francis Group, LLC, New York, 2006, p. 251.
15. J. Schleucher, M. Schwendinger, M. Sattler, P. Schmidt, O. Schedletzky, S.J. Glaser, O. W. Sorensen, C. Griesinger, *J. Biomol. NMR*, **4**, 301 (1994).
20. M. Simeonova, G. Ivanova, V. Enchev, N. Markova, M. Kamburov, Ch. Petkov, A. Devery, R. O'Connor, D. Brougham, *Acta Biomaterialia* **5**, 2109 (2009).
21. K. Momot, P. Kuchel, *Concepts. Magn. Reson. A,* **19**, 51 (2003).
22. Y. Cohen, L. Avram, L. Frish, *Angew. Chem. Int. Ed.*, **44**, 520 (2005).

ПОВЪРХНОСТНО МОДИФИЦИРАНИ ПОЛИБУТИЛЦИАНАКРИЛАТНИ НАНОЧАСТИЦИ, НАТОВАРЕНИ С ИНДОМЕТАЦИН: ПОЛУЧАВАНЕ И ФИЗИКОХИМИЧНО ОХАРАКТЕРИЗИРАНЕ

В. Станева[1], Г. Иванова[2], М. Симеонова[1*]

[1]Химикотехнологичен и металургичен университет, Катедра Полимерно инженерство, 1756 София, България;
[2]Мрежа за химия и технология-асоциран научен център, Департамент по химия и биохимия, Факултет на науките, Университет на Порто, 4169-007 Порто, Португалия

Постъпила на 25 юли 2014 г.; Коригирана на 9 февруари 2015 г.

(Резюме)

Полибутилцианакрилатните наночастици (ПБЦН) като биоразградими и биосъвместими средства привличат интерес като колоидни системи за доставяне на лекарства. Основното им технологично предимство е възможността за получаване чрез анионна полимеризаци във водна среда без добавне на инициатор, който би могъл да има старнични нежелани влияния. За съжаление, при такива условия възниква проблем с енкапсулирането на слабо разтворими във вода лекарства.

С цел преодоляване на този проблем, беше изследвана модифициращата способност на хидроксипропил-β-циклодекстрин (ХПВЦД) при получаването на ПБЦН, натоварени с индометацин. Повърхностно модифицирани ХПВЦД-ПБЦН бяха получени чрез анионна полимеризация на мономера в присъствието на ХПВЦД. Натоварването на индометацина беше извършено едновременно с формирането на наночастиците.

Физикохимичното охарактеризиране на натоварените с индометацин ХПВЦД-ПВЦН е извършено чрез динамично разсейване на светлината (фотонна корелационна спектроскопия), лазер Доплерова електрофореза, инфра червена и ЯМР спектроскопия. Всички потвърждават присъствието на лекарство в полимерната матрица на наночастиците.

Bulgarian Chemical Communications, Volume 47, Special issue (pp.100-105) 2015

Investigation on the effect of different tone value sum (TAC) of inks on the color reproduction accuracy of heatset web offset images

I.T. Spiridonov*, R.K. Boeva, T.Tz. Bozhkova, Y.V. Nedelchev

Department of Pulp, Paper and Printing Arts, University of Chemical Technology and Metallurgy, 1756 Sofia, Bulgaria

Submitted July 30, 2014; accepted January 29, 2014

The goal of the present study is to define the correlation between the tone value sum (total area coverage - TAC) and reproduction accuracy on heatset web offset images printed on LWC paper. In case of incorrect values usage - at relatively high or low levels of tone-value sum, press problems such as big amount ink consumption, poor ink trapping, back transfer and set-off due to insufficient ink drying might be encountered. That's why it is necessary to find and determine the optimal values of color separation parameters for each inks/paper/printing press combination.

A test form has been used that contains different control strips for densitometric, imetric measuring and test charts used for ICC profiles.

The reflection spectra of measured color patches in entire visible spectrum are used for determination the effect of different values of TAC. For study the effect of TAC values on color gamut and color accuracy, we have calculated color differences ΔE*ab, surface area and volumes of 2D cross-sections and 3D shape body in CIE L*a*b* system.

The results achieved are important from scientific and practical point of view. For the first time in an experimental way a well-grounded proof has been achieved with regard to the limits of the tone value sum and variation from the optimal values for TAC for heatset offset press, by provision of differences in compliance with the international standards.

Key words: total area coverage, total ink limit, color separation, spectral measurements, color gamut

INTRODUCTION

The paper presents investigation of the effect of different values of total area coverage of inks (TAC) on CIE Lab color characteristics, color differences and color gamut changes.

Total area coverage is the maximum total dot percentage of cyan, magenta, yellow and black ink used in the darkest areas and generally depends on the printing process and the type of paper. Total area coverage is a key factor for achieving of maximal volume of color gamut, especially in dark areas.

It generally depends on the printing process and the type of the paper. The most important parameters that have a significant influence on the TAC values are the papers, inks and printing presses specifications. For coated papers higher total area coverage than for uncoated papers is used. In addition, for web-fed printing presses, the TAC values are lower than these for sheet-fed printing presses. ISO 12647, Part 2, and organizations such as the German Printing and Media Industries Federation (bvdm) SWOP and GRACoL have different TAC recommendations [1-3].

Total area coverage is a key factor for achieving a maximal volume of color gamut, especially in dark areas. Theoretically, the maximal amount of process inksis 400 %, but in practice that will cause problems with ink trapping, decreasing of adhesion of inks layers, drying troubles, etc. Determination of TAC values depends of the exact CMYK combination, which is achieved with the highest optical density and with the least amount of ink [4-6].

The main goal of this study is development of methodology, which gives objective and analytical assessment, for determination of the optimal value of total area coverage (TAC) of inks in offset printing process. A practical implementation of the correct and optimal value of TAC should improve the print quality, printability, better ink layers adhesion, trapping and reducing the quantity of process inks [7-10].

The optimization and reduction of TAC leads to financial and ecological profits. Reduction of inks amounts used in print-production is a substantial part of decreasing the total printing cost. The ecological aspect of TAC optimizing is reduction of the emissions during manufacturing of the inks and the facilitation removal of the inks during the process of paper recycling [11].

To whom correspondence should be sent.
E-mail: i_spiridonov@abv.bg

EXPERIMENTAL

A special designed test form has been used for study of the effect of TAC values on color gamut and other reproduction parameters.The test form contains many different components for process control and spectra analyses: 100% solid patches for cyan, magenta, yellow and black – for control of optical density – Dv and characteristics, 80% patches for estimating print contrast, patches for estimating of dot gain and grey balance, strip which contains raster lines in different slope for doubling and slur control, registration marks, test charts containing about 1500 patches for ICC color profiles with different GCR and TAC values and etc. All measuring components are with screen value 60 cm^{-1} (150 lpi).

The paper, which has been used, is 56 g/m^2 LWC paper. A spectro-photometer/densitometer of type SpectroEye of X-rite has been used for measuring of optical density and the characteristics in the CIE Lab system. All measurements are in accordance with ISO 12647-1: D50 illuminant, 2° observer, 0/45 or 45/0 geometry, black backing and excluded polarization filter. The test chart ECI 2002 is measured with i1Profiler software and X-Rite i1i0 spectrophotometer and automatic scanning device. The offset printing machine, which has been used, is five heatset web-fed KOMORI. The value of pH of dampening solution was 5.3 and the temperature – 11°C. The relative humidity of the air in the printing house was 60% and the temperature near by the printing press – 26°C.

We have made two printing runs on the heatset offset printing press. The designation of first one was to make the test of the printing system, and for generating of ICC profile for the exact print conditions. The main goals of second print run, was to make a prints of test charts and images with different TAC settings.

RESULTS AND DISCUSSIONS

In order to achieve the goals of the experiment, series of measurements of Dv and Print Contrast have been performed. For defining the optimal inking by the method of maximum print contrast for Cyan, Magenta, Yellow and Black, the samples have been made by gradual smooth changes in ink quantity - from under-inking to over-inking. A statistical analysis of the results was performed.

Experimentally obtained values of optimal inking expressed by optical density of solid 100% tone - Dv and corresponding values print contrast are shown in Table 1. All of test sheets in this experiment have been printed using the values of optimal inking shown in Table 1.

Investigation and comparison of 3D and 2D color gamuts in dependence total area coverage

The graphically presentation of color gamuts – 3D and 2D, gives valuable and comprehensive information for the colors, that can be reproduced in specific printing and color separation conditions. In this study for precise determination of influence of TAC settings we have investigated the changes in 2D and 3D color gamuts volume and shape.

The color gamut range, especially the volume of the tree dimensional (3D) color gamut body, is one of the most important characteristics of an output device. Research on the color gamut surface size and shape is useful for many color science-related tasks such as visualization, gamut volume and surface calculation, and choosing of a color rendering intent method. Reducing the TAC values clips colors of the dark areas of the color gamut.

3D presentation and comparison of color gamuts for 280% and 300% TAC are presented on figures 1 and 2. Two different software products were used for more precise presentation of specific 3D body shape in dependence of TAC values. It is clearly visible from both figures 1 and 2, that the 3D body of 300% TAC has biggest volume especialy in middle and dark tones. The 3D shapes for 320%, 340% and 400% are not graphically presented, because they are similar and equal to 300% TAC.

Table 1. Experimentally obtained values of optimal inking expressed by Dv and corresponding values print contrast

Process colors	Experimentally obtained values of optimal inking expressed by Dv [Dv]	Print Contrast - Cmax, (highest value) [%]
Black	1.69	41%
Cyan	1.48	33%
Magenta	1.53	36%
Yellow	1.36	32%

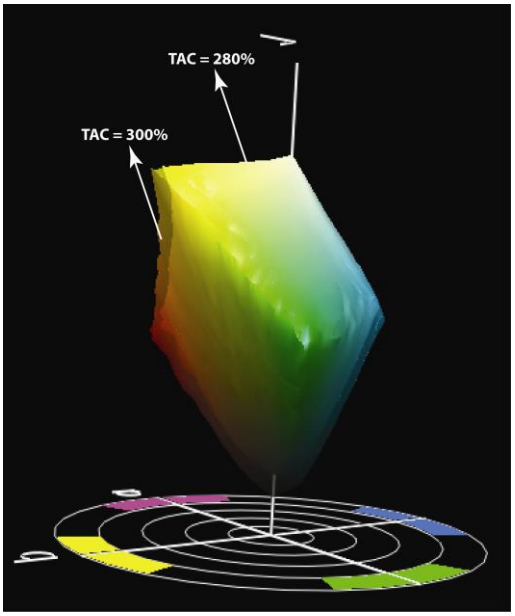

Fig. 1. 3D presentation of color gamuts in dependence of TAC value in CIE Lab, (graph is generated by X-Rite ProfileMaker).

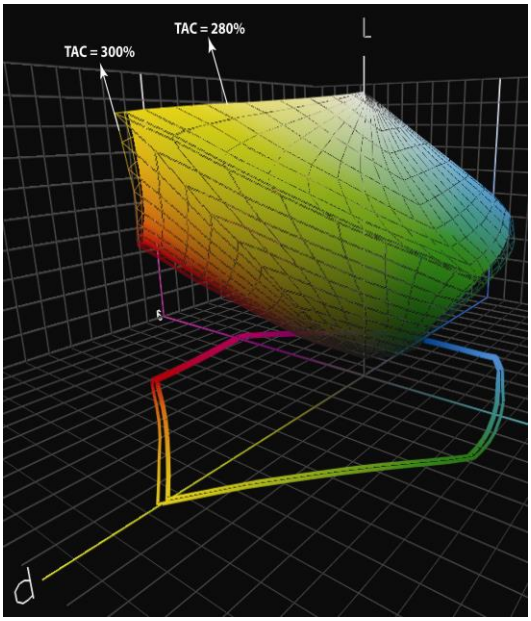

Fig. 2. 3D presentation of color gamuts in dependence of TAC value in CIE Lab, (graph is generated by Chromix Color ThinkPro).

In order to obtain complete assessment of the effect of TAC values on gamuts, we have compared the surface areas of 2D color gamuts for different CIE L* coordinates.

A comparison of 2D color gamuts is performed to obtain comprehensive characterization of colors depending on TAC value. The presentation of 2D color gamuts gives precise and detailed information of colors that can be reproduced in the specific conditions for all tonal range – from highlights to dark tones. These 2D gamuts are cross sections of 3D gamuts at different values of the CIE L*-coordinate. CIE L* is the coordinate corresponding to color lightness and has value from 0 (black) to 100 (white) units. The other two coordinates of the CIE L*a*b* color system - CIE a* and CIE b* correspond to red (+a*) – green (-a), and yellow (+b*) – blue (-b*).

The graphical presentation for the surface areas of 2D-cross sections in highlights, middle and dark tones are presented at Figure 3

Fig. 3 shows, that in the dark tones, at CIE L* = 20 (b) the color gamut at 300 % TAC is the largest one. The smallest color gamut is obtained at 280 % TAC value.

The color gamuts at others TAC values are similar to each other. They have surface area like the color gamut at 300% TAC value and larger than the gamut at 280 % TAC value, that's why they are not presented in the figures.

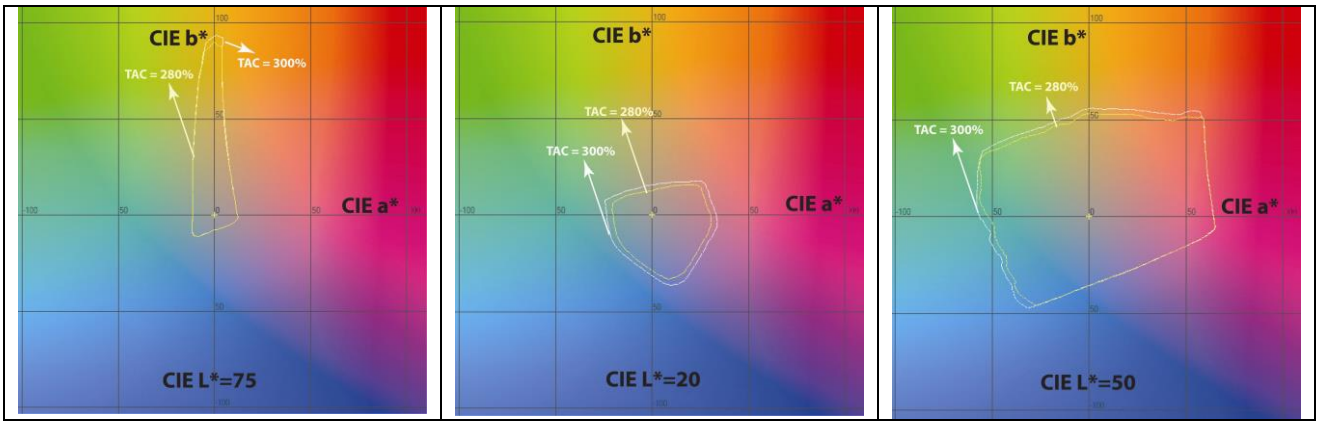

(a) Light tones at CIE L*=75 (b) Dark tones at CIE L*=20 (c) Middle tones at CIE L*=50

Fig. 3. 2D presentation of color gamuts in dependence of TAC value in CIE Lab.

The conclusion is that TAC values havea relatively significant effect on color gamuts in dark and middle tones. The results show, that the 300% TAC gamut is the optimal value (from 2D and 3D point of view) with relatively big color gamut and lower ink consumption compared to 280%, 320%, 340%, 400%.

Investigation of Color Gamut Volumes - ΔE³, CIE Lmin and Average Color Difference - ΔEab in dependence of total area coverage

For better quantitative analysis and assessment of the effect of TAC on color gamuts we have calculated the color gamut volumes – ΔE^3. Graphical presentation of the results is given in Figure 4. According to the results shown in Figure 4, the biggest color gamut volume is obtained at maximal level of TAC at 400% and the smallest – at minimal level of TAC at 280%. There is a relatively big difference about 8% in volumes of color gamuts between 280% and 300% TAC. The difference between 300%, 320%, 340% and 400% is insignificant – about 1-2 %. That means, that the 300% value of TAC is leading to one of the biggest gamut volumes and in the same time is one of the lowest ink consumption comparing to others technological situations. One of the most important factors that affect human perception is the possibility to reproduce the darkest tones and colors. That is one of the reasons to generate the "rich black" from all process colors – C, M, Y, K. The best way to investigate the darkest colors and tones is measuring and finding the patch with lower lightness coordinate - Lmin in CIE L*a*b* color system.

The graphically presentation of influence of TAC values on CIE Lmin is shown on Figure 5.

The results shows, that total area coverage affects the darkest reproducible color. The biggest difference between different TAC in CIE L*min value is 4.80 units – 280% TAC has Lmin=15.20 and 400% TAC has Lmin=10.40 value. The differences in L*min between 400%, 340%, 320% and 300% TAC are between 0.40-1.70 units. The results shows that the darkest and better from human perception point of view colors could be achieved with 400% TAC value. The worst results are for 280% TAC. The experimental data swows that the Lmin value for 300%, 320% and 340% are almost equal each to other and they are close to the best results for 400% TAC.

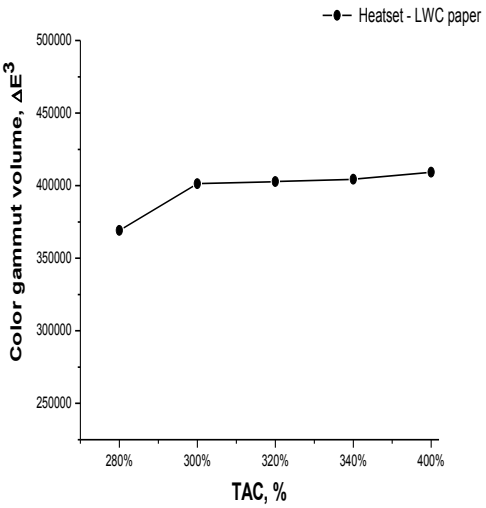

Fig. 4. Color gamut volume in dependence of TAC values.

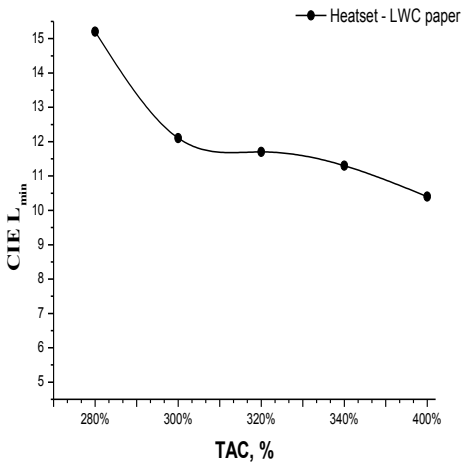

Fig. 5. CIE Lmin in dependence of TAC values.

One of the most important parameters, which defines the effect of TAC on image quality, is the color reproduction accuracy. Color difference expressed by ΔE*ab gives very valuable and reliable information for color reproduction correctness. So we have calculated ΔE*ab from spectral measurement data. The calculations for ΔE*ab were performed to 400 % TAC value as a reference. The obtained results for average colour difference depending on TAC value for all 1485 patches are given in Figure 6.

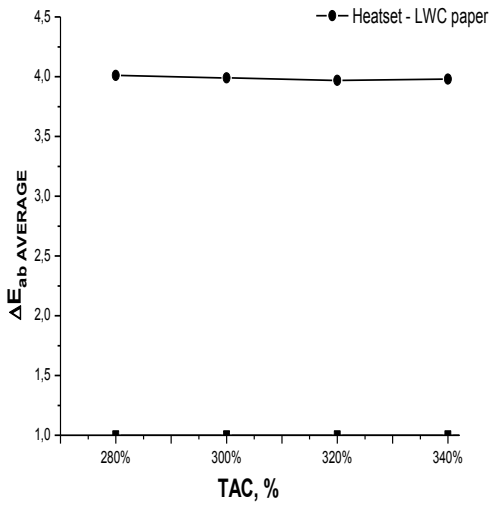

Fig. 6. Average difference in dependence of TAC values.

The graph (Fig. 6) shows that the color difference for printed dark tones for all TAC values is lower than 4.01 units. The lowest value of average color difference is obtained for total area coverage 320 % - about 3.97 units. The difference between them is only 0.04. It could be assumed that the TAC value (280-340%) do not influence color reproduction accuracy.

Except average color difference, we have calculated maximal and minimal color difference from the obtained spectral data for all 1485 patches. The trend and the results for minimal and maximal values are the same like average color difference. So by cause of shortness they are not included in the paper. According to the obtained results for ΔE*ab, it could me made a conclusion, that all TAC values are suitable, but from financial, ecological and for more fast dryness reasons - the lowest TAC values are preferable.

CONCLUSIONS

The results achieved are important from practical point of view. They lead to the conclusion that it is necessarily taking into strict consideration the TAC value, because relatively big differences in color reproduction parameters are occurred.

In an experimental way a well-grounded proof has been achieved for a substantial difference in color reproduction for 4 different TAC values with comparison of different quality parameters.

According to the results of investigation of color reproduction accuracy, switching the TAC values leads to changes in color gamut volumes and shapes (2D and 3D). The changes affect mostly dark and middle tones. There is about 2-8% difference in surface areas and volumes between different TAC values. The results shows, that total area coverage affects the darkest reproducible colour. The difference between different TAC in CIE L*min value is up to 4.80 units.

The evaluation of all color quality reproduction parameters from this research leads to conclusion that the 300% TAC is the best and optimal value of tone value sum. That is the lower TAC value, which gives good color reproduction accuracy, obtained and proofed by experiment performed in real industrial conditions. A practical implementation of the correct and optimal value of 300 % TAC should improve the print quality, printability, better ink layers adhesion, trapping and reducing the quantity of process inks.

We have introduced a new methodology for determination the optimal value of total area coverage by assessing few parameters obtained by measurement of big number of color patches. The methodology includes investigation of reflection spectra, 2D and 3D colour gamuts, color gamut volumes, surface areas of colour gamuts, achievement of darkest printed colour and colour reproduction accuracy. The optimal value of the TAC determined by this new methodology helps to achieve a significant reduction of ink cost and a maximal color gamut volume, i.e. improve the quality of printed image and reduce financial costs.

***Acknowledgements**: This paper is based upon work supported by the Bulgarian Science Fund under Grant No. DMU 03/69/2011.*

REFERENCES

1. ISO 12647-2, Graphic technology - Process control for the production of half-tone separations, proof and production prints, *Part 2: Offset lithographic processes, (*2004)
2. Medien Standard Druck 2010 – Technische Richtlinienfür Daten, Filme, Prüfdruck und Auflagendruck, *BundesverbandDruck und Mediene.V. (bvdm)*, Wiesbaden, (2010)
3. Guidelines & specifications, GRACoL specifications 2007, A special supplement to graphic arts monthly, *IDEAlliance*, 29-31, (2007).
4. G. Sharma, Digital Color Imaging Handbook, *CPC Press LLC*, Boca Raton, FL, Chapter **5**, (2002).
5. H. Kipphan, Handbook of Print Media, Technologies and Production Methods, *Springer-Verlag Heidelberg*, Berlin, (2001).
6. T. Costa, Effect of GCR and TAC in Color Gamut Volume, Test Targets **4.0**, *Advanced Color Management RIT School of Print Media*, Rochester, New York, USA, (2004).
7. I. Spiridonov, M. Shopova, R. Boeva, R., "Study of the effect of gray component replacement level on reflectance spectra and color reproduction accuracy",

8. *Proc. SPIE (International society for optics and photonics)*, **8770**, 17th IS on Quantum Electronics: Laser Physics and Applications, (2013)
9. I. Spiridonov, M. Shopova, R. Boeva, Investigation of effect of different total area coverage values of inks on reflection spectra and color gamut", *Proc. SPIE (International society for optics and photonics)*, **8770**, 17th IS on Quantum Electronics: Laser Physics and Applications, (2013).
10. I. Spiridonov, M. Shopova, J. *Chem. Technol. Metall.*, **48**, 47 (2013).
11. I. Spiridonov, M. Shopova, N. Galabov, K. Ivanova, *J. Chem. Technol. Metall.*, **48**, 247 (2013).
12. L. Shapira, B. Oicherman, *Eurographics*, **2**, 31 (2012
13.).

ИЗСЛЕДВАНЕ НА ВЛИЯНИЕТО НА СУМАРНОТО КОЛИЧЕСТВО НА МАСТИЛАТА В ТЪМНИТЕ ТОНОВЕ (TAC) ВЪРХУ ТОЧНОСТТА НА ТОНО- И ЦВЕТОВЪЗПРОИЗВЕЖДАНЕТО ПРИ ИЗОБРАЖЕНИЯ ОТПЕЧАТАНИ НА РОЛЕН ОФСЕТОВ ХИЙТСЕТ ПЕЧАТ

И.Т. Спиридонов*, Р.К. Боева, Т.Цв. Божкова, Я.В. Неделчев

**Катедра „Целулоза, хартия и полиграфия", Химикотехнологичен и металургичен Университет, бул. Климент Охридски 8., София 1756, България*

Постъпила на 30 юли, 2014 г.; приета на 29 януари, 2015 г.

(Резюме)

Целта на настоящото изследване е разработване на методика за дефиниране на оптимални стойности на сумарното количество на мастилата в тъмните тонове (TAC) и определяне влиянието му върху точността на тоно- и цветовъзпроизвеждането при ролния хийтсет офсетов печат върху LWC хартия. При избор на неоптимални стойности на TAC – по-ниски и по-високи от необходимата, се получават редица проблеми като висок разход на мастило, лоша адхезия на мастилата, ниски стойности на трапинга, копиране при печат, бавно съхнене на мастилата и др. Ето защо е изключително важно да се определят оптимални стойности на параметрите на цветоотделяне за всяка различна комбинация мастило/печатна машина/формена технология/хартия.

За постигане на целите на експеримента е моделирана специална тестова форма, съдържаща множество различни контролни елементи за денситометрични, колориметрични измервания и моделни скали за генериране на ICC профили.

Чрез изследване на резултатите получени от измерените спектрални данни във видимата част на спектъра на тестовите контролни скали и полета е определено влиянието на различните стойности на TAC върху цветовия обхват и точността на тоно- и цветовъзпроизвеждането. Изчислени са цветовите разлики ΔE*ab, площта на 2D разрезите и обемите на 3D тримерното тяло на цветовите обхвати в системата CIE L*a*b*.

Постигнатите резултати и изводи имат научен и научно-приложен характер и практическо приложение. За първи път по експериментален път са определени границите на вариране и оптималните стойности на TAC за хийтсет ролен офсетов печат, спазвайки всички дефинирани цветови толеранси на международните ISO стандарти.

.

Bulgarian Chemical Communications, Volume 47, Special issue A (pp. 106-111) 2015

Sulfuric acid autoclave dissolution of Ni-Co sulfide deposit

P. Iliev*, V. Stefanova, B. Lucheva

University of Chemical Technology and Metallurgy, 8 Kl. Ohridski, 1756 Sofia, Bulgaria

Received June 30, 2014; Accepted April 6, 2015

With increasing use of Cu, Ni and Co metals for different applications and fast depletion of natural land based resources, worldwide efforts are being made to look for alternative resources for the recovery of these metals. One such alternative resource could be the vast oceans, containing these metals in the form of manganese nodules at a depth of about 4–5 km. Many research groups in different countries have been working for more than three decades on the development of copper, nickel, cobalt and manganese recovery processes from manganese nodules by pyro-/or hydrometallurgical routes.

During processing deep ocean manganese nodules from the Clairon-Clipperton fraction zone of the Pacific Ocean by combined pyro-hydrometallurgical route the non-ferrous metals were concentrated in two sulfide deposits – copper and mixed nickel-cobalt. In the present work the experimental results on sulfuric acid autoclave dissolution of the Ni-Co sulfide deposit, containing in mass. %: 30.37 Ni, 3.13 Co, 8.36 Fe, 0.08 Cu, 0.16 Mn, 36.8 S are presented. The effect of the main technological parameters on nickel and cobalt extraction and iron hydrolytic precipitation from the solution were studied. The degree of nickel and cobalt extraction at T= 363K, Po_2 = 0.35MPa, mol H_2SO_4/g-ion(Ni+Co) = 0.19, pulp density = 10 % and dissolution time = 180 min were respectively 97.71% and 96.25%, while the degree of iron hydrolytic precipitation was 99.68%.

Keywords*: manganese nodules, Ni-Co sulfide deposit, sulfuric acid, autoclave dissolution*

INTRODUCTION

With increasing consumption of copper, nickel, cobalt and the fast depletion of natural land ores, worldwide efforts are being made to look for alternative resources for the recovery of these metals. One such alternative resource could be the vast oceans, containing these metals in the form of polymetallic nodules (PN) at a depth of about 2–5 km. The largest congregations are registered in Pacific Ocean between Hawaii and California and around Polynesia. According to Metal Bulletin Research (2005) the reserves of metals (Mn, Ni, Co, Cu, Zn etc.) in them are comparable to those of continental ores. The thorough analysis in this region, were made by R.Kotlinski [1], Andreew et all. [2], B.Agraval at all. [3] and others [4-7].

Many research groups in different countries have been working for more than three decades on the extraction of copper, nickel, cobalt from manganese nodules by pyro-/or hydrometallurgical routes.

Currently, the combined pyro-hydro-metallurgical methods are considered as the most promising methods of PN processing [8-11]. In the pyrometallurgical route of these schemes the non-ferrous metals are concentrated in an intermediate product, a polymetallic alloy (FeCuNiCoMn). One specific feature of that alloy is the high Fe content (>65 %) compared to that of Cu and Ni (~12-13 %), and especially that of Co (~1.5 %). The Mn content in the alloy is 5-6 %. Further, for extraction of non-ferrous metals and manganese the alloy is treated with sulfuric or hydrochloric acid. The alloy can be also sulfidized with elemental sulfur to matte before the hydrometallurgical treatment [10].

In our previously investigation aqueous SO_2-H_2SO_4-H_2O medium has been used for dissolution of the polymetallic alloy with composition in mass %: 65.90 Fe, 12.07 Cu, 12.81 Ni, 1.33 Co, 5.33 Mn and 2.56 others. [11]. The alloy was obtained by pyrometallurgical processing of PN with composition in mass. %: 24.0 Mn, 5.75 Fe, 1.11 Ni, 1.04 Cu and 0.12Co from Clairon Clipperton Zone of the Pacific Ocean after drying at a temperature of 723K and reduction smelting at 1723-1773K in the present of coke. It has been established that the presence of SO_2 in the solution led to selective dissolution of the alloy: copper was concentrated into insoluble residue with composition in mass %: 54.9 Cu, 4.8 Fe, 3.3 Ni, 0.3 Co, 0.4 Mn and 30.9 S, while Fe, Ni, Co and Mn were extracted in the leach solution. The chemical composition of the solution, in $g.L^{-1}$ was: 32.44 Fe, 0.05 Cu, 6.02 Ni, 0.62 Co, 2.62 Mn.

*To whom correspondence should be sent.
E-mail: pkiliev@uctm.edu

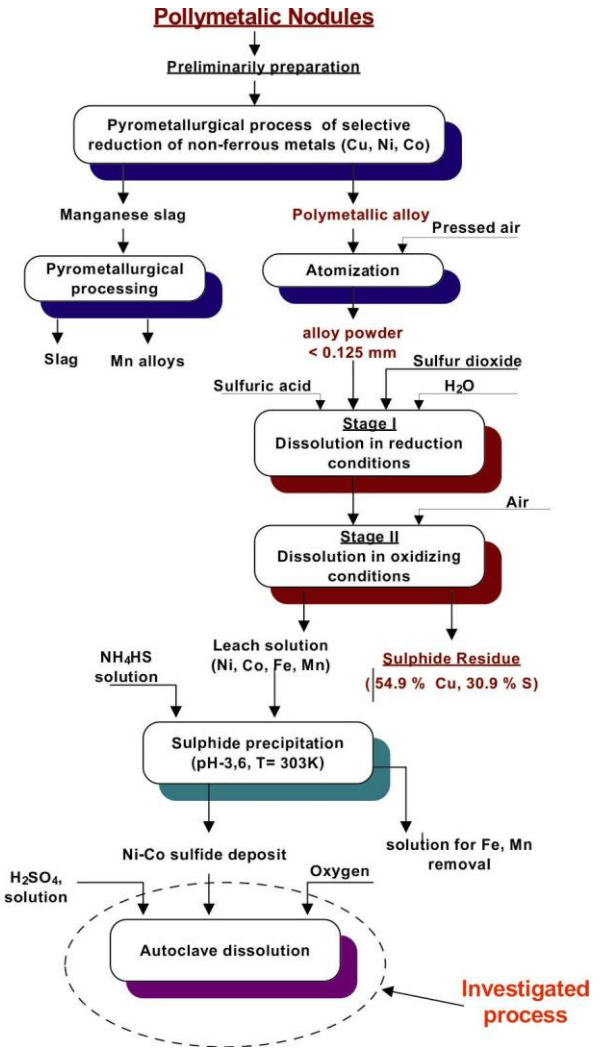

Fig.1. Combined pyro-hydrometallurgical scheme for obtaining of mixed Ni-Co concentrate from polymetallic manganese nodules.

Further Ni and Co were separated from the solution by sulfide precipitation with NH_4HS. In Figure 1 a schematic flow sheet for hydrometallurgical treatment of polymetallic alloy with recovery of copper and mixed Ni-Co concentrate is shown.

The concentrates can be directly processed into copper or nickel plant working on pyrometallurgical scheme. Conventional smelting techniques for processing nickel sulphide concentrates suffer from high capital and energy costs and from the emission of sulphur dioxide into the atmosphere. It is for this reason the hydrometallurgical processes gradually gain an advantage over the pyrometallurgical for production of nickel from sulphide ores. Many of the processes studied to date involve the leaching of an aqueous slurry of the sulphides concentrate in an air or enriched oxygen atmosphere in a pressure vessel (autoclave) at temperatures ranging from 120 to 230 ^{0}C.

In the present work the experimental results on acid autoclave dissolution of the Ni-Co sulfide deposit was presented. The effect of the main technological parameters on nickel and cobalt extraction and iron hydrolytic precipitation from the solution were studied.

EXPERIMENTAL

The process of Ni-Co sulfide deposit precipitation from leach solution was conducted at following conditions: equilibrium pH = 3.6, excess of NH_4HS - 150% more than the required stoichiometric and temperature =30 ^{o}C. Neutralization of the solution to pH 1.5 was made with lime. The time for precipitation was 30 minute. The experimental conditions and chemical composition of Ni-Co concentrate is given in Table 1.

XRD analysis of the residue was carry out with apparatus TUR M62 with $CuK_{\alpha+\beta}$ radiation. It showed that the main phases present in deposit were nickel and cobalt sulphides (Ni_3S_2 and $CoNi_2S_4$). Identified were also lines of double salts: $NiSO_4.(NH_4)_2SO_4.6H_2O$and $(NH_4)_2.Fe(SO_4)_2.6H_2O$. Based on chemical and XRD analyzes the resulting sulphide residue can be classified as mixed nickel-cobalt concentrate.

Table 1. Chemical composition of the solution and sulfide concentrate obtained after sulfide precipitation of nickel and cobalt.

PRODUCT	CHEMICAL COMPOSITION					
	Fe	Ni	Co	Cu	Mn	S
Initial solution, g.L^{-1}	32.44	6.02	0.62	0.05	2.62	-
Ni-Co concentrate, %	8.36	30.37	3.13	0.08	0.16	36.8
Residual solution, g.L^{-1}	25.9	0.07	0.01	0.01	1.80	

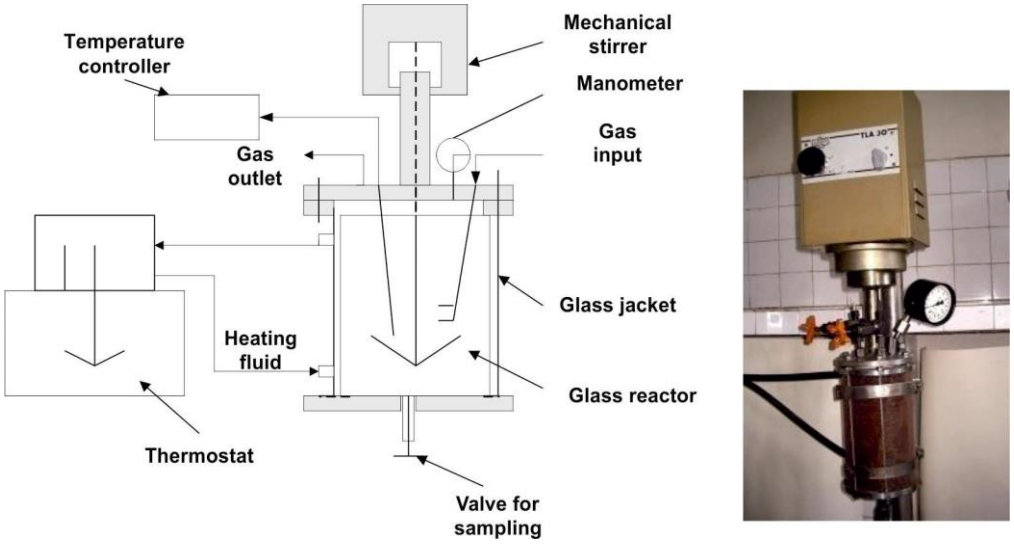

Fig.2. Scheme of laboratory apparatus with an autoclave TLA 30.

RESULTS AND DISCUSSION

The experimental conditions of the conducted experiments and chemical composition of the dissolution products of mixed Ni-Co concentrate are given in Table 2.

Effect of sulfuric acid consumption

For the assessment of this parameter a series of experiments (№ 1, 3 and 5) with duration of 180 min has been carried out. The degree of extraction of nickel and cobalt in solution during the experiment are shown in Fig.3a and b.

Analysis of the results shows that the increase in the sulfuric acid consumption from 0.19 to 1.0 mol H_2SO_4 /g-ion (Ni+Co) ions leads to a slight increase in the degree of extraction of nickel in solution. The degree of cobalt extraction in the solution decreases with decreasing initial concentration of H_2SO_4, which indicates a more difficult dissolution of the cobalt sulphide (Fig 3b)

Effect of temperature and oxygen partial pressure

The oxygen partial pressure and temperature are parameters that influencing on the rate of chemical dissolution of the sulfides and on degree of iron oxidation and its hydrolysis. They were estimated with series of experiments (№1, 2, and 4) carried out at P_{O2}=0.2 и 0.35 MPa, T=363K and 393K and initial ratio of mol H_2SO_4/g-ion (Ni+Co) = 0.19. In Figure 4 are shown respectively the degree of extraction of Ni and Co into solution.

The analysis of the obtained results showed that at T=363K and P_{O2} = 0.35 MPa the extraction of nickel (α_{Ni} = 97.71%) and cobalt (α_{Co} = 96.25%) are carried out with simultaneous purification of the solution from iron (α_{Fe} = 99.68%). With the decrease of P_{O2} up to 0.2 MPa the extraction degree of Ni and Co is increased about 2%, but the conditions of hydrolyses purification of solution from iron significantly are deteriorated (α_{Fe} ~11-13%).

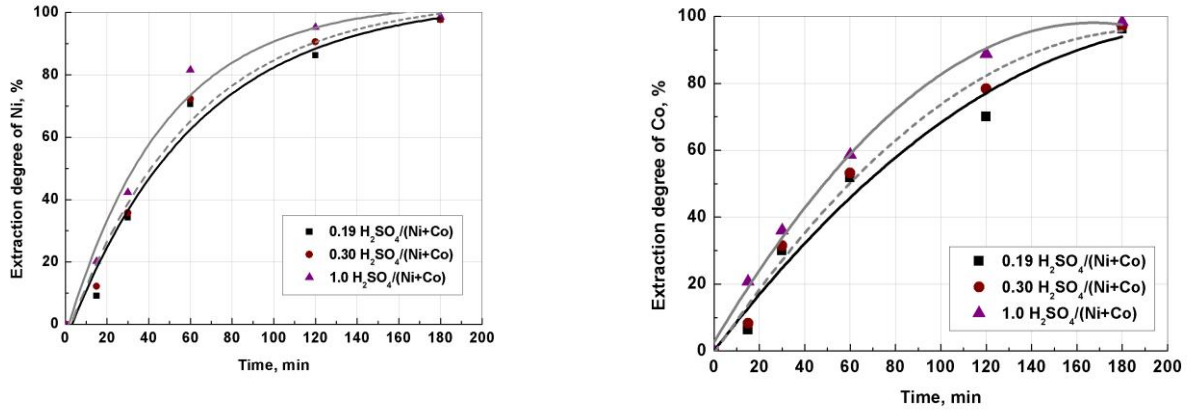

Fig.3. Effect of sulfuric acid concentration on (a) nickel and (b) cobalt extraction degree at T=363 K, P_{O2}=0.35 MPa, 500 rpm and pulp density 10%.

Table 2. The test conditions and experimental results obtained after autoclave dissolution of mixed Ni and Co concentrate.

Test conditions				Product	Chemical composition			
H_2SO_4/(Ni+Co) mol/g-ion	T, K	P_{O2}, MPa	S:L (rpm)		Ni	Co	Fe	S
0.19	363	.35	1:10 (500)	Solution, g/L	29.67	3.01	0.02	-
				Residue, % (m= 2.41g)	2.87	0.48	34.50 (99.68)*	21.05
0.19	393	0.35	1:10 (500)	Solution, g/L	29.91	2.99	0.14	-
				Residue, % (m=2.367g)	1.92	0.60	34.64 (98.09)*	18.95
0.3	363	0.35	1:10 (500)	Solution, g/L	29.68	3.02	0.24	-
				Residue, % (m=2.050g)	3.36	0.50	27.31 (67.03)*	17.34
0.19	363	0.20	1:10 (500)	Solution, g/L	29.66	3.01	6.42	-
				Residue, % (m= 1.03g)	6.87	1.11	18.77 (23.12)*	9.36
1.0	363	0.35	1:10 (500)	Solution, g/L	30.27	3.07	6.52	-
				Residue, % (m= 0.907g)	1.10	0.57	10.5 (11.40)*	82.56
0.19	363	0.35	1:5 (500)	Solution, g/L	57.87	5.78	0.10	-
				Residue, % (m=5.14g)	5.58	0.93	32.10 (98.69)*	18.30
0.19	363	0.35	1:20 (300)	Solution, g/L	12.03	0.86	0.01	-
				Residue, % (m=2.23g)	14.14	3.14	18.70 (99.73)*	6.22
0.19	363	0.35	1:20 (500)	Solution, g/L	14.96	1.52	0.06	
				Residue, % (m=1.19g)	1.88	0.38	34.50 (98.12)*	20.05
0.19	363	0.35	1:20 (700)	Solution, g/L	13.06	0.89	1.34	
				Residue, % (m= 1.469g)	14.42	4.60	19.32 (67.94)*	22.08

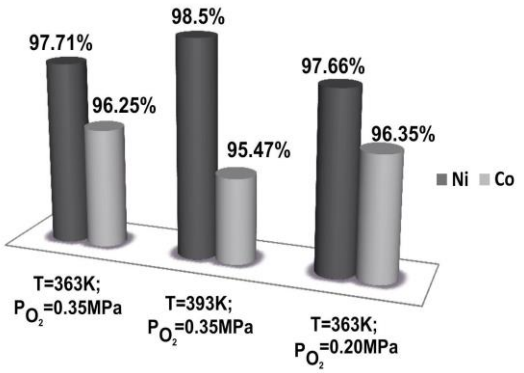

Fig. 4. Effect of temperature and P_{O2} on extraction degree of (a) nickel and (b) cobalt at mol H_2SO_4/g-ions (Ni+Co) = 0.19 and pulp density 10 %.

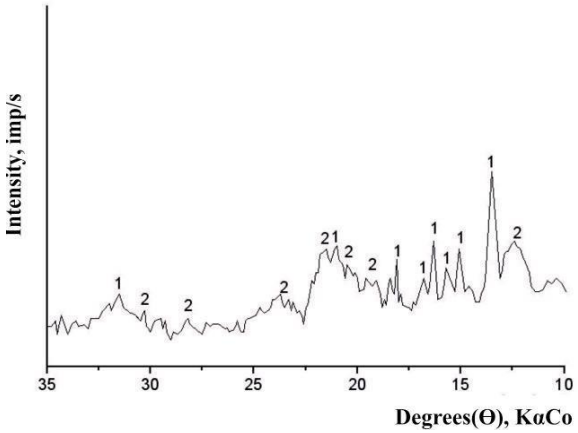

Fig.5. XRD of the residue obtained after dissolution of Ni-Co sulphide deposit at T=363K and P_{O2}=0.2 MPa, Phases: 1 – S^o; 2 – FeO.OH.

At the XRD of the insoluble residue obtained at P_{O2} = 0.2 MPa elemental sulfur and iron oxide phase - goethite (FeO.OH) were identified (Fig.5). The absence of distinct peaks of goethite on the XRD shows that he is in amorphous form. Therefore, the decrease in the oxygen partial pressure leads to decrease in the rate of oxidation of Fe^{2+} to Fe^{3+} and deterioration of the conditions for hydrolysis purification of the solution from iron.

Effect of pulp density

To assess the influence of this parameter are carried out experiments (№ 6, 1 and 7) at 5, 10 and 20 % pulp density at constant others parameter. The resulting degree of extraction of nickel and cobalt in the solution are shown in Figure 6.

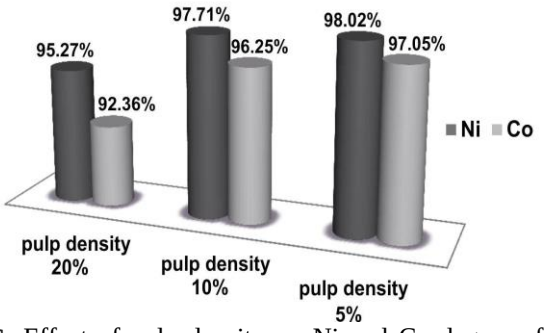

Fig. 6. Effect of pulp density on Ni and Co degree of extraction at T=363 K, P_{O2}=0.35 MPa, mol H_2SO_4/g-ions (Ni+Co) = 0.19 and 500 rpm.

Obviously, the increase of volume of the liquid phase leads to a significant decrease of the concentration of Ni and Co in solution. At all experiments in the insoluble residue about 98% of iron and ~19% elementary sulfur were passed.

Effect of intensity agitation

At diffusion-controllable processes the intensity of stirring has significantly effect on the rate of dissolution. It should be noted that the results give only a qualitative assessment, as the intensity of mixing is determined not only by the speed of the stirrer, but also from the geometric shape of the reactor and stirrer.

The influence of this parameter was evaluated with a series of experiments (№ 7, 8 and 9) at T = 363K, P_{O2} = 0.35MPa, pulp density 5%, initial sulfuric acid expense mol H_2SO_4/g-ion(Ni + Co) = 0.19 and extraction duration = 180 minutes. The dynamics of the Ni and Co dissolution from the concentrate is shown in Figure 7. The chemical compositions of the resulting dissolution products are shown in Table 3.

The analysis of the obtained results showed that maximum degree of metals extraction is reached at 500 rpm. At agitation 300 and 700 rpm a significant decrease in the rate of recovery of nickel and cobalt in the solution was observed. This effect is related to the deterioration of wrapping the solid sulphide particles and dispersion of gas phase in the solution. The last factor influences especially strong on the degree of oxidation of the iron ions and its hydrolysis.

CONCLUSIONS

On the basis of experimental results the optimal technological parameters on sulphuric acid autoclave dissolution of Ni-Co sulphide concentrate obtained during processing of polymetallic nodules have been established: mol ratio of H_2SO_4/gram-ion

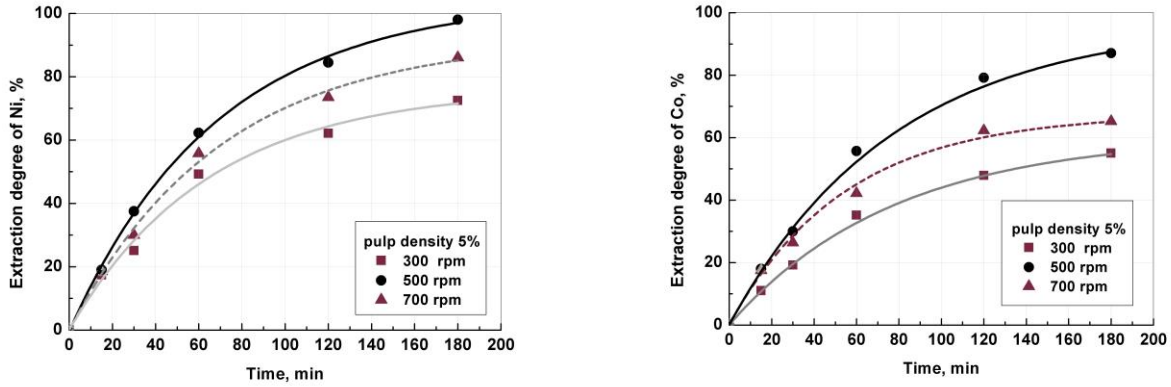

Fig.7. Effect of intensity agitation on (a) nickel and (b) cobalt extraction degree at T=363 K, P_{O2}=0.35 MPa, and mol H_2SO_4/g-ions(Ni+Co) = 0.19.

Table 3. The chemical composition of the products of autoclave dissolution of Ni-Co sulfide concentrate

Products	Ni	Co	Fe	S^o	α_{Ni}, %	α_{Co}, %	α_{Fe}, %	α_S, %
Leach liquor, $g.L^{-1}$	29.67	3.01	0.02	-	97.71	96.25	-	-
Residue, mass %	2.87	0.48	34.50	21.05	-	-	99.68	13.78

(Ni and Co) = 0.19; Oxygen partial pressure = 0.35 MPa; Temperature = 363K; Intensity of agitation – 500 rpm; Pulp density = 10% w/v; Dissolution time = 3h.

Under these conditions the dissolution of concentrate was carried out with simultaneous purification of the solution from iron in the form of goethite. The composition of leach liquor and insoluble residue are given in Table 3.

Under optimum leaching conditions a leaching efficiency of 97.71 % Ni and 96.25 % Co were achieved. Further the leach liquor can be used to recover Ni and Co, for example by solvent extraction and electrowinning.

The quantity of goethite residue was 0.241 g/g sulphide concentrate. Degree extraction of the iron and sulphur were respectively 99.68 % and 13.78 %. Extraction of sulfur from the residue can be performed by well-known in the metallurgical practice methods.

REFERENCES

1. R. Kotlinski, (2001). "Mineral Resources of the World Ocean – Their Importance for Global Economy in the 21-st Century*", Proc. 5th Ocean Mining Symp.* ISOPE, Szczecin, pp 1-7.
2. S.I. Andreev, (2000), "Metallogenic of the World Ocean" *(1:15000000), St. Peterburg*.
4. B. Agrawal, M. Placidi, H. Santo and J. Zhou, (2012), "Feasibility Study on Manganese Nodules Recovery in the Clairon Clipperton Zone", *The LRET Collegiums Tvet. Met.*, **3**, 17, (in Russian).
5. A. Avramov, *J. Univ. Chem. Technol. Met*, **40**, 275 (2005).
6. "A Companion to Global Economic Prospects", (2010), Global Commodity Markets, Review and price forecast, The Int. Bank for Reconstruction and Development, The World Bank, Washington, USA, 1-36.
7. T. Yamazaki, (2008), "Model Mining Units of the 20th Century and the Economies (Production Requirements, Area Requirements and Vertical Integration), *Technical paper for ISA Workshop on Polymetallic Nodule Mining Technology - Current Status and Challenges Ahead-Feb.*, Chennai, India, 18-22.
8. H. Zequan, X. Duan, Z. Xiang, *Min and Met. Eng*,, **16**, 40 (1996).
9. K. Tetsuyoshi, M. Imamura, J. Takahashi, N. Taanaka, T. Nishizawa, *J. Metallurgy*, **47,** 40 (1995).
10. S. Satyabrata, S. Anand, CW. Nam, K.H. Park, and R.P. Das, (2003), "Dissolution Studies on Cu-Ni-Co-Fe Matte Obtained from Manganese Nodules", *Proc 5th Ocean Min Symp*,Tsukuba, 231-237.
11. V. Stefanova, P. Iliev, B. Stefanov, (2009), "Selective Dissolution of FeCuNiCoMn Alloy Obtained during Pyrometallurgical Processing of Polymetallic Noduls", *Proc 8th ISOPE Ocean Min Symp*, Chennai, India, September 22-24, pp 186-189.
12. P.Iliev, V. Stefanova, "Autoclave Dissolution of Sulphide Copper Concentrate Obtained during Processing of Polymetallic Nodules", (2006), *Izv.Vuz. and Univ. of Southampton*, Eds. Shenoi, RA, Wilson, PA and Benet SS, pp 1-127.

СЯРНО-КИСЕЛО АВТОКЛАВНО РАЗТВАРЯНЕ НА Ni-Co СУЛФИДНА УТАЙКА

П. Илиев, Вл. Стефанова, Б. Лучева

Химикотехнологичен и металургичен университет,1756 София,България

Постъпила на 30 юни, 2014 г.; приета на 6 април, 2015 г.

(Резюме)

Поради нарастващото потребление на Cu, Ni и Co за различни цели и бързото изчерпване на континенталните им находища, в световен мащаб се полагат усилия за намиране на алтернативни суровини за техния добив. Такъв алтернативен източник могат да бъдат световните океани съдържащи тези метали под формата на манганови конкреции на дълбочина около 4-5 км. Много изследователски групи в различни страни работят вече в продължение на повече от три десетилетия по разработването на технологии за извличане на мед, никел, кобалт и манган от манганови конкреции по хидрометалургичен или пиро-хидрометалургичен път.

При преработване на дълбоководни манганови конкреции от областта Клайрон – Клипертон на Тихия океан по комбинирана пиро-хидрометалургична схема, цветните метали са концентрирани в две сулфидни утайки – медна и смесена никелово-кобалтова. В настоящата статия са представени експериментални резултати по сярнокисело автоклавно разтваряне на получената Ni-Co сулфидна утайка, съдържаща в мас. %: 30.37 Ni, 3.13 Co, 8.36 Fe, 0.08 Cu, 0.16 Mn, 36.8 S. Изследвано е влиянието на основните технологични параметри влияещи върху степента на извличане на никела и кобалта, и хидролизното утаяване на желязото от разтворите. Достигнатите степени на извличане на никела и кобалта при T= 363K, P_{O_2} = 0.35МПа, молH_2SO_4/молNi+Co = 0.19, плътност на пулпа = 10% и продължителност на разтварянето = 240 мин са съответно 97.71 % и 96.25%, докато степента на хидролизно утаяване на желязото е 99.68%.

Bulgarian Chemical Communications, Volume 47, Special issue A (pp. 112 - 117) 2015

Recovery of silver from zinc cakes

B. I. Lucheva*, P. K. Iliev, Vl. P. Stefanova

Department of Non-ferrous Metals, University of Chemical Technology and Metallurgy,Sofia 1718, Bulgaria

Received June 27, 2014; Accepted April 8, 2015

The present experimental study investigates the feasibility of thiosulfate recovery of silver from zinc cakes produced in the process of wet recovery of zinc cakes at the KCM Ltd in Bulgaria. The impact of various factors on the rate of silver recovery through thiosulfate leaching is studied. It is found that the rate of silver recovery is 70-74 % within the temperature range of 30-50°C at 20% pulp density and leaching time of 30 min, irrespective of the solution pH. The behavior of copper, lead, zinc and iron during thiosulfate extraction is also observed. The thiosulfate solution pH is maintained to 7-8 in order to reduce by hydrolization the concentration of the metals that have been transferred to the solution except silver. After subsequent precipitation of the silver by means of Na_2S, silver concentrate is produced. The possibility of regeneration of the thiosulfate solution is discussed. The solid residue from thiosulfate leaching contains 10-40 g/t silver and can be processed by a Waelz process.

Keywords: *zinc cake, silver, thiosulfate leaching.*

1. INTRODUCTION

The wet recovery of zinc by the technology adopted at KCM Ltd in Bulgaria takes place at relatively low acidity of the solution without bringing the impurities contained in the zinc concentrates into the solution. Thereupon, the metals are concentrated in the zinc cake which subsequently is subjected to Waelz-processing. After Waelz-processing the precious metals completely pass into the clinker and, due to the lack of a proper technology for their recovery they are irretrievably lost.

To prevent the loss of precious metals, attempts for their recovery from the zinc cakes are made at some plants with similar technology.

All known methods for zinc cakes processing in the world-wide practice can be divided into three groups [1]:

1. Waelz-process; reductive flash roasting; smelting in gas-generator, shaft, reverberatory, cyclone, and electric furnaces.
2. Roasting of the cakes in a mix with zinc or pyrite concentrates; treatment with SO_2 or sulfation with sulfuric acid.
3. Direct dissolution of the cakes in sulfuric acid at increased acidity and temperature.

Usually the hydrometallurgical methods of zinc cakes processing based on the reactions of ferrite decomposition using sulfuric acid at atmospheric or higher pressure have achieved greater development.

The complex composition and a large amount of very small size classes in the zinc cake make it a difficult object for leaching and flotation.

In recent years, there has been renewed interest in the use of thiosulfate as a substitute for cyanide in gold and silver leaching [2]. Many attempts have been taken for leaching silver sulfide with thiosulfate, each utilizing different additional reagents and conditions [3,4]. The cupric-ammonia catalyzed system has been the most commonly studied system because of its ability to leach gold, silver and silver sulfide.

The developed and patented hydrometallurgical method of zinc cake processing [5] is of certain interest. It is based on silver recovery by means of sodium thiosulfate in the presence of ammonium sulfate as an activator at a temperature of 30-60°C and pH=4-6. In this process, the silver passes into the solution wherefrom it is recovered by cementation with zinc powder. The solid residue is re-pulped by the same thiosulfate solution and is subjected to floatation. The drawbacks of that method are the low rate of silver recovery in the cement precipitate, its circulation in turnover with the flotation concentrate, considerable losses (over 10 %) with the clinker, as well as considerable loss of zinc in the thiosulfate solutions.

The purpose of this experimental work is to determine the behavior of silver and other metals contained in the zinc cakes at thiosulfate leaching and to investigate the feasibility of solution regeneration after precipitation of the silver by Na_2S.

* To whom correspondence should be sent.
E-mail: plasma@dir.bg

2. EXPERIMENTAL

2.1. Materials

The subject of the investigation is a zinc cake – a waste product from the wet recovery of zinc cakes at KCM Ltd. The chemical composition of the cake was determined through atomic absorption analysis as presented in Table 1.

The phase analysis of zinc cake obtained at similar plant applying the same technology for zinc cakes processing [6] shows that:

1. The zinc exists in the form of sulfate, oxide, silicate, sulfide and ferrite.
2. The lead in the cake exists in the form of anglesite ($PbSO_4$), cerusite ($PbCO_3$), galenite (PbS), plumbojarosite $PbFe(SO_4)_3(OH)_{12}$.
3. The copper is a very thin (up to 3 microns) edging of sulfide Cu_2S on zinc silicate and zinc oxide grains and as isomorphic admixture in sphalerite and zinc ferrite.
4. The silver in the zinc cake is mainly contained in the crystal lattice of the secondary covelline, while part of it is adsorbed by the iron hydroxides [7]. According to the authors, in the process of recovery of the zinc cakes, the copper and silver pass into the solution, and after that their ions interact with the zinc sulfide by the reaction:

$$(Cu,Ag)SO_4+ZnS = (Cu,Ag)S+ZnSO_4 \quad (1)$$

Cake, for the most part, consists of particle aggregates with size 10-15 microns. The latter contain particles to submicron size. More than 90% of the silver is concentrated in size classes less than 40 microns [6].

Upon recovery of the zinc cake with water for 1 hour at a temperature of 70°C, 3.97 % of the copper and 16.19 % of the zinc pass into the solution. The total content of water-soluble compounds in the zinc cake is 18.75 %.

For recovery of silver from the cake a sodium thiosulfate pentahydrate solution was used. Water solution of sodium sulfide was used as precipitator of the silver.

2.2. Methods

The leaching experiments for silver recovery from the cake were carried out in a thermostat in order to maintain the defined temperature. The stirring of the pulp was realized by means of a mechanical stirrer. The defined level of solution pH was reached and maintained by means of lime milk.

The silver precipitation experiments were carried out using a magnetic stirrer at room temperature. Atomic absorption analysis was used to determine the concentration of Ag, Cu, Fe, Pb, Zn in the thiosulfate solution, the solid residue, and the sulfide concentrate.

RESULTS AND DISSCUSION

3.1. Thiosulfate recovery of silver from zinc cake

The factors influencing the rate of silver recovery by thiosulfate leaching of zinc cake are: sodium thiosulfate concentration, type and quantity of the additions which stabilize the solution, temperature, pulp density, leaching time and pH of the medium.

Thiosulfate ion is a metastable anion with a tendency to chemical decomposition in water solutions. The oxidation of thiosulfate is fast in neutral and acidic solutions.

For the purpose of reducing thiosulfate consumption, various researchers propose addition of sulfites and sulfates that would transform the free sulfide ion into thiosulfate during the recovery process or would retard the decomposition process by increasing the concentration of decomposition products.

Ammonium sulfate was used in the subsequent experiments as activator of the process of thiosulfate recovery of silver from the zinc cake and as inhibitor of the thiosulfate ion decomposition, in analogy to [5].

The following conclusions can be drawn from the experiments performed to determine the factors influencing the rate of recovery, the results of which are presented in Figures 1-5:

- With the increase of sodium thiosulfate concentration up to 25 g/l the rate of silver leached increases. The increase of thiosulfate concentration above 25 g/l does not result in a higher rate of silver recovery (Figure 1).
- The joint action of sodium thiosulfate and ammonium sulfate increases the rate of silver recovery. As illustrated by Figure 2, an increase of the $Na_2S_2O_3$:$(NH_4)_2SO_4$ ratio above 1 does not lead to further increase of the rate of silver recovery. For this reason the experiments were carried out at a ratio $Na_2S_2O_3$:$(NH_4)_2SO_4$=1.
- The decomposition rate of the thiosulfate leachant is directly proportional to sodium thiosulfate concentration in the solution. Upon rising of the temperature to 40 - 80°C, the thiosulfate decomposition increases four times. There are two temperature zones of thiosulfate decomposition, from 40 to 60°C and from 60 to 80°C, which are related to different decomposition mechanisms. The maximum

rate of decomposition of the thiosulfate ions is observed at 80°C and sodium thiosulfate concentration 80g/l. The experiments carried out in the temperature range up to 50°C showed that the increase of temperature above 30°C does not result in any significant increase of silver recovery from the zinc cake (Figure 3).

- The lowest rate of silver recovery is achieved at solid:liquid ratio = 1:3 (Figure 4). This is most probably due to the depletion of thiosulfate, because other metals also simultaneously pass into the solution with the silver.
- The results of the experiments showed (Figure 5) that pH of the solution does not influence the rate of silver recovery.
- In all experiments, the highest reached silver recovery degree is 74 %.

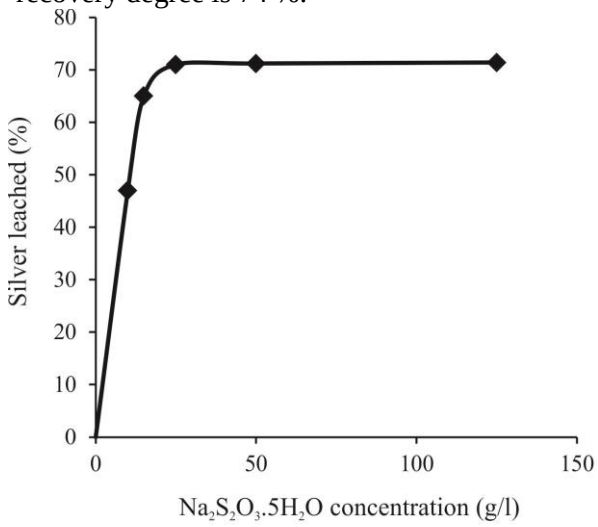

Fig. 1. Effect of thiosulfate concentration on silver leaching (T=50°C, τ=60 min, S:L=1:10, pH=6).

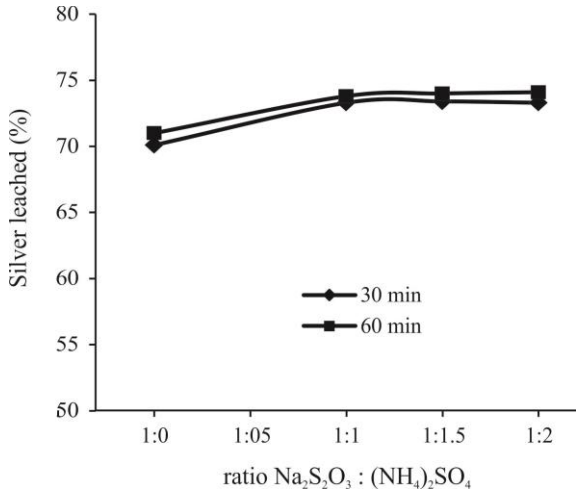

Fig. 2. Effect of ratio $Na_2S_2O_3$:$(NH_4)_2SO_4$ on silver leaching (25 g/l $Na_2S_2O_3.5H_2O$, T=50°C, S:L=1:10, pH=6).

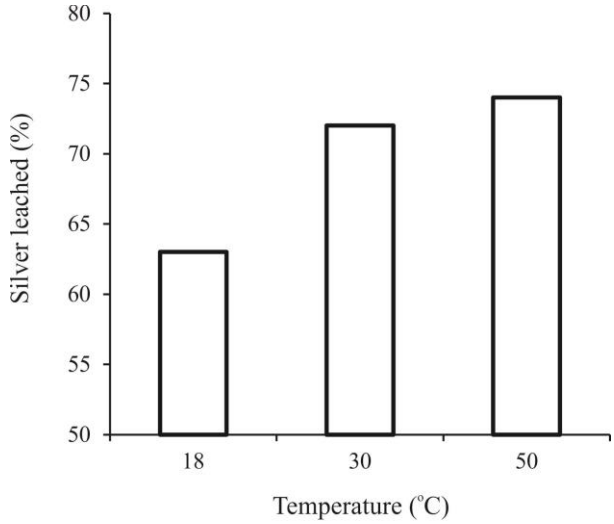

Fig. 3. Effect of temperature on silver leaching (25 g/l $Na_2S_2O_3.5H_2O$, 15 g/l $(NH_4)_2SO_4$, t =60 min, S:L=1:10, pH=6)

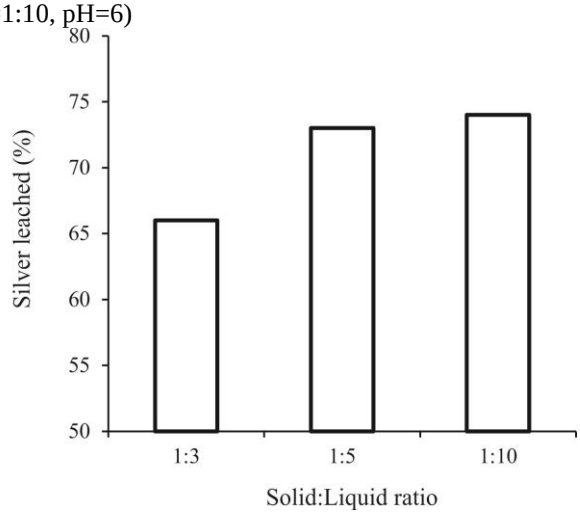

Fig. 4. Effect of solid:liquid ratio on silver leaching (25 g/l $Na_2S_2O_3.5H_2O$, 15 g/l $(NH_4)_2SO_4$, T=50°C, τ =60 min, pH=6)

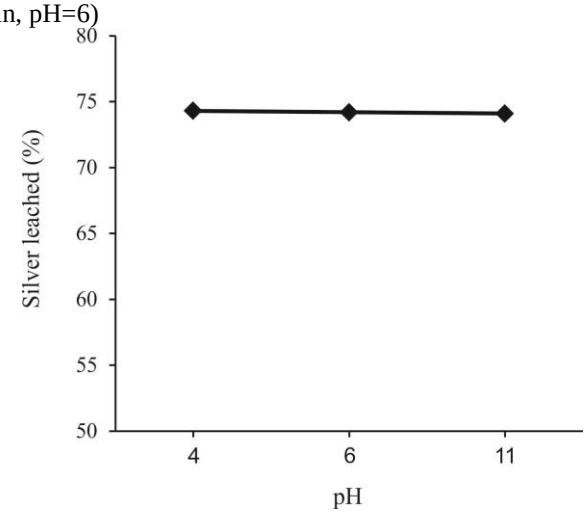

Fig. 5. Effect of pH on silver leaching (25 g/l $Na_2S_2O_3.5H_2O$, 15 g/l $(NH_4)_2SO_4$, T=50°C, S:L=1:5, τ =60 min

As a result of thiosulfate leaching of the zinc cake at 25 g/l $Na_2S_2O_3.5H_2O$, 15 g/l $(NH_4)_2SO_4$, 20 % pulp density, 30 min process duration and pH=6, a solution with chemical composition as presented in Table 2 is obtained.

Table 1. Chemical composition of zinc cake, %

Cu	Pb	Fe	Zn	Ag, g/t
1.27	4.40	27.69	18.10	158

Table 2. Chemical composition of thiosulfate solutions, g/l

Cu	Pb	Fe	Zn	Ag
0.07	0.64	1.81	4.65	0.026

Table 3. Chemical composition of undissolved residue, %

Cu	Pb	Fe	Zn	Ag, g/t
1.14	4.85	31.95	17.00	30

As can be seen in Table 2, the thiosulfate solution contains predominantly zinc.

The chemical composition of the solid residue obtained after thiosulfate leaching of the zinc cake at these conditions is presented in Table 3.

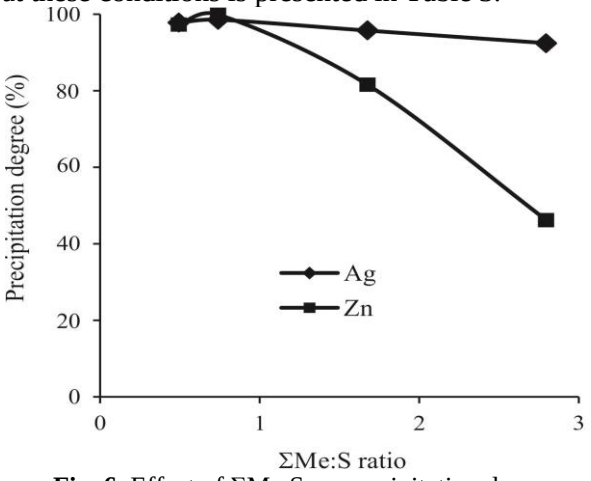

Fig. 6. Effect of ΣMe:S on precipitation degree.

Silver can be extracted from the thiosulfate solutions through cementation, electrolysis or precipitation of low-soluble compounds. The choice of a proper method will be determined by the regeneration capability of the solution. Probably the most suitable method of silver recovery is precipitation of silver sulfide by means of sodium sulfide.

3.2. Precipitation of silver from thiosulfate solutions

Of all reagents proposed for silver precipitation, sodium sulfide is the most affordable, inexpensive and reliable in terms of completeness and rate of the reaction which is described with the following equation:

$$2Na_5[Ag(S_2O_3)_3] + Na_2S \rightarrow Ag_2S + 6Na_2S_2O_3 \quad (2)$$

Various quantities of 10 % Na_2S solution are used for metal precipitation from solution produced as a result of thiosulfate leaching of zinc cake. The dependency of the rate of silver and zinc precipitation on the ratio of the sum of metals (ΣMe) in the solution to the amount of sulphur introduced with Na_2S is presented in Figure 6.

Depending on the quantity of Na_2S, pH of the thiosulfate solution varies from 6 to 11, whereupon, to different degrees, the zinc is precipitated as a hydroxide. The chemical composition of the hydroxide-sulfide precipitate obtained at ΣMe:S = 0,74 is presented in Table 4.

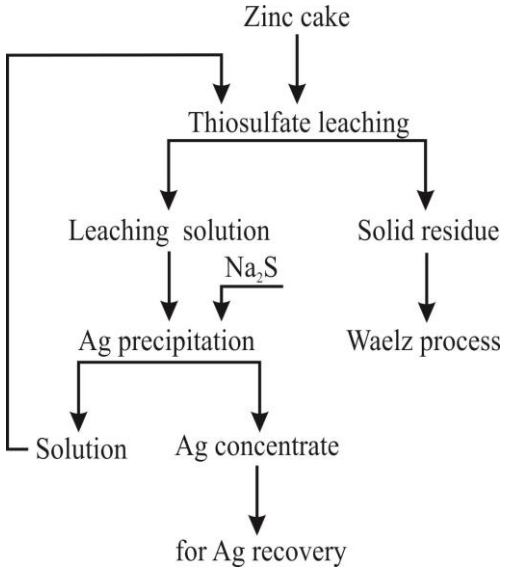

Fig. 7. Conceptual flow sheet for treatment of zinc cake.

Table 4. Chemical composition of sulfide concentrate, %

Cu	Pb	Fe	Zn	Ag	S
0.93	3.55	0.27	43.09	0.1616	10.74

Table 5. Metal precipitation degree, %

Cu	Pb	Fe	Zn	Ag
97.80	99.58	92.32	99.93	99.99

Table 6. Chemical composition of leaching solution (pH=7) and obtained concentrate

	Cu	Pb	Fe	Zn	Ag
Leaching solution, g/l	0.334	0.122	0.016	6.5	0.115
Concentrate, %	14.29	5.65	0.19	44.73	5.18

In that case, the degree of precipitation of the examined metals varies between 92 and 100% (Table 5).The technology of thiosulfate recovery of silver from zinc cake is attractive only if the solution is regenerated and reused, in which case the silver concentration is gradually increased to higher levels. Experiments for repeated use of the thiosulfate solution for dissolution of new batches of zinc cake were carried out and the precipitator consumption is being determined by the ratio ΣMe:S =1. It was found that upon dissolution of the second batch of cake the degree of silver recovery decreased from 74 % to 6 %, which was due to the presence of free S^{2-}, because of the high consumption of precipitator. Therefore, for successful regeneration of the thiosulfate solution the leaching process should be performed while maintaining pH=7-8, so as to secure hydrolization of the other metals except silver. Then, the consumption of precipitator will be considerably lower. For that purpose, experiments were carried out for quintuple use of the thiosulfate solution while maintaining pH=7 by means of lime milk. The consumption of sodium sulfide for silver precipitation is 1,1 g per 1 g of silver in the solution. After recovery of the fifth batch the thiosulfate solution has the chemical composition presented in Table 6. The chemical composition of the hydroxide-sulfide concentrate obtained after precipitation is also presented in the same table.

As a result of the quintuple use of the thiosulfate solution, the rate of silver recovery in the concentrate decreases from 74 to 70 %. It means that the thiosulfate solution should be adjusted at regular intervals. It can be assumed that if an even higher pH is maintained during the recovery, for example pH=8, whereby fuller hydrolization of the metals is secured, the silver content in the produced concentrate will increase significantly.

For treatment of the solid residue after thiosulfate leaching there are two possible ways – Waelz-process or floatation and Waelz-process.

The conceptual flow sheet for treatment of the zinc cake is presented in Fig. 7.

CONCLUSIONS

As demonstrated by the obtained experimental results, about 74% of the silver contained in the zinc cake can be recovered by thiosulfate technology and subsequent precipitation with Na_2S to produce silver concentrate. The proposed process diagram can be successfully applied in the end of the cycle of wet recovery of zinc cakes.

REFERENCES

1. N. B. Kokoeva, *Trudy molodykh uchenykh*, **2,** 35 (2005).
2. M.G Aylmore, D.M Muir, *Minerals Engineering,* **14,** 135 (2001).
3. J. L. Deutsch and D. B. Dreisinger, *Hydrometallurgy*, **137**, 156 (2013).
4. J. L. Deutsch, D. B. Dreisinger, *Hydrometallurgy*, **137**, 165 (2013).
5. Maksimov, O. K. Kuznetsov, N. V. Khodov, V. M. Alkatsev, N. I. Bekarevich, I. S. Sataev, L. A. Otrozhdennova, N. D. Malinovskaya, *RU Patent* 2002828 (1993).
6. L. A. Otrozhdenova, N. D. Malinovskaya, I. I. Maksi-mov, N. D. Khodov, O. K. Kuznetzov, XIX IMPC Precious Metals Processing & Mineral Waste & the Environment, San Francisco Vol. 4, (1995), pp. 75-77.
7. V. V. Geykhman, L. A. Kazanbaev, P. A. Kozlov, A.V.Kolesnikov, V. B. Chinkin, *Tsvetnye Metally (Non-Ferrous Metals),* **1,** 25 (2003).

ИЗВЛИЧАНЕ НА СРЕБРО ОТ ЦИНКОВИ КЕКОВЕ

Б. И. Лучева *, П. К. Илиев, Вл. П. Стефанова

Департамент по цветни метали, Химико-технологичен и металургичен университет, София 1718,България

Постъпила на 27 юни, 2014 г.; приета на 8 април, 2014 г.

(Резюме)

В настоящата експериментална работа е изследвана възможността за тиосулфатно извличане на среброто от цинковите кекове, получени при мокрото извличане на цинкова угарка в КЦМ-Пловдив. Изследвано е влиянието на различни фактори върху степента на тиосулфатно извличане на среброто. Установено, е че степента на извличане на среброто е 70-74 % в температурния диапазон 30-50^{o}C при плътност на пулпа 20% и времетраене на извличането 30 min, независимо от pH на разтвора. Проследено е поведението на медта, оловото, цинка и желязото при тиосулфатното извличане. При поддържане на pH на тиосулфатния разтвор 7-8 с цел хидролизиране на металите, преминали в разтвора и следващо утаяване на среброто с Na_2S се получава сребърен концентрат. Разгледана е възможността за регенериране на тиосулфатния разтвор. Твърдият остатък от извличането съдържа 10-40 g/t и може да бъде преработван чрез Велц-процес.

Bulgarian Chemical Communications, Volume 47, Special issue A (pp. 118 - 123) 2015

Application of waste glycerol from biodiesel productionfor obtaining of modifiers for reduced friction of different motor oils

Z. Glavcheva-Laleva[1], L. Varadinova[2], St. Kerekov[3], D. Pavlov[4], Iv. Glavchev[2*]

[1]Institute for Organic Chemistry, Bulgarian Academy of Science, Acad. G. Bonchev Street, Building 9, 1113 Sofia, Bulgaria,[2]University of Chemical Technology and Metallurgy, Sofia, Bulgaria,[3]Director "NITIAT"OOD,Sofia, Bulgaria,[4]University of Russe „Angel Kanchev",Russe, Bulgaria

Received August 11, 2014; Revised April 8, 2015

Glycerol mono oleate (GMO) was made from waste glycerol (WG) from biodiesel productions by condensation with oleic acid in presence of titanium alcoholate as catalyst. The total acid number was obtained with titration of the samples of GMO with alcohol solution of potassium hydroxide (ASKON). The neutralization of extra oleic acid was made by alcohol solution of methyl amine or 25% amonia. The prepared sample from the obtained modifier was analysed by standard method with four-ball method and the reduced friction was assessed.

Key words: *waste glycerol, glycerol monooleate, titanium catalysts, friction modifiers*

INTRODUCTION

In a number of publications was described the obtaining of GMO started from 30th years of the last century. It was known that this compound can be obtain from:

- Glycerolize
- Hydrolyses of triglycerides
- Direct esterification of glycerol with oleic acid

The third method was possible to be made with or without catalysts. The first possibility was made usually at high temperature or pressure. The applied catalysts were acids [1,2] or basis [3,4]. Usually the application of catalysts decreases the temperature and the time. The application of solid catalysts (oxides, zeflites and others)widely investigated and it will not be described in this paper. The reaction between oleic acid (OA) and ammonia or ammines was well known, because –COOH was acidic, but amines were bases. In [6] was described the obtaining of amides from fatty acids and methylamine. The same authors have another article, published in 2013 year. The application of enzymes was described in a lot of articles [7]. We investigated the possibility for making of glycerol mono oleate from waste glycerol obtained in biodiesel production. The reaction was made in the presence of a new titan tetra alcoholic containing catalysts (TiAl) applied in syntheses of synthetic oils [8]. Becausethey have some excess of oleic acid, we decided to combine itwith methyl amine.The reaction between glycerol –OH groups and oleic acid in the presence of TiAl was investigated at two temperatures and the activation energy ($E_{act.}$) was determined.

EXPERIMENTAL

The compound WG was investigated by elemental analysis (EA) with apparatus Euro EA 3000 (Euro Vector Sp A, Italy). The carbon, nitrogen and hydrogen content were measured in the analyzed samples by burning of the material with weight 0.5 – 1.5 mg at 980^0C in oxygen atmosphere. The obtained gas mixture passed through chemical/absorption zone. Then CO_2,N_2 and H_2O were separated by gas chromatography. It was known, that glycerol have no nitrogen in his molecule, but in WG it was possible to have some small amount of nitrogen from protein of the raw oils applied in biodiesel production. The standard curve was made through analyses of acetonilile (C_8H_9NO) with computer product Calligus. From the obtained results, the content of glycerol (G)was calculated.The results from EA were compared by data obtained with UV-VIS analyses, made by apparatus Cary 100 Scan UV-VIS spectrophotometer (Varian, Germany) by obtaining the spectra of WG and pharmacopeiusG,99% product of Chemapol Ltd, Dimitrovgrad, Bulgaria and of G, p.a., product ofValerus Ltd, Sofia, Bulgaria. From the obtained spectra of the second company,the dependence concentration of G – C, / absorption A was made and there were calculated the equations of several maxima in the specter of G with different values of accuracy of the obtained

* To whom correspondence should be sent.
E-mail: ivgl@uctm.edu

equations and experimental values(correlation coefficient R^2). With the equations at 222 n.m.and A from spectrum of WG it was calculated the glycerol content in the WG. The obtained value was 62%.The syntheses of GMO were made in 150^0C for 3 h in the presence of 0.43 ml TiAl, 0.5 mol. standard OK, p.a., product of Valerus Ltd. and 0.6 mol. WG. The same synthesis was made with standard OK and G, p.a.The obtained products wereinvestigated by ^{1}H NMR(by apparatus BrukerAvance DRX250),UV-VIS and FTIR spectroscopies (by apparatus Cary 100 Scan UV-VIS and Varian FTIR). The investigation with UV-VISwere made in 10 mm cuvettes. The investigation with FTIR were made in thin layers of the obtained materials. Thefriction properties of GMO obtained from WG and from pure raw materials were investigated by standard method like additive of engine oil with four boll machine [9].

RESULTS AND DISSCUSION

The characteristics of WG were investigated with elemental analyses, UV-VIS and FTIR spectroscopes. The spectra of G, product of Chemapol Ltd, Dimitrovgrad, Bulgaria were made with UV-VIS spectroscopy but they have not maxima in the area 200 – 400 nm(fig. 1).

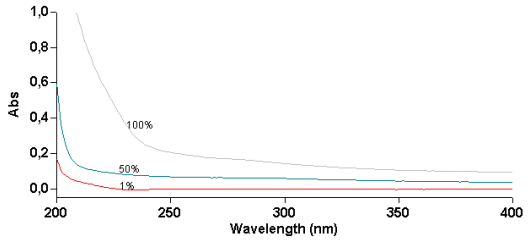

Fig. 1. UV-VIS spectra of G, product of Chemapol Ltd, Dimitrovgrad

The spectra of glycerol published in the literature have several maxima in this area. This is the reason to make the same investigations with G, p.a., product of Valerus Ltd, Sofia, Bulgaria. The obtained spectra are presented in fig.2

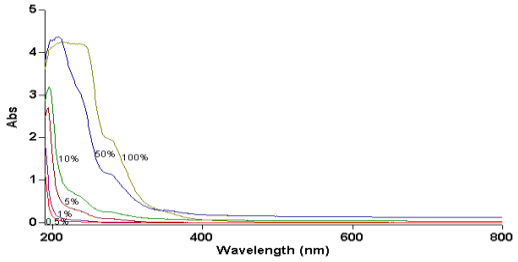

Fig. 2. UV-VIS spectra of G, product of Valerus Ltd, Sofia, Bulgaria

From the obtained spectra were made equations concentration C, % / absorption A.for maxima at 285, 225, 222 and 218 nm. It was known, that the equations are true if R2 > 0.99. This is the reason to make calculations only with equation at 222 nm. From this equation and from the data for WG given in fig. 3 the concentration of G in WG was calculated, namely 62%.

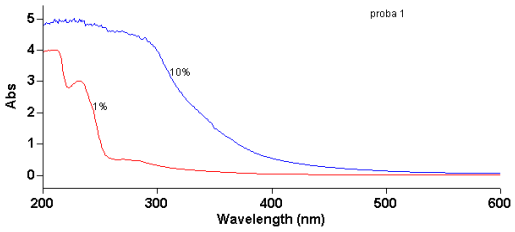

Fig. 3. UV-VIS spectra of water solutions of WG

ГIn ^{1}H NMR spectrum of WG have maxima for protons in –CH- , -CH и –OH groups. Thesegroupswerewithbands, shownin FTIR spectrum of WG. Forexample –OH was with band at 3354.45 sm^{-1}, Because WG was very reactive, was made spectrum in thin layer on the plate from CaF_2 with apparatus ThermoScietificNicolet 6700

GMO, obtained from WG and standard OA , like product, made only from standard G and OA were investigated with^{1}H NMR, UV-VIS and FTIR spectroscopes. Data for ^{1}H NMR of GMO, made from WG was analogical of data for this compound, published in[10].In fig. 4 was given UV-VIS spectrum ofGMO from WG and standard OA. The place oftwo maxima for 1% -en alcoholsolution of GMO was under of 300 n.m

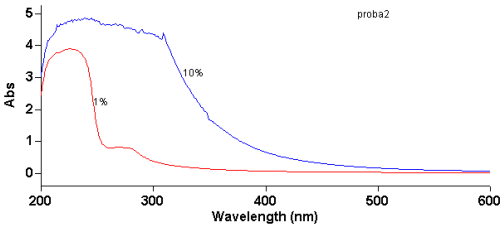

Fig. 4. UV-VIS spectra of alcoholsolutions of GMO, made from WG with TiA.

FTIR spectrum of GMO, obtained with the same catalyst from WG and standard OA was shown in fig. 5. The bands for–OH group was at 3382.660 cm^{-1}, for–CH- and CH_2groups were at 2926.058, 2853.929, 1463.020, 1410.009 and 723.009 $cm^1$and for –CO was at 1711.729 cm^1. The values of some bands were at the same position, like in row glycerol, but in some bands were in a new places, because were for a new compound.In FTIR spectrum of GMO, obtained at the same catalyst from stanfard row materials, shown in fig. 7 had the same bands. The differences in the values of some bands were so small, that were after decimal point.

In the spectra of GMO after neutralization of the remained acidswith alcohol solution of methylamine ore with 25% water solution of ammonia, shown in figures 7 and 8 had analogical bands.

The activation energy$E_{actt.}$ of the esterification of –OH groups in GMO with OA was obtained in the investigation of the reactionin two temperatures – room at 80^0C. From the values of the velocities W_1 = 0.052 mg KOH/g.h. andW_2 = 0.7515 mg. KOH/g.h. was obtained the value of activation energy E_{actt}=.9.15kJ/mol.The values of acid numbers (AN) were obtained with alcohol solution of KOH by standard method, described in[11]. The obtained values were in table 1.

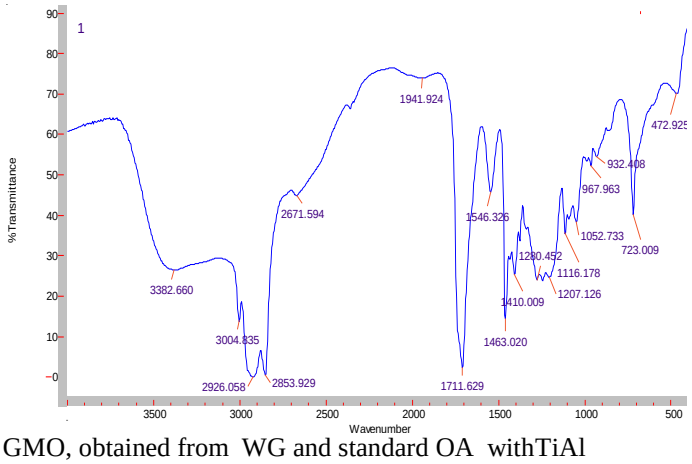

Fig 5 FTIR spectrum of GMO, obtained from WG and standard OA withTiAl

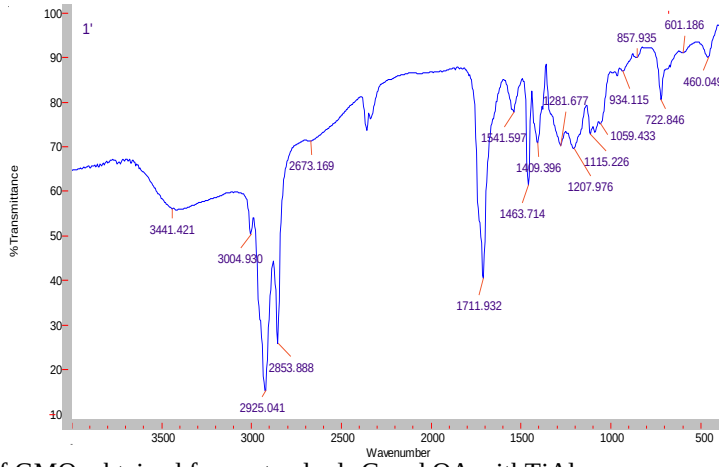

Fig. 6. FTIR spectrum of GMO, obtained from standards G and OA withTiAl.

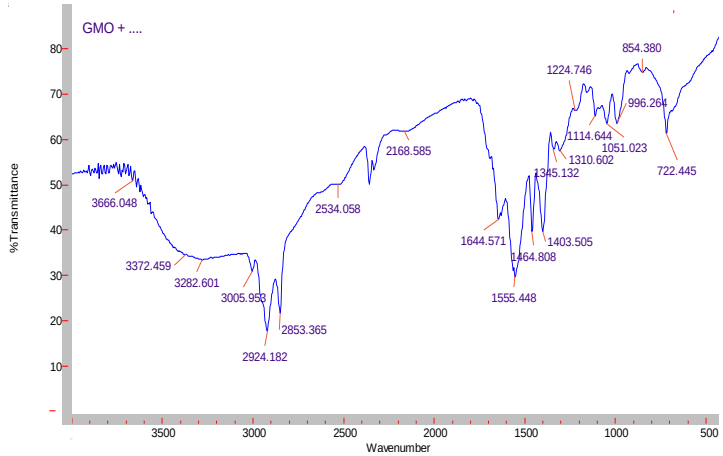

Fig. 7. FTIR spectrum of GMO, obtained from WG with catalystTiAl and after neutralization of the remained acids with alcohol solution of methylamine.

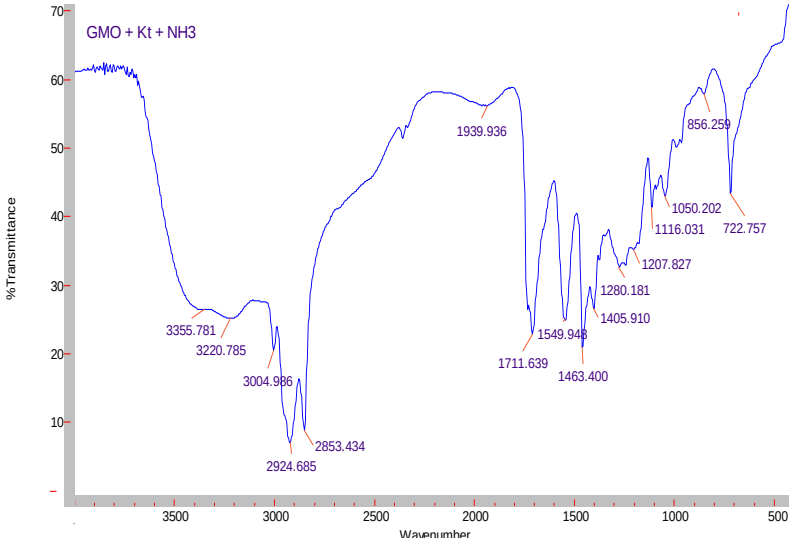

Fig. 8. FTIR spectrum of GMO obtained from WG with catalystTiAl and after neutralization of the remained acids with water solution of 25% ammonia

Table 1. Data for A.N. of GMO and its mixtures with methilamine (MA)(1 -11.02, 2 – 19.02, 3 – 02.04)in room temperature

N	Probe (ml/ml)	A.N.1,mg KOH*/ g	A.N. 2,mg KOH*/ g	A.N..3,mg KOH*/ g
1	GMO from WG	101.15	80.53	79.68
2	GMO: MA= 5 :1	71.34	51.78	51.55
3	GMO: MA = 5 : 3	61.97	alkaline	alkaline
4	GMO: MA = 5 : 5	42.28	alkaline	alkaline

Table 2. Dependences between average diameter of wearing of the balls (d_{eva}) and of anti wearing index (AWI),from the quantity, % and the kind of investigated modifiersin mineral motor oil M10D$_2$/E$_1$

№	Quantity,% and the kind of modifier ,	$d_{eva}$of wearing,mm	AWI, N
1	0	0.60	243
2	2, Zn sucsinide	0.36	346
3	0.5, Zn sucsinide	0.39	329
4	0.5, Cu oleate	0.45	-
5	GMO obtained from WG	0.43	302
6	GMO obtained from standard materials	0.42	324

Table3. Dependences between average diameter of wearing of the balls (d_{av}), % , Δfrom the quantity, % and the kind of investigated modifiersin motor oilSN 500

№	Quantity,% and the kind of modifier ,	$d_{av}$of wearing, mm., %, Δ
1	0 , Mineral motor oil SN 500,	0.70, 100, 0
2	1, anilidoleate	0.57, 81.43, 18.57
3	0.5, anilidoleate	0.62, 88.57, 11,43
4	1, Cu oleate	0.65, 92.86, 7.14
5	0.5, Cu oleate	0.60, 85.71, 14.29
6	2, Complex polyester	0.63, 90, 10
7	1, Complex polyester	0.63, 90, 10
8	2, GO obtained from WG	0.60, 85,71, 14.29
9	1, GO obtained from WG	0,56, 80, 20
10	0,5, GO obtained from WG	0,56, 80, 20
11	2, GO obtained from standard materials	0.60, 85.71, 14.29
12	1, GO obtained from standard materials	0,55, 78.57, 21.13
13	0,5, GO obtained from standard materials	0,55, 78.57, 21.13

Table 4. Dependences between average diameter of wearing of the balls (d_{av}), %, Δfrom the quantity, % and the kind of investigated modifiersin synthetic motor oil5W40 according SAESL/CF по API

№	Quantity,% and the kind of modifier ,	$d_{av}$of wearing, mm., %, Δ
1	0 , syntetic motor oil 5W40	0.59, 100, 0
2	1, anilidoleate	0.53, 89.83, 10.17
3	0.5, anilidoleate	0.54, 91.53, 8.47
4	1, Cu oleate	0.50, 84.75, 15.24
5	0.5, Cu oleate	0.55, 93.22, 6.78
6	2, Complex polyester	0.47, 79.66, 20.34
7	1, Complex polyester	0.50, 84.75, 15.24
8	0,5, Complex polyester	0,55, 93.22, 6.78
8	2, GO obtained from WG	0.55, 93.22, 6.78
9	1, GO obtained from WG	0,55, 93.22, 6.78
10	0,5, GO obtained from WG	0,54, 91.53, 8.47
11	2, GO obtained from standard materials	0.52, 88.14, 11.86
12	1, GO obtained from standard materials	0,52, 88.14, 11.86
13	0,5, GO obtained from standard materials	0,54, 91.53, 8.47
14	1, Zn oleate	0,55, 93.22, 6.78
15	0,5, Zn oleate	0,55, 93.22, 6.78
16	1, Titanium oleate	0,52, 88.14, 11.86
17	0,5, Titanium oleate	0.55, 93.22, 6.78

Data for AN of GMO, obtained at 80^0C were analogical. .MA was 33% solution of the gazeCH_3NH_2in pure ethanol. If the sample was alkalinewas no possible the determination of AN. Maybe the esterification of GMO and OA prolonged, because in the molecule of Ghave3 OH groups, capable to react with – COOH groups of OA.In the presence of MA this possibility increased (probes NN 3 and 4).

The properties of the obtained compounds like friction modifier of different motor oils were determined with four ball machine by standard method. For comparison were made investigations with standard friction modifiers. The investigations were made in acridities laboratory for oil products of" "Prista Oil" Ltd. In120^0C for1h – table 2 and in laboratories of university of Russe "ÄngelKanchev", given in tables 3, and 4.

From the results, shown in table 2 was evident, that anti wearing properties of the oil with frictions modifiers (d_{eva} mm and AWI) increased with friction modifier Zn sucsinidewith 30%. With the decreasing of the concentration of the modifier those % was decreased from d_{eva}= 0,36mm for 2% to 0,39 mmfor 0,5%, but was enough for anti wearing properties of motor oil. With anti wearing modifier Cu oleate were obtained the bed results, compared with results of friction modifier GMO, obtained with catalyst TiAl. From the data in table 2 was evident, that the modifier GMO, made from WG and OA were similar with the anti wearing properties of GMO, obtained from standard materials. The increasing was about 25%. From the results, shown in tables 3 and 4 were evident, that the obtaining materials were the good frictions modifiers

CONCLUSION

The results for decreasing of the quantity of different friction modifiers, given in tables 2, 3 and 4 in mineral and synthetic motor oils were no every time in connection with theory of friction modifiers, but the results, obtained with investigated materials from WG were comparable or better with data, obtained with known friction modifiers.

Acknowledgment: *This study is a part of ou rinvestigations and fulfilling of the scientific project "Modifiers for reducing the friction and wear in machinery", financed by Operational programme "Development of the Competitiveness of the Bulgarian Economy" 2007-2013.*

We thanks to Assoc. Prof. Galina Gencheva, PhD, Laboratory of Molecular Spectroscopy, Department of Analytical Chemistry, faculty of Chemistry and Pharmacy,SofiaUniversity for permit ion of making of FTIR spectrum of WG.

REFERENCES

1. Is. Díaz, C. Márquez-Alvarez, F. Mohino, J. P. Pariente[1], E. Sastre, *Journal of Catalysis*, **193-2,** 295 (2000).
2. Is.Díaz, F. Mohino, J. Pérez-Pariente, E. Sastre, *Applied Catalysis A: General*, **242-1**, 161 (2003).
3. M. Berrios, J. Siles, M. A. Martín, A. Martín, *Fuel*, **86-15**, 2383 (2007).
4. M. Zong, Z. QunDuan,W. Lou,T. J. Smithand, H. Wu, *Green Chemistry*, **5,** (2007).

5. S. Abro, Y. Pouilloux, J. Barroult, S*tud. Surf. Sci. Catal*, **108**, 539 (1997).
6. F. Ergan, M. Trani , G. André, *Biotechnology and Bioengineering*, **35**, 195 (1990).
7. O. Abel-Anyebe, K. I. Ekpenyong, A. Eseyin**,** *International Journal of Chemistry*, **5-1**, 80 (2013).
8. D. J. Pavlov, N. N. Gospodinova, I. K. Glavchev, *Industrial Lubrication and Tribology*, **56**, 19 (2004).
9. BSS 9786-84
10. C. Yu, Y. Lee, B. Cheon, S. Lee, *Bull. Korean Chem. Soc.*, **24** 1224 (2003).
11. БДСENISO 660 – 2009.

ПРИЛОЖЕНИЕ НА ОТПАДЪЧЕН ГЛИЦЕРОЛ ОТ ПРОИЗВОДСТВОТО НА БИОДИЗЕЛ ЗА ПОЛУЧАВАНЕ НА МОДИФИКАТОР НА ТРИЕНЕ НА РАЗЛИЧНИ МОТОРНИ МАСЛА

З. Главчева-Лалева[1], Л. Варадинова[2], Ст. Кереков[3], Д. Павлов[4], Ив. Главчев[2]

[1]Институт по Органична химия, Българска академия на науката, Акад. „Г.Бончев", сгр. 9,1113 София, България,
[2]Университет по химична технология и металургия, София, България,
[3]Директор „НИТИАТ" ООД, София, България,
[4]Университет на Русе, „А.Кънчев", Русе, България

Постъпила на 11 август, 2014 г., коригирана на 8 април, 2015 г.

(Резюме)

Глицерол моно олеат (ГМО) беше получен от отпадъчен глицерол (ОГ) от производството на биодизел при кондензация с олеинова киселина с катализатор титанов алкохолат. Общото киселинно число беше получено с титруване на проби от ГМО с алкохолен разтвор на калиева основа (АРКОН). Неутрализацията на излишната олеинова киселина беше направено с алкохолен разтвор на метиламин или 25% амоняк при стайна температура. Получените проби от модификатора на триене бяха изследвани със стандартен метод с четирисачмяна машина и промяната на триенето беше оценена.

BULGARIAN CHEMICAL COMMUNICATIONS

Instructions about Preparation of Manuscripts

General remarks: Manuscripts are submitted in English by e-mail or by mail (in duplicate). The text must be typed double-spaced, on A4 format paper using Times New Roman font size 12, normal character spacing. The manuscript should not exceed 15 pages (about 3500 words), including photographs, tables, drawings, formulae, etc. Authors are requested to use margins of 3 cm on all sides. For mail submission hard copies, made by a clearly legible duplication process, are requested. Manuscripts should be subdivided into labelled sections, e.g. **Introduction, Experimental, Results and Discussion**, *etc*.

The title page comprises headline, author's names and affiliations, abstract and key words.

Attention is drawn to the following:

a) **The title** of the manuscript should reflect concisely the purpose and findings of the work. Abbreviations, symbols, chemical formulas, references and footnotes should be avoided. If indispensable, abbreviations and formulas should be given in parentheses immediately after the respective full form.

b) **The author**'s first and middle name initials, and family name in full should be given, followed by the address (or addresses) of the contributing laboratory (laboratories). **The affiliation** of the author(s) should be listed in detail (no abbreviations!). The author to whom correspondence and/or inquiries should be sent should be indicated by asterisk (*).

The abstract should be self-explanatory and intelligible without any references to the text and containing not more than 250 words. It should be followed by key words (not more than six).

References should be numbered sequentially in the order, in which they are cited in the text. The numbers in the text should be enclosed in brackets [2], [5, 6], [9–12], etc., set on the text line. References, typed with double spacing, are to be listed in numerical order on a separate sheet. All references are to be given in Latin letters. The names of the authors are given without inversion. Titles of journals must be abbreviated according to Chemical Abstracts and given in italics, the volume is typed in bold, the initial page is given and the year in parentheses. Attention is drawn to the following conventions:

a) The names of all authors of a certain publications should be given. The use of "*et al*." in the list of references is not acceptable.

b) Only the initials of the first and middle names should be given.

In the manuscripts, the reference to author(s) of cited works should be made without giving initials, e.g. "Bush and Smith [7] pioneered...". If the reference carries the names of three or more authors it should be quoted as "Bush *et al*. [7]", if Bush is the first author, or as "Bush and co-workers [7]", if Bush is the senior author.

Footnotes should be reduced to a minimum. Each footnote should be typed double-spaced at the bottom of the page, on which its subject is first mentioned.

Tables are numbered with Arabic numerals on the left-hand top. Each table should be referred to in the text. Column headings should be as short as possible but they must define units unambiguously. The units are to be separated from the preceding symbols by a comma or brackets.

Note: The following format should be used when figures, equations, *etc*. are referred to the text (followed by the respective numbers): Fig., Eqns., Table, Scheme.

Schemes and figures. Each manuscript (hard copy) should contain or be accompanied by the respective illustrative material as well as by the respective figure captions in a separate file (sheet). As far as presentation of units is concerned, SI units are to be used. However, some non-SI units are also acceptable, such as °C, ml, l, etc.

The author(s) name(s), the title of the manuscript, the number of drawings, photographs, diagrams, etc., should be written in black pencil on the back of the illustrative material (hard copies) in accordance with the list enclosed. Avoid using more than 6 (12 for reviews, respectively) figures in the manuscript. Since most of the illustrative materials are to be presented as 8-cm wide pictures, attention should be paid that all axis titles, numerals, legend(s) and texts are legible.

The authors are asked to submit **the final text** (after the manuscript has been accepted for

publication) in electronic form either by e-mail or mail on a 3.5'' diskette (CD) using a PC Word-processor. The main text, list of references, tables and figure captions should be saved in separate files (as *.rtf or *.doc) with clearly identifiable file names. It is essential that the name and version of the word-processing program and the format of the text files is clearly indicated. It is recommended that the pictures are presented in *.tif, *.jpg, *.cdr or *.bmp format, the equations are written using "Equation Editor" and chemical reaction schemes are written using ISIS Draw or ChemDraw programme.

The authors are required to submit the final text with a list of three individuals and their e-mail addresses that can be considered by the Editors as potential reviewers. Please, note that the reviewers should be outside the authors' own institution or organization. The Editorial Board of the journal is not obliged to accept these proposals.

EXAMPLES FOR PRESENTATION OF REFERENCES

REFERENCES

1. D. S. Newsome, *Catal. Rev.–Sci. Eng*., **21**, 275 (1980).
2. C.-H. Lin, C.-Y. Hsu, *J. Chem. Soc. Chem. Commun*., 1479 (1992).
3. R. G. Parr, W. Yang, Density Functional Theory of Atoms and Molecules, Oxford Univ. Press, New York, 1989.
4. V. Ponec, G. C. Bond, Catalysis by Metals and Alloys (Stud. Surf. Sci. Catal., vol. 95), Elsevier, Amsterdam, 1995.
5. G. Kadinov, S. Todorova, A. Palazov, in: New Frontiers in Catalysis (Proc. 10th Int. Congr. Catal., Budapest, 1992), L. Guczi, F. Solymosi, P. Tetenyi (eds.), Akademiai Kiado, Budapest, 1993, Part C, p. 2817.
6. G. L. C. Maire, F. Garin, in: Catalysis. Science and Technology, J. R. Anderson, M. Boudart (eds), vol. 6, Springer-Verlag, Berlin, 1984, p. 161.
7. D. Pocknell, *GB Patent* 2 207 355 (1949).
8. G. Angelov, PhD Thesis, UCTM, Sofia, 2001.
9. JCPDS International Center for Diffraction Data, Power Diffraction File, Swarthmore, PA, 1991.
10. CA **127**, 184 762q (1998).
11. P. Hou, H. Wise, *J. Catal.*, in press.
12. M. Sinev, private communication.
13. http://www.chemweb.com/alchem/articles/1051611477211.html.

CONTENTS

СЪДЪРЖАНИЕ